

## The Yuanjue Grottos in Anyue



# **The Yuanjue Grottos in Anyue**

**Annual Report 2007–2009**

**BMBF Project 01 GWS 079**

**Technische Universität München,  
Lehrstuhl für Restaurierung, Kunsttechnologie und  
Konservierungswissenschaft**

**Chinese Academy of Cultural Heritage (CACH)**

GEFÖRDERT VOM



© Technische Universität München und Chinese Academy of Cultural Heritage, Beijing, 2009

Herausgeber: Technische Universität München  
Lehrstuhl für Restaurierung, Kunsttechnologie und Konservierungswissenschaft,  
Oettingenstr. 15, 80538 München, [www.rkk.arch.tu-muenchen.de](http://www.rkk.arch.tu-muenchen.de)

Chinese Academy of Cultural Heritage  
No. 2 Gaoyuan Street, North 4<sup>th</sup> Ring Road, East Road, Beijing, 100029 P. R. China

Konzeption: Dr. Mathias Kocher  
Redaktion: Sabine Tönnies M.A., Dr. Mathias Kocher, Prof. Dipl.-Restaurator Erwin Emmerling  
Satz und Layout: Sabine Tönnies M.A.  
Umschlaggestaltung: Dipl.-Restaurator Felix Horn

---

**Inhalt/Content**

Einleitung/Introduction .....	7
<i>Wang Jinhua, Zhang Jinfeng</i> Research Report on Control Strategy of Environmental Geological Diseases of Yuan Jue Carving Protected Area .....	13
<i>Rolf Snethlage, Erwin Emmerling, Mathias Kocher, Melanie Eibl</i> Examination of the stone samples from the Yuanjue grottos, Anyue in the province Sichuan .....	131
<i>Felix Horn</i> 3-D-Vermessung und Texturierung der Grotte Nr. 10 des Buddha Shakyamuni und der Grotte Nr. 37 .....	161
<i>Felix Horn</i> 3-D-Dokumentation der Grotte Nr. 10 des Buddha Shakyamuni .....	179
<i>Ursula G. Drewello, Mathias Kocher</i> Biological investigations of grotto no. 37 .....	187
<i>Zhang Jinfeng, Melanie Eibl, Felix Horn, Mathias Kocher</i> Garden maintenance- and Landscape management plan .....	201
<i>Lin Chunmei</i> Die Kunst der Grotte Nr. 10 in der Grottenanlage Yuanjue .....	207
<i>Zhao Zhou</i> Kunsthistorische und religionshistorische Grundlagen der Restaurierung buddhistischer Kulthöhlen in China (Arbeitsbericht 2008) .....	215
<i>Zhao Zhou</i> Frontal Buildings and Niche No. 10 at Yuanjuedong in Anyue County .....	219



# Einleitung

Mathias Kocher

Im Januar 2006 wurde in der 11. Lenkungsausschusssitzung in Xian die Ausweitung der bisherigen Forschungen auf landesweit ausgewählte Denkmäler der VR China beschlossen.

In Süd-West China, in der Provinz Sichuan und im Gebiet von Congqing, befinden sich eine Vielzahl von außergewöhnlichen Steinskulpturen, die für die Entwicklung der chinesischen Bildhauerei und Kunstgeschichte von außergewöhnlicher Bedeutung und in ganz China einzigartig sind. Der Bezirk Anyue mit seiner Bezirkshauptstadt gleichen Namens ist ein nahezu unbekannter kleiner Kreis, der in der Mitte zwischen den beiden Metropolen Chengdu (Provinzhauptstadt von Sichuan) und Congqing (Hauptstadt des gleichnamigen Stadtbezirks) liegt.

Der anstehende rötliche Sandstein und die schweren braunen Lehmböden der Region haben der Gegend ihren Namen gegeben – das Rote Becken.

Zurückgehend bis auf die Südliche Dynastie (um 500 n. Chr.) überblickt man hier eine mehr als 1500-jährige Geschichte der Bildhauerei und Bildhauerkunst mit deren kulturwissenschaftlichem Hintergrund.

Die Blütezeit wurde während der Song-Dynastie (960–1279 n. Chr.) erreicht. Heute zählt man 200 Grotten mit mehr als 100 000 Buddha-Statuen.

Die Yuanjuedong Grottenanlage liegt ca. 2 km südöstlich der Stadt Anyue, am Mount Yunju. Die Anlage geht auf die Tang-Dynastie (618–907 n. Chr.) zurück. Ihre Blütezeit erreichte sie während



Abb. 1: Die Provinz Sichuan in Süd-West China

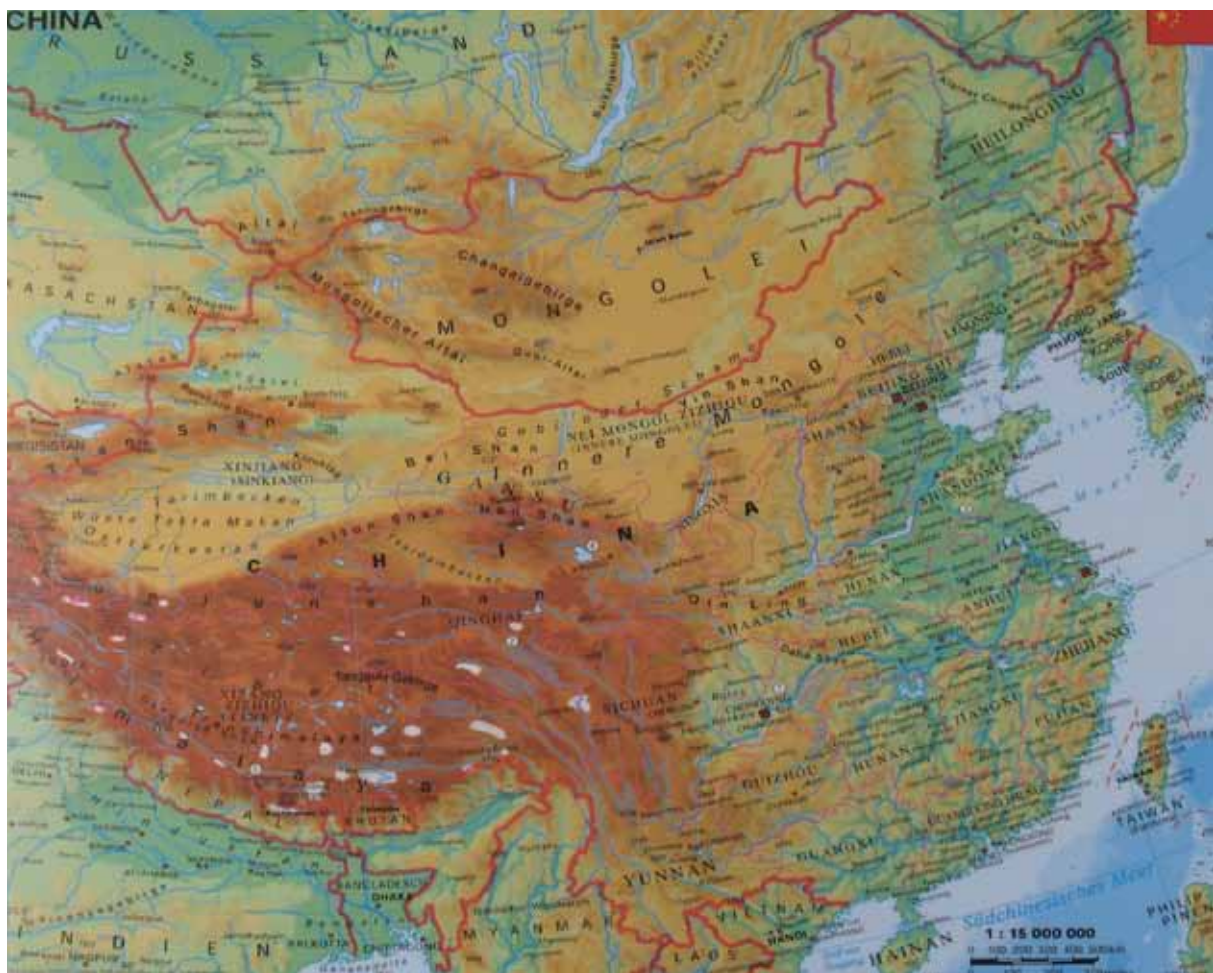


Abb. 2: Geografische Karte China



Abb. 3: Das Rote Becken mit der Stadt Anyue

der Fünf Dynastien (907–960 n. Chr.) und der Song-Dynastie (960–1280 n. Chr.). 400 Jahre Bildhauerei hinterließen mehr als 100 Grotten mit nahezu 2 000 Statuen von unterschiedlicher Größe.

Während sich auf der Südseite hauptsächlich kleinere Nischen und Grotten mit Höhen von 2–3 Metern befinden, sind auf der Nordseite drei große Grotten mit sehr großen und gut erhaltenen Statuen zu finden, eine des Buddha Shakyamuni und zwei des Buddha Guanyin.

Die Statue des Buddha Shakyamuni (Grotte Nr. 10) ist 7 Meter hoch. Sein Kopf ist leicht nach unten geneigt und wohlwollend lächelnd einer weiteren Figur zugewandt. Der „Lotusblüten-haltende“ Buddha Guanyin ist 6,5 Meter hoch. Er trägt eine Krone, die mittig mit einem sitzenden Buddha verziert ist, und hält einen Strauß Lotusblüten in seiner Hand. Der „Vase-haltende“ Buddha Guanyin ist mit 7 Metern etwas größer. Die Figur ist ähnlich der des Lotusblüten-haltenden Guanyin.

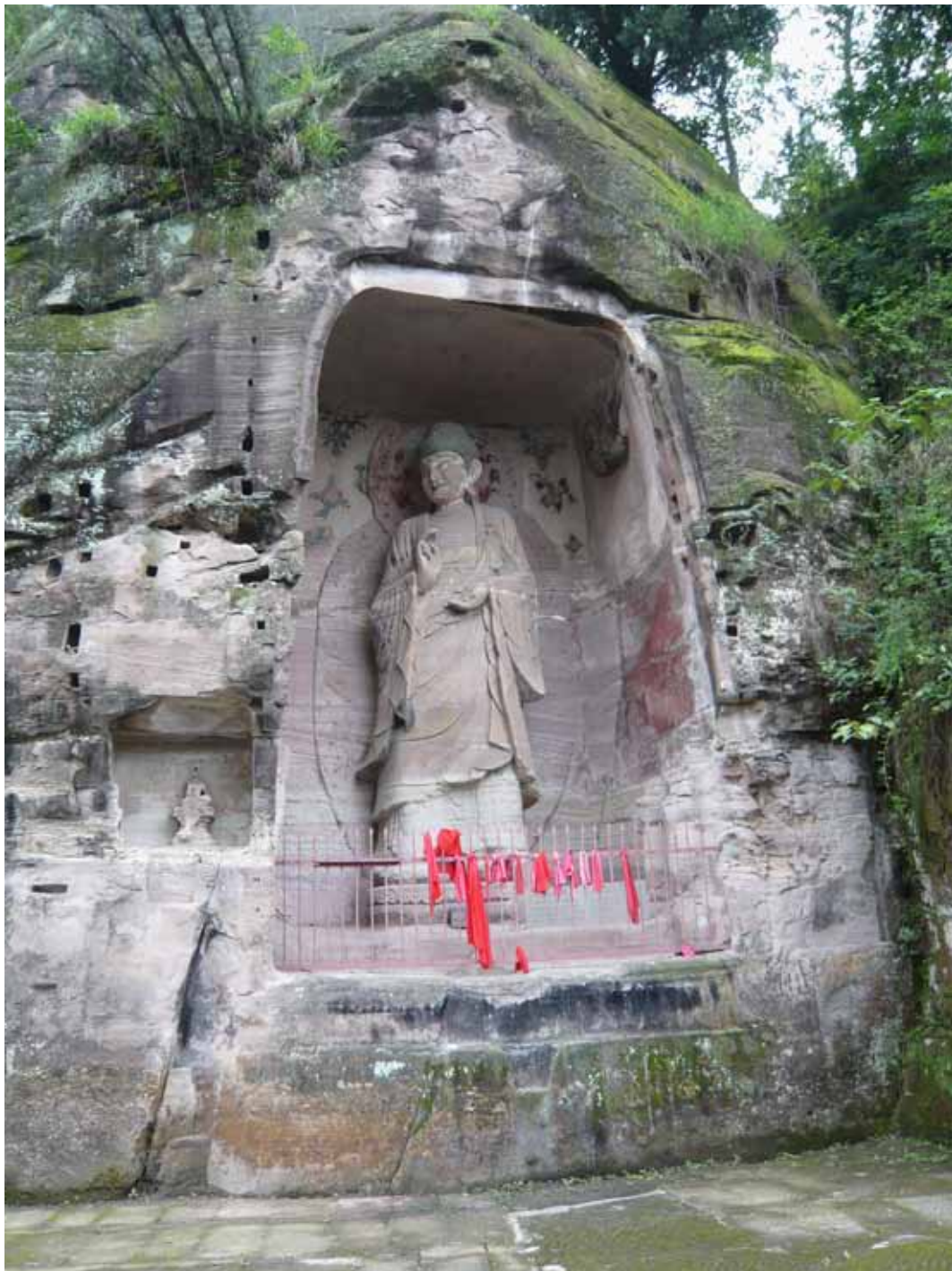
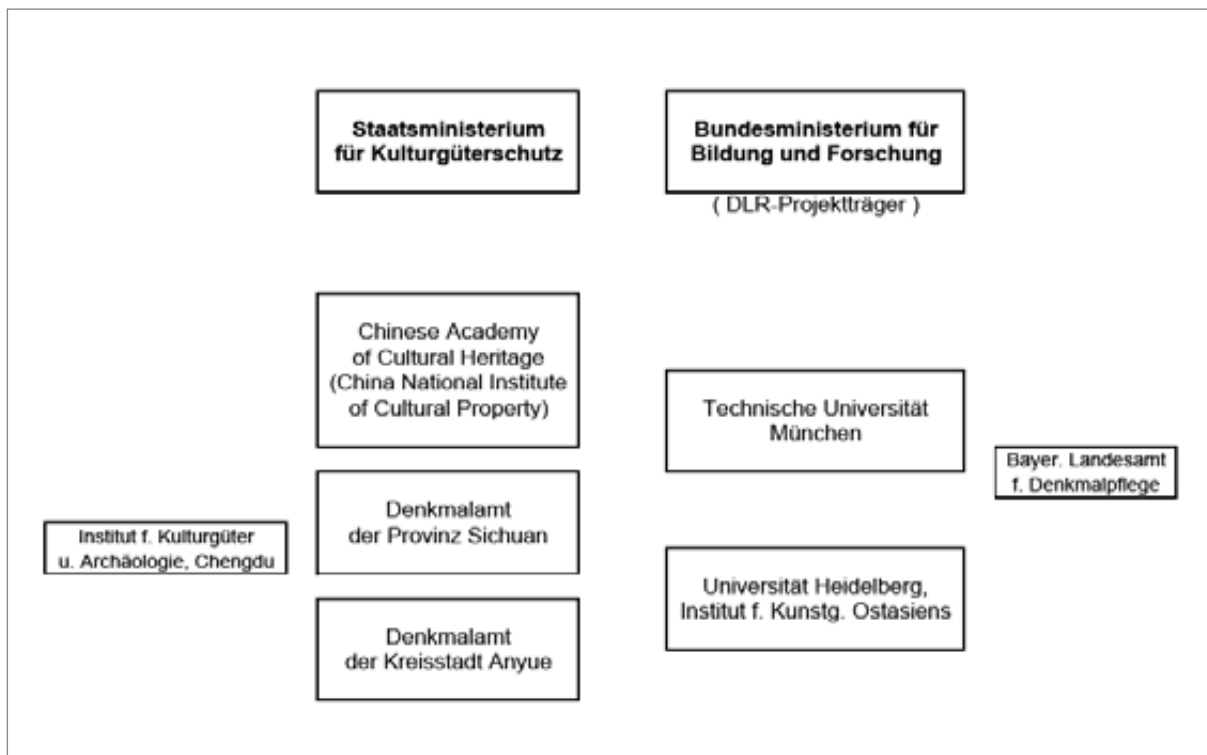


Abb. 4: Die Grotte Nr. 10 der Yuanjuedong Anlage

## Die beteiligten Institutionen



## Aufgabenstellungen

- Dokumentation und Aufnahme des momentanen Zustandes (2007)
- Fotografische Dokumentation
- Erstellung eines Sofortmaßnahmenplans, Stabilisierung des Ist-Zustandes (2007)
- Ermittlung der Schadensursachen (2007, 2008)
- Petrografische Bestimmung der Gesteine und Gesteinseigenschaften (2007, 2008)
- Erstellung eines Restaurierungskonzeptes mit der Entwicklung geeigneter Steinschutzmittel und Hinterfüllmassen (2008, 2009)

## Arbeitsaufenthalte 2007

**9. Juli bis 20. Juli 2007:**  
Auswahl der zu untersuchenden Grotten (Grotte Nr. 10, Nordseite und Grotte Nr. 37, Südseite)

**17. November bis 30. November 2007:**  
Erstellung einer Übersichtsaufnahme des gesamten Grottenhügels (Laserscanner) und detaillierte Aufnahmen der beiden ausgewählten Grotten (Streifenlichtscanner)

## Arbeitsaufenthalte 2008

**26. Mai bis 6. Juni 2008:**  
Wegen des schweren Erdbebens vom 12. Mai 2008 konnte der Arbeitsaufenthalt nicht stattfinden.

**13. Oktober bis 24. Oktober 2008:**  
Auswahl einer geeigneten Musterfläche zur Festigung und Fortführung der 3-D-basierten Dokumentation.

## Arbeitsaufenthalt 2009

**4. Mai bis 15. Mai 2009:**  
Bohrhärtemessungen an der zuvor ausgewählten Musterfläche mit anschließender Festigung.

## Juli 2007 – Arbeitsaufenthalt in Anyue

Der Arbeitsaufenthalt in Anyue dauerte vom 9. bis 20. Juli 2007. Teilnehmer waren Herr Dr. Mathias Kocher, Herr Dipl.-Rest. Felix Horn (beide Technische Universität München), Frau Dr. Zhang Jinfeng (Chinese Academy of Cultural Heritage) und Frau Prof. Dr. Lin Chunmei (Tainan University College of the Arts, Conservation of Cultural Relics).

Der Schwerpunkt des Aufenthalts war die Erkundung, Dokumentation und Auswahl der exemplarisch zu bearbeitenden Grotten der ca. 2 km außerhalb von Anyue auf einem Hügel gelegenen Grottenanlage Yuanjuedong („Grotten der vollkommenen Erleuchtung“).

Bei einer ersten Besichtigung der Grotten zusammen mit Liao Shunyong, dem vor Ort Verantwortlichen, wurden erste historische Details in Erfahrung gebracht. Neben ersten Untersuchungen an den Grotten wurde mit der Dokumentation durch Digital- und Videoaufnahmen begonnen. Mit Frau Dr. Zhang wurden nach umfassender Erkundung der Grottenanlagen Kriterien (Größe, Gesteinsqualität, Polychromie, Zustand, Zeitaufwand, Situation für Schutzbau etc.) für die Wahl der exemplarisch zu bearbeitenden Grotte erstellt.

Dabei wurden das weitere Vorgehen und der künftige Arbeitsplan abgestimmt. Zunächst wurden für die Bearbeitung auf der Vorderseite des Hügels (nordöstliche Ausrichtung) Grotte Nr. 10 mit der Skulptur des Buddha Shakyamuni und auf der Rückseite (südwestliche Ausrichtung) Grotte Nr. 37 ausgewählt. Diese Auswahl der Grotten sollte dann bei einer Besprechung mit den chinesischen Kollegen in Beijing erörtert werden. Bei der abschließenden Besprechung in Anyue wurden folgende Maßnahmen festgelegt:

- Grotte Nr. 10: Dokumentation, Kartierung von lockerem Gestein, Untersuchungen von Gestein und Pigmenten.
- Grotte Nr. 37: Diskussion von Schutzbauten, Verbesserung der Wasserführung, Entfernung von biologischem Bewuchs, Reinigung, Gesteinsfestigung, Stabilisierung der Felsen.

Beim anschließenden Treffen in Beijing an der Chinese Academy of Cultural Heritage wurde dem Vorschlag, die Grotten Nr. 10 und Nr. 37 zu bearbeiten, zugestimmt. Als Ansprechpartner wurden für China Frau Dr. Zhang und für Deutschland Herr Dr. Kocher festgelegt. Dem Vorschlag von Herrn Horn, die Grotte Nr. 10 digital zu vermessen, wurde zugestimmt. Das 3-D-Modell kann als Grundlage für die Schadenskartierung sowie für die virtuelle Konstruktion eines Schutzbaues verwendet werden. Die chinesische Seite begrüßt die 3-D-Vermessung. Weiter berichtet Herr Ma Qinglin, dass die Chine-

se Academy of Cultural Heritage voraussichtlich im Herbst 2007 eine eigene Abteilung für 3-D-Vermessung einrichten will. Die noch anzuschaffenden Gerätschaften könnten dann auch in Anyue verwendet werden.

## November 2007 – Arbeitsaufenthalt in Anyue

Der zweite Arbeitsaufenthalt des Jahres 2007 fand vom 17. bis 30. November 2007 statt. Teilnehmer auf deutscher Seite waren Herr Dr. Mathias Kocher, Herr Dipl.-Rest. Felix Horn (beide TU München), Herr Martin Scheich und Herr Lars Langheinrich (Firma ArcTron, 3-D-Vermessungstechnik, Altenthann). Auf chinesischer Seite Frau Prof. Dr. Lin Chunmei (Tainan University College of the Arts, Conservation of Cultural Relics), Herr Prof. Wang Liang, Herr Dr. Wu Yuhua, Frau Dr. Zhang Jinfeng (Chinese Academy of Cultural Heritage, Beijing), Frau Prof. Lei Yu Hua, (Archaeological Institut, Chengdu) und Liao Shunyong (Denkmalamt Anyue) sowie weitere Mitarbeiter aus Beijing und Anyue.

Ziel des Arbeitsaufenthaltes war die 3-D-Vermessung der Anlage mit den beiden detaillierter zu untersuchenden Grotten Nr. 10 und Nr. 37 sowie die geologische Erkundung. Von der Firma ArcTron wurde mittels Laser-Scans der gesamte Hauptgrottenhügel vermessen. Von den Grotten Nr. 10 und Nr. 37 wurden zusätzlich Streifenlicht-Scans angefertigt. Die 3-D-Vermessung der Anlage soll zum einen als Dokumentationsgrundlage des Ist-Zustandes dienen und zum anderen die Dokumentation der durchgeföhrten Maßnahmen erleichtern.

Beim anschließenden Treffen der beiden Arbeitsgruppen in Beijing wurden die nächsten Schritte für das Jahr 2008 erörtert und in gegenseitigem Einvernehmen festgelegt.

## Mai 2008 – Arbeitsaufenthalt in Anyue

Wegen des verheerenden Erdbebens vom 12. Mai 2008 musste der geplante Arbeitsaufenthalt (26. Mai bis 6. Juni 2008) für dieses Frühjahr ausgesetzt werden. Die chinesische Seite wies mit Nachdruck auf die Unwägbarkeiten und Schwierigkeiten eines Arbeitsaufenthaltes zu diesem Zeitpunkt hin.

## Oktober 2008 – Arbeitsaufenthalt in Anyue

Der Aufenthalt fand im Herbst 2008 vom 13. bis 24. Oktober 2008 statt. Die Teilnehmer auf deutscher Seite waren Herr Dipl.-Rest. Felix Horn, Herr Dr. Mathias Kocher (beide TU München), Herr Vojislav Tucic (Bayerisches Landesamt für Denkmalpflege, München) und Herr Zhao Zhou (Universität Hei-

delberg). Die Teilnehmer auf chinesischer Seite waren Herr Prof. Wang Jinhua, Frau Dr. Zhang Jinfeng, Herr Dr. Wu Yuhua, Herr Yuxinxin (alle Chinese Academy of Cultural Heritage, Beijing), Frau Prof. Lei Yu Hua (Archaeological Institut, Chengdu), Herr Yanmin Guo (Guangzhou Baiyun Cultural Heritage Conservation Materials Research Center, Taihe Town) sowie weitere Mitarbeiter des Denkmalamtes Anyue.

Ziel des Aufenthaltes war die Auswahl einer geeigneten Musterfläche zur Festigung sowie die Weiterführung der Dokumentation der Grotte Nr. 10 mittels klassischer und 3-D-basierter Methoden. Die Musterfläche wurde in Übereinkunft mit der chinesischen Seite festgelegt und erste Festigkeitsmessungen mit dem Intender durchgeführt (Messgerät zur Ermittlung der Eindringtiefe einer definierten Metallkugel).

### Mai 2009 – Arbeitsaufenthalt in Anyue

Ziel des Arbeitsaufenthaltes war die Ermittlung der Bohrhärte des Sandsteins von Anyue. Die Bestimmung der Bohrhärte wurde mit dem nach China exportierten DRM-System durchgeführt. Dabei wurden die chinesischen Kollegen sowohl in die Messtechnik (Anwendung des Gerätes) wie auch in die Interpretation (Auswertung) der Ergebnisse eingeführt. Anschließend erfolgte die Festigung der Musterfläche mit Remmers KSEOH.

Die Teilnehmer auf chinesischer Seite waren: Prof. Wang Jinhua, Dr. Wu Yuhua, Dr. Liuyiou, Herr Yuxinxin, (Chinese Academy of Cultural Heritage, Beijing) Yang Sheng (Jinsha Site Museum, Chengdu) sowie mehrere Mitarbeiter des Kulturgüteramtes des Kreises Anyue und der Stadt Anyue.

Teilnehmer von deutscher Seite waren: Herr Vojislav Tucic (Bayerisches Landesamt für Denkmalpflege, München), Herr Dr. Mathias Kocher (TU München) und Frau Lin Chunmei.

# **Research Report on Control Strategy of Environmental Geological Diseases of Yuan Jue Carving Area**

**Wang Jinhua, Zhan Jinfeng**

**Engineering Center of Protection of Cultural Heritage and  
Relics of Rocks and Soils, China University of Geoscience**

**November 2007**



## Contents

Chapter 1	Introduction .....	17
Chapter 2	Environmental Geological Condition in Yuanjuedong .....	20
Chapter 3	Rock Engineering Properties in Yuanjuedong .....	41
Chapter 4	Environmental Geological Disease Investigation about Yuanjuedong Rock Carving Area .....	78
Chapter 5	Analysis of disease forming mechanism and influencing factors .....	85
Chapter 6	Evaluation on stability of dangerous rock in Yuanjue carving .....	95
Chapter 7	Preventional and treatmental countermeasures of geological hazard .....	109
Chapter 8	Conclusions and suggestions .....	114

## Illustrations

Illustration 1	Topographic map of Yuanjue protected area .....	117
Illustration 2	Topographic map of Yuanjue protected area .....	118
Illustration 3	Relief Map of Yuanjuedong .....	119
Illustration 4	Engineering geology map of Yuanjue carving .....	120
Illustration 5	Distribution of the fissures in Yuanjue carving protected area .....	121
Illustration 6	I-I' Geological section map of protected area .....	122
Illustration 7	II-II' Geological section map of protected area .....	123
Illustration 8	Profile map of grotto no. 9 and 10 .....	124
Illustration 9	Profile map of grotto no. 10 .....	125
Illustration 10	Section map of north wall of Yuanjue protected area .....	126
Illustration 11	Decay survey map of Yuanjue carving .....	127
Illustration 12	Section map of southern wall of Yuanjue protected area .....	128
Illustration 13	Decay survey map of south wall of Yuanjue protected area .....	129



## 第一章 前言

安岳石刻，盛于唐、五代、北宋、明和清。现存的最早造像题记为唐开元 11 年（723 年），最多的造像为唐代、五代和北宋（723~1110 年）。安岳县境内有摩崖石刻造像 140 余处，其中具有一定规模和文物价值且保存较好的有 69 处，造像 10 万躯左右，另有盛唐石刻佛经 40 万字。安岳石刻继承了我国北方石窟艺术，并独立创造出具有我国民族特色的生动的艺术形象，被誉为“我国古代雕刻的伟大宝库”。

安岳石刻以佛教造像为主，也有少数道教造像和儒、释、道三教合龛造像，多数是摩崖造像，也有单个圆雕造像。各文物点碑刻题记甚多。这些都为研究古代社会、文化、地方史和宗教的发展变化提供了可靠的物证。

安岳石刻大量雕造于我国石窟艺术由北向南发展的高峰时期。造像大胆突破宗教仪轨，创造出多姿多彩的艺术形象。安岳石刻通过宗教的事迹具体刻画出人民群众的爱憎和生活情

## 1 Introduction

Anyue Rock Carvings refers to all the rock carvings in Anyue County, which was quite prosperous during Tang Dynasty, the Five Dynasties, Northern Song, Ming and Qing Dynasty (from 723 AD to 1900 AD). The existing statue inscription can be traced back to 11<sup>th</sup> Year of Kai Yuan Era of Tang Dynasty (723 AD), and most of the statues were built during Tang Dynasty, the Five Dynasties and Song Dynasty (from 723 AD to 1110 AD). There are more than 140 sites in Anyue, 69 (more than 100,000 figures) of which are of certain scale, historical value and well-preserved, and over 40,000 rock Buddhist scriptures of Tang Dynasty can be also found. Anyue Rock Carving created the vivid image of Chinese minority nationality characteristic on the base of Grotto Art of Northern China. Thus, Anyue County is reputed as “The Great Treasure House for Ancient Carvings of China”.

Most of Anyue Rock Carvings are cliff sculptures except for some single full relief figures, and most of them are about Buddhism solely, while the others are about Taoism or related to Confucianism, Buddhism and Taoism together. Almost all of the locations have some inscribed steles, which provide reliable material evidence for the research on the change and development of ancient society, culture, history and religion.

Most of Anyue Rock Carvings are sculpted during the period when Grotto art spread from North to South China, and some of them go beyond the religion restriction, thus lead to the colorful and diverse artistic figures. Through the religion stories, Anyue Stone Carvings depicted the general life, love and hate of ordinary people, which illustrated the beauty of human nature and body.

趣，展现了人体美和人性美。

安岳石刻的古、多、精、美，在全国石窟艺术中是罕见的。特别是大量保存完好的唐、五代、北宋的石刻，具有很高的历史价值和艺术价值。

Because of its long-history, richness, diversity and exquisiteness, Anyue Rock Carvings has a unique position among the Grottoes in China. Especially the well-preserved stone carvings of Tang Dynasty, the Five Dynasties and Northern Song Dynasty are of high historical and artistic value.



图 1-1 安岳圆觉洞石刻地理位置  
Fig. 1-1 Geographical Position of Yuanjuedong Cave

圆觉洞石刻区位于安岳县城南 1km 的云居山上（图 1）。石刻均分布于云居山顶南北两侧的砂岩陡崖之上，长 186m，现存摩崖造像 103 壑窟，造像 1933 躯，碑刻题记 25 处，唐代浮雕

Yuanjuedong, one of the major sculptural centers in Anyue County, meaning Complete Enlightenment Cave, is one of the locations of Anyue Rock Carvings where rock carvings exist intensively, which is located on the Mt. Yunjushan, 1 kilometer north to Anyue county town (Fig.1). The statues are about evenly distributed on the southern and northern side of peak which is 186 meters long with 103

1座。1961年圆觉洞被公布为四川省文物保护单位，2005年5月被国务院公布为全国重点文物保护单位。

近千年,在长期自然营力作用的影响下,四川安岳石刻岩体产生了严重的环境地质病害。构造裂隙、卸荷裂隙及层面裂隙交错切割,将石窟区的岩体切割成巨块状,形成危岩体,威胁游客和文物的安全,需要及时采取科学保护措施进行治理。因此,查明圆觉洞石刻环境地质病害的现状和成因,是四川安岳圆觉洞石刻区文物保护的首要任务。

groups, 1933 statues, 25 inscribed steles and 1 relief sculpture of Tang Dynasty. Yuanjuedong was listed to Provincial Historical and Cultural Protection Sites of Sichuan in 1961, and National Historical and Cultural Protection Sites by State Council in May, 2005.

Exposed to nature for more than one thousand years, serious environmental geological damage occurred on the rock carvings. The decay of some exposed cliff grottoes is getting worse and worse. The tectonic fissure, relief joint and horizontal fissure are crossed with each other, and the rock body of the Yuanjuedong is cut into huge pieces, which threaten the safety of the tourists and cultural relics themselves. Therefore, it is very urgent to take scientific measures to prevent further deterioration, and a thorough investigation into the decay reasons related to geology, climate and environment, etc. is the top priority for the Yuanjuedong cultural relics protection.

## 第二章 圆觉洞石刻区环境地质条件

### 2.1 地形地貌

圆觉洞石刻区位于安岳县城南1km的云居山上，石刻区的地形为“坪状”丘陵，区内制高点海拔高度为404.9m。台坪状残丘呈串珠状分布于石刻区周围，形成圆觉洞石刻区的地表分水岭。由遂宁组泥岩构成丘体，水平状砂岩构成丘顶。东北及西南大沟为深切沟谷（图 2-1），相对高差84.2m，沟头由巨厚层状砂岩形成5~15m高的陡崖。丘陵斜坡由砂、泥岩叠置而成，向四周逐渐变缓，岩层产状近水平。砂岩在地形上形成陡崖或陡坡，泥岩组成缓坡。山顶处以砂岩为主，地形坡度陡，约60°~80°。山体下部以泥岩为主，坡度变缓，山脚处坡度为20°~30°（图 2-2）。圆觉洞石刻造像分布在山顶的弧形砂岩崖壁上，崖壁长约210m。

### 2.2 地层岩性

圆觉洞石刻区出露的地层为侏罗系上统遂宁组( $J_{3sn}$ )的紫红色泥岩与紫灰、灰白色砂岩不等厚互层，以及第四系松散堆积物(Q)。

## 2 Environmental Geological Condition in Yuanjuedong

### 2.1 Topography and Geomorphology

Yuanjuedong is located on the Mt. Yunjushan, which lies 1km north to Anyue County town. Flat-top hills, which are scattered like a string of beads around with highest elevation of 404.9m. delineate the watershed of Yuanjuedong. The flat-top hills is composed of Suining formation mudstone (Jurassic Period) whose top constitutes horizontal sandstone. As shown in fig. 2-1, the incised gully in northeast and southwest is deep cut, and the relative height difference is 84.2 m, while 5 to 15 meter high steep cliff composed of thick laminar sandstone situated in the entrance of the gully. The slope of the hills is mainly piled up by sand and mudstone, which extend gently to the bottom, and the rock stratum is about flat. The top of the mountain is mainly composed of sandstone with a dip angle of 60°-80°. The bottom of the mountain is mainly composed of mudstone with a dip angle of 20°-30°, which can be seen from figure 2-2. As shown in Appendix figure 1 to 3, Yuanjuedong rock carvings are distributed on the 210-meter-long arched sandstone rock wall on the mountain peak.

### 2.2 Characteristic of the stratum and rock

The outcrop is the interbedded layers of mauve mudstone, grey-violet sandstone and off-white sandstone in different thickness of the Suining Formation of Upper Jurassic ( $J_{3sn-1}$ ), and loose deposit of Quaternary System(Q) can also be found.

根据遂宁组泥岩～砂岩～泥岩～砂岩的沉积旋回，在研究区范围内，自下而上可以分为四段(附图二～附图三)。



According to the mudstone ~ sandstone ~ mudstone ~ sandstone sedimentary cycle, the stratum of the research area can be classified into 4 layers from top to bottom, which can be observed from appendix 2 to 3.



图 2-1 保护区沟谷发育

Fig.2-1 Incised Gully of Yuanjuedong



图 2-2 圆觉洞石刻区地形

Fig2-2 Topography of Yuanjuedong



图 2-3 遂宁组第一段泥岩

Fig.2-3 Mudstone of Jurassic Period ( $J_{3sn-1}$ )

**第一段( $J_{3sn-1}$ )：**该段岩性为紫红色泥岩(图2-3)，厚层状，夹褐黄色～褐色薄层状粉砂岩，在泥岩中发育青灰色弱胶结粉砂岩。主要分布于研究区地势低洼的山沟范围内，表面大部分为第四系覆盖。

**第二段( $J_{3sn-2}$ )：**青灰色钙质胶结粉细砂岩，风化后岩石表面为褐红色(图2-4)。该岩层主要出露在石刻区的东南部。岩性为巨厚层～块状，完整性好，并形成坡度为60度左右的陡崖。该岩层在石刻区的西北角渐变为砂岩夹泥岩(图2-5)，或砂泥岩互层，泥岩以褐红色为主，其中发育灰白色粉砂质条带。

该岩层在石刻区内主要形成天然陡坎。

**第1段与第2段之间分界明显，并在接触面形成下降泉。**

**第三段( $J_{3sn-3}$ )：**该段岩性为紫红色～褐红色泥岩夹褐黄色粉砂质泥岩，厚层状，中见灰白色粉砂质条带，开挖后容易形成干缩裂缝，导致岩体表面破碎。该岩层在地形上形成小型陡坎(图2-6)。该层主要被第四系残积土、耕植土所覆盖，天然露头主要为粉砂质泥岩。

**First Stratum ( $J_{3sn-1}$ )：** Mauve thick-bedded mudstone (Fig.2-3), interbedded thin layers of siltstone with brown yellow to maroon color, and caesious weakly-cemented siltstone is developed in the mudstone. Which is mainly distributed in the low-lying gully of the research area, and the surface is covered by the deposit of Quaternary System.

**Second Stratum ( $J_{3sn-2}$ )：** Calcareous cemented siltstone, whose surface is of maroon color after weathering (Fig.2-4). This rock stratum is emerged in the southeast of the Yuanjuedong. between huge thick layer to massive stone with comparatively integration and a steep dip angle of 60°. This rock stratum change into sandstone interbedded with mudstone when it extends to the northwest part of Yuanjuedong (Fig. 2-5), and the mudstone color is mainly maroon, while off-white siltstone stripes are developed.

The natural steep slope of the Yuanjuedong rock carving area. Consists of mainly this stratum.

The delimitation boundary of the first and the second stratum is quite obvious, and the descending springs are generated in the contact surface.

**Third Stratum ( $J_{3sn-3}$ )：** This stratum is mauve to maroon mudstone interbedded by brown yellow silty mudstone in the shape of thick layer, while off-white siltstone stripes can be found inside. Desiccation fissures are easily formed after dug open to the air, which lead to the skin breakage of the rocks. This rock stratum, which is mainly covered by the residual soil of Quaternary System or cultivating soil, appeared as small steep ridge (Figure 2-4). The natural outcrop of this stratum is mainly composed of silty mudstone.



图 2-4 遂宁组第二段砂岩



图 2-5 砂岩夹泥岩

**Fig.2-4 Sandstone of Jurassic Period ( $J_{3sn-2}$ )****Fig.2-5 Sandstone interbedded mudstone**

图 2-6 泥岩夹粉砂质泥岩（天然陡坎）

**Fig.2-6 Mudstone interbedded silty mudstone (natural steep ridge)**

图 2-7 第三段泥岩与第四段砂岩接触界线

**Fig. 2-7 Delimitation boundary between sandstone of Third Stratum and mudstone of the Fourth Stratum**

第四段( $J_{3sn-4}$ )：主要为厚层~巨厚层、灰黄色~褐红色粉细砂岩，钙质胶结为主，沿层理发育较多定向排列的云母片。该岩层上下部位水平层理发育，而中部发育交错层理。该砂岩层与下覆泥岩分界明显(图2-7)。沿接触面见地下水渗出。该段岩体主要分布于山顶部，形成陡崖。圆觉洞

Fourth Stratum (( $J_{3sn-4}$ )): Calcite cementation siltstone with sallow to maroon color in general to extraordinary thick layer, and quiet some directional arrayed sheet mica is developed according to the stratification of this section. The horizontal bedding developed well in the upper and lower part of this stratum, while the middle part is cross-bedding. This sandstone layer has clear delimitation boundary with the lower mudstone layer (Fig. 2-7), and ground water seepage can be observed along the contact surface. This

石刻区的龛窟造像主要分布在该段砂岩陡崖上(图 2-8),是本次工作的重点研究区域。



**图 2-8 第四段厚层~巨厚层砂岩  
Fig. 2-8 Thick sandstone of Jurassic  
Period ( $J_{3\text{sn-4}}$ )**

研究区砂岩完整性较好,容易形成陡崖,是石窟开凿的良好场所。泥岩粘土矿物含量较高,在干湿交替循环作用下易崩解,抗风化能力差。

stratum rock is mainly distributed in the top of the mountain, which forms the steep cliff. Most of the statues and grottoes of Yuanjuedong are located in sandstone cliff of this stratum (Fig. 2-8), which is the key research region of this project.



**图 2-9 泥岩风化形成残积土  
Fig. 2-9 Residual soil formed by mudstone  
weathering**

The sandstone in the research region is relatively integrated, which easily generate steep cliff, thus provide good foundation for grotto excavation. Mudstone clay is rich in mineral substances, which subject to disintegration under the alternation of the dry and humid circumstances, so its resistance capacity to weathering is low.

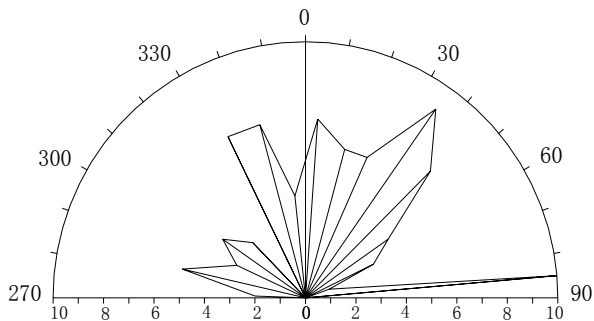


**图 2-10 裂隙走向玫瑰图  
Fig. 2-10 Rose map for the fissure strike**

在自然营力的长期作用下,研究区的地貌剥蚀变换模式为泥岩剥蚀

Under the long term natural agency, the geomorphy disintegration mode is mudstone disintegration ~ sandstone crack devolution

——砂岩体开裂崩塌——泥岩进一步剥蚀——再诱发砂岩体的开裂垮塌。

## 2.3 地质构造

圆觉洞石刻区位于川中平缓褶皱带中部,龙女寺半环状构造与威远辐射状构造之间。其总体特征为构造简单,地层单一,岩性简单。石刻区地层缓倾,为近水平状岩层,倾向 $3\sim10^\circ$ ,倾角为 $1\sim10^\circ$ 。砂岩内具交错层理和斜层理,岩层产状变化较大。区内岩体完整性好,未发现断裂构造,主要以构造裂隙和卸荷裂隙为主(表 2-1),广泛分布于西山的石刻分布区,东山相对较少。

图 2-10 为裂隙走向玫瑰花图。

### 2.3.1 构造裂隙

根据裂隙统计调查结果可知,区内主要发育两组构造裂隙,其中一组近似垂直于崖壁,另一组近似平行于崖面(附图四);在崖壁及窟边周围发育有一组卸荷裂隙;岩体中的构造裂隙近直立,由于植物根系的劈裂及雨水的冲蚀,常使构造裂隙在崖壁处形成宽大裂隙。在近地表处裂隙最大张开度达 1m,向岩体深处渐变闭合。

圆觉洞石刻区发育的裂隙,其特点与岩性组合有关。在相互叠置的砂

~ further disintegration of the mudstone ~ re-induced sandstone crack and break down.

## 2.3 Geological Structure

Yuanjuedong lies in the middle of broad fold belt of central Sichuan Province, between the Longnusi Halfring structure and Weiyuan Radiating structure. The general characteristic of Yuanjuedong is simple structure, unitary stratum and simple lithology, and the stratum is of gentle slope like horizontal layer with a dip direction of  $3^\circ$  to  $10^\circ$  and a dip angle of  $1^\circ$  to  $10^\circ$ . There are crossbedding and oblique-bedding in the sandstone, and the attitude of rock mass changes greatly. The rock integration is rather well without rift structure, but relief joints and tectonic fissures are widely scattered in the stone carving area of west part of the mountain, and the number of fissures in east mountain is relatively low.

### 2.3.1 Tectonic fissure

According to the fissure investigation and statistic results, two sets of tectonic fissures are developed in the Yuanjuedong region, one of which is almost perpendicular to the cliff wall, while the other is parallel to the cliff surface (Appendix Figure 4); a set of relief joint is developed near the cliff wall and grotto edge; the tectonic fissure in the rock body is about vertical, which always forms wide crack in the cliff wall because of the rainwater erosion and flerry by the plant root. The maximum crack width near the surface is about 1m, which gets narrower and narrower when goes into the rock body. The fissure characteristic of Yuanjuedong has close correlation with the lithology. In the overriding of sandstone and mudstone,

泥岩中，砂岩为脆性岩，泥岩为塑性岩，砂岩中发育的构造裂隙一般都没有贯穿泥岩，而是突然尖灭，延伸比较短，表现为层间裂隙的形态。与崖壁延展方向垂直或斜交的构造裂隙一般对岩体的稳定性影响不大，主要形成渗水的贮存、运移通道，诱发渗水病害。

### 2.3.2 层面裂隙

圆觉洞石刻砂岩中沉积层理发育，层面裂隙中夹有云母类粘土矿物。经风化剥蚀和水的侵蚀，层面裂隙不断扩大，成为岩体中的软弱结构面。层面裂隙与构造裂隙、卸荷裂隙相互交切连通，易诱发岩体垮塌破坏，常常为渗水病害提供渗流通道。

### 2.3.3 卸荷裂隙

由于山体向崖壁临空方向产生位移变形，拉裂岩体，形成与崖壁平行的卸荷裂隙。卸荷裂隙具有延伸长，张开度大的特点。平行崖壁的卸荷裂隙往往构成分离岩块的后缘切割面，导致岩体失稳病害。开凿龛窟，在龛窟顶板、侧壁和后壁，由于岩体应力释放，卸荷拉裂，也会造成龛窟

the sandstone is brittle while the mudstone is plastic. Therefore, the tectonic fissure developed in the sandstone can not penetrate the mudstone, and it always suddenly pinch out with short extension, which appears as inter-layer fissures. Generally speaking, the tectonic fissures perpendicular to or oblique crossing the cliff stretch have minor influence on the stability of the rock body, however, those fissures will form storage and travel passage for the seepage water, which may lead to seepage diseases.

### 2.3.2 Bedding fissure

The bedding structure of sandstone in Yuanjuedong is developed well, and the clay minerals as mica are interbeded in the stratification plane fissure. The stratification plane fissure will be expanded through weathering disintegration and water erosion, which result in the weak structure surface of the rock body. The connection, interaction and intersection of the bedding fissure, tectonic fissure and relief joint will induce the breakdown of the rock mass and thus supply flow channel for the seepage.

### 2.3.3 Relief joint

Because of the displacement and deformation of the mountain to the free face, and relief joint parallel to the cliff wall will be generated. Relief joint usually has long extension and wide opening, and the relief joint parallel to the cliff wall always form the rear cutting surface of separated rock body, which result in the destabilization of the rock. During the grotto excavation, the stress of the apical plate, side wall and back wall will be relieved, and the relief joint will lead to the crack and deformation of the grotto roof, wall and

顶板、壁面、棱边的开裂变形，甚至垮塌。如果卸荷裂隙发育在造像上，会造成造像掉块破坏。

### 2.3.4 风化裂隙

除构造裂隙和卸荷裂隙外，岩体表层还发育有风化裂隙。石刻区风化裂隙有两种类型。（1）在层面裂隙、构造裂隙、卸荷裂隙上进一步扩展，具有继承性；（2）在表生作用下，在岩体表层形成不规则网状微裂隙网络。第一类风化裂隙，使各类裂隙进一步恶化。第二类风化裂隙，如果发育在石刻造像表面，危害性极大。

卸荷裂隙、构造裂隙和层面裂隙互相交切，将区内岩体切割成巨块状。这些巨块石在重力作用下，易产生向临空方向的崩塌。在圆觉洞石刻区内，崩塌是主要的不良地质现象。

构造裂隙、层面裂隙和风化卸荷裂隙相互交切，构成了区内的渗水裂隙网络系统，成为地下水的主要渗流通道和储存空间。

edge, which might be result in the breakdown of the grotto. If the relief joint developed on the statue, it might be result in the break and rock-falling destroy of the statue.

### 2.3.4 Weathering fissure

Except for tectonic fissure and relief joint, the weathering fissure can also be found on the rock surface. There are two types of weathering fissure in the Yuanjuedong: Type 1 is the further extension of the tectonic fissure, relief joint and stratification plane fissure, which has adoptive characteristic; Type 2 is the irregular reticulate micro-fissure network on the rock surface under the influence of epidemiogenesis. Type 1 fissure will make the other kinds of fissures even worse, and Type 2 fissure have tremendous damage if it is developed on the stone carving surface.

The interaction and intersection of the relief joint, tectonic fissure and stratification plane fissure will cut the rock body into huge pieces. Under the influence of gravity, these huge rock pieces will easily break down towards the free face, which is the cardinal geological disease in the Yuanjuedong.

Through the interaction and intersection of the tectonic fissure, stratification plane fissure and weathering fissure, the fissure network system for seepage will be formed, which will serve as the travel passage and storage space for the ground water.

表 2-1 圆觉洞石刻区主要裂隙统计表  
Tab.2-1 Fissure Statistic of Yuanjuedong



图 2-11 裂隙  $J_1$ 、 $J_2$ 、 $J_3$   
Fig.2-11 Joint  $J_1$ ,  $J_2$ ,  $J_3$



图 2-12 园觉洞旁裂隙  $J_4$   
Fig.2-12 Joint  $J_4$  beside Nich 9



图 2-13 园觉洞顶部裂隙  $J_5$   
Fig.2-13 Joints of  $J_5$  at the top of Yuanjuedong Cave



图 2-14 5 号龛旁裂隙  $J_6$   
Fig.2-14 Joints of  $J_6$  near the niche of No.6



图 2-15 裂隙  $J_7$   
Fig.2-15 Joint  $J_7$



图 2-16 裂隙  $J_{10}$   
Fig.2-16 Joint  $J_{10}$



图 2-17 裂隙 J<sub>12</sub> 导致石窟破損  
Fig.2-17 Grotto Damage Resulted from J<sub>12</sub>



图 2-18 裂隙 J<sub>14</sub> 松散层堆积  
Fig.2-18 J<sub>14</sub> in Loose Deposit



图 2-19 卸荷裂隙 J<sub>17</sub> 和 J<sub>18</sub>  
Fig. 2-19 Relief Joint J<sub>17</sub> and J<sub>18</sub>

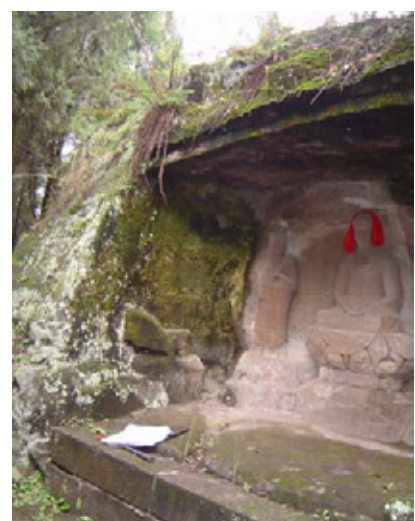


图 2-20 卸荷裂隙 J<sub>18</sub> 在 67 号龛边缘  
2-20 Relief Joint J<sub>18</sub> beside Niche No. 67

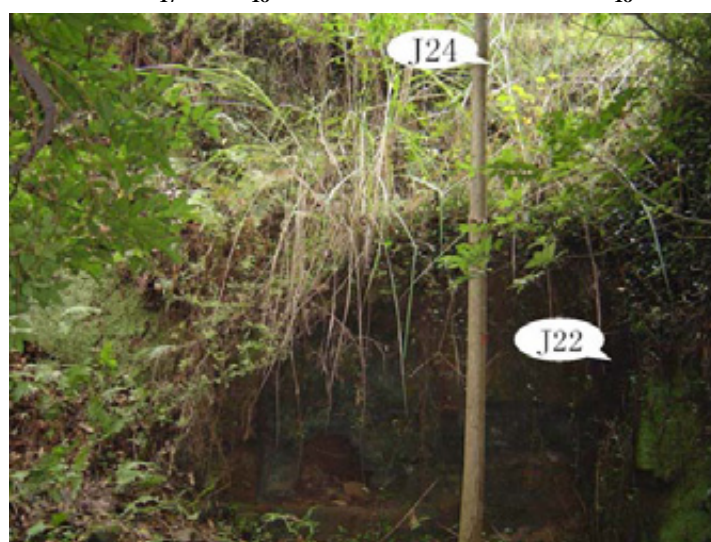


图 2-21 裂隙 J<sub>22</sub> 于 J<sub>24</sub> 切割形成危岩体  
Fig. 2-21 Unstable Rock Cut by J<sub>22</sub> and J<sub>24</sub> Joint



图 2-22 14 号龛后发育的卸荷裂隙  $J_{31}$

Fig. 2-22 Relief Joint  $J_{31}$  in the Back of Niche No.14

另外，需要注意的是，在东山新开凿的卧佛和紫竹观音处发育多条裂隙，对新开凿的石刻造像造成不利影响。应提前对其防治。

In addition, quite some fissures are developed in the new excavated Sleeping Buddha and Zizhu Kwan-yin in East Mountain, which has adverse influence on the new rock carvings. Prevention and control of the influence of such fissures should be carried out earlier.

## 2.4 水文地质条件

如前所述，石刻区主要的地层为泥岩、砂岩互层的组合关系。泥岩完整性好，透水性差，属于相对隔水层，而区内砂岩主要为粉细砂岩，为弱透水层。地下水主要储存在砂岩裂隙之中，并沿砂岩裂隙和砂泥岩之间的交界面产生渗流。研究区的地层整体为水平展布，岩体结构控制着石刻区的水文地质条件。

## 2.4 Hydro-geological Condition

As mentioned above, the stratum in Yuanjuedong is mainly mudstone interbedded with sandstone. The integrity of mudstone is rather good with low water penetration, which can be classified as relative water-resisting layer. The sandstone is mainly composed of siltstone, which can be classified as weak permeable layer. The groundwater is mostly stored in the fissures of sandstone, and seepage will occur in sandstone fissure and the interface of sandstone and mudstone. The researched strata are horizontally distributed as a whole, and the hydro-geological condition in yuanjuedong is controlled by the rock structure.

圆觉洞石刻区为一相对独立的水文地质单元。所在的山顶为区内地表分水岭的脊。研究区主要接受大气降水补给，汇水面积小。石刻区的补给径流排泄条件为，大气降水除了以面流的形式顺地表排出外，部分大气降水经残坡积层垂直入渗，以山脊为地下水的分水岭，向四周产生径流，以缓坡地带及沟谷作为排泄区，以井泉的方式排泄。石刻岩体孤立突出于周围地表，高于当地的地下水位，因此地下水对石刻岩体基本不存在直接影响。从本次调查来看，对石窟具有明显影响的主要表面流、局部裂隙渗水等影响，而大部分龛窟内部，总体比较干燥。

在圆觉洞石刻保护区外云居山东北侧半山坡及北侧，省道公路以东民房旁各有一水井。井口标高分别为366.2m、355.1m，水位埋深分别约为3.0m、2.0m，常年有水，主要为第四系孔隙水和泥岩裂隙水。在火葬场东南侧小路旁的砂岩和泥岩分界处附近出露一泉水（如图2-20），泉眼高程为334m，泉眼旁的泥岩为褐红色。上

Yuanjuedong is a relatively independent hydro-geological unit, and the mountaintop is the division ridge of the surface watershed in this area. The water supply in the research area, whose catchment is rather small, is mainly from atmospheric precipitation. The runoff discharge condition in Yuanjuedong is as follows: most of the precipitation will discharge as surface runoff, part of the precipitation will vertically infiltrated through the residual slide rock and flow away from the mountain ridge, which is the groundwater dividing ridge; the gentle slope and clough are served as outflow area, and the discharge will be in form of wells or springs. The stone carvings lie in the isolated rocks which are stuck out the ambient ground surface. So, the rock elevation is higher than the local ground water level, and there is no direct influence of ground water on the carvings. It can be concluded from this investigation that the apparent influence on the grottoes and niches is from surface runoff, regional fissure seepage, while inside of the grotto and niche is relatively dry.

Out of Yuanjuedong, there are two wells on the north side and northeast side of Mt.Yunjushan. The elevation of the wells is 366.2m and 355.1 m with buried depth of 3.0m and 2.0m respectively, and the perennial water flow in the wells is mainly the fissure water of mudstone and the pore water of Quaternary System. Beside the road on southeast of crematory, a spring emerged near the interface of the sandstone and mudstone stratum, which can be seen from Figure 2-20. The spring mouth elevation is 334m, with maroon mudstone around.

部砂岩裂隙中储存的地下水被下部相对隔水的泥岩阻隔，导致沿砂岩和泥岩交界面溢出成泉。

Because of the obstruction of the waterproof mudstone, the ground water stored in the sandstone fissures always overflowed as spring in the interface of sandstone and mudstone.



图 2-23 保护区西南角小路旁泉眼

**Fig. 2-23 Spring beside the Road of Southwest Yuanjuedong**

分别采取井水、雨水及消防池中水样进行了水化学分析，其分析成果列于表 2-2。由井水的测试结果可知，按库尔洛夫分类标准，石刻区地下水属  $\text{HCO}_3-\text{Ca}$  型水（重碳酸钙型水）。井水的 PH 值为 6.83，略偏酸性。而消防池的水质成分与井水类似，地下水化学类型相同。消防池水主要为从保护区井内不定期抽水和雨水的混合体，取样期间地表蒸发较弱，消防池的水基本保持原有井水的化学特征。

雨水化学成分表明，雨水为  $\text{HCO}_3-\text{Ca}-\text{Na}$  型水（重碳酸钙钠型水）。

对比分析可知，石刻保护区地下

Chemical analysis about the water samples from the well, precipitation and fire fighting pool were carried out, and the results were presented in Table 2-2. It can be concluded from the analyzing results that the underground water of Yuanjuedong is  $\text{HCO}_3\text{-Ca}$  type (calcium bicarbonate water). The well water is metaacid with pH of 6.83. The water quality of fire fighting pool is similar to that of well, which belongs to  $\text{HCO}_3\text{-Ca}$  type. The water in the fire fighting pool is the mixture of rainfall and groundwater from well, which is of the original chemical characteristic of well water because of the low evaporation during the sampling period.

Chemical analysis indicated that the rainfall water belongs to  $\text{HCO}_3\text{-Ca-Na}$  type (calcium-sodium bicarbonate water). It can be deducted from the comparative analysis that the groundwater cycle condition in Yuanjuedong is rather good,

水的循环条件较好,为大气降水补给。and the groundwater will be recharged by atmospheric precipitation.

表 2-2 地下水水质分析成果表

Tab.2-2 Quality Analysis of Groundwater

分析编号 1 送样编号 采样地点 四川安岳园觉洞(消防池)  
Analysis No. 1 Sample No. Sampling place: Fire fighting pool of Yuanjuedong

离子	mg/L	Meq/L	meq%	采样日期	2007.10.9	采样深度	地面下 米、水面下 米
Ion	mg/L	Meq/L	meq%	Sampling Date	2007.10.9	Depth of Sampling	Underground m; Under water level m
阳离子 cation	Ca <sup>+2</sup>	56.11	2.80	54.79	水温 water temperature		气温 air temperature °C
	Mg <sup>+2</sup>	14.58	1.20	23.48	嗅 olfaction		浊度
	Fe <sup>+3</sup>				PH 值 PH value	6.70	沉淀 sedimentation 采样方法 sampling method
	Fe <sup>+2</sup>				项目 item	毫克/升 mg/l	项目 item 德度
	NH <sub>4</sub> <sup>+1</sup>				矿化度 mineralization	381.12	As 全硬度 overall hardness 11.22
	Na <sup>+1</sup> K <sup>+1</sup>	27.75	1.11	21.72	游 CO <sub>2</sub> free carbon dioxide	5.28	Hg <sup>+2</sup> 永久硬度 permanent hardness 1.67
					侵 CO <sub>2</sub>	0.00	CN 暂时硬度 temporary hardness 9.53
					耗氧量 oxygen consumption		Cr <sup>+6</sup> 负硬度 negative hardness -
	合计 total	98.44	5.10	100.0	可溶 SiO <sub>2</sub> soluble SiO <sub>2</sub>		Cr <sup>+3</sup> 总碱度 total alkalinity 9.53
阴离子 anion	Cl <sup>-1</sup>	19.50	0.55	10.76	H <sub>2</sub> S		Pb <sup>+2</sup>
	SO <sub>4</sub> <sup>-2</sup>	55.71	1.16	22.70	酚 phenol		Zn <sup>+2</sup>
	HCO <sub>3</sub> <sup>-1</sup>	207.47	3.40	66.54	库尔洛夫表示式	$M_{0.381} \frac{HCO_3^{-1}}{C_{a54.79}} \frac{^{366.54}}{^{66.54}} {}^{\circ}\text{C}$	
	CO <sub>3</sub> <sup>-2</sup>						
	OH <sup>-1</sup>				细菌分析 analysis of bacteria	细菌总数 number	大肠杆菌 Escherichia coli
	NO <sub>3</sub> <sup>-1</sup>					个/ml	指数 个/升 菌值 ml
	NO <sub>2</sub> <sup>-1</sup>				备注 remarks		
合计 total	282.68	5.11	100.0				

分析编号 2 送样编号 \_\_\_\_\_ 采样地点 四川安岳园觉洞（雨水）

Analysis No. 2 Sample No. Sampling place: Fire fighting pool of Yuanjuedong

离子 ion		mg/L	Meq/L	meq%	采样日期 sampling date	2007.10. 9	采样深度 sampling depth	地面下____米、水面下____米 Underground ____m; Under water level ____m		
阳离子 cation	Ca <sup>+2</sup>	8.02	0.40	56.34	水温 water temperature		气温 air temperature	℃	色 color	
	Mg <sup>+2</sup>	0.97	0.08		嗅 olfaction		味 taste		浊度	
	Fe <sup>+3</sup>				PH值 PH value	6.70	沉淀 sedimentation		采样方法 sampling method	
	Fe <sup>+2</sup>				项目 item	毫克/升	项目 item	毫克/升	项目 item	硬度
	NH <sub>4</sub> <sup>+1</sup>				矿化度 mineralization	54.70	As		全硬度 overall hardness	1.35
	Na <sup>+1</sup> K <sup>+1</sup>	5.75	0.23	32.39	游 CO <sub>2</sub> free CO <sub>2</sub>	5.28	Hg <sup>+2</sup>		永久硬度 permanent hardness	---
					侵 CO <sub>2</sub>	0.00	CN <sup>-</sup>		暂时硬度 temporary hardness	1.40
					耗氧量 oxygen consumption		Cr <sup>+6</sup>		负硬度 negative hardness	0.05
	合计	14.74	0.71	100.0	可溶 SiO <sub>2</sub> soluble SiO <sub>2</sub>		Cr <sup>+3</sup>		总碱度 total alkalinity	1.40
					F <sup>-1</sup>		Cu <sup>+2</sup>			
阴离子 anion	Cl <sup>-1</sup>	1.77	0.05	7.04	H <sub>2</sub> S		Pb <sup>+2</sup>			
	SO <sub>4</sub> <sup>-2</sup>	7.68	0.16	22.54	酚 phenol		Zn <sup>+2</sup>			
	HCO <sub>3</sub> <sup>-1</sup>	30.51	0.50	70.42	库尔洛夫表示式		$M_{0.054} \frac{HCO_3^{-1}}{C_{a56.34}(K + N_a)_{32.39}} {}^{\circ}\text{C}$			
	CO <sub>3</sub> <sup>-2</sup>									
	OH <sup>-1</sup>				细菌分析 analysis of bacteria		细菌总数 number	大肠杆菌 Escherichia coli		
	NO <sub>3</sub> <sup>-1</sup>						个/ml	指数____个/升	菌值____ml	
	NO <sub>2</sub> <sup>-1</sup>				备注 remarks					
	合计	39.86	0.71	100.0						

分析编号 3 送样编号 \_\_\_\_\_ 采样地点 保护区公路旁水井  
 Analysis No. 1 Sample No. Sampling place: Well near the Yuanjuedong cave

离子		mg/L	Meq/L	meq%	采样日期 sampling data	2007. 10. 24	采样深度 sampling depth	地面下米、水面下米 Underground m; Under water level m	
阳离子 cation	Ca <sup>+2</sup>	65.73	3.28	75.58	水温 water temperature		气温 air temperature	℃	色 color
	Mg <sup>+2</sup>	7.78	0.64	14.75	嗅 olfaction		味 taste		浊度
	Fe <sup>+3</sup>				PH值 PH value	6.83	沉淀 sedimentation		采样方法 sampling method
	Fe <sup>+2</sup>				项目 item	毫克/升	项目 item	毫克/升	项目 item
	NH <sub>4</sub> <sup>+1</sup>				矿化度 mineralization	326.65	As		全硬度 overall hardness
	Na <sup>+1</sup> K <sup>+1</sup>	10.50	0.42	9.67	游 CO <sub>2</sub> free CO <sub>2</sub>	5.28	Hg <sup>+2</sup>		永久硬度 permanent hardness
					侵 CO <sub>2</sub>	0.00	CN <sup>-</sup>		暂时硬度 temporary hardness
					耗氧量 oxygen consumption		Cr <sup>+6</sup>		负硬度 negative hardness
	合计	84.01	4.34	100.0	可溶 SiO <sub>2</sub> soluble SiO <sub>2</sub>		Cr <sup>+3</sup>		总碱度 total alkalinity
					F <sup>-1</sup>		Cu <sup>+2</sup>		
阴离子 anion	Cl <sup>-1</sup>	13.47	0.38	8.76	H <sub>2</sub> S		Pb <sup>+2</sup>		
	SO <sub>4</sub> <sup>-2</sup>	46.11	0.96	22.12	酚 phenol		Zn <sup>+2</sup>		
	HCO <sub>3</sub> <sup>-1</sup>	183.06	3.00	69.12	库尔洛夫表示式		$M_{0.326} \frac{HCO_3^3}{C_{a75.58}} {}^\circ C$		
	CO <sub>3</sub> <sup>-2</sup>								
	OH <sup>-1</sup>				细菌分析 analysis of bacteria		细菌总数 number	大肠杆菌 Escherichia coli	
	NO <sub>3</sub> <sup>-1</sup>						个/ml	指数 个/ 升	菌值 ml
	NO <sub>2</sub> <sup>-1</sup>				备注 remarks				
合计		242.64	4.34	100.0					

分析: 曹李靖 复核: 审阅: 日期: 2007 年 10 月 26 日

## 2.5 气候条件

安岳县境气候属中部亚热带季风性湿润气候, 四季分明, 气候温暖, 热

## 2.5 Climatic Condition

The weather of Anyue County is subtropical humid climate of middle monsoon area, with four clear seasons,

量光足，雨量丰沛，无霜期长，云雾较多，日照偏少；具有春早、夏长、秋凉、冬暖，夜雨多、风速小、湿度大，夏季雨量集中、多旱涝，秋季绵雨频率高等特征。

安岳县境内太阳辐射量随地形的变化而变化，丘顶多于丘谷。夏季日照充足，春季多于秋季，冬季最弱。全年中的5至9月太阳总辐射值与日照时数均占全年52%以上。

境内多年日平均气温为17.6℃，年均气温变化不大。最冷月是1月，平均为6.7℃；最高月是7月和8月，平均气温皆为27.6℃；年内2至5月气温回升较快，每月平均上升5℃左右；6月上升较小，为2.6℃左右；7至8月高温较稳定；8月后气温下降明显，平均每月下降5℃左右，由盛暑很快转入凉秋；形成春早、夏长、秋凉、冬暖的气候。极端最高气温为40.2℃（1972年8月13日），极端最低气温为-3.7℃（1975年12月16日），最大温差达43.9℃。1961年～1985年期间，最高地面温度

mild temperature, abundant heat, plentiful rainfall, long frost-free period, much fog and cloud and less sunlight. Anyue County has early spring, long summer, cool fall and warm winter with low wind speed, high humidity and plenty of rainfall during the night. Flood and drought occurs quite often because of the concentrated precipitation in summer time, while continuous rainfall has high frequency in the fall.

The radiation quantity of sunlight is changed with topographical variation in Anyue County, and the sunlight radiation on the mountain top is higher than bottom of hills and gullies. Summer sunlight is abundant while winter sunlight is the weakest, and sunshine of spring is better than that of autumn. The total radiation quantity of sunlight from May to September accounts for 52 % of that of the whole year.

The average daily temperature of long term is 17.6℃ without great changes in the whole year. The coldest month is January with average 6.7℃, while the hottest are July and August with average 27.6 ℃ . The temperature increases rather quickly from February to May, which is about 5℃ per month, and the increase of June is about 2.6. The temperature is quite hot and stable during July and august, and then decreases rapidly to fall. The maximum temperature is 40.2℃ (on 13th, Aug. 1972), while the minimum is -3.7℃ (on 16th, Dec. 1975), and the difference is as high as 43.9℃. The maximum ground surface temperature is 69.8℃ (on 13th, Aug. 1972), while the minimum is minus 5.9℃ (on 16th,

为 $69.8^{\circ}\text{C}$ (1972年8月13日), 最低地  
面温度为 $-5.9^{\circ}\text{C}$ (1975年12月16日),  
极差 $75.7^{\circ}\text{C}$ 。

区内多年平均降水量 $1025.8\text{mm}$ ,  
县域降雨量年际变化大, 最多年与最少  
年相差1倍以上。1958年至1985年间  
降雨量高于或低于多年平均降雨量值  
的各14年, 各占50% (图2-21)。最  
大年降雨量为 $1420.2\text{mm}$ (1962年), 最  
小年降雨量为 $688.3\text{mm}$ (1977年)。

Dec. 1975), and the extreme difference  
is  $75.7^{\circ}\text{C}$ .

The precipitation in Anyue Country  
varies greatly, which is averaged  
 $1025.8\text{ mm per year}$ , and the maximum  
rainfall in wet year may be two times of  
that in dry year. During 1958 to 1985,  
there are 14 years with precipitation  
higher than the average, which accounts  
for 50 percent of that period. The  
maximum annual rainfall is  $1420.2\text{ mm}$   
in 1962, while the minimum is  $688.3\text{ mm}$   
in 1977.

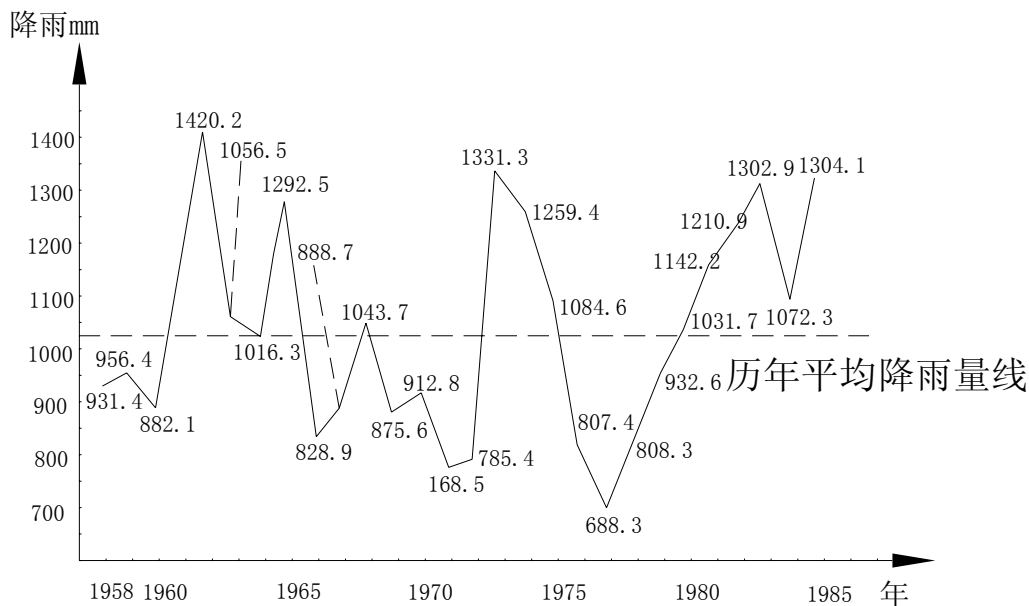


图 2-24 安岳县 1958 至 1985 年降雨量年际变化

Fig. 2-24 Rainfall Variation from 1958 to 1985

雨量季节分配不均, 夏季(6至8  
月)多年平均 $488.4\text{mm}$ , 占年均降雨总  
量48%。冬季(12至2月)仅有 $48.2\text{mm}$ ,  
仅占年均降雨总量5%。夏湿冬干。多  
年雨量按月统计数据显示(图2-22):

The rainfall distributes unevenly in  
different season, and the average  
summer precipitation (from June to  
August) is  $488.4\text{ mm}$ , which accounts  
for 48% of the whole year, while the  
winter precipitation (from December to  
next February) only accounts for 5  
percent, i.e.  $48.2\text{ mm}$ . The monthly

12月和1月雨量最少，以后逐月上升，春雨较早。5月、6月梅雨季节常有绵雨、雷雨，雨量显著增多，仅次于7至9月。7月雷雨，雨量达到最高值，以后逐月下降。8月和9月多雷暴雨，雨量次于7月，高于5月、6月；雨量集中、地域分布不均，常有伏旱发生。10月雨量锐减，雨时增多，秋雨连绵。11月雨量仅占10月的一半。

多年平均降雨天数为147天（日降雨量 $\geq 0.1\text{mm}$ ），在过去28年的日降雨量统计中：日雨量 $\geq 10\text{mm}$ 的小雨天气年均26.4天。日雨量 $\geq 25\text{mm}$ 的大雨天气年均8.7天，多出现在6月中旬后期至10月上旬。日雨量 $\geq 50\text{mm}$ 的暴雨，计有76次，年均3次。日雨量 $\geq 100\text{mm}$ 的特大暴雨计12次，年均1次不足。连续性降雨多发生在初夏到秋季，最长为15天。连续无降雨，以冬、春季为多，最长达31天。

安岳县境多年平均蒸发量为

statistic about the long term rainfall is presented in figure 2-22, from which it can be concluded that the rainfall in spring comes early with low quantity in December and January, continuous rainfall and thunderstorm are always occurred during May and June with high precipitation quantity, the period of July to September is plenty of thunderstorm while the maximum rainfall of the year appears in July. The rainfall is generally concentrated and uneven distributed in this region, and drought often happens during hot summer days. The precipitation quantity decreases rapidly from October with higher raining time, and the quantity of November is only half of that in October.

The average raining time with no less than 0.1 mm daily precipitation is 147 days per year. According to the statistics of daily precipitation during the past 28 years, the average raining time with no less than 10 mm daily precipitation is 26.4 days per year; the average raining time with no less than 25 mm daily precipitation is 8.7 days per year, which generally occurs between middle June to the beginning of October; the average raining time with no less than 50 mm daily precipitation is 3 days per year; and 12 extraordinary storm with no less than 100 mm daily precipitation is observed. Continuous rainfall always takes place during the beginning of summer to autumn, and the longest continuous rainfall lasted for 15 days. Continuous dry weather without rainfall often occurs in winter and spring, and the longest dry weather lasted for 31 days.

The long term average evaporation is

1168.3mm。夏季持续高温，蒸发量大。月蒸发量最大一般出现在8月，最小出现在冬季的12月。

1168.3 mm per year. The continuous high temperature of summer time leads to high evaporation capacity. The maximum evaporation capacity generally observed in August, while the minimum occurs in December.

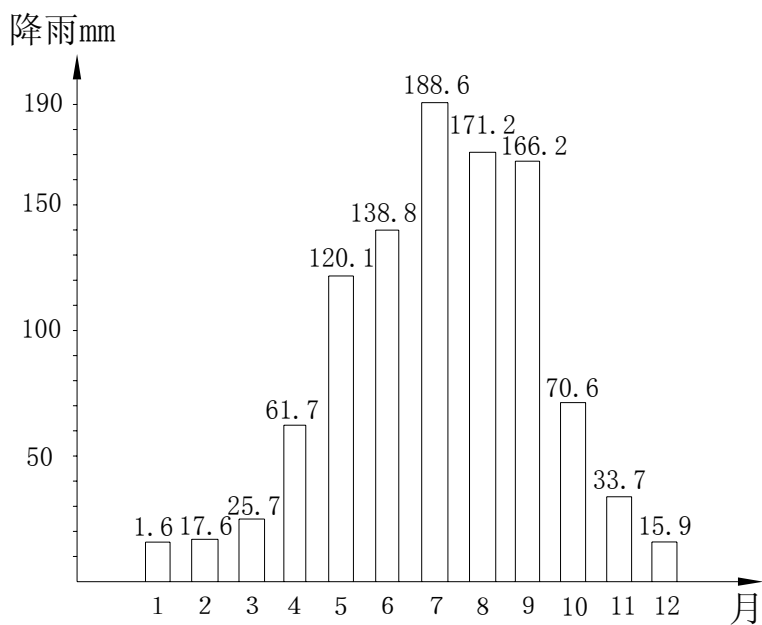


图 2-25 安岳县历年各月雨量比较

Fig. 2-25 Monthly Rainfall in the Past Years

安岳地处中亚热带季风区，9至3月受北方冷空气入侵，为偏北风；4至8月受西南暖湿季风和亚热带高气压影响，为偏南风。县域位于盆地中部，空气流动不畅，多静风，石刻区处于县域东北部，地形低导致东北风较多。多年年均风速为1.4m/s。4月、5月平均风速最大，均为1.7m/s，11月最小，为1.0m/s。一般风力小，一、二级风、静风多；但当寒潮、雷暴雨、冰雹来临，风力骤然增大，常伴大风。

Anyue County lies in middle subtropical monsoon area, whose wind direction from September to next March is about north, which is resulted from the cold air flow from northern area; and because of the influence of subtropical anticyclone and southwest humid and warm monsoon, the wind direction from April to August is approximately south. Anyue County lies in the basin center, which impedes the airflow and leads to calm wind. The Yuanjuedong lies to northeast of Anyue County, and its low elevation leads to comparatively more northeast wind. The long-term average wind velocity is 1.4m/s, with a maximum of 1.7 m/s in April to May, while the lowest average velocity occurs in November, i.e. 1.0

m/s. The wind velocity is always low as light air or light breeze and even static wind, while gale often accompanies with cold wave, thunder storm and hail.

## 2.6 地震

安岳地质构造运动反应微弱，地壳比较稳定，属于地震波及区或弱震区。自 1488 年至今，县域出现过 9 次弱震或地动反应，且震源多在县外。总体来说，地震对石刻区整个区域岩体的稳定性影响较小，仅对由裂隙切割及软弱夹层组合形成的局部危岩体的稳定性影响较大。

据《建筑抗震设计规范》(GB50011—2001)，安岳地区抗震设防烈度为 6 度，设计基本地震加速度为 0.05g。从地形上看，石窟分布范围主要为孤立的山体，地震效应将会在局部放大，属于抗震不利地段。

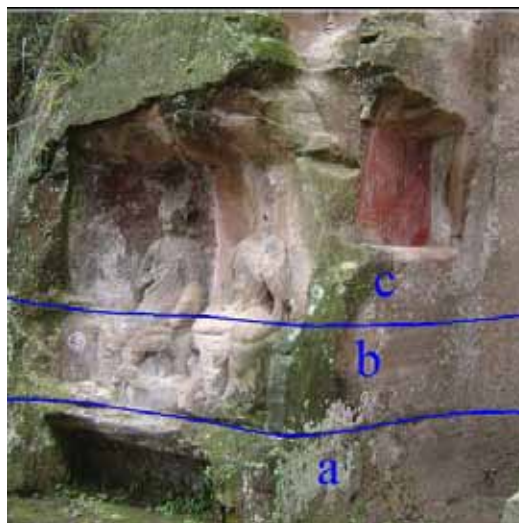
### 2.6 Earthquake

The geological structure of Anyue has weak motion reaction with relatively stable earth crust, which belongs to weak earthquake zone or felt area. There are 9 weak earthquakes or quake reactions from 1488, and the earthquake centers are all out of Anyue County. Generally speaking, earthquake has very low influence on the rock stability in the Yuanjuedong, but it will impact the stability of local rock which is composed of soft embedding stratum and fissures .

According to *Code for seismic design of buildings*. GB 50011 — 2001, seismic fortification intensity is 6 degree, and design basic acceleration of ground motion is 0.05 g. Form the viewpoint of topographic form, the rocks where the grottoes located are mainly isolated hills, and the earthquake influence will be regionally amplified, which makes the earthquake resistance difficult in this area.

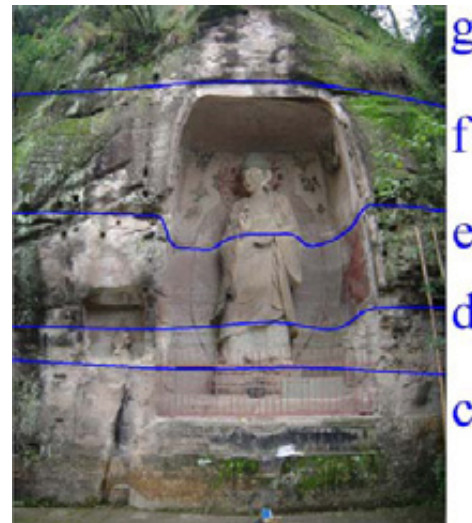
### 第三章 圆觉洞岩体工程性质

根据野外观察岩性色调、宏观结构等变化规律，将圆觉洞石刻岩体自下而上划分为 a、b、c、d、e、f、g 共 7 层（图 3-1）。各岩样取样地点及实验项目见表 3-1。



5 号窟

Group 5



10 号窟

Group 10

图 1-1 石刻岩层分层

**Fig. 3-1 Lithostratigraphic Classification**

a 层：灰黄色厚层状粉砂岩。新鲜岩石为青灰色，风化后颜色发黄。岩石中见黑色矿物，层理不太发育。A 层顶部层面见铁锈，宽约 3mm，沿该层面风化较严重。

b 层：褐黄色、灰黄色粉细砂岩，层理密集发育，间距 2~5cm 不等，底部密度大于上部，顺层理容易形成小型风化掉块。含顺层排列的云母片。在层

### Chapter 3 Rock Engineering Properties in Yuanjuedong

According to color, structure etc., the rock can be divided into 7 layers with a respective name of a, b, c, d, e, f, g. Group 10 covers layers from c to g. Group 5, which is near to Group 10 to be chosen to describe the rock layers integrally, covers from a to c.



10 号窟

Group 10

Layer a is grey-yellow thick-bedded silt sandstone. The fresh rock is steel grey, and the weathered is yellowed. There is black mineral, and the bedding didn't develop. At the top of this layer, there exists rust with a width of 3mm, where serious weathering occurs.

Layer b is from brown yellow to grey yellow silt sandstone. The bedding developed densely with a interval of 2cm~5cm. the density at the bottom is bigger than that at the top. Small scale off-falling blocks forms easily along

面上见黄褐色铁质，风化后形成红色锈斑。

c 层：底部一层厚约 15cm，上部为厚层状，青灰～黄灰色细砂岩，表面风化后呈红色。岩性较均匀，主要病害以风化起壳剥落为主。

d 层：灰白色夹褐红色粉砂岩，风化严重，在 10 号龛的左壁门口主要以风化掉块破坏为主，在窟内主要为起壳、砂化等破坏形式。是 10 号龛的风化最严重的层位，其中左壁相对右壁风化更为严重。

e 层：中厚层粉细砂岩，中间发育两层交错层理，岩石的抗风化能力较强，主要顺斜层理出现差异风化。

f 层：巨厚层褐黄色～褐红色粉细砂岩，水平层理相对发育。抗风化能力强，在 10 号龛内该层风化相对较弱。

在 e 和 f 之间具一层面，沿层面出现破坏，历史上进行过修补，主要措施为水泥等材料进行封堵。

g 层：位于 10 号龛以上，主要为褐黄色、厚层粉砂岩。

bedding. There is some mica lamination which arrange along bedding plane. There exist tawny iron which form red rusty spot after weathered.

Layer c has two sub-layers with a thickness of 15cm at the lower part and thick-bedded sandstone at the upper part. The weathered surface turns from caesious to red. Lithology is well-proportioned, and the encrustation-spalling is the main weathered form.

Layer d is grey intermingled with maroon silt sandstone and badly weathered. The off-falling blocks is the main decay form at the left wall, while encrustation and sand-like forming at the back wall. This layers is the most severely damage location, and left wall is more serious than the right.

Layer e is a fine-silt sandstone, and there exist two layers of crossing bedding. This layer is rather weatherproof, and differential weathering exist along oblique bedding.

Layer f is brown yellow and maroon thick-bedding fine-silt sandstone. The rock is comparatively Weakly weathered.

There is a layer between layer e and f, and where cement was used to repair.

Layer g is brown yellow thick-bedding silt sandstone.

石刻区的地层岩性特点是砂岩与泥岩互层，相互叠加，层位平缓。砂岩为岩屑质细~粉砂岩，易于雕凿。



图 3-2 4 号龛 b 层水平层理发育

Fig. 3-2 Horizontal bedding in Group 4

在岩壁上发育有数条层面裂隙。由于沿层面裂隙发生渗水、风化，导致沿层面裂隙形成风化凹槽，特别是在 10 号龛的 e、f 层之间最为明显（图 3-4）。

Sandstone and mudstone interbedded with a gently dip angle. Sandstone is easy to carve.



图 3-3 10 号龛 e 层中交错层理

Fig.3-3 Cross bedding in Group 10

There are several bedding fissures developed in the rock, where seepage and weathering took place, leading to the weathering flute, especially between layer e and layer f.



图 3-4 岩壁层面形成凹槽

Fig.3-4 Weathering flute in the rock wall

为了对影响 5 号龛和 10 号龛风化破坏的原因进行调查分析，采取了 b~f 层岩样进行了测试，特别对 d 层进行多点采样（图 3-5）。

In order to investigate and analyze the reasons influencing the weathering of sculpture, rock samples from b to f stratum are tested, and quite some samples are taken from d stratum (Figure 3-5).

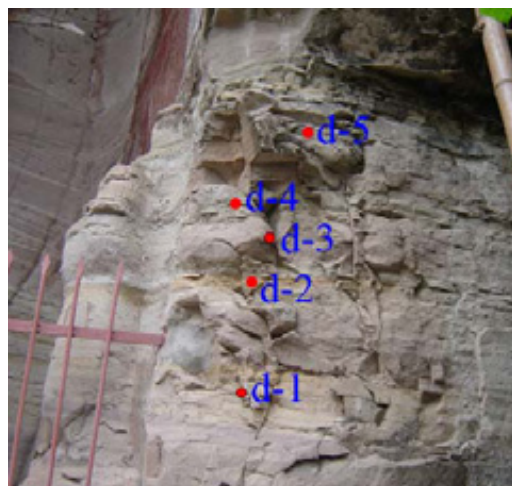


图 3-5 d 层取样点

Fig.3-5 Sampling spots for layer d

表 3-1 取样位置

Tab.3-1 Sampling Positions

序号 No.	编号 Sample No.	位置 Location
1	b	4号龛左壁 left wall of Group 4
2	c	4号龛左壁 left wall of Group 4
3	5-1	5号龛右佛 right Buddha of Group 5
4	d-1	10号龛左壁 left wall of Group 10
5	d-2	10号龛左壁 left wall of Group 10
6	d-3	10号龛左壁 left wall of Group 10
7	d-4-1	10号龛左壁 left wall of Group 10
8	d-4-2	10号龛左壁 left wall of Group 10
9	d-5	10号龛左壁 left wall of Group 10
10	e-1	紫竹观音西 western spot of Yuanjuedong
11	f-1	东山 western spot of Yuanjuedong
12	w	东山卧佛 western spot of Yuanjuedong

### 3.1 岩石薄片鉴定分析

对石刻区北壁 10 号释迦佛龛及东山卧佛处采集的岩样做薄片鉴定结果表明（表 3-2），石刻区砂岩主要为钙质与绢云母胶结岩屑质细~粉砂岩，岩石的矿物成分为：碎屑石英含量 70%~90

### 3.1 Identification Analysis of the rock slice

The identification of the rock slice samples were carried out, and the results are listed in Table 3-2. The sandstone in Yuanjuedong is mainly calcic and sericite cemented pack sand and siltsand of syrosem characteristic. The mineral indigent of the rock is as follows: 70 to 90 percent clastic quartz,

%、粘土岩屑 5%~14%，斜长石碎屑含量 1%~4%、白云母 2%~3%。基质组分为细晶方解石和绢云母。孔隙式胶结，细粒砂状结构和细砂~粉砂结构，基质具粉晶~细晶结构和微细鳞片结构。

5 to 14 percent clastic claystone, 1 to 4 percent clastic plagioclase and 2 to 3% muscovite. The stromata component is cryptomere calcite and sericite.

**表 3-2-1 岩石薄片鉴定成果表**  
**Tab. 3-2-1 Identification of the Thin Section of rocks**

样号 Sample No.	碎屑组份 component	基质组份 Matrix	胶结类型 Bonding	结构构造 texture	鉴定名称 Given name
b	1. 碎屑石英，次棱角状，粒度 0.03~0.1mm, 83% 2. 粉砂质粘土岩屑，次圆状，零散分布，粒度 0.06~0.1, 9% 3. 石英泥质碎屑，零星分布，粒度 0.1~0.2mm, 少数呈片状，3% 4. 鳞片状黑云母及白云母，长轴无定向，零散分布，长径粒度 0.2~0.3mm, 2% 5. 斜长石碎屑，零星分布，粒度 0.08mm, 1%	绢云母	微孔隙式	细砂~粉砂状结构，基质具微细鳞片结构	含岩屑细~粉砂岩
b	1. clastic quartz, subangular, 0.03 to 0.1mm, 83% 2. siltsand-clay debris, sub-circular, 0.06 to 0.1 mm, 9% 3. quartz-mud debris, distributed sporadically , 0.1-0.2mm, 3% 4. biotite and common mica, distributed sporadically, without obvious macro-axis direction. 0.2-0.3mm, 2% 5. anorthose debris, 0.08mm, 1%.	Sericite	Pore mode	Finesand-siltsand structure, with micro-scale structure	Sandstone with debris
c	1. 碎屑石英均匀分布，次棱角状~棱角状，粒度，0.1~0.15mm, 82% 2. 绢云母粘土岩屑，次棱角状，零散分布，粒度 0.1~0.15mm, 5%	绢云母 4%	孔隙式	细粒砂状结构，基质具微细鳞片结构	含岩屑细砂岩

	3.石英质碎屑，形态不规则，少量呈拉长条带状，定向分布，长径粒度 0.1~0.5mm, 5% 4. 细粒鳞片状白云母，长轴无定向，零星分布，长径粒度 0.05~0.2mm, 2% 5. 斜长石碎屑，粒度 0.1mm, 1% 6. 少量泥质岩屑次角状，粒度 0.6 mm, 1%				
c	1. clastic quartz, evenly distribution, angular and subangular, 0.1 to 0.15 mm 82% 2. sericite claystone, distributed sporadically in subangular form, 0.1 to 0.15 mm, 5%. 3. quartz debris, without specific shape, 0.1-0.5mm, 5%. 4. scaly common mica, without obvious macro-axis direction, distributed sporadically, 0.1mm, 1%. 5. anorthose debris, 0.1mm, 1%.	Sericite 4%	Pore mode	Finesand structure, with micro-scale	Sandstone with debris
d-1	1.碎屑石英，棱角状~次棱角状，均匀分布，粒度 0.1~0.15mm, 81% 2. 粘土岩屑，次棱角状，均匀分布，粒度 0.1~0.2mm, 8% 3. 形状不规则的碳化碎屑，零散分布，粒度 0.05~0.25mm, 3% 4. 斜长石碎屑，零散分布，粒度 0.1mm, 2% 5. 鳞片状白云母，零星分布，长径粒度 0.2mm, 2%	绢云母 5%	孔隙式	细粒砂状结构，基质具微细鳞片结构	绢云母胶结含岩屑细砂岩
d-1	1. clastic quartz, distributed evenly in angular and subangular form, 0.1 to 0.15 mm, 81%. 2. clay debris, subangular, distributed evenly, 0.1-0.2mm, 8%. 3. debries carbide, distributed sporadically, 0.05-0.25mm, 3%. 4. anorthose debris, distributed sporadically, 0.1mm, 2%. 5. scaly common mica,	Sericite 5%	Pore mode	Fine granular structure, matrix with fine scaly structure	Fine sandstone with sericite bonding containing febris

	distributed sporadically, 0.2mm, 2%.				
d-2	1. 碎屑石英, 次棱角状, 均匀分布, 粒度 0.05~0.1mm, 80% 2. 粘土岩屑, 次圆状, 零散分布, 粒度 0.1~0.15mm, 12% 3. 微粒状及微片状石英质碎屑, 零散分布, 长轴略定向, 粒度 0.05~0.2mm, 3% 4. 鳞片状白云母, 零星分布, 长轴粒度 0.1mm, 2%	绢云母 3%	孔隙式	细砂~粉砂状结构, 基质具微细鳞片结构	绢云母胶结含岩屑细~粉砂岩
d-2	1. clastic quartz, distributed evenly in subangular form, 0.05 to 0.1 mm, 80%. 2. clay debris, in sub-circular form, 0.1-0.15mm, 12%. 3. quartz debris, distributed sporadically, 0.05-0.2mm, 3%. 4. scaly common mica, distributed sporadically, 0.1mm, 2%.	Sericite 3%	Pore mode	Fine-silt granular structure, matrix with fine scaly structure	Fine sandstone with sericite bonding containing febris

表 3-2-2 岩石薄片鉴定成果表

Tab. 3-2-2 Identification of the Thin Section of rocks

样号	碎屑组份	基质组份	胶结类型	结构构造	鉴定名称
Sample No.	component	Matrix	Bonding	texture	Given name
d-3	1.碎屑石英, 棱角状~次棱角状, 均匀分布, 粒度 0.03~0.1mm, 70% 2.粘土岩屑, 次圆状, 零散分布, 粒度 0.1~0.15mm, 17% 3.泥质和碳质碎屑, 零星分布, 粒度 0.1~0.25mm, 4% 4.微细鳞片状黑云母及白云母, 零散分布, 长径略变向, 长径粒度 0.25~0.4mm, 3% 5.粘土碎屑, 零散分布, 粒度 0.05~0.1mm, 2%	绢云母 4%	孔隙式	细砂 ~ 粗粉砂状结构, 基质具微细鳞片结构	绢云母胶结岩屑质细砂~粗粉砂岩
d-3	1. clastic quartz, distributed evenly in angular and subangular form, 0.03 to 0.1 mm , 70% 2. clay debris, distributed sporadically in sub-circular form, 0.1-0.15 mm, 17%. 3. muddy carbon debris, distributed sporadically, 0.1-0.25 mm, 4%	Sericite 4%	Pore mode	Fine granular structure, with fine crystal matrix	Fine sandstone with sericite-calcite cementation

	4. slightly scaly biotite and common mica, clastic muscovite in laminar form, distributed sporadically, 0.1 mm, 2%. distributed sporadically, 0.25-0.4mm, 3%. 5. clay debris, distributed sporadically , 0.05-0.1mm,2%.				
d-4	1. 碎屑石英, 棱角状~次棱角状, 均匀分布,粒度 0.05~0.15mm, 85% 2. 粉砂质粘土岩屑, 次圆状, 零星分布, 粒度 0.1mm, 5% 3. 石英质碎屑, 零星分布, 粒度 0.1~0.2mm, 3% 4. 镰石岩屑, 次圆状, 零散分布, 粒度 0.1mm, 2%	绢云母 5%	孔隙式	细砂 ~粗粉砂状结构, 基质具微细鳞片结构	含岩屑细砂 ~ 粗粉砂岩
e-1	1. clastic quartz, distributed evenly in angular and subangular form, 0.05 to 0.15 mm , 85% 2. clay debris, distributed sporadically in sub-circular form, 0.1 mm, 5%. 3. clastic firestone in subangular and sub-circular form, 0.08 mm, 2% 4. quartz debris, distributed sporadically ,0.1-0.2mm, 3%. 5. chert debris, distributed sporadically in sub-circular form, 0.1 mm, 2%.	Sericite 3%	Pore mode	Fine granular structure, with fine scaly matrix	Fine –coarse sandstone with rock debris
d-5	1. 碎屑石英, 棱角状~次棱角状, 均匀分布,粒度 0.05~0.1mm, 80% 2. 粘土岩屑, 次圆状, 零散分布, 粒度 0.06 ~ 0.1 mm, 14% 3. 鳞片状白云母, 零星分布, 粒度 0.05~0.08mm, 2% 4. 石英碎屑, 多数呈粒状, 少数呈片状, 零散分布, 粒度 0.1~0.3mm, 2% 5. 斜长石碎屑, 粒度 0.05mm, 1%	绢云母 3%, 方解石 细晶 2%	孔隙式	细砂 ~粉砂状结构, 基质具微细鳞片及细晶结构	绢云母钙质胶结细砂 ~ 粉砂岩
d-5	1. clastic quartz, distributed evenly in angular and subangular form, 0.05-0.1mm 80%. 2. clay debris, in sub-circular form, 0.1 mm, 14%. 3. scaly common mica, distributed sporadically, 0.05-0.08mm, 2%. 4. clastic muscovite in laminar form, distributed sporadically, 0.1 mm granularity, accounts for 2 percent 5. clastic plagioclase, 0.05mm, 1%.	Sericite 3%, Fine crystal calcite 5%	Pore mode	Fine granular structure, with fine crystal matrix	Fine sandstone with calcite cementation
e-1	1.碎屑石英, 棱角状~次棱角状, 均	细晶方	孔	细粒砂	钙质胶结

	匀分布,粒度 0.06~0.1mm, 79% 2. 细粉砂质粘土岩屑, 次棱角状, 粒度 0.1mm, 5% 3. 火成岩屑, 次棱角状~次圆状, 粒度 0.08mm, 3% 4. 碎屑白云母, 片状, 零星分布, 粒度 0.1mm, 2% 5. 斜长石碎屑, 零星分布, 粒度 0.1mm, 1%	解石, 5 %	隙式	状结构, 基质具细晶结构	含岩屑细砂岩
e-1	1. clastic quartz, distributed evenly in angular and subangular form, 0.06 to 0.1 mm , 79% 2. clastic fine silt sandy clay, in sub-circular form, 0.1 mm granularity, 5%. 3. clastic firestone in subangular and sub-circular form, 0.08 mm, 2% 4. clastic muscovite in laminar form, distributed sporadically, 0.1 mm, 2%. 5. clastic plagioclase, distributed sporadically, 0.1 mm, 1%.	Fine crystal calcite 5%	Pore mode	Fine granular structure, with fine crystal matrix	Fine sandstone with calcite cementation

表 3-2-3 岩石薄片鉴定成果表

Tab. 3-2-3 Identification of the Thin Section of rocks

样号	碎屑组份	基质组份	胶结类型	结构构造	鉴定名称
Sample No.	component	Matrix	Bonding	texture	Given name
f-1	1. 碎屑石英, 棱角状~次棱角状, 均匀分布, 粒度 0.1~0.25mm, 75% 2. 绢云母粘土岩屑, 次圆状, 零散分布, 粒度 0.15~0.2mm, 11% 3. 碎屑斜长石, 可见薄片双晶, 零散分布, 粒度 0.15mm, 4% 4. 鳞片状白云母, 零散分布, 长径粒度 0.2mm, 2%	绢云母 3% 细晶斜长石 5%	孔隙式	细粒砂状结构, 基质具微细鳞片及细晶结构	绢云母钙质胶结合岩屑细砂岩
f-1	1. clastic quartz, distributed evenly in angular and subangular form, 0.1 to 0.2 mm, 70% 2. clastic sericite claystone, distributed sporadically in sub-circular form, 0.15 to 0.2 mm, 11%.	Sericite 3 %, Fine crystal plagioclase	Pore mode	Fine sand structure, with micro-scaly and fine crystal	Fine sandstone with sericite calcic cementation

	3. clastic plagioclase, slice double crystal is observed, distributed sporadically, 0.15 mm, 4%. 4. scaly muscovite, distributed sporadically, 0.2 mm ribbon width granularity, 4%			matrix	
g	1.碎屑石英, 棱角状的~次棱角状均匀分布, 粒度 0.1 ~ 0.2mm, 70% 2.粘土岩屑及粉砂质粘土岩屑, 次圆状, 均匀分布, 粒度 0.1 ~ 0.5mm, 15% 3.粒状及片状石英质碎屑, 形状不规则, 粒度 0.1 ~ 0.5mm, 5 % 4.斜长石碎屑, 零星分布, 粒度 0.1mm, 2%	细晶方解石 8%	孔隙式	细粒砂状结构, 基质具细晶结构	钙质胶结岩屑质细砂岩
g	1. clastic quartz, distributed evenly in angular and subangular form, 0.1 to 0.2 mm, 70% 2. clastic claystone and clastic silt claystone, distributed evenly in sub-circular form, 0.1 to 0.5 mm, 15%. 3. granular and laminar clastic quartz in irregular form, 0.1 to 0.5 mm, 15%. 4. clastic plagioclase, distributed sporadically, 0.1 mm, 2%.	Fine calcite 8%	Pore mode	Fine granular structure, with fine crystal structure matrix	Calcareous cemented fine sandstone

3.2 砂岩 X 衍射物像分析	3.2 X-ray Diffraction Analysis of the sandstone
表 3-3 为石刻区 10 号龛处所取岩样的 X 衍射矿物成分分析结果, 图 3-7 为其矿物成份的 X 衍射图谱。由分析成果可知, 砂岩岩样中石英含量最高, 均在 30% 以上, 其次为蒙脱石、斜长石、钾长石、伊利石和方解石。其中蒙脱石、斜长石、钾长石、伊利石为可溶性矿物。粘土矿物蒙脱石、伊利石遇水很不稳定。	The X-ray diffraction analysis results of the mineral contents in the sample taking from Group 10 Niche in Yuanjuedong are listed in Table 3-3, and the X-ray diffraction pattern of its mineral contents is shown in Figure 3-7. It can be concluded from the experimental results that the quartz content in the sandstone samples is the highest, i.e. higher than 30%, and then follows montmorillonite, plagioclase, potash feldspar, illite and calcite. The

<p>定，含蒙脱石矿物的岩石具有较强的亲水性和较大的胀缩性，因此蒙脱石含量较高的泥岩在干湿交替的环境下容易崩解，风化形成缓坡状地形。砂岩中蒙脱石矿物含量较高时，易风化形成风化凹槽。</p>	<p>montmorillonite, plagioclase, potash feldspar and illite are solvable minerals. Clay minerals montmorillonite and illite is unstable when contact with water, and the rock containing montmorillonite has high hydrophilicity and strong swell-shrink characteristics. Therefore, the mudstone, which is rich in montmorillonite minerals, is easy to break down under the dry and humid alternative circumstance, and then generates the gentle slope landform due to weathering effect. Weathering flute is easily formed in the sandstone which is abundant in montmorillonite minerals.</p>
--	--

表 3-3 X 衍射物相分析成果

Tab.3-3 Analysis Results of X-Ray Diffraction

送样号	蒙脱石	伊利石	石英	钾长石	斜长石	白云石	方解石
Sample No.	Montmorillonite	Illite	Quartz	potash feldspar	Plagioclase	Dolomite	Calcite
5-1	25	10	35	10	15	0	5
b	25	10	35	5	20	0	5
c	17	10	35	10	25	0	3
d-1	17	10	35	10	25	0	3
d-2	25	10	30	10	20	0	5
d-3	17	10	35	10	25	0	3
d-4-1	22	10	30	5	30	0	3
d-4-2	15	10	35	10	25	0	5
d-5	20	10	30	5	25	0	10
e-1	12	5	40	10	30	0	3
f-1	12	5	35	10	25	5	8
J <sub>3</sub> <sup>S-3</sup>	35	25	15	5	10	0	10

测试类别：X 衍射矿物成分分析

测试依据：JCPDS 卡片(国际粉末衍射标准联合委员会)

主要测试仪器名称及编号：荷兰 X' Pert PRO 衍射仪 DY2198

测试环境（温度）：20°C （湿度）：50%

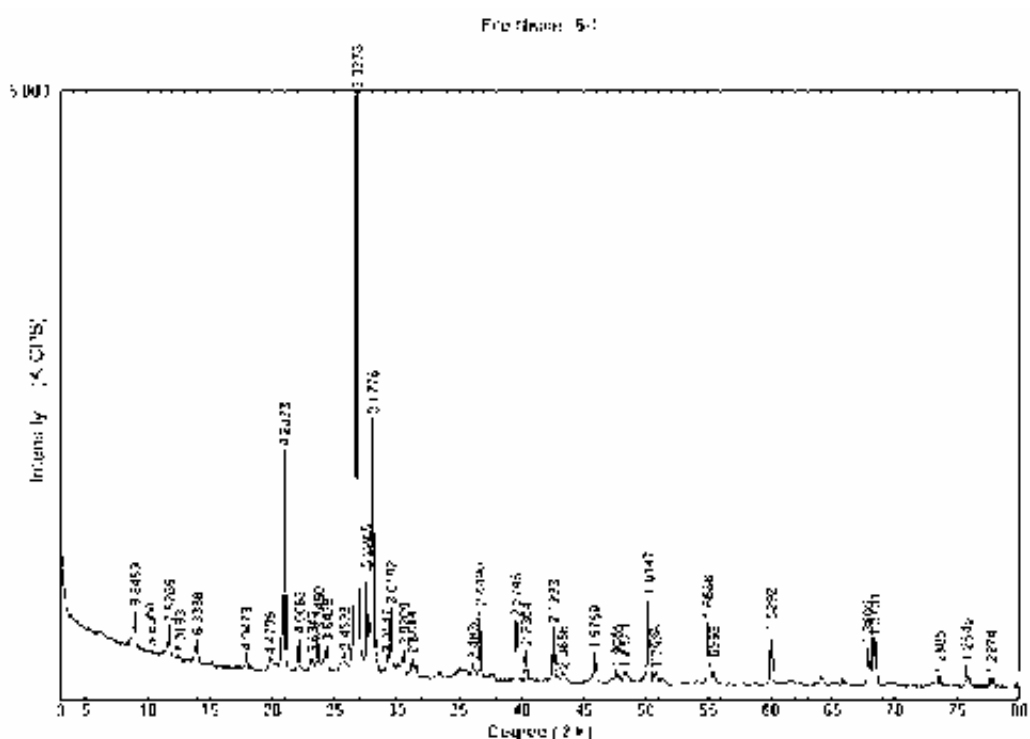


图 3-7-1 5-1 号样 X 衍射图谱

Fig.3-7-1 X-ray spectrum analysis of sample No.5-1

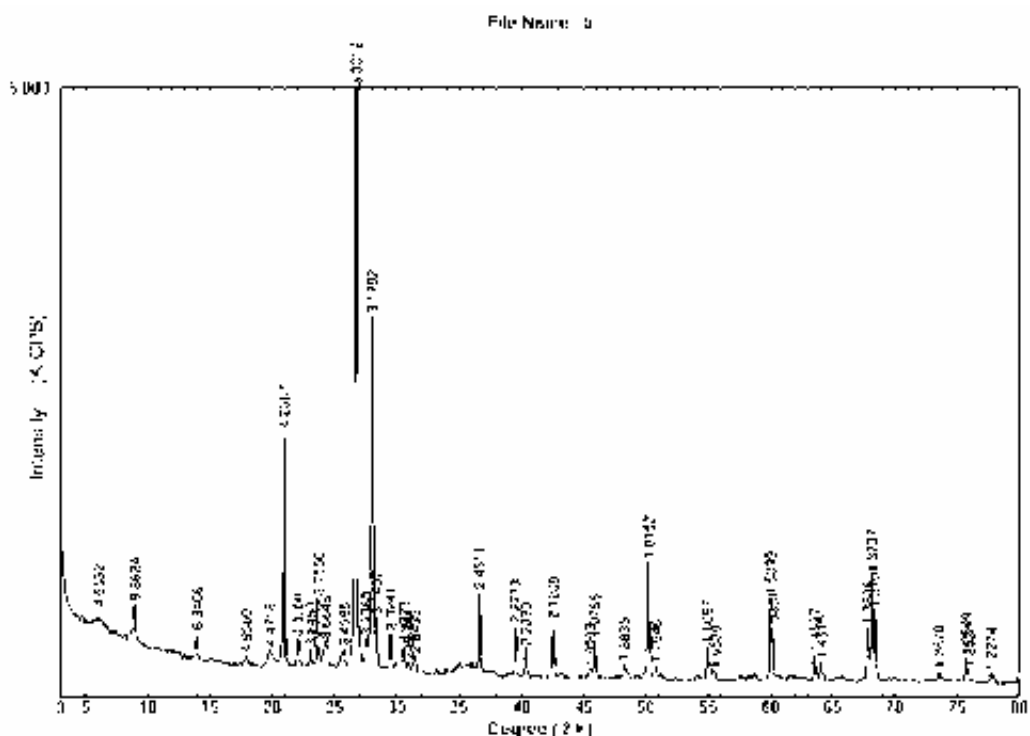


图 3-7-2 b 号样 X 衍射图谱

Fig.3-7-2 X-ray spectrum analysis of sample of No.b

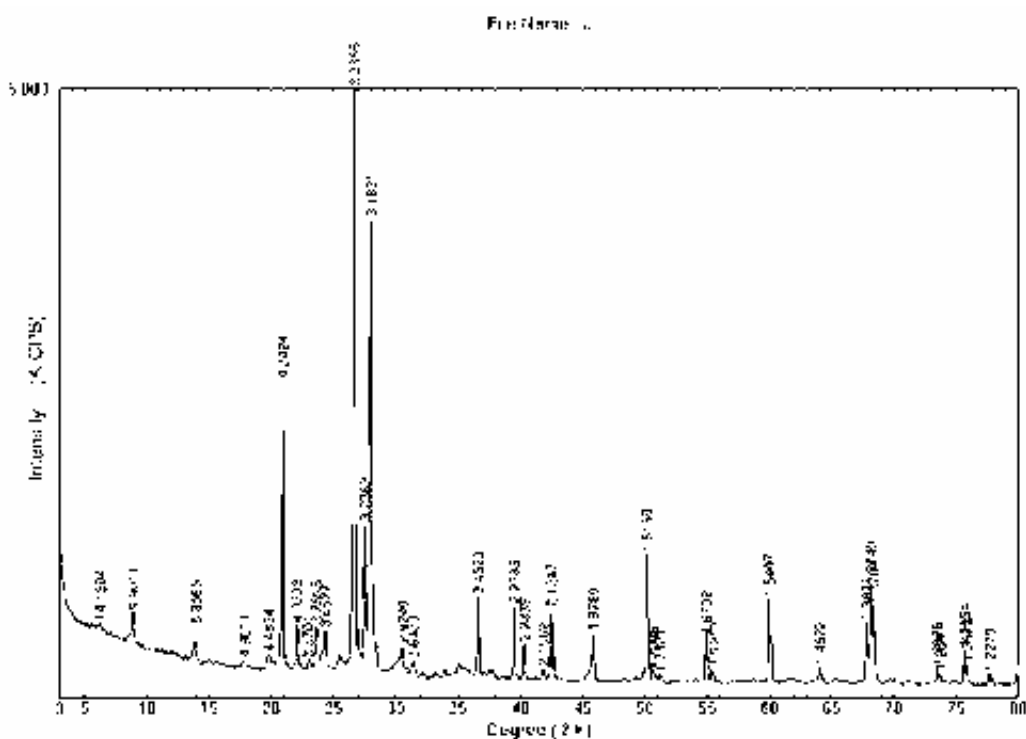


图 3-7-3 c 号样 X 衍射图谱

Fig.3-7-3 X-ray spectrum analysis of sample of No.c

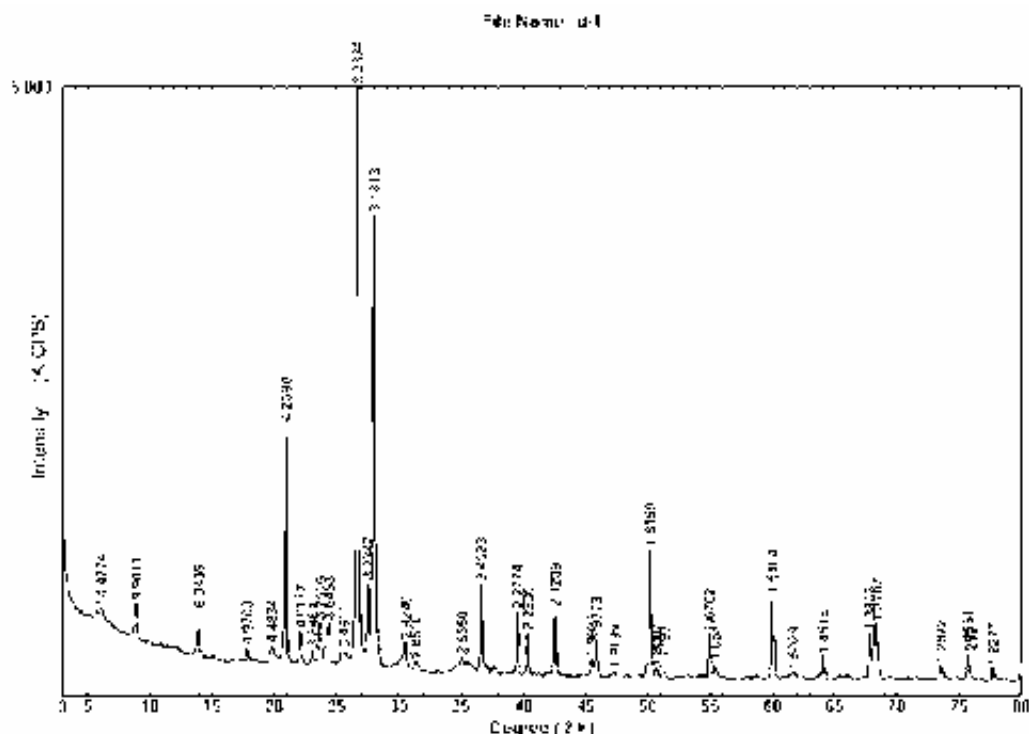


图 3-7-4 d-1 号样 X 衍射图谱

Fig.3-7-4 X-ray spectrum analysis of sample of No.d-1

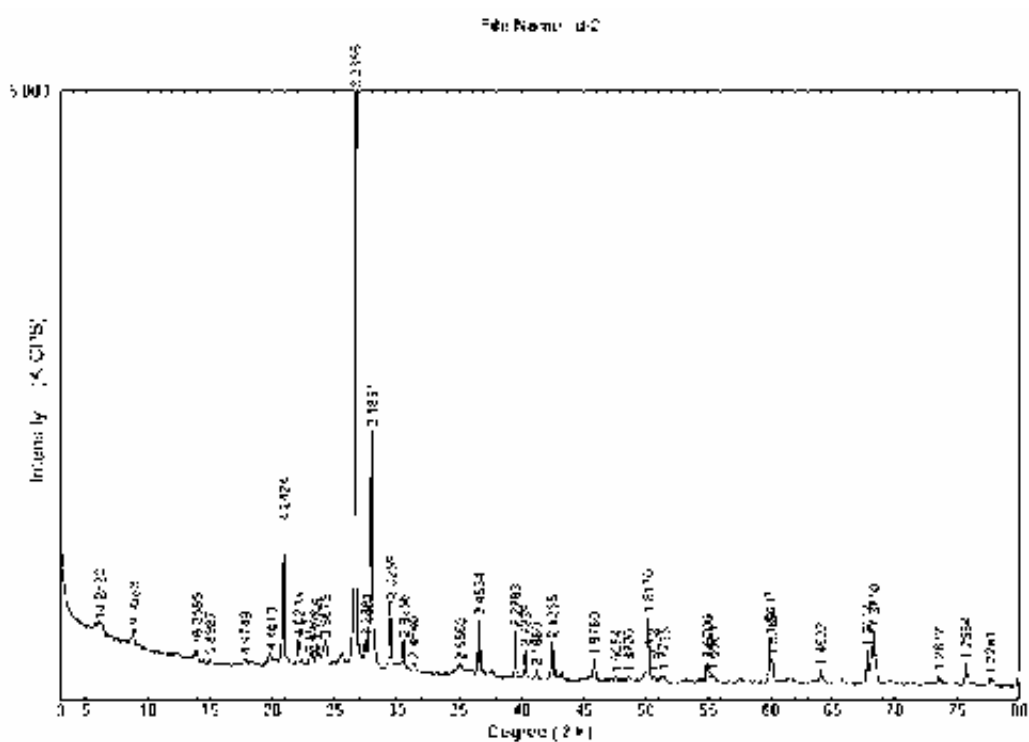


图 3-7-5 d-2 号样 X 衍射图谱

Fig.3-7-5 X-ray spectrum analysis of sample of No.d-2

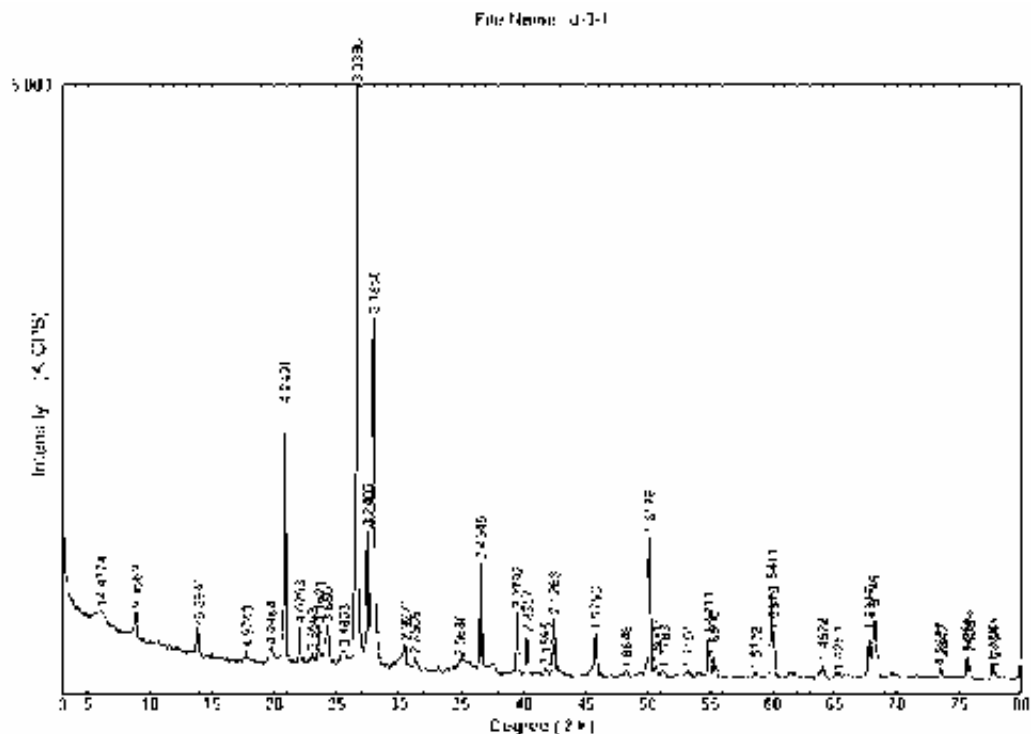


图 3-7-6 d-3 号样 X 衍射图谱

Fig.3-7-6 X-ray spectrum analysis of sample of No.d-3

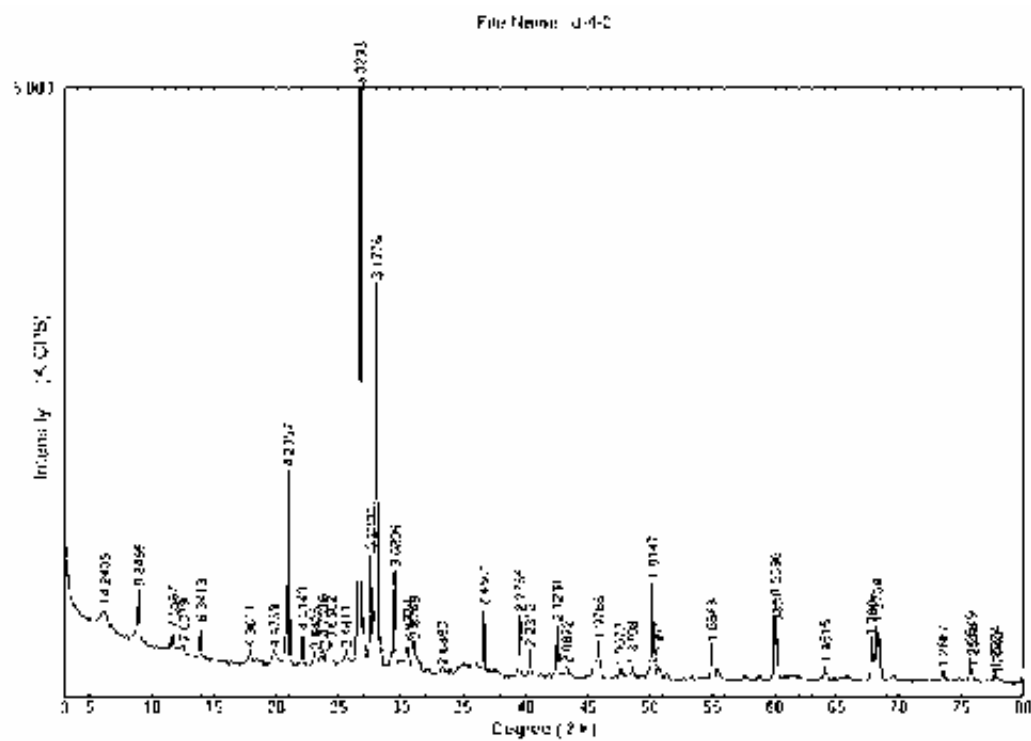


图 3-7-7 d-4-2 号样 X 衍射图谱

Fig.3-7-7 X-ray spectrum analysis of sample of No.d-4-2

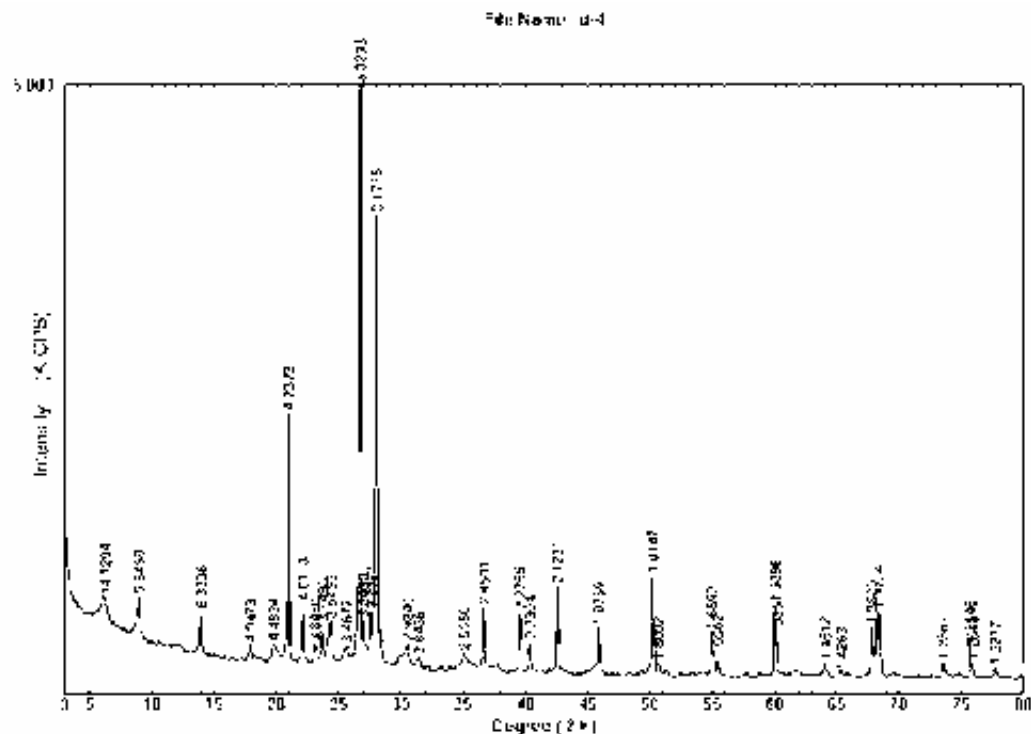


图 3-7-8 d-4 号样 X 衍射图谱

Fig.3-7-8 X-ray spectrum analysis of sample of No.d-4

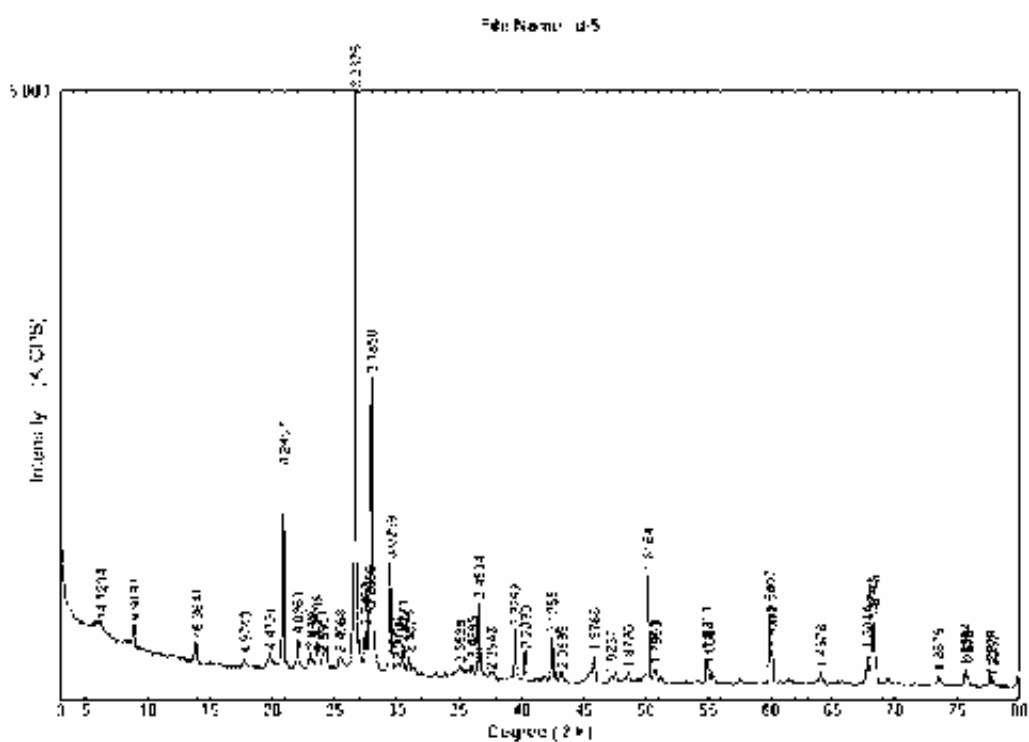


图 3-7-9 d-5 号样 X 衍射图谱

Fig.3-7-9 X-ray spectrum analysis of sample of No.d-5

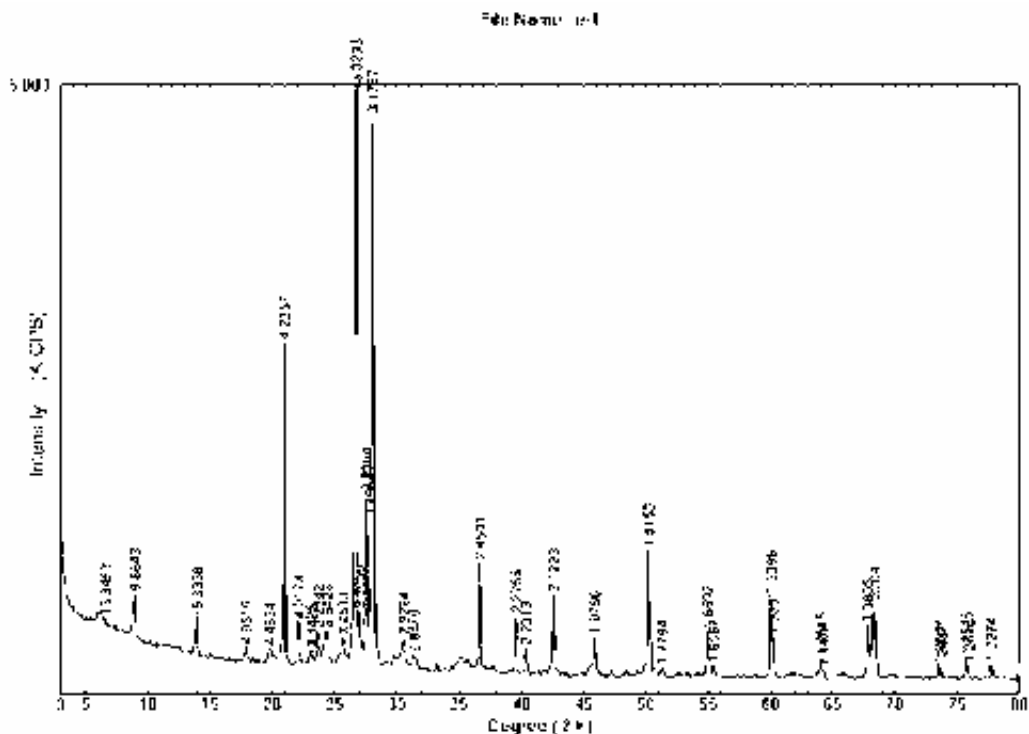


图 3-7-10 e-1 号样 X 衍射图谱

Fig.3-7-10 X-ray spectrum analysis of sample of No.e-1

Fig. Figure 3-1

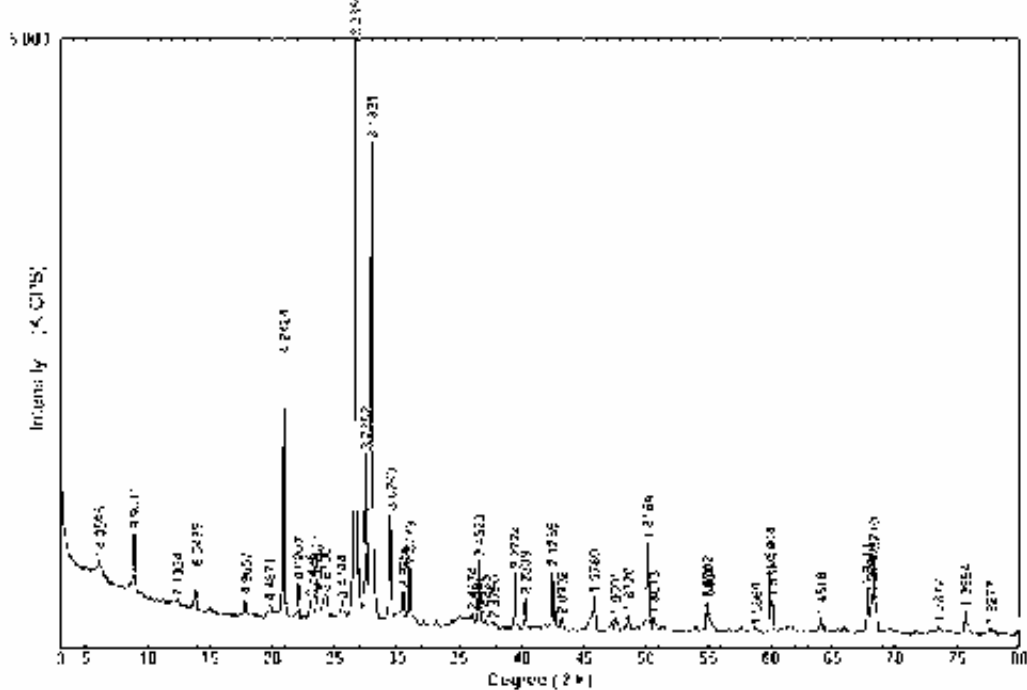
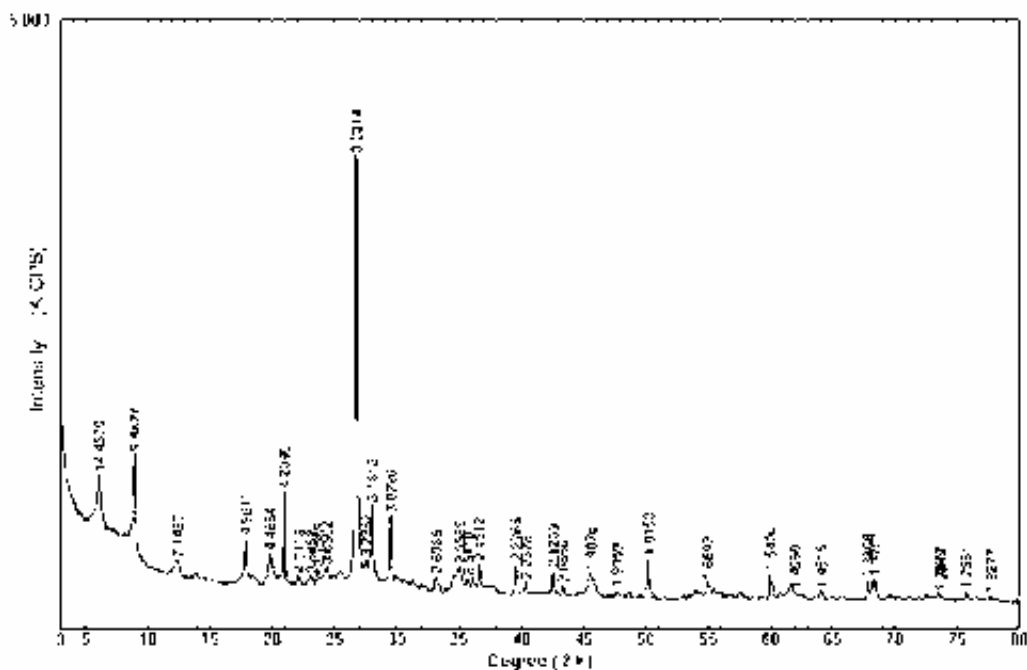


图 3-7-11 f-1 号样 X 衍射图谱

Fig.3-7-11 X-ray spectrum analysis of sample of No.f-1

File Name: J3(s-3)

图 3-7-12 J<sub>3</sub><sup>S-3</sup> 号样 X 衍射图谱Fig.3-7-12 X-ray spectrum analysis of sample of No.J<sub>3</sub><sup>S-3</sup>

### 3.3 岩样 X-荧光分析

对 10 号龛处五个层位岩石表面的风化样品进行X-荧光分析，结果见表 3-4。由测试结果可以看出，样品的化学成分主要为 $\text{SiO}_2$ ，其次为 $\text{Al}_2\text{O}_3$ 。由 $\text{Al}_2\text{O}_3$ 含量的多少，可间接判断出岩石抗风化能力的强弱。 $\text{Fe}_2\text{O}_3$ 、 $\text{Na}_2\text{O}$ 、 $\text{K}_2\text{O}$ 、 $\text{MgO}$ 、 $\text{CaO}$ 的含量均超过 1%，其它氧化物含量甚微。比较各个样品，其中 b 号样品的 $\text{SiO}_2$ 含量相对较少，而 $\text{Al}_2\text{O}_3$ 、 $\text{Na}_2\text{O}$ 、 $\text{K}_2\text{O}$ 含量最高。

### 3.3 X-ray Fluorescence analysis of the rock samples

The X-ray fluorescence analysis for the weathering samples taking from the rock surface of 5 different layers of Group 10 Niche is carried out, and the results were listed in Table 3-4. It can be concluded from the experimental results that the primary chemical component of the samples is  $\text{SiO}_2$ , and the secondary one is  $\text{Al}_2\text{O}_3$ , from the content of which the weathering resistance capacity can be deduced indirectly. The contents of  $\text{Fe}_2\text{O}_3$ ,  $\text{Na}_2\text{O}$ ,  $\text{K}_2\text{O}$ ,  $\text{MgO}$  and  $\text{CaO}$  are all higher than 1 percent, while the content of other oxide is very low. It can be concluded from the comparison of the samples that the  $\text{SiO}_2$  content in Sample b is relatively low, while the  $\text{Al}_2\text{O}_3$ ,  $\text{Na}_2\text{O}$  and  $\text{K}_2\text{O}$  content is the highest.

表 3-4 10 号龛处岩样 X-荧光分析成果

Tab.3-4 Analysis Results of the X-ray fluorescence

样品编号		b	c	d-2	d-4	e-1	f-1
化 学 成 分 含 量 %	$\text{Na}_2\text{O}$	3.78	2.96	2.61	2.74	3.04	2.83
	$\text{MgO}$	2.25	1.47	2.02	2.33	1.33	1.48
	$\text{Al}_2\text{O}_3$	16.5	15.3	14.1	15.7	13.2	13.0
	$\text{SiO}_2$	68.9	74.3	71.5	71.6	75.8	71.7
	$\text{P}_2\text{O}_5$	0.152	0.108	0.158	0.137	0.169	0.0846
	$\text{SO}_3$	0.283	0.0899	0.0765	0.0591	0.113	0.0845
	Cl	0.590	0.0155	0.0275	0.0174	0.189	0.0187
	$\text{K}_2\text{O}$	2.54	2.28	2.07	2.18	2.03	2.38
	$\text{CaO}$	1.63	0.754	3.95	1.96	1.18	5.97
	$\text{TiO}_2$	0.526	0.397	0.466	0.412	0.428	0.244
	$\text{Cr}_2\text{O}_3$	0.0180	0.0139	0.0126	0.0118	0.0131	0.0125
	$\text{MnO}$	0.0576	0.0695	0.0474	0.0547	0.0724	0.0510
	$\text{Fe}_2\text{O}_3$	2.76	2.10	2.80	2.73	2.26	2.07

	<b>CoO</b>	<b>0.0179</b>	<b>0.0270</b>	<b>0.0409</b>	<b>0.0266</b>	<b>0.0528</b>	<b>0.0431</b>
	<b>NiO</b>	<b>0.00666</b>	<b>0.00431</b>	<b>0.00650</b>	<b>0.00636</b>	<b>0.00571</b>	<b>0.00583</b>
	<b>CuO</b>	<b>0.00889</b>	<b>0.00673</b>	<b>0.0113</b>	<b>0.00735</b>	<b>0.00733</b>	<b>0.00791</b>
	<b>ZnO</b>	<b>0.00818</b>	<b>0.00633</b>	<b>0.00760</b>	<b>0.00811</b>	<b>0.00699</b>	<b>0.00560</b>
	<b>Ga<sub>2</sub>O<sub>3</sub></b>	<b>0.00257</b>	/	<b>0.0149</b>	<b>0.00215</b>	/	/
	<b>Rb<sub>2</sub>O</b>	<b>0.00857</b>	<b>0.00807</b>	<b>0.00770</b>	<b>0.00790</b>	<b>0.00744</b>	<b>0.00843</b>
	<b>SrO</b>	<b>0.0223</b>	<b>0.0191</b>	<b>0.0191</b>	<b>0.0181</b>	<b>0.0205</b>	<b>0.0212</b>
	<b>ZrO<sub>2</sub></b>	<b>0.0378</b>	<b>0.0295</b>	<b>0.0323</b>	<b>0.0251</b>	<b>0.0452</b>	<b>0.0133</b>
	<b>BaO</b>	<b>0.0458</b>	<b>0.0418</b>	<b>0.0462</b>	<b>0.0480</b>	<b>0.0475</b>	<b>0.0518</b>
	<b>Norm.%</b>	<b>100.10</b>	<b>100.00</b>	<b>100.00</b>	<b>100.00</b>	<b>100.00</b>	<b>100.00</b>

### 3.4 砂岩微观结构扫描电镜分析

从表 3-5 和扫描电镜图谱分析可知, 石刻区岩体微观结构松散, 粒状矿物主要为石英。片状矿物主要为蒙脱石和伊利石。微孔隙和微裂隙发育, 孔隙大小一般为 2~20 μm, 孔隙率为 5%~30%。微观结构的疏松导致圆觉洞岩石的抗风化能力较弱。

### 3.4 SEM analysis of the sandstone microstructure

It can be concluded from the SEM analysis and Table 3-5 that the rock in Yuanjuedong is of loosening microstructure, and the granular minerals are mainly quartz, the laminar minerals are mainly montmorillonite and illites. The micro pores and micro fissures range from 2 to 20 μm are developed in the rock, and the porosity ranges from 5 to 30 percent. The loosening microstructure results in relatively poor weathering-resistance capacity of the rock in Yuanjuedong.

表 3-5 扫描电镜分析成果

Tab.3-5 Analysis Results of the SEM

送样单位: 工程学院	送样人: 方云	送样日期: 2007-10-22
样品名称: 砂岩等		
样 品 号	照片号	放 大 倍 数
Sample No.	Photo No.	magnification ratio
b	2_008	×500
	2_007	×600
	2_003	×1000

	2_006	×1000	长石蚀变蒙脱石
	2_004	×2000	长石解理
	2_001	×2000	蒙脱石
	2_002	×2000	长石, 石英
该样品主要由石英, 长石, 绿泥石, 伊利石及方解石组成。结构松散, 粒状矿物主要为长石及石英, 长石多蚀变为绿泥石。片状矿物主要为绿泥石和伊利石。微孔隙和微裂隙发育, 孔隙大小一般为 1~20 μm, 孔隙率约 30%。			
c	7_006	×300	长石与石英, 表面溶蚀
	7_001	×600	粒间孔隙较大
	7_004	×2000	薄片状伊利石
	7_003	×5000	薄层状伊利石
	7_005	×5000	溶蚀空洞
	7_002	×6000	蒙脱石
	7_007	×6000	石英
该样品主要由石英、长石、蒙脱石、伊利石组成。结构较松散, 粒状矿物主要为长石及石英, 长石多蚀变为绿泥石。微孔隙和微裂隙发育, 孔隙大小一般为 2~10 μm, 孔隙率约 20%。			
d-1	21_001	×400	结构较致密, 偶有孔洞
	21_007	×500	结构较致密, 表面上有溶蚀
	21_008	×1000	长石蚀变蒙脱石
	21_003	×1500	长石
	21_002	×2000	结构松散的伊利石
	21_006	×2000	石英颗粒及表面上溶蚀
	21_005	×5000	蒙脱石
	21_004	×8000	长石表面溶蚀
该样品主要由石英、长石、蒙脱石、伊利石、绿泥石组成, 长石多已蚀变为绿泥石、蒙脱石、伊利石。结构较致密, 微裂隙不太发育, 有微溶蚀孔洞, 孔隙率约 5%。			
d-2	25_007	×100	颗粒间隙紧凑, 有裂隙发育
	25_006	×500	结构较松散, 表面覆盖有蒙脱石, 并有溶蚀
	25_004	×800	长石蚀变蒙脱石
	25_005	×2000	长石蚀变蒙脱石
	25_003	×2500	长石风化
	25_002	×4000	蒙脱石
	25_001	×10000	方解石颗粒松散堆积
该样品主要含晶体状石英、薄片状绿泥石及长石, 长石部分蚀变为绿泥石, 结构较松散, 裂隙发育, 孔隙率约 20%。			
d-3-1	47_010	×400	结构较松散, 表面上有绿泥石及粘土矿物覆盖

	47_003	×500	长石, 蒙脱石, 粘土矿物, 结构相对致密
	47_006	×1000	表面溶蚀, 长石蚀变蒙脱石
	47_001	×2000	石英断裂面
	47_007	×2300	石英颗粒
	47_008	×2300	颗粒表面溶蚀及次生发育
	47_004	×2500	石英
	47_002	×4000	蒙脱石
	47_009	×10000	方解石

该样品主要由石英, 长石, 绿泥石, 伊利石及方解石组成。粒状矿物主要为长石及石英, 长石多蚀变为绿泥石。结构相对致密, 孔隙大小一般为 1~20 μm, 孔隙率约 15%。

d-4	57_004	×300	结构相对致密, 表面有粘土矿物及绿泥石覆盖
	57_006	×800	溶蚀空洞及次生矿物
	57_007	×800	次生矿物方解石
	57_005	×2000	长石
	57_001	×2500	蒙脱石
	57_002	×5000	图片 57_001 的局部放大, 蒙脱石

该样品主要由石英, 长石, 蒙脱石, 伊利石及方解石组成。结构相对致密, 孔隙大小一般为 1~20 μm, 孔隙率约 10%。

d-4-2	71_002	×500	结构疏松, 较多溶蚀空洞
	71_008	×500	结构较疏松, 表面有粘土矿物覆盖
	71_005	×1000	空洞发育
	71_006	×1500	粒间孔隙发育结构疏松
	71_007	×2000	棱角状石英颗粒
	71_003	×3000	层状矿物定向排列
	71_004	×3000	蒙脱石, 伊利石
	71_001	×5000	长石颗粒及蚀变

该样品主要由石英, 长石, 蒙脱石, 方解石组成。结构较致密, 孔隙大小一般为 1~10 μm, 孔隙率约 8%。

d-5	72_004	×600	结构较致密, 表面有粘土矿物覆盖
	72_001	×1500	蒙脱石, 伊利石
	72_002	×5000	方解石
	72_003	×5000	长石, 石英
	72_005	×5000	长石, 石英

该样品主要由石英, 长石, 蒙脱石, 方解石组成。结构较致密, 微裂隙不太发育, 有微溶蚀孔洞, 孔隙率约 5%。

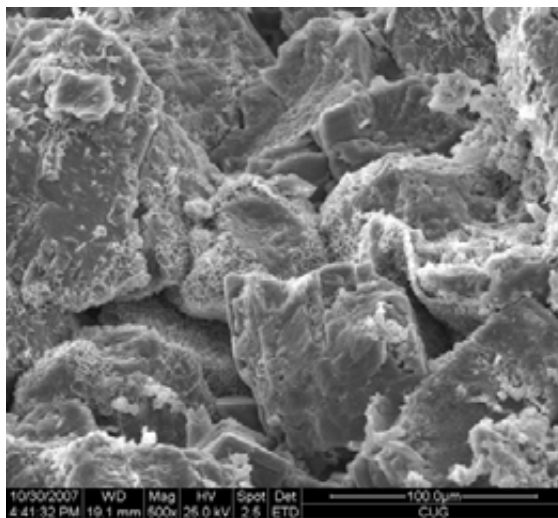
e-1	82_008	×200	颗粒间结构相对松散
	82_001	×300	结构相对松散

	82_005	×500	石英颗粒及次生矿物发育
	82_004	×1000	石英颗粒及次生粘土矿物
	82_007	×1000	石英蚀变
	82_002	×3000	基质溶蚀空洞
	82_003	×3000	次生片状及纤维状矿物
	82_006	×3000	蒙脱石
该样品主要由石英，长石，蒙脱石，方解石组成。结构相对松散，粒间孔隙几乎无粘土矿物填充，粒间微裂隙发育，一般为 1~8 μm，孔隙率约 10%。			
f-1	89_004	×200	结构致密，有粘土矿物覆盖
	89_003	×800	方解石解理面
	89_002	×1000	基质溶蚀空洞
	89_001	×2000	蒙脱石
该样品主要由石英、长石、方解石、绿泥石等组成。结构致密，含粘土矿物。			
J <sub>3</sub> <sup>s-3</sup>	90_006	×300	结构致密，无裂隙发育
	90_003	×1000	结构致密，表面溶蚀
	90_005	×2000	蒙脱石
	90_002	×3000	结构致密，粘土矿物粘接
	90_004	×3000	泥岩中含少量粒状矿物
	90_001	×5000	结构致密，偶有孔洞
该样品主要由石英，长石，蒙脱石，方解石组成。结构致密，偶有小孔洞，裂隙不发育。			

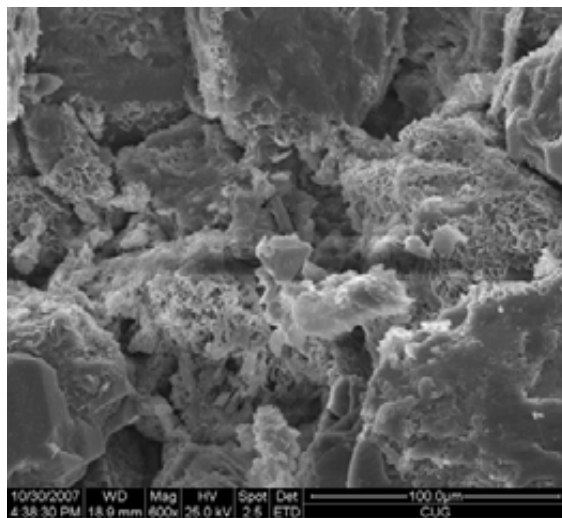
测试类别：扫描电镜分析 测试依据：GB/T17359-1998

主要测试仪器名称及编号：FEI.QUATA200

测试环境：(温度)：25°C (湿度)：48%



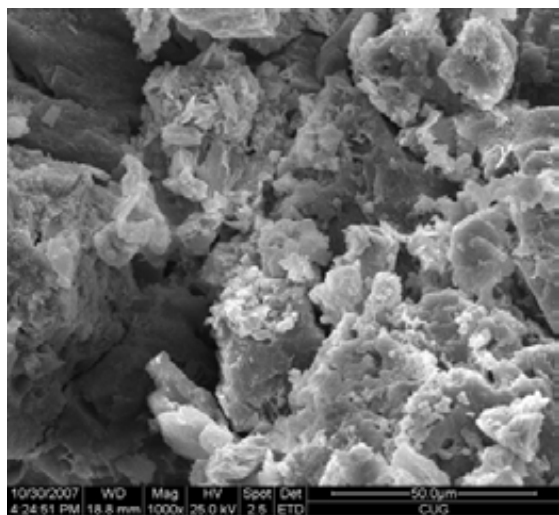
照片 2-008 ×500 结构松散



照片 2-007 ×600 孔洞发育，蒙脱石

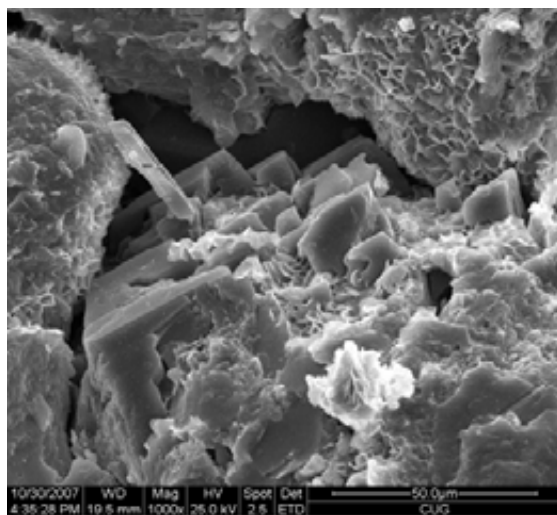
loose structure

pore developed, montmorillonite



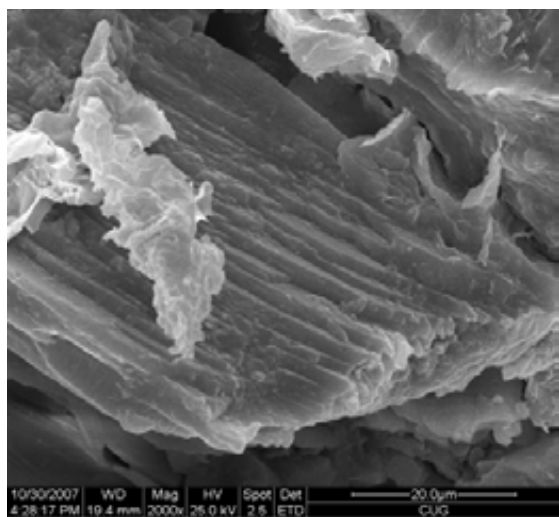
照片 2-003 ×1000 长石, 伊利石

feldspar, illite



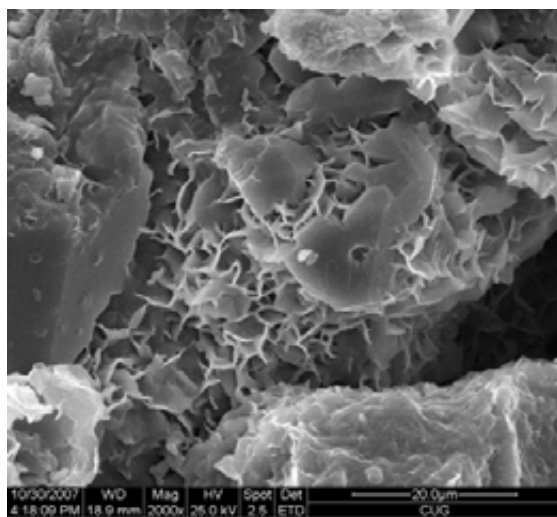
照片 2-006 ×1000 长石蚀变蒙脱石

feldspar -alter montmorillonite



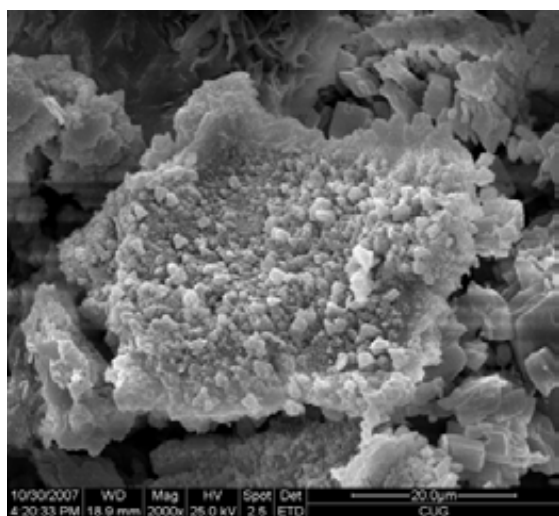
照片 2-004 ×2000 长石解理

feldspar cleavage



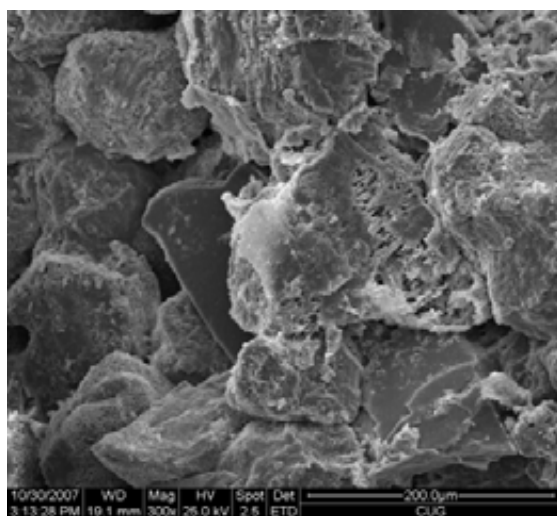
照片 2-001 ×2000 蒙脱石

montmorillonite



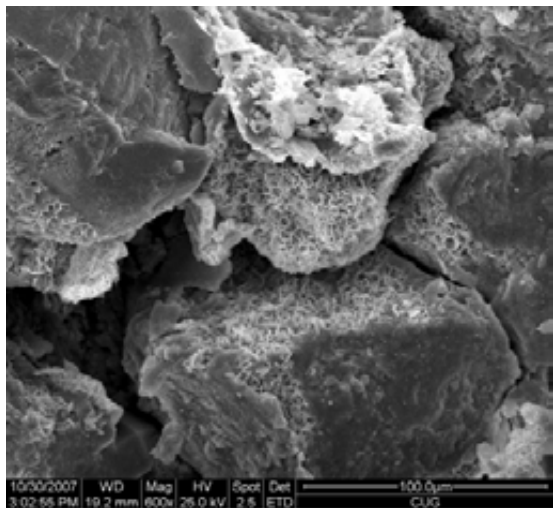
照片 2-002 ×2000 长石, 石英

feldspar, quartz



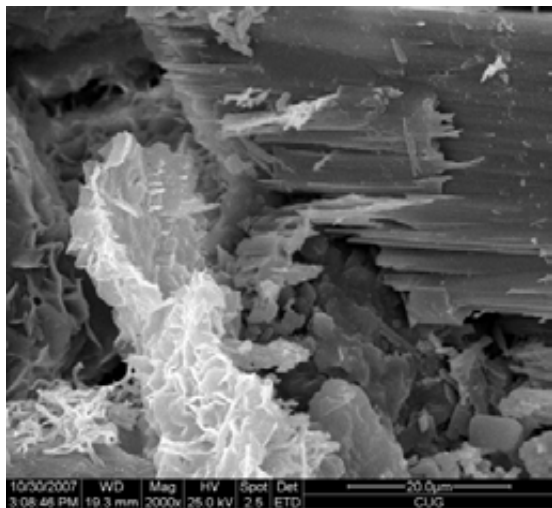
照片 7-006 ×300 长石与石英, 表面溶蚀

feldspar, quartz, surface erosion



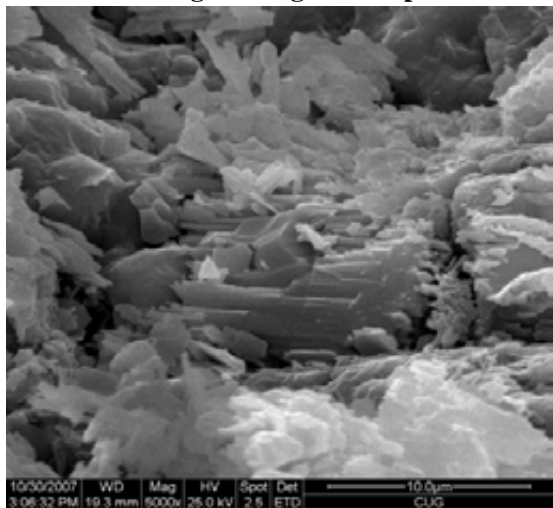
照片 7-001 ×600 粒间孔隙较大

large inter-granular pore



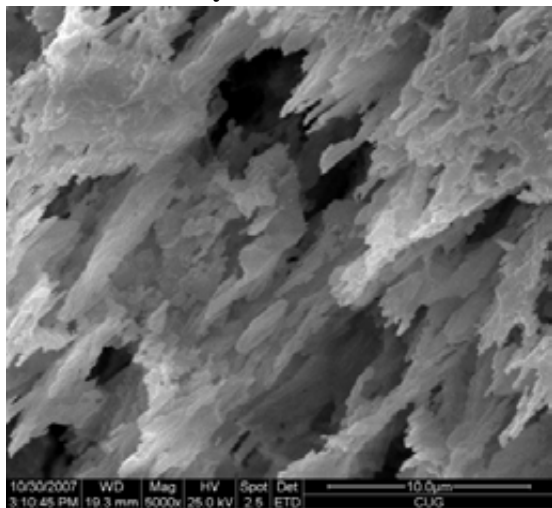
照片 7-004 ×2000 薄片状伊利石

scaly illite



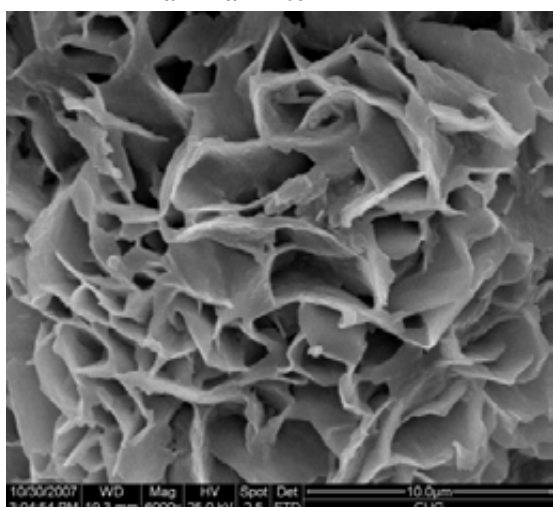
照片 7-003 ×5000 薄层状伊利石

laminal illite



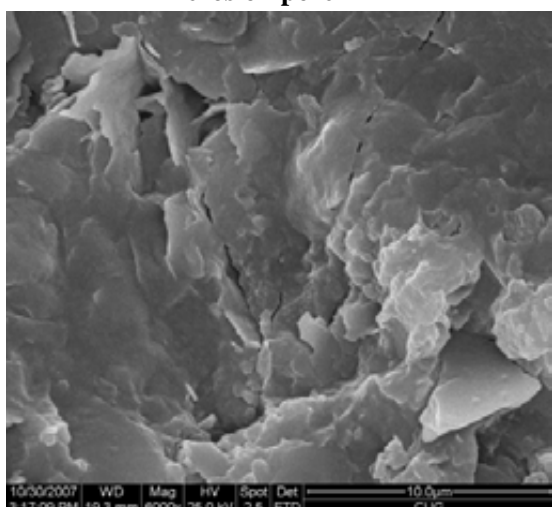
照片 7-005 ×5000 溶蚀空洞

erosion pore



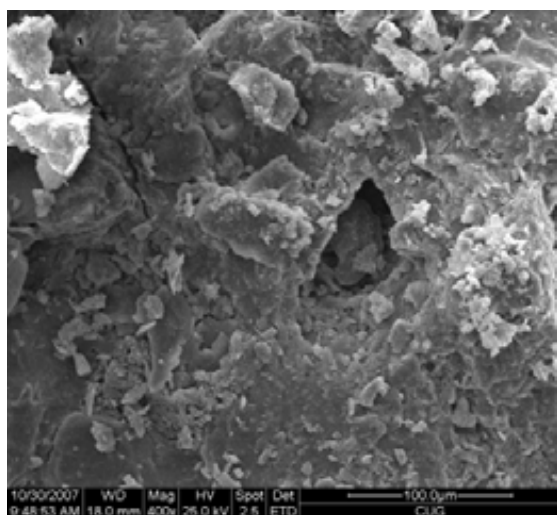
照片 7-002 ×6000 蒙脱石

montmorillonite

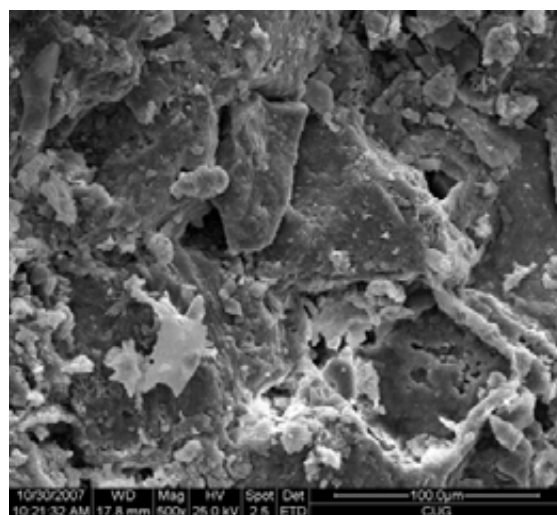


照片 7-007 ×6000 石英

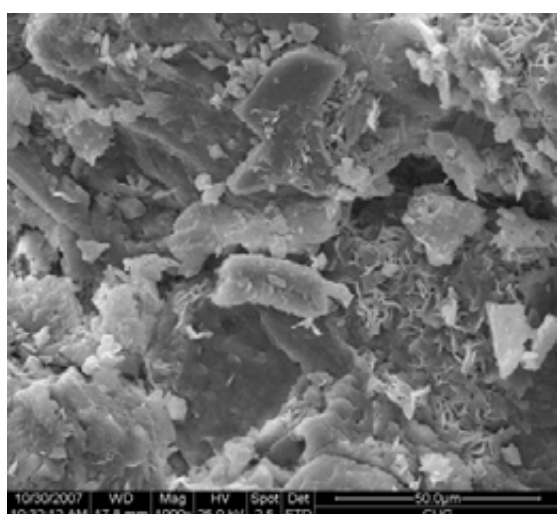
quartz



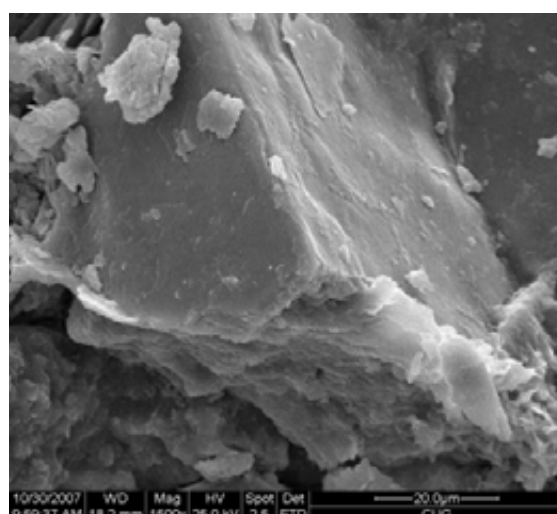
照片 21-001 ×400 结构较致密，偶有孔洞



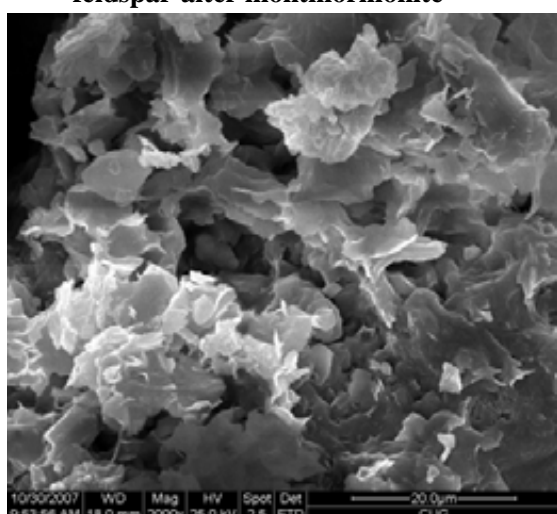
照片 21-007 ×500 结构较致密,表面有溶蚀



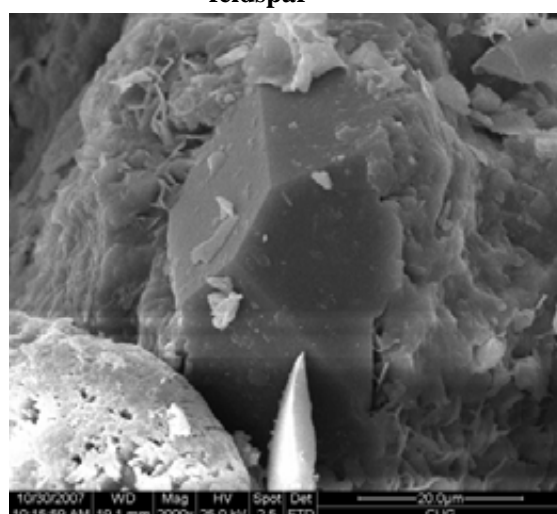
照片 21-008 ×1000 长石蚀变蒙脱石



照片 21-003 ×1500 长石



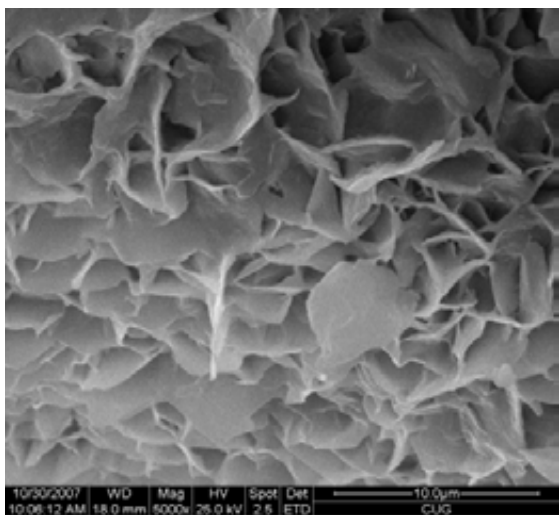
照片 21-002 ×2000 结构松散的伊利石



照片 21-006 ×2000 石英颗粒及表面溶蚀

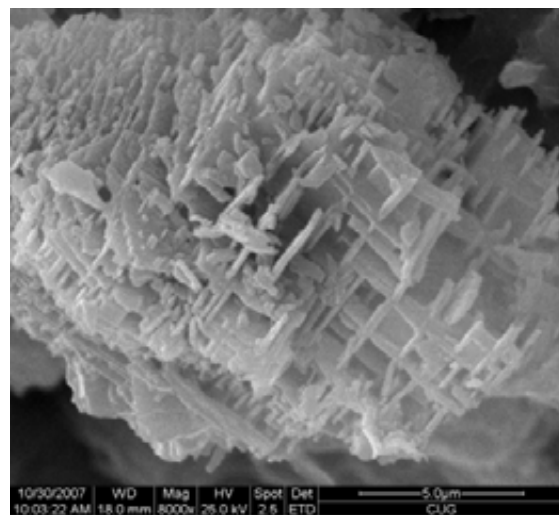
loose structure illite

quartz grain and surface erosion



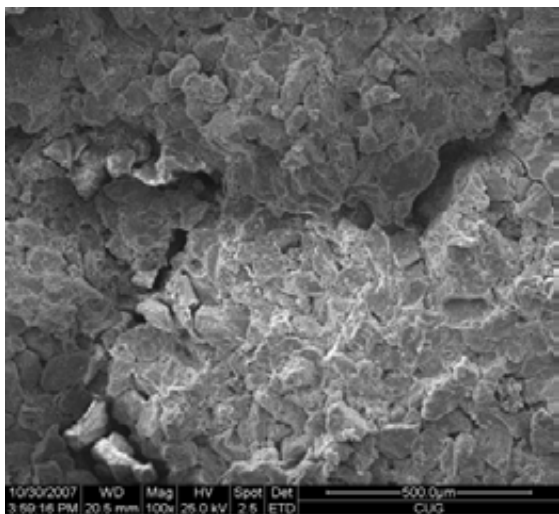
照片 21-005 ×5000 蒙脱石

montmorillonite



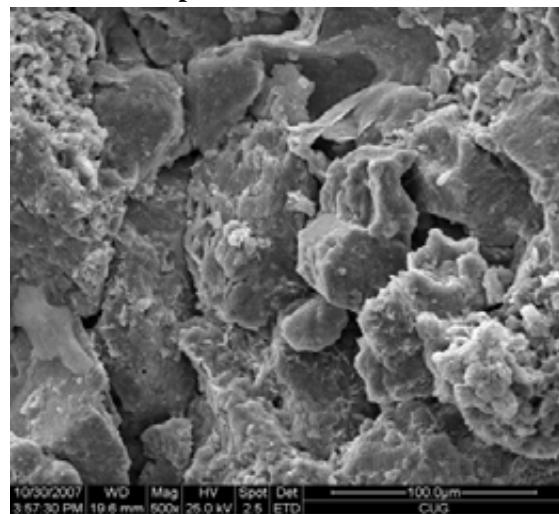
照片 21-004 ×8000 长石表面溶蚀

feldspar with surface erosion



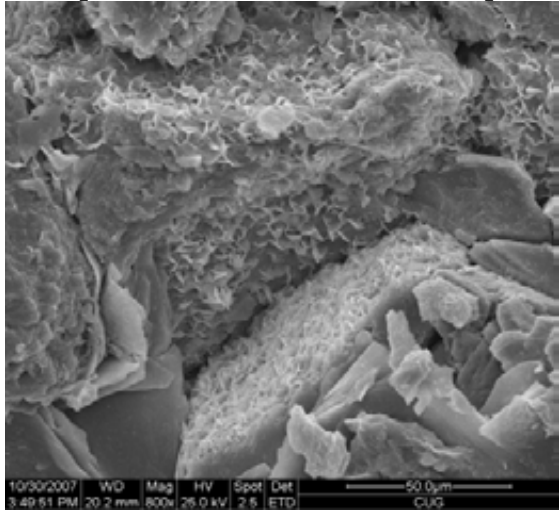
照片 25-007 ×100

颗粒间隙紧凑,有裂隙发育  
compact structure with fissure developed



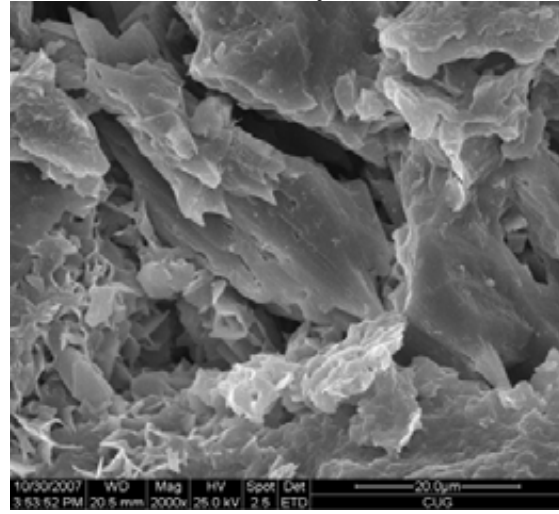
照片 25-006 ×500

结构较松散, 表面覆盖有蒙脱石, 并有溶蚀  
loose structure covered by montmorillonite



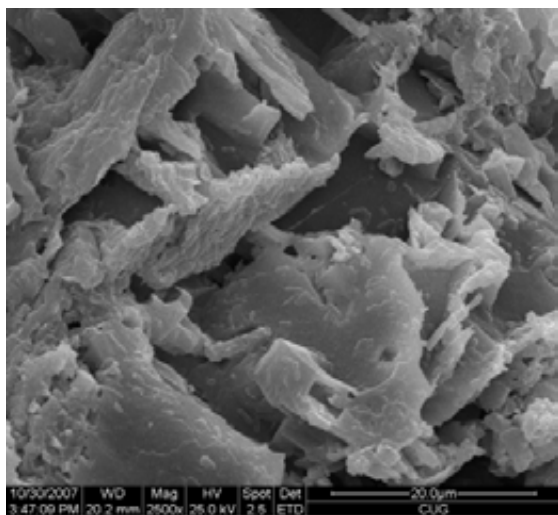
照片 25-004 ×800 长石蚀变蒙脱石

feldspar-alter montmorillonite



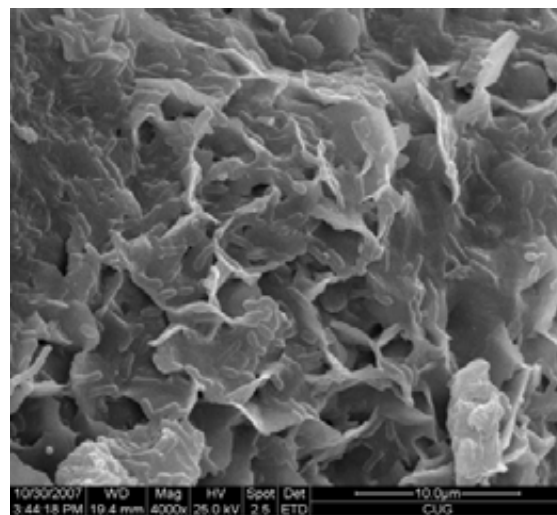
照片 25-005 ×2000 长石蚀变蒙脱石

feldspar-alter montmorillonite



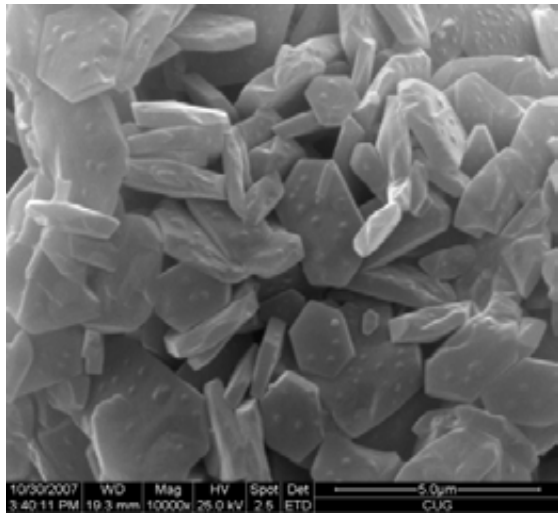
照片 25-003 ×2500 长石风化

feldspar weathering



照片 25-002 ×4000 蒙脱石

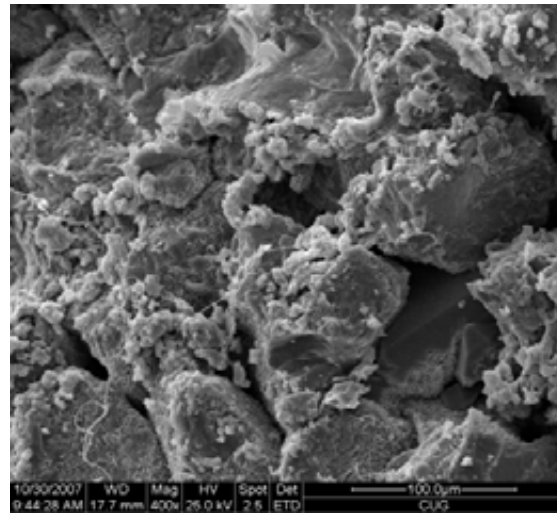
montmorillonite



照片 25-001 ×10000

方解石颗粒松散堆积

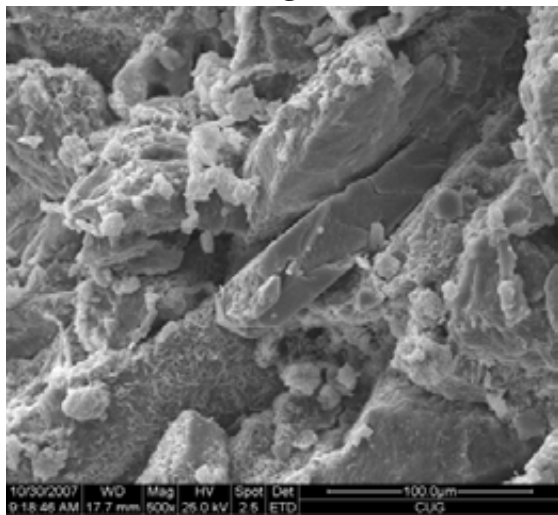
calcite grain



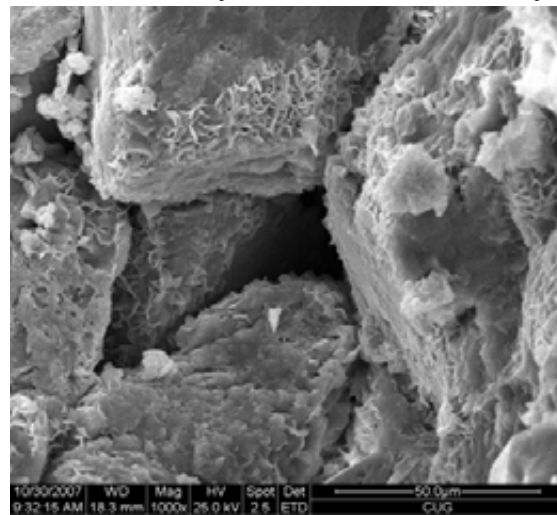
照片 47-010 ×400

结构较松散，表面有蒙脱石及粘土矿物覆盖

loose structure covered by montmorillonite and clay



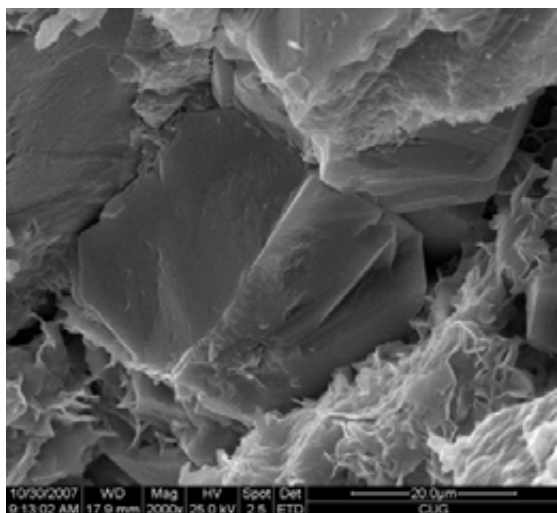
照片 47-003 ×500

长石，蒙脱石，粘土矿物。结构相对致密  
feldspar, montmorillonite and clay.

照片 47-006 ×1000

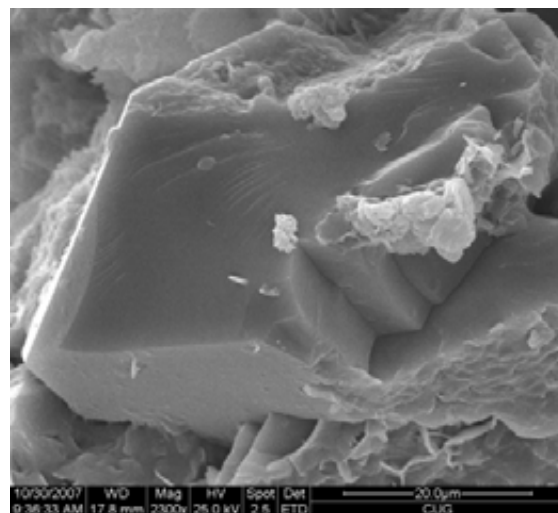
表面溶蚀，长石蚀变蒙脱石

Surface erosion, feldspar-alter montmorillonite



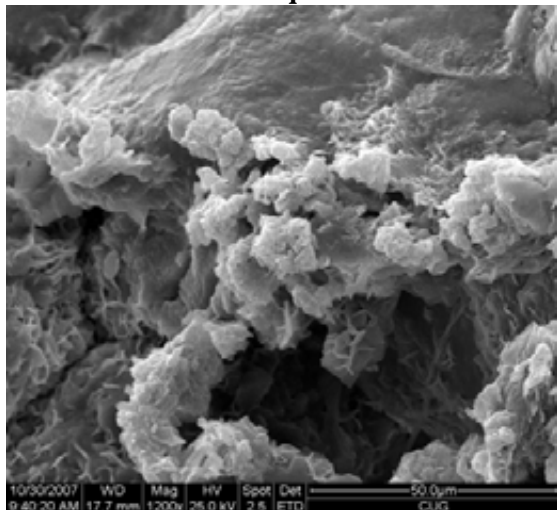
照片 47-001 ×2000 石英断裂面

quartz



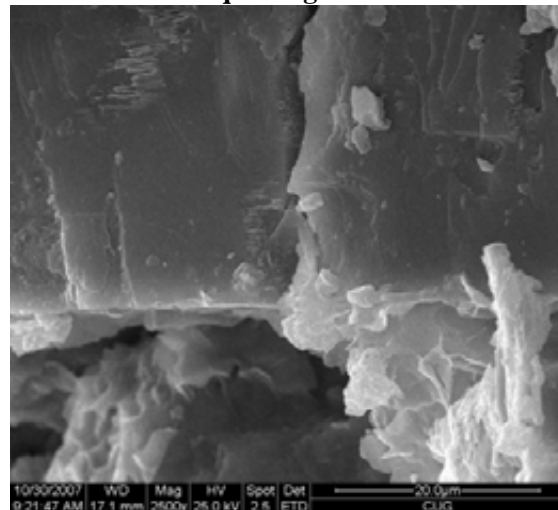
照片 47-007 ×2300 石英颗粒

quartz grain



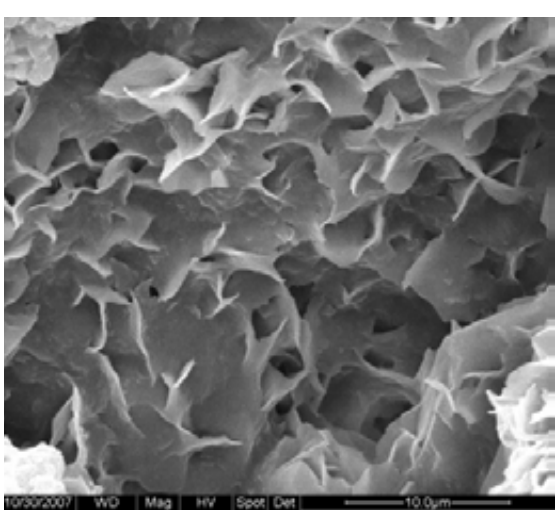
照片 47-008 ×2300 颗粒表面溶蚀及次生发育

surface erosion



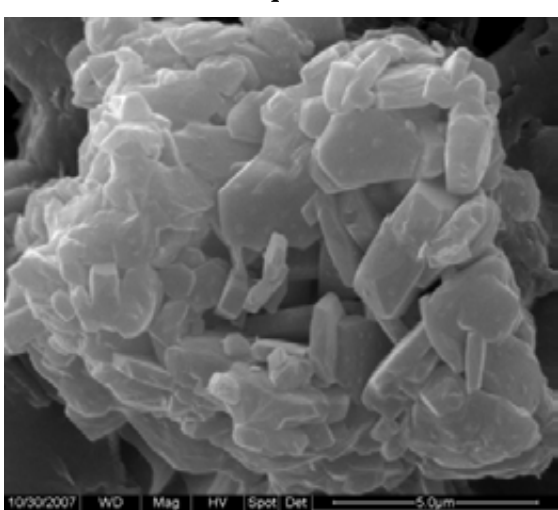
照片 47-004 ×2500 石英

quartz



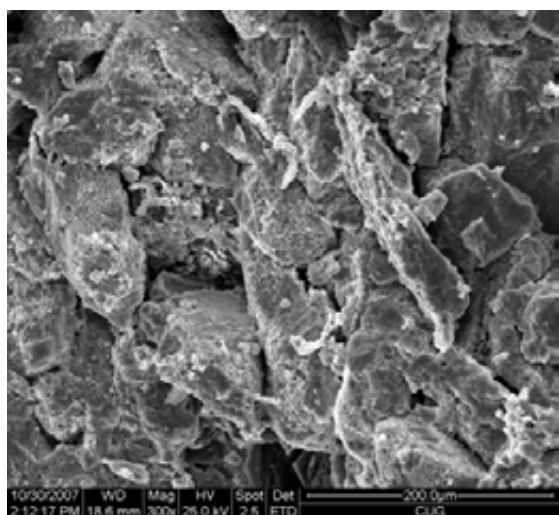
照片 47-002 ×4000 蒙脱石

montmorillonite

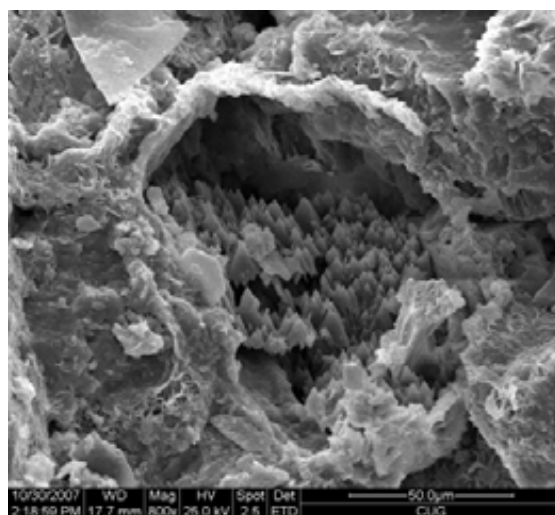


照片 47-009 ×10000 方解石

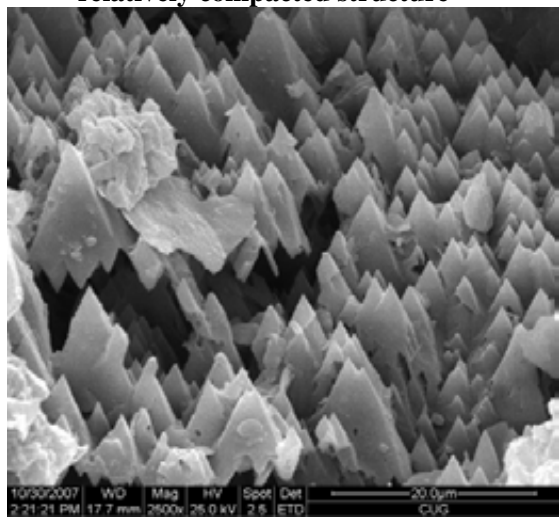
calcite



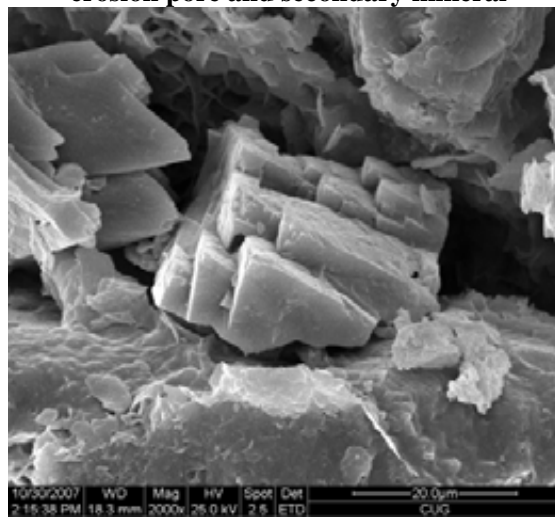
照片 57-004 ×300  
结构相对致密，表面有粘土矿物及蒙脱石覆盖  
relatively compacted structure



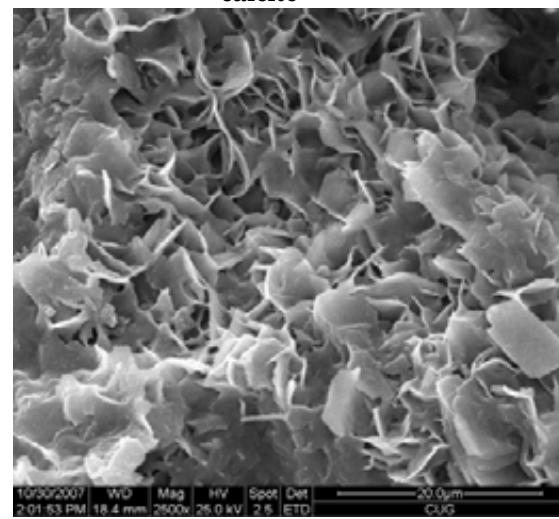
照片 57-006 ×800  
溶蚀空洞及次生矿物  
erosion pore and secondary mineral



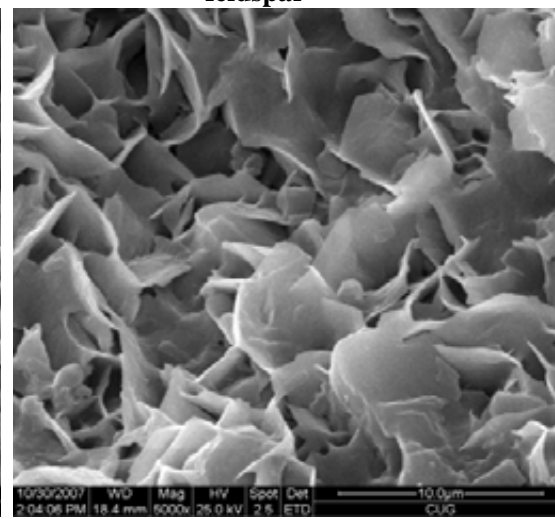
照片 57-007 ×800 次生矿物方解石  
calcite



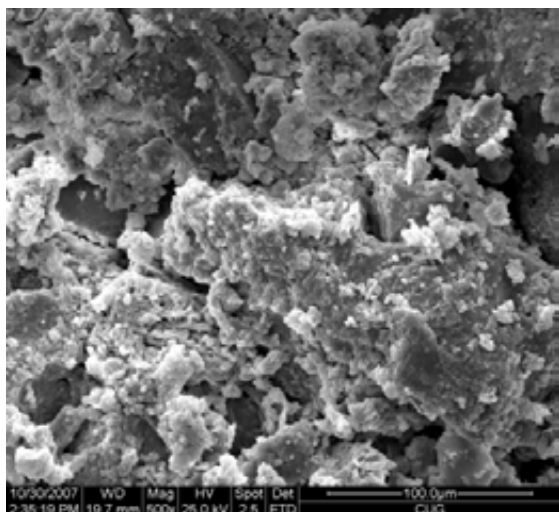
照片 57-005 ×2000 长石  
feldspar



照片 57-001 ×2500 蒙脱石  
montmorillonite



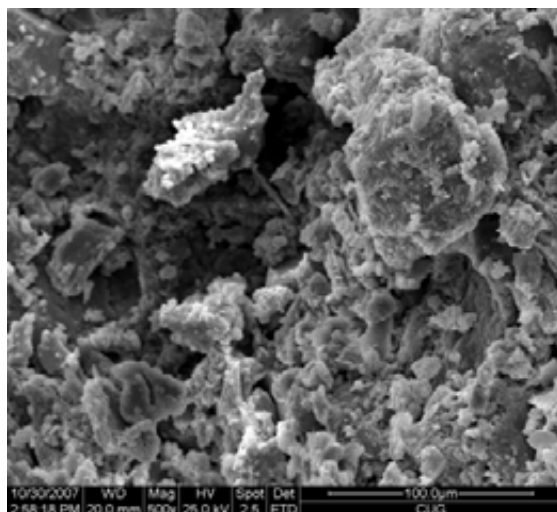
照片 57-002 ×5000  
照片 57-001 的局部放大，蒙脱石  
local part of photo 57-001



照片 71-002 ×500

结构疏松，较多溶蚀空洞

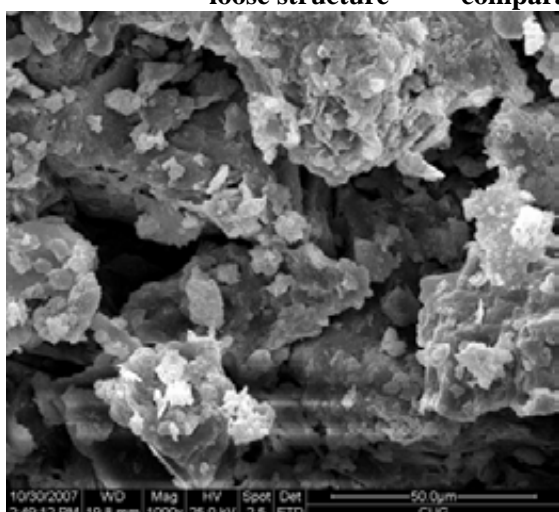
loose structure



照片 71-008 ×500

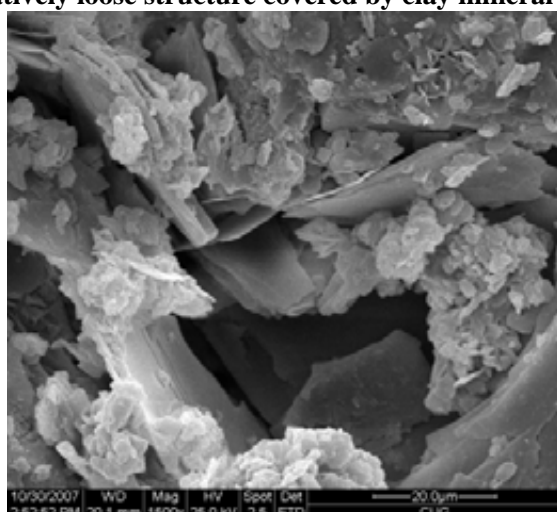
结构较疏松，表面有粘土矿物覆盖

comparatively loose structure covered by clay mineral



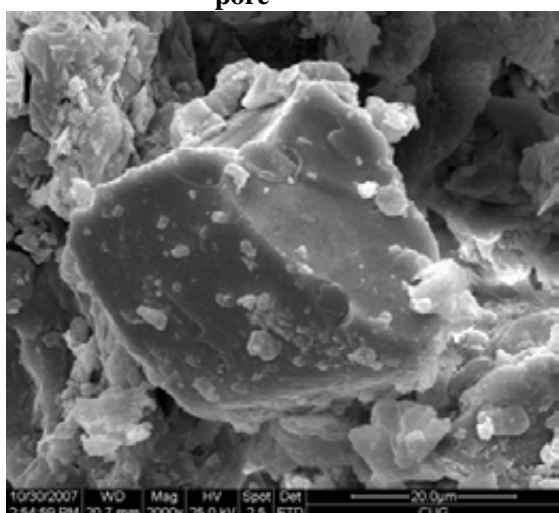
照片 71-005 ×1000 空洞发育

pore



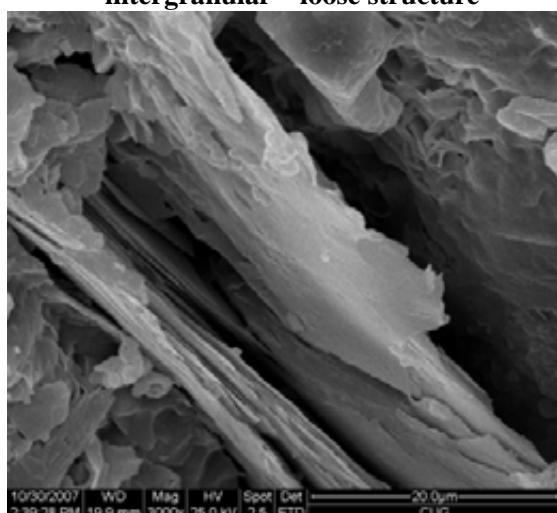
照片 71-006 ×1500 粒间孔隙发育结构疏松

intergranular loose structure



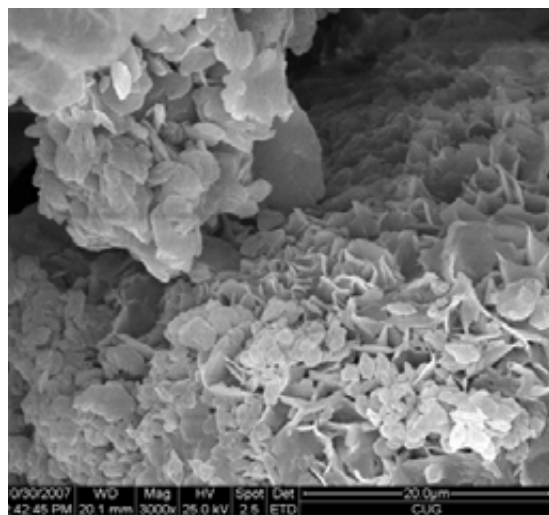
照片 71-007 ×2000 棱角状石英颗粒

angular quartz grain

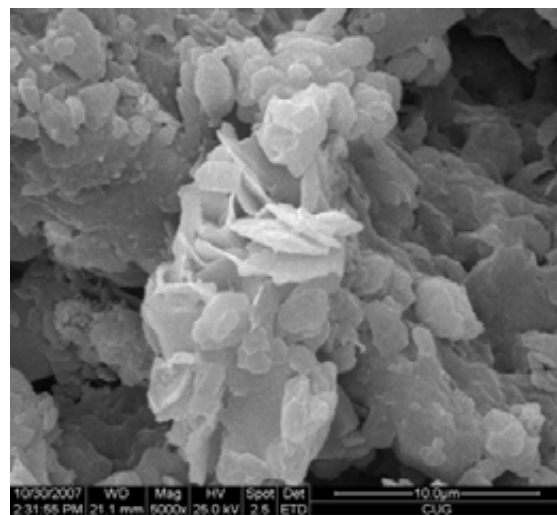


照片 71-003 ×3000 层状矿物定向排列

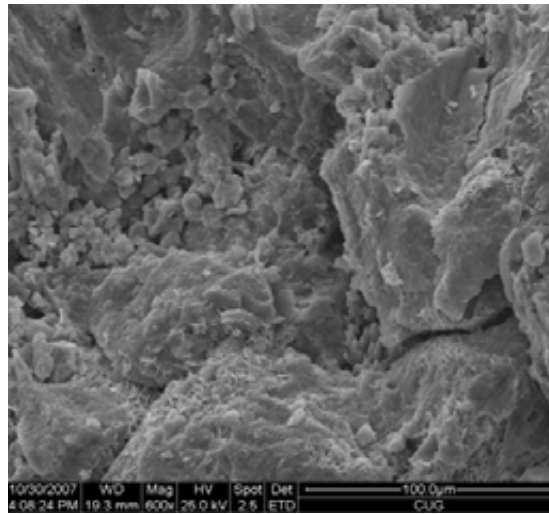
oriented mineral



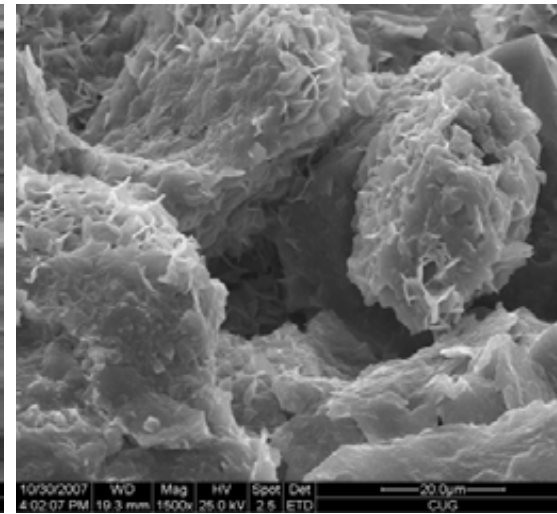
照片 71-004 ×3000 蒙脱石, 伊利石  
montmorillonite, illite



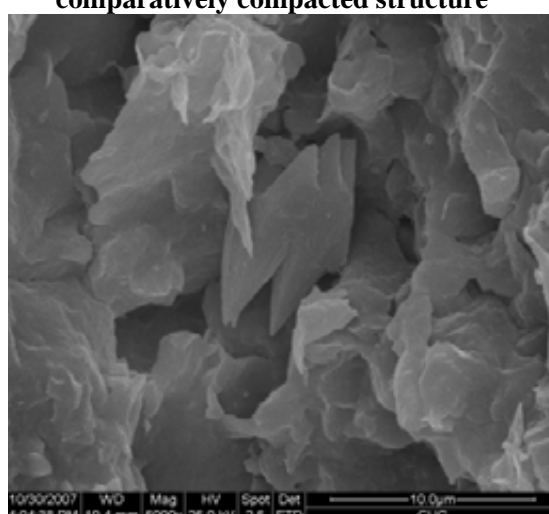
照片 71-001 ×5000 长石颗粒及蚀变  
feldspar, alteration



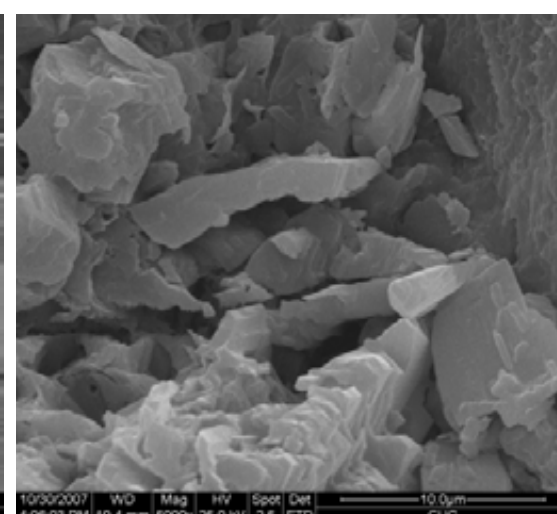
照片 72-004 ×600  
结构较致密, 表面有粘土矿物覆盖  
comparatively compacted structure



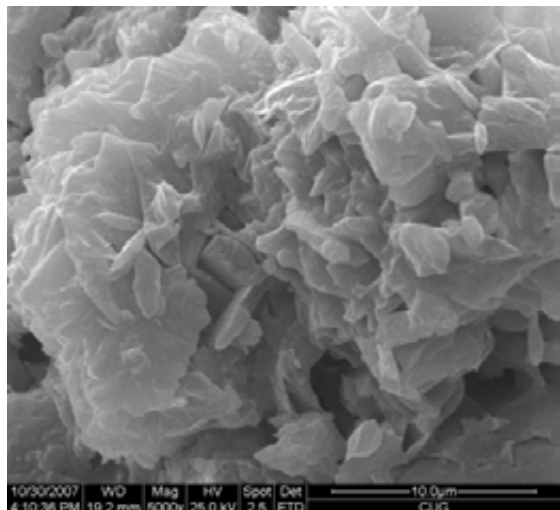
照片 72-001 ×1500 蒙脱石, 伊利石  
montmorillonite, illite



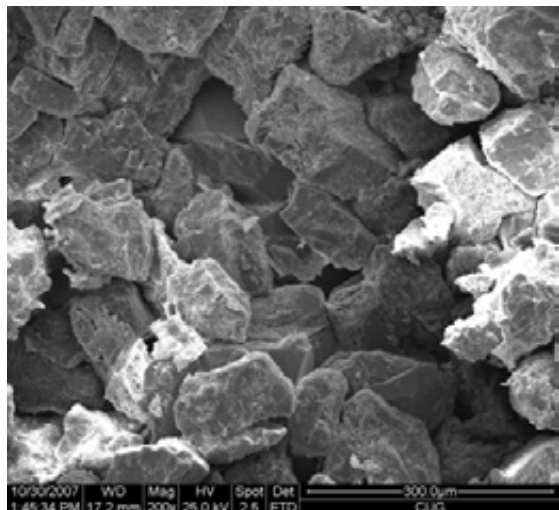
照片 72-002 ×5000 方解石  
calcite



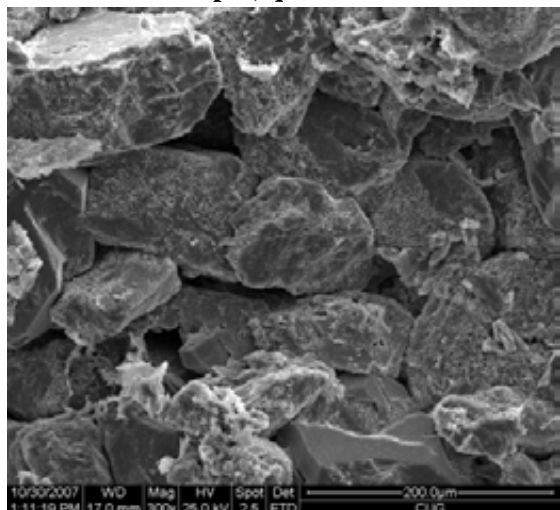
照片 72-003 ×5000 长石, 石英  
feldspar, quartz



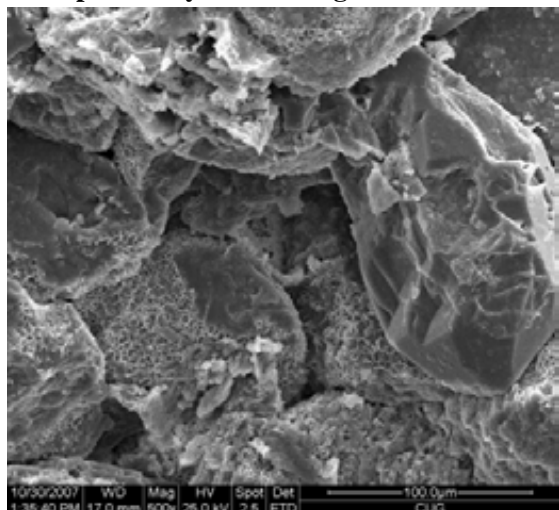
照片 72-005 ×5000 长石, 石英  
feldspar, quartz



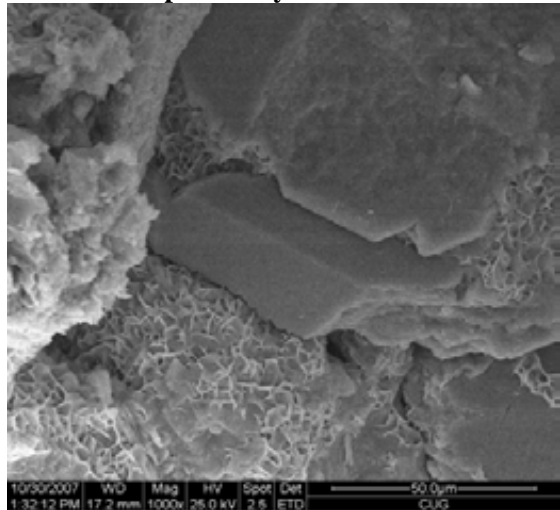
照片 82-008 ×200 颗粒间结构相对松散  
comparatively loose intergranular structure



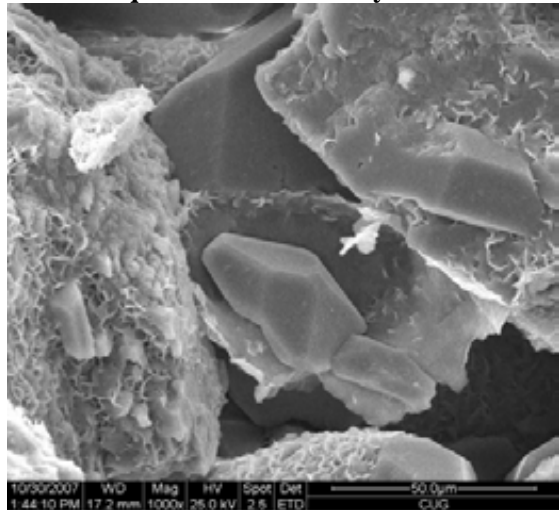
照片 82-001 ×300  
结构相对松散  
comparatively loose structure



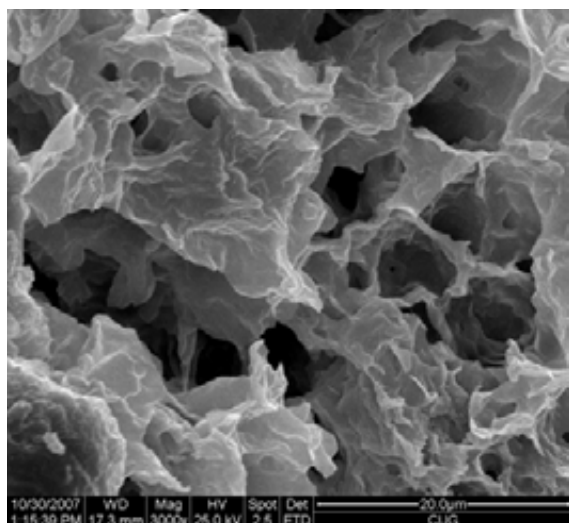
照片 82-005 ×500  
石英颗粒及次生矿物发育  
quartz and secondary mineral



照片 82-004 ×1000  
石英颗粒及次生粘土矿物  
quartz and secondary mineral

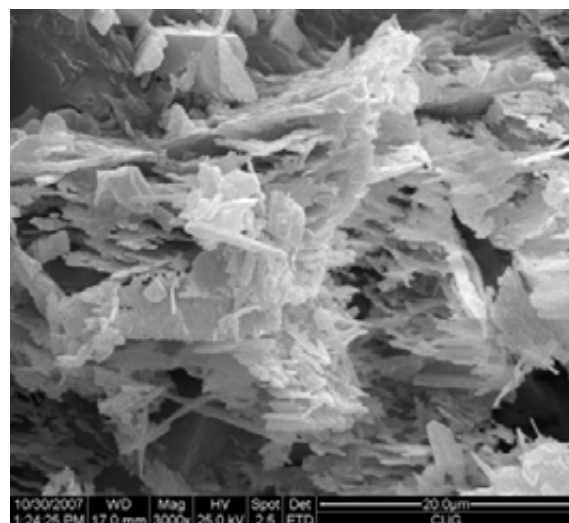


照片 82-007 ×1000  
石英蚀变  
quartz alteration



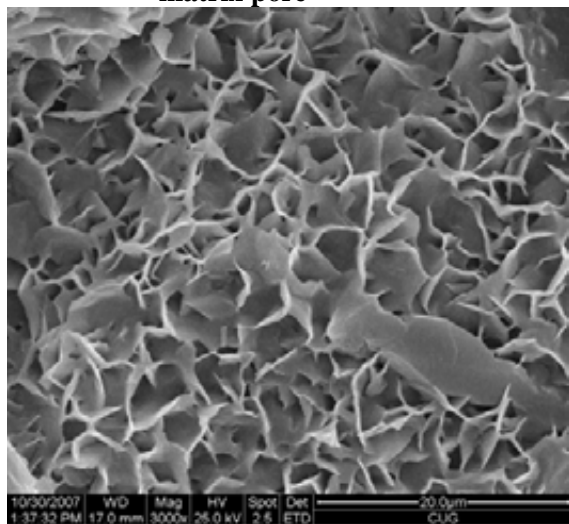
照片 82-002 ×3000

基质溶蚀空洞  
matrix pore



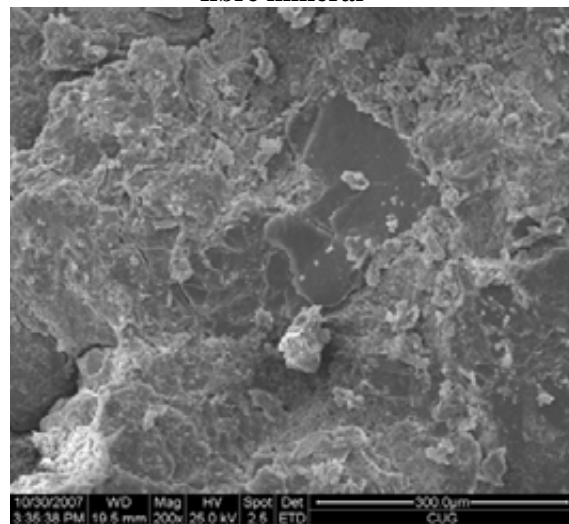
照片 82-003 ×3000

次生片状及纤维状矿物  
fibre mineral



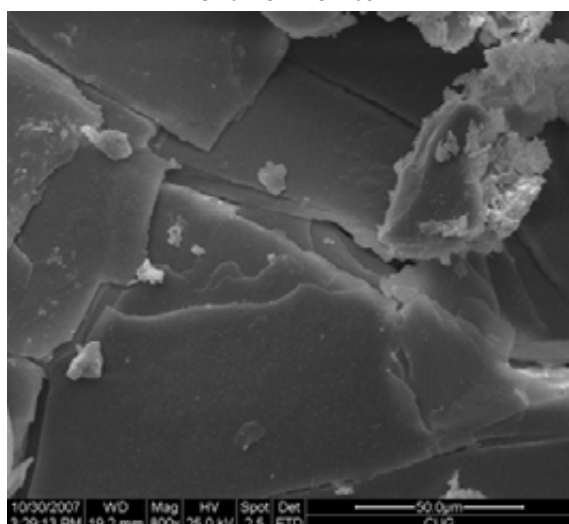
照片 82-006 ×3000 蒙脱石

montmorillonite



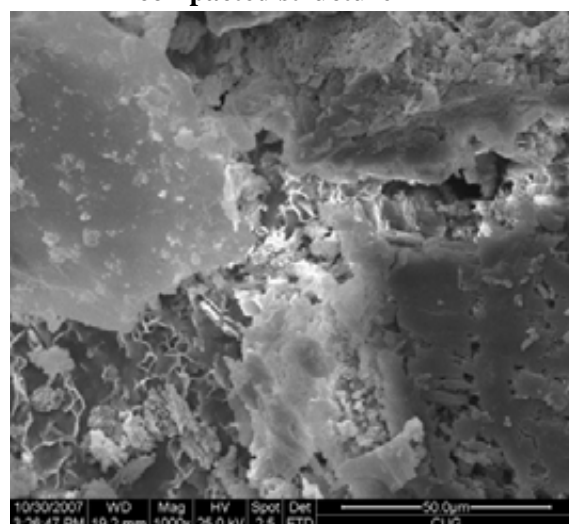
照片 89-004 ×200 结构致密，有粘土矿物覆盖

compacted structure



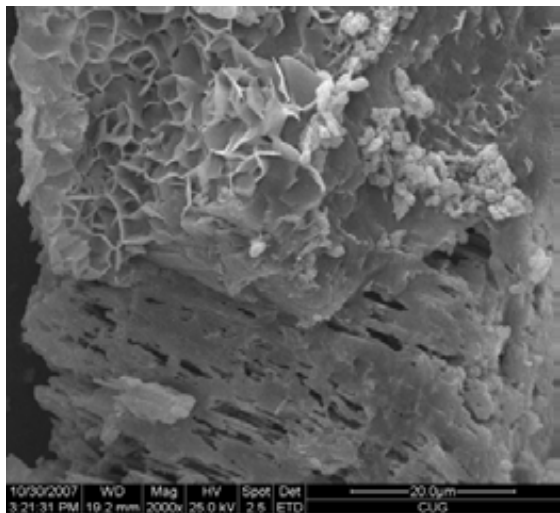
照片 89-003 ×800 长石解理面

feldspar cleavage

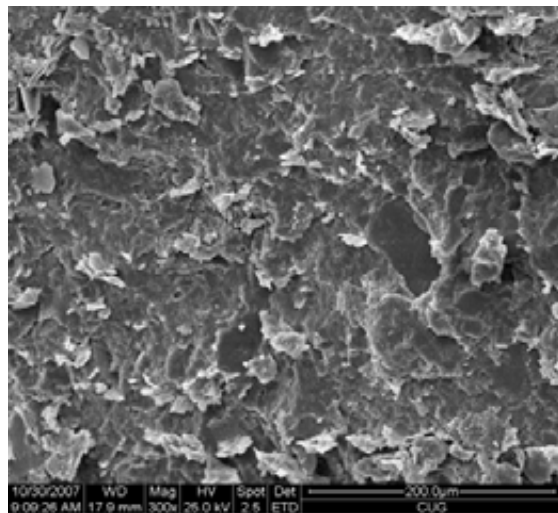


照片 89-002 ×1000 基质溶蚀空洞

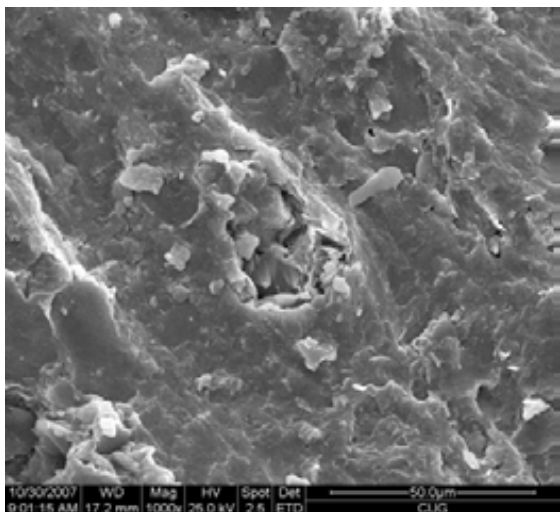
erosion pore



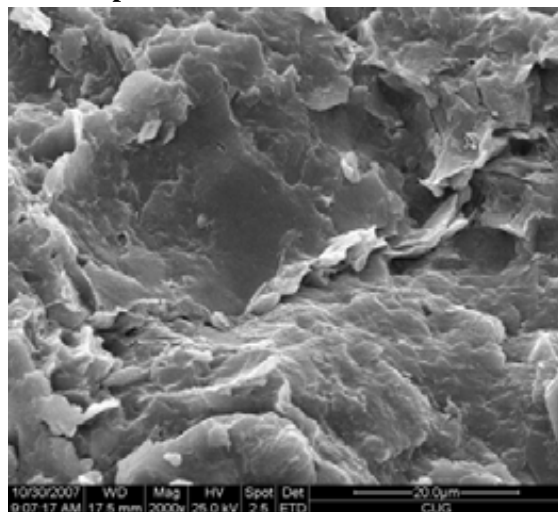
照片 89-001 ×2000 蒙脱石  
montmorillonite



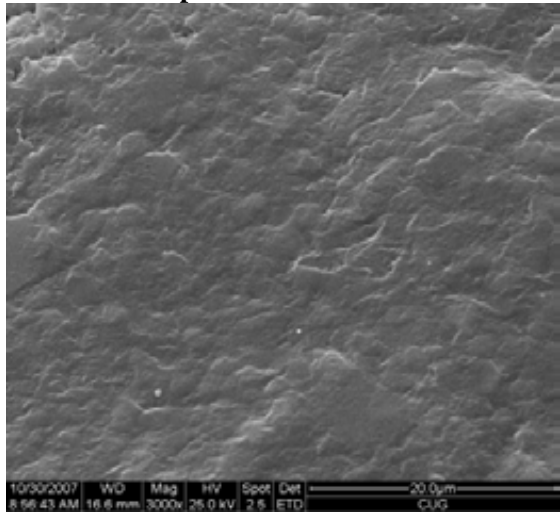
照片 90-006 ×300 结构致密, 无裂隙发育  
compacted structure without fissure



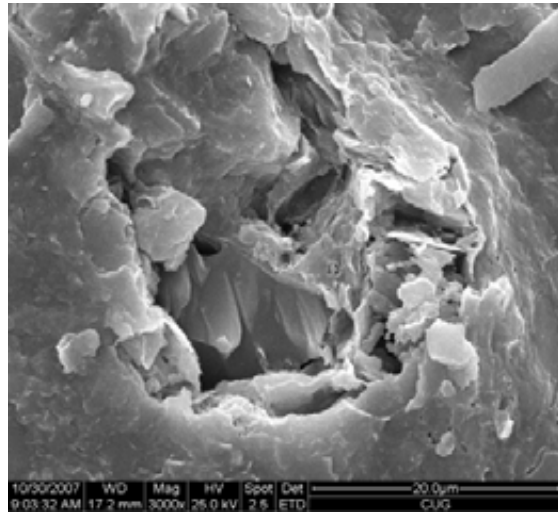
照片 90-003 ×1000 结构致密, 表面溶蚀  
compact structure



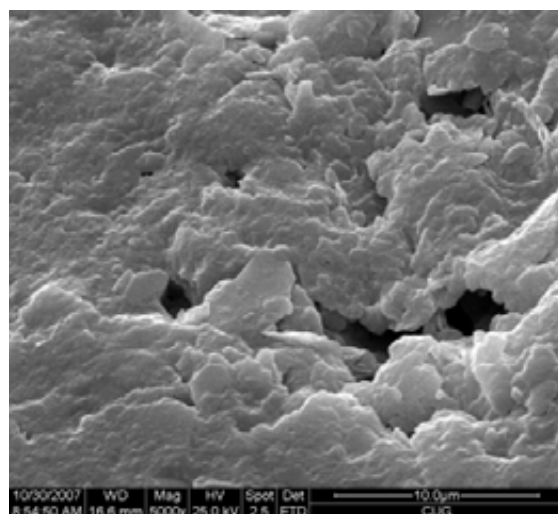
照片 90-005 ×2000 蒙脱石  
montmorillonite



照片 90-002 ×3000  
结构致密, 粘土矿物粘接  
compact structure



照片 90-004 ×3000  
泥岩中含少量粒状矿物  
claystone with a little granular mineral



照片 90-001 ×5000

结构致密，中偶有孔洞  
compact structure

3.5 砂岩物理力学性质	3.5 Physical Mechanical Characteristic of the Sandstone
<p>石刻区砂岩的岩石物理力学指标见表 3-6。由表可知，石刻砂岩的干单轴抗压强度为 30.65MPa，风干状态下抗压强度为 24.49 MPa，砂岩的饱和单轴抗压强度为 11.39MPa，软化系数为 0.46，属于易软化岩石。</p>	<p>The physical mechanical indices of the sandstone in Yuanjuedong is illustrated in Table 3-6, it can be seen from which that the dry monoaxial compressive strength of the sandstone is 30.65 MPa, the air-dried compressive strength is 24.49 MPa, the saturated monoaxial compressive strength is 11.39 MPa, the softening coefficient is 0.46. So, the sandstone in Yuanjuedong is easy for softening.</p>
<p>安岳圆觉洞石刻立壁岩体宏观结构上的一个明显特征是立壁砂岩体中发育有软弱泥质夹层。圆觉洞石刻区崖壁的砂岩体中发育有几层连续延伸的软弱泥质夹层，软弱夹层的形态为厚度不等的层状或透镜体状，成份多为泥质粉砂岩，孔隙率大，结构松散，强度低，软化系数低，抗风化能力差，在自然营</p>	<p>An obvious characteristic of the macrostructure of the Yuanjuedong stone carving standing wall is the weak muddy intercalation developed in the sandstone rock body. Several continuous extended weak muddy intercalations are developed in the sandstone of the cliff wall in Yuanjuedong, which are in laminar or lenticular form of different thickness. These ingredient of the weak intercalation is mainly pelitic siltstone, which is of high porosity, loosen structure,</p>

力作用下极易形成风化凹槽。

low intensity, low softening coefficient, poor weathering resistance capacity, and weathering flute is very easily formed in these weak intercalation area in the natural circumstance.

表 3-6 岩样物理力学性质试验成果

Tab.3-6 Experimental Results of the Physical Mechanical Characteristics of the Rock Samples

岩样 名称 Sample Name	状态 State	岩样编号 Sample No.	密度 density (g/cm <sup>3</sup> )	饱和吸水率 saturated water absorption rate (%)	单轴抗压强度 monoaixial compressive strength (MPa)	弹性模量 elastic modulus (GPa)	变形模量 deformation modulus (GPa)	泊松比 Poisson's ratio	软化系数 Softening coefficient
砂岩 Sandstone	烘干状态 Drying	B-1	2.19	7.71	29.972	4.018	2.734	0.200	0.46
		B-2			31.820	4.038	2.718	0.300	
		B-3			30.179	3.746	2.615	0.227	
	风干状态 Air drying	C-1	2.23	14.194	24.624	3.283	2.519	0.248	0.46
		C-2			24.360	3.11	2.221	0.284	
		A-1			14.199	2.199	1.759	0.249	
	饱水状态 Water	A-2	2.39	11.783	11.783	2.019	1.562	0.313	0.46
		Saturated			8.187	1.251	1.048	0.293	

Testing material: rock of geologic engineering

Testing reference: GB/T 50123-99

Testing Machine and Type: 电液伺服材料试验机 1346 型

Operated by Hu Xuejun

Calculated by Zhang Hui

Checked by Liu Jianhui

Reporting Date Nov. 10, 2007

测试类别: 地质工程岩土 测试依据: GB/T 50123-99

主要测试仪器及编号: 电液伺服材料试验机 1346 型

试验者: 胡学军 计算者: 张慧 校核者: 刘建辉

报出日期: 2007 年 11 月 10 日

## 第四章 圆觉洞环境地质 病害现状调查

在实施石窟保护工程前，首先要查明石窟有哪些病害以及病害的严重程度，才能采取有效的措施，消除或防止病害进一步的发展，以便在最小干预的原则下延长石窟的寿命，达到保护石窟的目的。

对于摩崖石刻等石质石窟，其病害主要是指由于自然地质作用和人类生产活动所引起的石窟主体和相关环境的破坏现象。根据导致病害的原因不同，环境地质病害可以分为两类：第一类环境地质病害，是由于自然地质环境引起的病害，如风化、岩体失稳等；第二类环境地质病害，是由于人类工程活动的影响，导致自然环境的变化，在改变后的自然环境影响下，引起原有（第一类）病害的加剧或诱发新的病害现象。如爆破震动，采矿引起的地面和边坡岩体的变形破坏，酸雨引起的岩石表面的风化加剧等。

根据对安岳圆觉洞石刻区的勘察调查，石刻区地下水的稳定水

## Chapter 4 Environmental Geological Disease Investigation about Yuanjuedong Rock Carving Area

The diseases category and their severity should be investigated clearly before the implementation about the grotto protection projects, which will improve the efficiency of the countermeasures and eliminate or prevent further deterioration of the diseases, thus to prolong the grotto life-span under the principle of minimum intervention.

The disease about stone grottoes as cliff sculptures means damage of the grotto itself and the relative circumstances, which resulted from natural geologic process or activities of human beings. According to the causes of the disease, the environmental geological diseases can be divided into two Classes: Class one is caused by the natural geological environment as weathering, rock destabilization, etc. Class two is the aggravation of Class one or newly induced disease under the altered natural circumstance, which is resulted from the engineering activity of mankind as blasting, deformation of the surface or slope rock caused by mining, amplified weathering of rock surface caused by acid rain, etc.

According to the investigation and exploration of Yuanjuedong, the permanent ground water level is far below the bottom

位远低于石刻底面，地下渗水对石刻的破坏不明显。由于圆觉洞大部分石刻造像均暴露于露天环境中，所以区内主要的环境地质病害为裂隙切割及其导致的掉块和岩体失稳、风化、苔藓等生物病害以及雨水冲刷的直接破坏。

中德合作研究项目选择 10 号龛和 37 号龛作为重点研究对象。

圆觉洞石刻区总计窟龛 103 个，造像 1933 尊。主要分布于云居山顶砂岩陡崖的南北两壁上，北崖壁雕凿有 1~14 号龛窟，其余窟龛分布在南崖壁上。

### 10 号龛：

释迦佛龛，龛形为方形平顶，高 6.4m，宽 4m，深 3m。正壁刻释迦牟尼佛立像，像高 6m。头高 1.3m，底座高 0.65m。

崖壁岩体砂岩呈现三种不同的韵律，地面以上 2.25m 范围内为微孔隙含岩屑质细砂岩，黄色为主，发灰。中部高 2.25m~3.70m 范围内岩体为软弱夹层，主要为青灰色孔隙式绢云母胶结含岩屑细~粉砂岩，夹有褐黄色泥质条带，其顶部斜层理发育。3.70m 以上范围为

of the stone carvings, and there is no obvious destroy caused by ground water seepage. Because most of the stone statues in Yuanjuedong are exposed in the open air, its key environmental geological diseases are the fissure cutting and resulting rock destabilization, dropping and weathering, biological damage by moss, and the direct destroy caused by rainwater erosion.

Group 10 and Group 37 in Yuanjuedong were chosen as the subjects investigated by Sino-German protection cooperation group.

There are 103 grottoes and niches and 1933 statues in Yuanjuedong, which are mainly distributed in the southern and northern side of the sandstone cliff of Mt. Yunjushan peak. Group No. 1 to 14 lie in the northern side of the cliff, and the others are located in the southern side.

### Group No. 10

The flat-top square grotto of Sakyamuni with height of 6.4m width of 4m and depth of 3 m. The front wall is carved with standing figure of Sakyamuni, and the figure is 6 meter high, while its head is 1.3 meter high and the base is 0.65 meter high.

The sandstone of the cliff rock presents three different layers. From the ground surface to 2.25 meter high is the lithic pack sand containing micro pore, which is mainly in the color of grey yellow. The middle part of the cliff from 2.25 to 3.70 meter is weak intercalation, which is mainly composed of lithic siltstone cemented with pore didrimit in caesious color, and brown yellow slime stripes in diagonal bedding on the top can be found. The upper part of the cliff (higher than 3.70m) is calcic syrosem-contained pack sand, which has relatively high capacity

钙质胶结含岩屑细砂岩，抗风化能力相对较高。

该龛整体保存相对完好。佛左手处有软弱夹层发育，厚度 5cm，历史上修补过。龛西壁外侧下部青灰色砂岩差异性风化，形成一个小凹槽，该区域风化掉块严重。由于受水冲刷，其上部形成小型掉块。主佛身上由于裂隙切割及风化影响多处产生掉块。龛左壁下侧有 20cm 宽，30cm 高，20cm 深的松动体。西壁两菩萨风化严重，形状不可辨，有水流冲刷的痕迹。

主佛右侧的东壁现存佛像的头部掉块，胸部受层面裂隙切割，形成宽 1mm 的裂隙，导致手部和头部破损。耳垂脱落，鼻子掉块，颈部风化严重。肘以下位于青灰色砂岩之中，风化起翘，形成掉块。腿部历史上做过修补。基座岩体风化起翘后形成空腔（图 4-1）。左壁西南角有一裂隙发育，上部闭合，下部较宽，曾封堵过。龛顶部有一水平状层面裂隙，宽 1cm，形成风化凹槽。

for weathering resistance

Grotto No. 10 is relatively well preserved. Weak intercalation is developed in the left hand of the Sakyamuni figure with 5 centimeter thick, which has been repaired before. Because of the differential weathering of the caesious sandstone on the outside of the west grotto wall, a small flute was formed, which causes serious rock falling in this area. Small falling pieces will be formed on the top of the grotto, which resulted from the water erosion. Because of the fissure cutting and weathering influence, quite a few falling pieces are formed on the Sakyamuni figure itself. A 20 cm wide, 30 cm high and 30 cm deep loosening rock can be found on the lower part of the grotto left side. The weathering of the two Bodhisattvas on the west wall is very serious, and the shape of which can not be identified, while clear water scouring can be observed.

On the right side of the Sakyamuni figure, i.e. the east wall, falling pieces can be observed on the existing Buddha head, whose breast is cut by the horizontal fissure with 1 mm gap, which damaged the Buddha hands and head, and the earlobe is broken off, the nose is loosened while the neck is seriously weathered. The part of Sakyamuni figure under the elbow is caesious sandstone, which is weathered to blister and lead to dropping pieces. Historical restoration has been made on the legs, and cavity resulted from weathering upwarping can be found in the base rock. A fissure, which is closed on the top with broad bottom, is developed on the southwest corner of the left wall, and historical blockage can be observed. A horizontal stratification fissure of 1 centimeter width lies in the grotto roof, which is weathered as flute.

左壁上部的飞天外侧由于雨水冲刷造成局部彩绘破坏，主佛后岩壁突出部位的彩绘保存较好。佛龛两侧青灰色砂岩以上部分岩体布满苔藓（图 4-2）。

The colored drawing outside of the Apsaras, which located in the upper part of the left wall, is partial destroyed by rainwater washing, while the colored drawing on the protruding part behind the Sakyamuni figure is well protected. The rock body above the caesious sandstone on each side of the grotto is covered by moss (Figure 4-2).



**图 4-1 10 号窟主佛右侧佛像风化病害现状**

**Fig.4-1 Weathering Condition of the Buddha on the Right Side of Sakyamuni figure in Group No.10**

### 37 号龛：

造像龛，方形平顶，高 1.00m，宽 0.90m，深 0.50m，龛内造像已毁。

该龛整体保存情况较差。主佛上半身缺失，龛顶层面处有一椭圆形掉块，龛右壁发育一条裂隙，隙宽 5mm。龛内风化严重，龛顶有风化

### Group No. 37

Flat-top square grotto of 1 meter high, 0.9 meter wide and 0.5 meter deep, and the figure of this grotto had been destroyed totally.

This grotto is badly preserved as a whole. The upper part of the Buddha figure is lost, an ellipse falling piece lies in the top stratification, and a fissure of 5 mm wide developed in the right wall. The weathering of this grotto is very serious, blister of the apical plate can be observed, and 1 to 5 mm thick



**图 4-2 10 号窟保存现状**

**Fig.4-2 Group No. 10**

起壳现象，壁面有剥落现象，剥落层厚度 1~5mm。沿龛两层壁面有苔藓覆盖（图 4-3）。

crumbling occurred on the wall. The two rock walls along the grotto are covered by moss.



图 4-3 37 号龛保存现状

Fig.4-3 Group No. 37



图 4-4 圆觉洞 10 号龛——释迦牟尼龛(2007.11)  
Fig. Group 10-Sakyamuni(Photodd in Nov. 2007)



图 4-5 圆觉洞 10 号龛——释迦牟尼龛(自《安岳石窟艺术》1997.04 出版)

Fig.4-5 Group 10-Sakyamuni from *The Grotto Art in Anyue*, Published in April, 1997

## 第五章 病害形成机理及影响因素分析

圆觉洞石刻处于自然地质环境中，长期经受各种自然营力和人类活动的影响和破坏，导致摩崖石刻产生了如前所述的风化病害、苔藓等生物风化病害、危岩体病害等。其中石刻表面的风化病害最为严重。

### 5.1 岩体表面风化

岩体表面的风化分为物理(机械)风化和化学风化。

#### 5.1.1 物理风化

岩石的物理风化作用是指使岩石发生机械破碎,而没有显著的化学成分变化的作用。物理风化的产物为：岩石碎屑、矿物碎屑。其方式和类型主要包括热力风化作用、冰劈(冰楔)作用、盐分结晶的撑裂作用、岩石卸荷引起的剥离作用

#### 5.1.2 化学风化

岩石发生化学成分的改变，形成新的次生矿物，称为化学风化。例如，岩石中含铁的矿物受到水和空气作用，氧化成红褐色的氧化铁；某些矿物吸收水分后体积膨胀；水和岩层中

### Chapter 5 Analysis about the Disease Mechanism and Its Influencing Factors

Yuanjuedong stone carvings exposed to the natural geological environment form a long term, and they are influenced and destroyed by natural agency and human activity. Therefore, diseases as weathering, biological influence caused by moss, unsafe rock, etc. are occurred on the cliff carvings, in which the weathering of the rock carving surface is the worst.

#### 5.1 Surface weathering of the rock body

Surface weathering of rock body can be classified into physical (mechanical) and chemical types.

##### 5.1.1 Physical weathering

Physical weathering means the mechanical crush of the rock without distinct change of the chemical ingredient, and the products of physical weathering will be rock and mineral fragment. Other types of physical weathering are as follows: heating power weathering, ice wedging, crystallization expansion, and load relief exfoliation, etc.

##### 5.1.2 Chemical weathering

Chemical weathering means the change of chemical ingredient of the rock, and new secondary mineral will be formed. For example, sorrel iron-oxide will be generated when the iron contained minerals in the rock react with water and air, the swell of certain minerals when they absorb water, the molecule structure change when the rock

的矿物作用，改变原来矿物的分子结构，形成新矿物。这些作用可使岩石硬度减弱、密度变小或体积膨胀，促使岩石分解。使石雕的结构构造遭到破坏，成分受到改造，并产生一些在地表条件下稳定的新矿物，例如石刻区砂岩中的长石经水解作用会形成高岭石、伊利石、绿泥石、氢氧化钾和二氧化硅。水化作用和氧化作用均会在石刻岩体表层产生褐铁矿交代浸染。

圆觉洞石刻区的物理风化类型，以热力风化作用和盐分结晶撑裂作用最为显著，结果常使岩石发生层层剥落，风化起翘、表面砂化等病害。此两种风化类型在安岳圆觉洞石刻区广泛存在，为岩石表面风化的主要类型。

圆觉洞石刻区气候温暖潮湿，有利于化学风化作用，因此化学风化也是安岳地区的主要风化类型。

## 5.2 生物风化

破坏石质文物的生物主要有两类：第一类为微生物即细菌、真菌、藻类及地衣等；第二类较高级生物：包括藓类、植物、昆虫等。

生物风化作用是指生物活动对岩石的破坏作用，一方面引起岩石的机

compositions react with water to form new mineral. The reaction mentioned above will reduce the hardness, decrease the density, and expand the volume of the rock, which leads to the break up of the rock body, and then destroy the stone carvings, change the rock ingredient, and produce new inactive minerals under the surface conditions. For instance, under the hydrolytic action, the feldspar in the sandstone of the carving area will form kaolinite, andreatite, chlorite, potassium hydroxide and silicon dioxide. Both hydration and oxidation will generate alternative impregnation of brown hematite on the carving stone surface.

The most prominent physical weathering in Yuanjuedong is heating power weathering and mineral crystallization expansion weathering, which often lead to the layered exfoliation, upwarping and smash of rock surface. These two kinds of weathering are widely existed in Yuanjuedong, which are the main types of rock surface weathering.

The warm and humid climate in Yuanjuedong is favorable for the chemical weathering, which also contributes greatly for the weathering in Anyue County.

## 5.2 Biological weathering

There are mainly two kinds of biology influencing the stone cultural relics, one is microbiology as bacteria, fungus, algae and lichens, while the other is higher level biology as moss, plants, insects, etc.

Biological weathering means the breakage influence of biological activities on the rock. On one hand, biological activity leads to mechanical destroy of the rock. For

械破坏，如树根生长对于岩石的压力可达 1.0~1.5MPa。这使深入岩石裂缝的植物根系能劈开岩石。另一方面植物根分泌出的有机酸，也可以使岩石分解破坏。此外，植物死亡分解可以形成腐殖酸，这种酸分解岩石的能力也很强。

安岳处于中部亚热带季风性湿润气候地区，空气潮湿、雨量充沛。圆觉洞崖壁上分布有大量的张开度很大的构造裂隙，且裂隙内被第四系泥土充填，给杂草、树木等植物创造了良好的生存环境。所以在保护区崖壁上，生长着大量的苔藓、野草及树木，这些植物尤其它们发达的根系，会对石刻产生以下影响：第一，延长了水分在岩体表面的储存时间，也就延长了向洞内渗水的时间，使得水和岩石作用的时间增加。第二，植物生长过程中，根系腐烂变质时会分泌出酸性物，加速岩石的溶解（蚀）作用。第三，树木杂草的根系会沿着裂缝往下不断发展，使裂缝不断扩大，造成岩体的崩塌及滑落。树木发育在裂隙内、风化凹槽及软弱夹层处对崖壁岩体破坏尤其显，其发达的根系使岩石崩解，使岩体失去强度，加速岩体失稳（图 5-1）。

example, the root growth of vegetables will generate 1.0 to 1.5 MPa press for the rock, so, the root system in the crack will split the rock. On the other hand, organic acid will be excreted from the plant root, which can decompose the rock. Furthermore, humic acid during the decomposition of the died vegetables has strong capacity for the destroy of the rock.

Anyue County lies in middle subtropical monsoon area with humid climate and plenty of rainfall. Lots of widely-opened structural fissures are distributed on the cliff wall of Yuanjuedong, which is filled in by the earth of Quaternary System, thus provide good living environment for the weed and tree. Large numbers of moss, weed and tree are grew on the cliff wall of SCA, these plants, especially their flourishing root system have great influence on the stone carvings. Firstly, the plants prolong the residence time of moisture on rock surface, and then extend the time of permeation to the grottoes, which will increase the acting time of water and rock. Secondly, during the plant growth, the rotting and deterioration of its root system will generate acid materials, which can accelerate the corrosion and dissolution of the rock. Thirdly, the plant root will extend continuously along the rock crack, which will expand the crack and lead to the break down and falling of the rocks. The trees growing in the fissure, weathering flute and weak interlayer have even greater influence on the cliff rock, and the flourishing root system will break down the rock, decrease its intensity and then increase the velocity of rock instability (Figure 5-1).



图 5-1 裂隙中根系发育产生生物风化病害

Fig.5-1 Biological Weathering Disease Resulted from Plant Root Growth

### 5.3 圆觉洞石刻病害的影响因素

影响圆觉洞摩崖石刻产生病害的因素主要有以下几方面：

#### 1、岩体材料的性质

圆觉洞所赋存的岩石为侏罗系厚层块状泥钙质胶结砂岩。其质地较坚硬，强度较高。但一般泥质胶结砂岩吸水率可高达 20%、饱水系数为 83%、软化系数为 0.21~0.70。垂直层面方向的饱和抗压强度为 5~12MPa。泥质钙胶结砂岩是一种软质易风化剥落的岩石，其主要造岩矿物长石在饱水条件下最易化学风化。这是崖壁上软弱夹层处产生风化凹槽的主要原因。

### 5.3 Influencing factors on the Disease of Yuanjuedong stone carvings

The main influencing factors on the disease of Yuanjuedong cliff carvings are as follows:

#### 1. Characteristic of the rock material

The rock of Yuanjuedong is the mud-calcic cementitious sandstone of the Jurassic Period ( $J_{3sn-1}$ ) in the form of thick layers, which is of high hardness and intensity. Generally speaking, the water absorption rate of mud cementitious sandstone is as high as 20 percent, the water saturation coefficient is 83 percent, the softening coefficient ranges from 0.21 to 0.70, and the saturated compression strength of vertical direction ranges from 5 to 12 MPa. The mud cementitious sandstone is soft rock and liable to weathering, the main composition of which, i.e. feldspar is very susceptible to chemical

## 2、裂隙效应

由于地质构造运动、自然环境及人类活动的影响,圆觉洞石刻区崖体中形成了大量的裂隙,这些裂隙大致可分为层面裂隙、构造裂隙、卸荷裂隙、风化裂隙。这些裂隙的切割,使崖壁岩体易发生滑动和倾覆破坏。影响了崖壁岩体的稳定性。

层面裂隙是在成岩过程中形成的。

构造裂隙主要指岩体受构造应力作用所产生的破裂面。

卸荷裂隙主要是在近地表的岩体中分布,它是由于岩体中应力释放和调整而造成的。

风化裂隙一般是指岩体表面风化带内产生的不规则裂隙。不过,当含有较多易风化矿物的岩层向下延伸得比较深时,它也有可能沿裂隙带伸展到岩体的内部很深的部位。

圆觉洞石刻区岩层构造主要包括构造裂隙与卸荷裂隙。构造裂隙一般倾角近于直立。卸荷裂隙一般隙宽较大。这些裂隙的存在,不仅破坏了岩体完整性,同时成为空气、水气和水的循环通道。这些裂

weathering under the water saturation condition, which is the main reason for the weathering flute in the weak embedding stratum of the cliff.

### 2. Fissure effect

Because of the influence of geological structure movement, natural environment and human activity, plenty of fissures are formed in the cliff of YJD SCA, which can be classified as horizon fissure, tectonic fissure, relief joint and weathering fissure. Under the cutting effect of these fissures, the cliff rock body is subject to sliding and turning over, thus influence the stability of the rock body itself.

Horizon fissure is generated during the formation of the rock.

Tectonic fissure means the fracture surface produced by the influence of tectonic stress on the rock body.

Relief joint is mainly distributed in the rock near the ground surface, which is resulted from the stress relief and adjustment.

Generally speaking, weathering fissure refers to the irregular crack in the weathering zone of rock surface. However, when the rock containing easy weathering minerals extends deep to ground, the weathering fissure will also spread to the deep part of the rock body.

The rock stratum structure disease in Yuanjuedong is mainly composed of tectonic fissure and relief fissure. The tilt angle of tectonic fissure is almost perpendicular, and the relief fissure is always of greater width. These fissures not only destroy the integrity of the rock body, but also provide the passage for

隙的存在，在影响岩体稳定性的同时还加剧了风化作用的发展。

### 3、气温效应

安岳的气候为亚热带季风性湿润气候，四季分明，气候温暖，雨量丰沛，蒸发量稍大于降雨量，日照偏少、湿度大，夏长、冬暖。年平均气温  $17.6^{\circ}\text{C}$ ，年均气温变化不大，极端高温  $40.2^{\circ}\text{C}$ ，极端低温  $-3.7^{\circ}\text{C}$ 。昼夜温差，季度温差可引起岩体热胀冷缩，产生温度应力，破坏岩石的表面浅层结构，加速岩石风化剥落。

### 4、水侵蚀

岩石中的水包括结合水和自由水，它们对岩体的作用主要是改变岩体的物质成份和结构形态。水对岩体的作用主要有：

(1) 楔劈作用：水分子在浸润作用下，挤入细微裂缝中，对裂缝两壁施加一定的压力，使裂缝增大。

(2) 润滑作用：水进入各种裂隙中，形成结合水膜，当裂隙两壁发生相对剪切位移时，水分子将固体表面隔开而起到润

the air, water and aqueous gas, and then decreases the stability of the rock body while accelerate its weathering.

### 3. Temperature effect

The weather of Anyue County is subtropical humid climate of middle monsoon area, with four clear seasons, mild temperature, abundant heat, plentiful rainfall, less sunshine, high humid, long summer and warm winter, while the evaporation is slightly higher than precipitation. The average temperature of long term is  $17.6$  degree centigrade without great changes during the whole year. The maximum temperature is  $40.2$  degree centigrade while the minimum is minus  $3.7$ . The temperature difference between day and night and between different seasons causes the swell and shrink of the rock, which generates temperature stress and then destroys the superficial structure of rock surface, accelerates the weathering exfoliation.

### 4. Water erosion

The water in the rock includes free water and bound water, and their main influence on the rock is to change the substance ingredient and structural form. The influences of water on rock are as follows:

(1) Wedging action: water molecular will wedge into the micro fissures under the sweating action, and then exert certain stress to the fissure wall to make it wider.

(2) Lubrication: the water molecular in the fissure forms bound water film, which will separate the solid surface of the fissure wall during their relative shear displacement, and act as lubricant

滑作用，使岩体摩擦力减少，变形性能提高。

(3) 溶解作用：有可溶盐或胶体矿物连接的岩石浸水时，可溶盐或胶体水解，使原来较强的胶结连结变为较弱的水胶连结，连结力减弱，摩擦力降低，岩体强度降低。如果某些铝硅酸盐矿物在水参与下分解成新的次生粘土矿物，岩体强度会显著地降低。

(4) 潜蚀作用：渗透水流将岩石中的可溶物质溶解带走，有时将岩体中的细颗粒冲走，这种潜蚀作用大大的降低了岩体强度。

(5) 水、岩之间的应力耦合作用：岩体中的渗透水流通过各种裂隙流动，而裂隙的渗透性对应力是极为敏感的。岩体中应力的作用极大地影响着岩体的渗透性，而渗透性的变化又反过来影响岩体中的应力分布，进而影响岩体的强度和稳定性。

水对岩体的影响往往是几种作用同时发生。饱水后，岩体的强度和变形模量都降低，常用软化性来表征饱水后水对岩石强度影响。由于水的影响，岩体的力学性质有所下降。当饱水的裂隙化岩体突然受力，水来不及排出时，岩体空隙中将产

to reduce the friction force and increase the deformation capacity.

(3) Dissolution: when the rock containing soluble salt or connected with colloid mineral submerge is soaked with water, the slat or colloid will be hydrolyzed, and the strong agglutination will change to weak water colloid connection, which will reduce the friction force and decrease the intensity of the rock. For example, some aluminumsilicate minerals will be decomposed to new secondary clay minerals when reacting with water, which will remarkably reduce the rock intensity.

(4) Underground erosion: the permeated water will take away the soluble substance and even the fine particles in the rock, which will greatly decrease the rock intensity.

(5) Stress coupling between water and rock: the permeated water in the rock will flow through the fissures, whose permeability is very sensitive to the stress. The stress in the rock influences its permeability greatly, and contrarily, the change of permeability will influence the stress distribution in the rock, which then affects the intensity and stability of the rock body.

The influences of water on rock body are always happened simultaneously. The rock intensity and deformation modulus will decrease when saturated with water, so softness will be used to characterize the intensity of water saturated rock. The mechanical property of rock will decrease under the influence of water. When the water

生一定的空隙水压力,从而降低了岩体的抗剪强度,甚至使岩石微裂隙端部处于受拉状态而破坏岩石的连结。

安岳圆觉洞石刻区的水侵害主要是由降雨引起的。

安岳县年降雨量为 1025.8mm,最大年份年为 1420.2mm,最小年份年为 688mm。降水多集中在 7—9 月,又以 7 月份居多。暴雨、大雨等冲刷岩体表面,雨水渗入裂隙中形成较高的静水压力和渗透压力,破坏岩体。水会破坏岩石中的胶结物,砂岩在接近饱和时可损失强度的 15%。

## 5、空气作用

大气环境质量的恶化,也是石质文物损坏的因素之一。虽然大气对岩石材料的破坏作用在一般情况下是比较缓慢的,不易被人们所察觉,但它确实每日每时都在影响着石刻材料的耐久性。有害气体与大气中的洁净程度有关,随着工业的发展,在城市中大气污染问题日益严重,有害气体对文物制成材料的不利影响也就日趋突出。对石质文物危害性较大的几种典型

saturated rock suddenly under stress and the water can not be discharged, certain pore water pressure will be generated in the open space of the rock. Consequently, the shear strength will be reduced, which may even destroy the rock cohesion by pulling the top of micro fissure in the rock.

The water erosion in Yuanuedong is mainly caused by rainfall.

The average precipitation in Anyue Country is 1025.8 mm per year, and the maximum annual rainfall is 1420.2 mm while the minimum is 688.3 mm. The precipitation is often occurred from July to September, and July is always of the highest volume of rainfall. The rainstorm and heavy rain will flush the rock surface and infiltrated into the fissure, which will generate high hydrostatic pressure and osmotic pressure and then destroy the rock body. Water can destroy the cementing material, and the sandstone will lose 15 percent of its intensity when saturated with water.

## 5. Atmosphere effect

Air quality deterioration is also one of the influencing factors on the stone cultural relics of Anyue County. Although the influence of atmosphere on rock material is very slow, which is often imperceptible, it affects the durability of the stone carvings all the time. With the industrial development, the air pollution in urban area becomes more and more serious, and its adverse impact on the material of the cultural relics gets more and more remarkable. Some typical gases which have relatively great influence on the stone

气体有：二氧化硫、三硫化氢、臭氧( $O_3$ )和氯气。



**图 5-2 人为刻画形成文物损害**  
**Fig.5-2 Damage Caused by Human Activity**

## 6、人类活动影响

人类的活动对安岳石刻文物也造成了极大的伤害，如历史上的几次灭佛运动，很多文物尽遭破坏。一些石窟内的石造像、浮雕石刻、碑刻题记都毁坏消失。

现在，随着旅游行业的发展，景区每年要接待大量的游客，游客的一些不文明活动对也有一定的破坏，如，在文物上乱写乱画(图 5—2)，肆意毁坏等。祭祀的

carvings are as follows: sulfur dioxide, sulfur trioxide, ozone and chlorine.



**图 5-3 祭祀烧香对文物的烟熏**  
**Fig.5-3 Smoking Disease Caused by Sacrifice and Perfume Burning**

## 6. Influence of Human Activity

Human activities have incredible adverse influence on the stone carvings of Anyue County, and lots of cultural relics have been destroyed during the anti-Buddhism movements in the history, some of the stone figures, emboss carvings and stele inscriptions in the grottoes were fully devastated.

With the thrive of tourism, quite a lot tourists will visit the Yuanjuedong stone carving area every year, and some of the incivilization activities as unexpected writing and inscription, willful destroy, etc., will influence on the rock cultural relics to some extent. Moreover, the

烟火对造像龛窟会造成烟熏破坏（图 5—3）。

smoke and fire during sacrifice will cause smoking diseases on the grottoes.

## 第六章 圆觉洞危岩体稳定性评价

根据现场调查,圆觉洞石刻区共发现4处危岩体。现分别对这4处危岩体进行分析评价如下。

根据室内试验的成果,砂岩的重度取 $\gamma=21.86\text{kN/m}^3$ ;砂岩体剪切强度参数取 $c=500\text{kPa}$ , $\varphi=32^\circ$ ;泥质粉砂岩剪切强度参数取(软弱夹层带) $c=10\text{kPa}$ , $\varphi=23^\circ$ ;按国家现行的《建筑抗震设计规范》(GB 50011—2001),考虑文物的价值和不可再生的特殊性,圆觉洞石刻保护区考虑地震力作用时,按地震烈度VII度设防,水平地震影响系数取 $\alpha_h=0.127$ ,(水平地震加速度值 $1.27\text{m/s}^2$ )。

圆觉洞石刻区的危岩体为各类裂隙和软弱夹层相交形成的孤立巨块石,其可能的破坏模式有2类。第1类破坏模式为单滑面滑动破坏。第2类岩体中有近直立的宽大裂隙及风化凹槽发育,岩体以块石底部风化凹槽最深处为支点,向临空方向发生拉裂倾覆破坏。岩土工程上多采用极限平衡理论计算危岩体的稳定性系数。

当危岩体稳定性系数 $K=1.0$ 时,危岩体处于极限平衡状态。在石质文

## Chapter 6 Stability Assessment about the Unsafe Rocks in Yuanjuedong Stone Carving Area

According to the onsite investigation, there are 4 unsafe rocks in Yuanjuedong. The analysis and assessment of the unsafe rocks are as follows:

It can be concluded from laboratory experiments that the density of the sandstone  $\gamma$  is  $21.86\text{kN/m}^3$ , the shear strength coefficients  $c$  and  $\varphi$  are  $500 \text{ kPa}$  and  $32^\circ$  respectively, and the shear strength coefficients of pelitic siltstone (weak embedded stratum)  $c$  and  $\varphi$  are  $10 \text{ kPa}$  and  $23^\circ$  respectively. Based on the Code for Seismic Design of Buildings (GB 50011-2001) and take into consideration of the value and irreproducibility of the cultural relics, the seismic intensity should be grade IV and the horizontal seismic influencing coefficient  $\alpha_h$  should be 0.127 (i.e., the horizontal seismic acceleration rate is  $1.27 \text{ m/s}^2$ ) during the design of the protection projects in Yuanjuedong.

The unsafe rocks in Yuanjuedong are isolated rock bodies resulted from the intersect of different fissures and weak intercalation, and there are two possible destroy types. Type one is sliding destroy caused by interface movement. Type two is break down destroy to the rock free face, which is resulted from the approximate vertical wide fissure and weather flute, i.e. the rock body will be pulling apart taking the deepest point of the flute as the pivot. The stability coefficient of the rock body is always calculated by theory of ultimate equilibrium in geotechnical engineering.

The unsafe rock body is in the state of ultimate equilibrium when the stability coefficient  $K$  equals 1.0. In the engineering practice of stone cultural relics protection,

文物保护工程实践中,  $K$  值等于 1 或稍大于 1, 并不能说明石刻岩体处于稳定状态。工程上  $K$  值必须满足一个最起码的安全需要, 称为容许安全系数, 用  $K_f$  表示。对于石质文物岩体加固的容许安全系数, 目前尚无明确规定。由于文物的重要性, 建议分析石质文物岩体的稳定性时, 取  $K_f=1.3$  作为容许安全系数, 并按下列标准进行稳定性分析。

$K < 1.0$	不稳定
$1.0 \leq K \leq 1.3$	欠稳定
$K > 1.3$	稳定

## 6.1 1号危岩体稳定性计算

1号危岩体位于7号净瓶观音龛的左壁, 高2.2m, 宽1.22m, 厚0.9m。危岩体下部距地面2.9m。在危岩体上下各有一层软弱夹层发育。由于倾角为65°的卸荷裂隙与软弱夹层的切割, 使危岩体上部与后方山体分离, 仅下部高约0.8m的岩体支撑上部危岩体的全部荷载(图6-1)。危岩体在重力和外界营力的作用下可能发生的破坏模式为沿裂隙面向下发生剪切滑动破坏。

$K$  等于或稍大于 1.0 并不意味着石刻在稳定情况下, 而  $K$  必须满足最起码的安全要求, 即所谓的容许安全系数  $K_f$ 。目前对石质文物岩体加固的容许安全系数没有明确规定。由于文物的重要性, 建议在分析石质文物岩体的稳定性时, 取  $K_f=1.3$  作为容许安全系数, 并按下列标准进行稳定性分析:

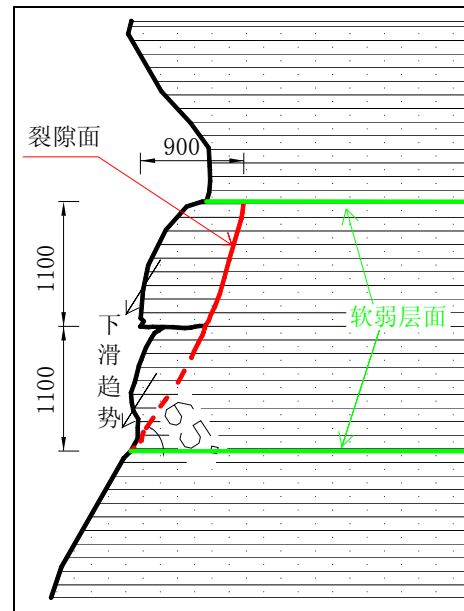
$K < 1.0$	unstable
$1.0 \leq K \leq 1.3$	metastable
$K > 1.3$	stable

### 6.1 Stability calculation for No. 1 unsafe rock

No. 1 unsafe rock lies on the left wall of No. 7 Jingping Kwan-yin Niche, which is 2.2 m high, 1.22 m wide, 0.9 m thick and 2.9 m above the ground surface. Both on the bottom and top of the unsafe rock No. 1, a weak intercalation is developed. Because of the intersect of the relief joint with 65° dip angle and the weak intercalation, the upper part of the unsafe rock is separated from the mountain body, and only the 0.8 m lower part supports the load of the whole unsafe rock, which can be seen from Fig 6-1. The possible destroy mode of this unsafe rock under the influence of gravity and circumstances is downward shear sliding destroy along the fissure surface.



(a)



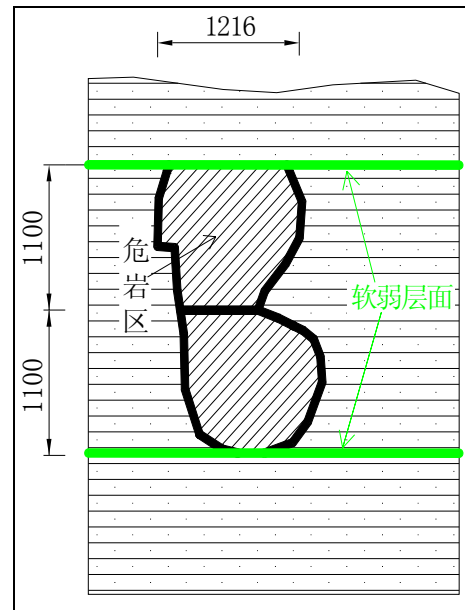
(b)

1号危岩体纵剖面图

Longitudinal Profile of No. 1 dangerous Rock



(c)



(d)

1号危岩体正面图  
Front View of No. 1 Unsafe Rock

图 6-1 1号危岩体

Fig. 6-1 Dangerous rock mass of No. 1

按单面滑动剪切破坏方式进行分析计算，  
其计算公式为：

The equation for one side sliding  
destroy resulted from shear force  
influence is as follows:

$$K = \frac{W_r}{W_s} = \frac{G \times \cos\alpha \times \tan\phi + c \times S}{G \times \sin\alpha} \quad (6-1)$$

考慮地震力作用時，其計算公式為：

$$K = \frac{W_r}{W_s} = \frac{(G \times \cos\alpha - Q \times \sin\alpha) \times \tan\phi + c \times S}{G \times \sin\alpha + Q \times \cos\alpha} \quad (6-2)$$

上式中：

K—危岩體穩定性系數；

$W_r$ —抗滑力(kN)；

$W_s$ —滑動力(kN)；

G—危岩體重力(kN)， $G = \gamma \times A \times B$ ；

$\gamma$ —危岩體的重度( $\text{kN}/\text{m}^3$ )；

A—危岩體在剖面上的面積( $\text{m}^2$ )；

B—危岩體在垂直於剖面方向上的寬度(m)；

$\alpha$ —危岩體滑面與水平方向的夾角( $^\circ$ )；

$Q$ —作用在危岩體上的水平地震力(kN)， $Q = \alpha_h \times G$ ；

$\alpha_h$ —水平地震影響系數；

$\phi$ —危岩體破壞面的內摩擦角( $^\circ$ )；

c—危岩體破壞面的粘聚力(kPa)；

S—危岩體潛在破壞面的粘着部分的面積( $\text{m}^2$ )。

不考慮地震力作用的影響：

The calculation equation will be changed as 6-2 when the seismic effect is taken into consideration:

Where

K is the stability coefficient of the unsafe rock

$W_r$  is the skid resistance force (kN)

$W_s$  is the skid force (kN)

G is the gravity of the unsafe rock, which equals  $\gamma \times A \times B$ , and  $\gamma$  is the unsafe rock density ( $\text{kN}/\text{m}^3$ ), A is the sectional area ( $\text{m}^2$ ) and B is the width perpendicular to the plane section of the unsafe rock (m)

$\alpha$  is the included angle of the sliding face to the horizontal direction ( $^\circ$ )

$Q$  is the horizontal seismic force influencing on the unsafe rock, which equals  $\alpha_h \times G$ , and  $\alpha_h$  is the horizontal influencing coefficient by earthquake

$\phi$  is internal friction angle of the failure plane of the unsafe rock ( $^\circ$ )

c is the cohesion force of the failure plane of the unsafe rock (kPa)

S is the adhesion area of the potential failure plane of the unsafe rock ( $\text{m}^2$ )

When the seismic influence is not considered:

危岩体的重力

$$G = \gamma \times A \times B = 21.86 \times 1.0 \times 0.9 = 196.74 \text{ kN}$$

根据现场调查裂隙的连通情况，确定危岩体潜在破坏面的粘着部分面积为  $S=0.97\text{m}^2$ 。

将已知各参数带入式（6-1）中，得

$$K = \frac{W_r}{W_s} = \frac{G \times \cos \alpha \times \tan \phi + c \times S}{G \times \sin \alpha} = \frac{196.74 \times \cos 65^\circ \times \tan 32^\circ + 10 \times 0.97}{196.74 \times \sin 65^\circ} = 1.001$$

考虑地震力作用的影响：

水平地震力

$$Q = \alpha_h \times G = 0.127 \times 196.74 = 24.99 \text{ kN}$$

$$K = \frac{W_r}{W_s} = \frac{(G \times \cos \alpha - Q \times \sin \alpha) \times \tan \phi + c \times S}{G \times \sin \alpha + Q \times \cos \alpha} = 0.87$$

计算结果表明，在不考虑地震影响的条件下，1号危岩体处于极限平衡状态。在考虑地震因素影响的条件下，危岩体的稳定性系数仅为0.87，将发生危岩体崩塌。应及时采取措施对1号危岩体进行加固处理。建议进行锚固处理。

The gravity of the unsafe rock is

According to the onsite fissure connection investigation results, the adhesion area of the potential failure plane of the unsafe rock is determined, i.e.  $S=0.97\text{m}^2$ .

Then, it can be calculated from equation 6-1

When the seismic influence is considered:

The horizontal seismic force is

It can be concluded from the calculation results that the No. 1 unsafe rock is in the state of ultimate equilibrium when the seismic influence is not taken into consideration. However, when the seismic influence is taken into consideration, the rock stability coefficient is only 0.87, which means break down will occur about this rock. Therefore, the reinforcement about No. 1 unsafe rock should be carried out timely, and anchoring measures are recommended.

## 6.2 2号危岩体稳定性计算

2号危岩体位于7号净瓶观音龛的右壁（图6-2）。裂隙J1、J2在7号龛的右壁上部飞天部位与软

## 6.2 Stability calculation for No. 2 unsafe rock

As shown in Figure 6-2, No. 2 unsafe rock lies on the right wall of No. 7 Jingping Kwan-yin Niche. J1 and J2 fissure intersect with the weak intercalation on the upper part of right wall of No.7 Niche, which is in the

弱夹层交切组合，形成一高 1.6m，上部宽 1.2m，下部宽 0.6m，厚 0.6m 的危岩体。飞天石刻部分赋存于危岩之上。危岩体受裂隙切割，上部与后方岩体分离，仅下部小部分与山体粘结。危岩体的可能破坏形式为沿裂隙面剪切滑动破坏。

## 2 号危岩体的重力

$$G = \gamma \times A \times B = 21.86 \times 0.53 \times 0.6 = 69.51 \text{ kN}$$

根据现场调查裂隙的连通情况，确定危岩体潜在破坏面的粘着部分的面积  $S=0.48\text{m}^2$ 。

在不考虑地震力作用下的影响时：

将已知各参数带入式（6-1）中，得：

$$K = \frac{W_r}{W_s} = \frac{G \times \cos \alpha \times \tan \phi + c \times S}{G \times \sin \alpha} = \frac{69.51 \times \cos 64^\circ \times \tan 32^\circ + 10 \times 0.48}{69.51 \times \sin 64^\circ} = 1.303$$

考虑地震力作用的影响：

水平地震力

$$Q_h = \alpha_h \times G = 0.127 \times 69.51 = 8.83 \text{ kN}$$

将已知各参数带入式（6-2）中，得：

$$K = \frac{W_r}{W_s} = \frac{(G \times \cos \alpha - Q_h \times \sin \alpha) \times \tan \phi + c \times S}{G \times \sin \alpha + Q_h \times \cos \alpha} = 1.15$$

计算结果表明，在不考虑地震因素影响的条件下，危岩体的稳定性系数为 1.303，处于稳定状态。

position of the apsaras, and lead to an unsafe rock with 1.6 m high, 0.6 m thick, 1.2 m wide in the top and 0.6 m thick in the bottom. The stone carving of apsaras lies on the unsafe rock. The unsafe rock is intersected by the fissures, which results in the separation of the upper part from the mountain body, and only small lower part is adhered on the mountain. The possible destroy mode of this unsafe rock is shear sliding destroy along the fissure surface.

The gravity of No.2 unsafe rock is

$$G = \gamma \times A \times B = 21.86 \times 0.53 \times 0.6 = 69.51 \text{ kN}$$

According to the onsite fissure connection investigation results, the adhesion area of the potential failure plane of the unsafe rock is determined, i.e.  $S=0.48\text{m}^2$ .

When the seismic influence is not considered:

It can be calculated from equation 6-1 that

When the seismic influence is considered:

The horizontal seismic force is

$$Q_h = \alpha_h \times G = 0.127 \times 69.51 = 8.83 \text{ kN}$$

It can be calculated from equation 6-2 that

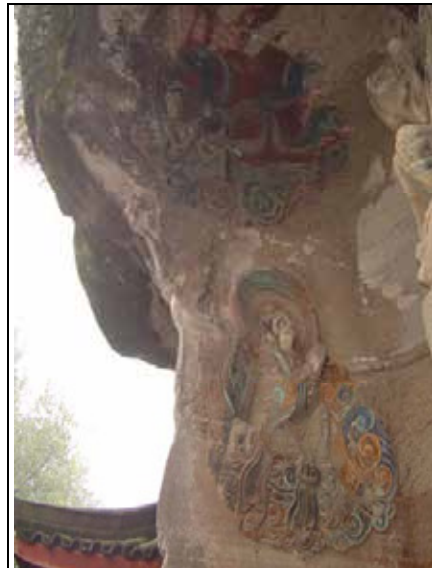
It can be concluded from the calculation results that the stability coefficient of No. 1 unsafe rock is 1.303 when the seismic influence is not taken into consideration, which means the state of stable. However,

考虑地震影响因素时，稳定性系数为 1.15，岩体处于欠稳定状态，需要对其进行加固处理。

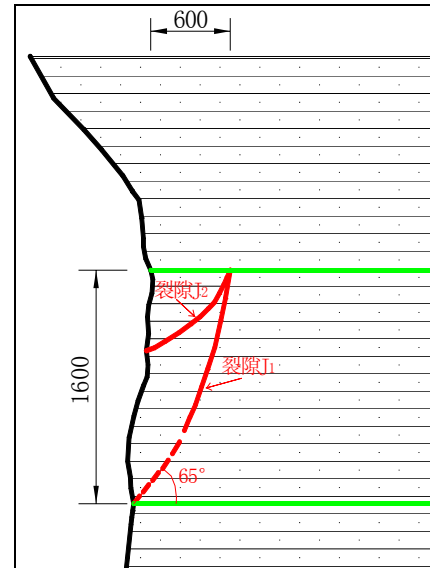
建议进行锚固处理。

when the seismic influence is taken into consideration, the rock stability coefficient is 1.15, which means the state of meta stable, and reinforcement is needed.

Anchoring measures are recommended for the reinforcement of No.2 unsafe rock.



(a)



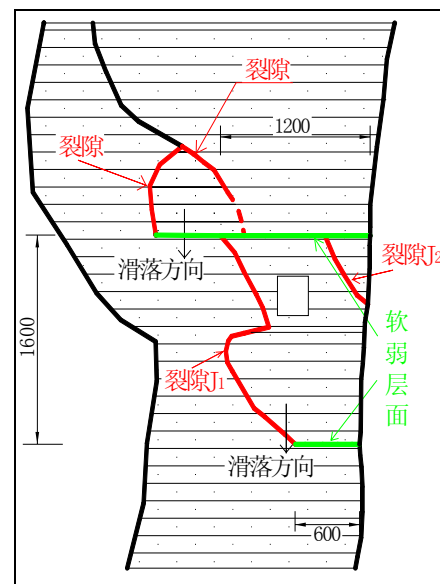
(b)

2号危岩体侧剖面图

Longitudinal Profile of No. 2 Unsafe Rock



(c)



(d)

2号危岩体正面图  
Front View of No. 2 Unsafe Rock

图 6-2 2号危岩体

Fig. 6-2 Dangerous rock mass of No. 2

在 2 号危岩体的左上角（面对危岩区）有一局部突出的小危岩，小危岩受裂隙及软弱层面切割，仅局部有很小的面积与山体相连，已接近极限平衡状态，受轻微扰动后极易发生掉块，威胁游客安全，应尽快对其进行处理。由于该小危岩体上无石刻赋存，建议对其进行清除。

### 6.3 3 号危岩体稳定性计算

3 号危岩体位于 15 号“龟鹤”题字龛处，危岩体为两条近于直立的宽大裂隙切割而成，“龟鹤”题刻上方的卸荷裂隙产状为  $84^{\circ} \angle 82^{\circ}$ ，裂隙顶部被泥土充填，有植物生长；另一条裂隙近直立，隙宽 20~40cm，裂隙内有泥土充填，有植物发育。两裂隙之间形成一高 5.5m，厚 3.6m 的孤立巨石（图 6-3）。“龟鹤”题刻区右边缘（面对题刻）岩体在上下两软弱夹层处受风化作用形成风化凹槽，沿凹槽产生掉块。后期曾进行过修砌，修砌体现已松动。危岩体在自身重力及外界营力作用下，使卸荷裂隙端部产生拉应力集中，使裂隙逐渐向深部发展。危岩体以岩体底部风化凹槽最深处为支点，可能向临空方向发生拉裂倾覆破坏，裂隙内植物根系的

There is a small extrusive local unsafe rock lies on the top left corner of No. 2 unsafe rock (face to the unsafe rock area), which is under the intersect of fissure and weak intercalation, and only connect very small part with the mountain. The small local unsafe rock is in the ultimate equilibrium state, and break down will occur even under minor disturb, which will threat the safety of tourists and need urgent reinforcement. Since no inscription lies on this small local unsafe rock, it is suggested to remove it.

### 6.3 Stability calculation for No. 3 unsafe rock

No. 3 unsafe rock lies on the position of No. 15 “龟鹤(GUI HE)” inscription, which is formed by the scission of two wide fissures of almost vertical direction. One fissure, i.e. the relief joint up to the “GUI HE” inscription, occurs in the angle of  $840 \angle 820$ , whose top is filled with earth and growing plants. The other fissure is approximately vertical with 20 to 40 cm width, which is also filled with earth and growing plants. A 5.5m high and 3.6 m thick separate huge rock body is formed between these two fissures, which can be seen from Figure 6-3.

On the very right side of the “GUI HE” inscription area (facing to the inscription), between the two weak intercalation, a weathering flute is developed, and falling pieces is observed along the flute. The flute has been restored after its destroy, but the restoration is loosening now. Under the influence of gravity and circumstances, the tensile stress will be concentrated on the end of the relief joint, which will further deepen the fissure. Taking the deepest point of the flute as the pivot, the unsafe rock maybe break down to the free face, and the splitting

劈裂作用加剧了危岩体的失稳可能性。

按拉裂倾覆破坏方式进行稳定性评价分析的计算公式为：

$$K = \frac{G_2 \times L_2 + M}{G_1 \times L_1} \quad (6-3)$$

考虑地震力作用时，其计算公式为：

$$K = \frac{G_2 \times L_2 + M}{G_1 \times L_1 + F_{h2} \times L_{h2} + F_{h1} \times L_{h1}} \quad (6-4)$$

式中：

$M$ —I 破坏面砂岩抗拉力对支点 O 的力矩；

$L_1$ 、 $L_2$ —支点 O 两侧岩体重力相对于 O 点的力臂；

$L_{h1}$ 、 $L_{h2}$ —水平地震力相对于支点 O 的力臂；

$F_{h1}$ 、 $F_{h2}$ —水平地震力。

在不考虑地震力作用下，对 I 破坏面：砂岩的抗拉强度取  $\sigma_t = 0.28 \text{ MP}_a$ ；

在支点 O 右侧：

危岩体重力  $G_1 = \gamma \times A \times B = 21.86 \times 8.87 \times 3.0 = 581.695 \text{ kN}$ ，力臂  $L_1 = 1.45 \text{ m}$ ；

在支点 O 左侧：

危岩体重力  $G_2 = \gamma \times A \times B = 21.86 \times 9.14 \times 3.0 = 599.401 \text{ kN}$ ，力臂  $L_2 = 1.74 \text{ m}$ 。

of the plant root system in the fissure will exacerbate the destabilization possibility of the unsafe rock.

Assuming the destroy mode is pulling breakdown, the equation for the stability assessment will be as follows:

$$K = \frac{G_2 \times L_2 + M}{G_1 \times L_1 + F_{h2} \times L_{h2} + F_{h1} \times L_{h1}} \quad (6-4)$$

When the seismic influence is considered:

Where

$M$  is the moment of the sandstone stretching resistance of I failure plane to pivot O

$L_1$  and  $L_2$  are the arm of force relative to O pivot results from the rock gravity beside pivot O respectively

$L_{h1}$  and  $L_{h2}$  are the arm of force relative to O pivot results from the horizontal seismic force respectively

$F_{h1}$  and  $F_{h2}$  are the horizontal seismic force respectively

When seismic influence is not considered, for I failure plane: the tensile strength of the sandstone  $\sigma_t$  is  $0.28 \text{ MP}_a$

On the right side of pivot O:

The gravity of the unsafe rock  $G_1 = \gamma \times A \times B = 21.86 \times 8.87 \times 3.0 = 581.695 \text{ kN}$ , and the arm of force  $L_1$  is  $1.45 \text{ m}$ .

On the left side of pivot O:

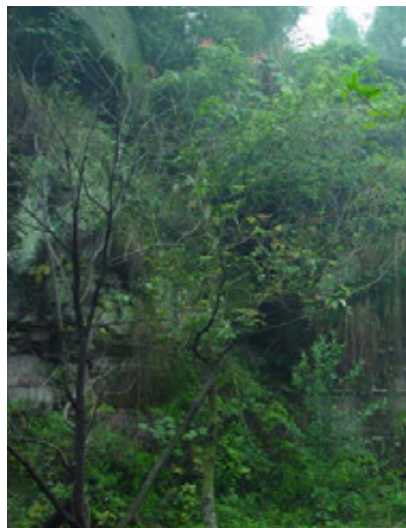
The gravity of the unsafe rock  $G_2 = \gamma \times A \times B = 21.86 \times 9.14 \times 3.0 = 599.401 \text{ kN}$ , and the arm of force  $L_2$  is  $1.74 \text{ m}$ .

将各参数带入式 (6-3) 中, 得

$$K = \frac{G_2 \times L_2 + M}{G_1 \times L_1} = \frac{599.401 \times 1.74 + 487.21}{581.695 \times 1.45} = 1.24$$

考虑地震力作用的影响时, 对 I 破坏面:

支点 O 右侧, 地震作用力  $F_{h1}=a_h \times G_1 = 0.127 \times 581.695 = 73.875 \text{ kN}$ , 力臂  $L_{h1}=2.53 \text{ m}$ ;



(a) 3号危岩体右侧裂隙

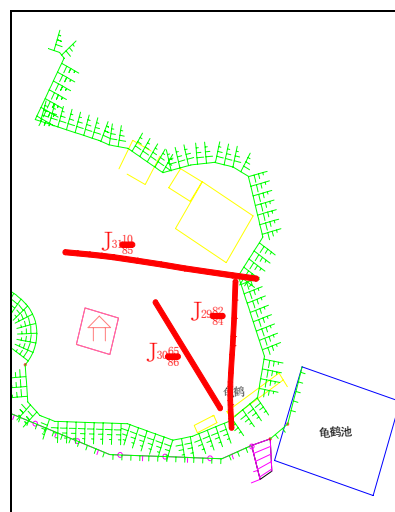
(a) Fissure on the Right Side of No. 3

Then, it can be calculated from equation 6-3 that

$$K = \frac{G_2 \times L_2 + M}{G_1 \times L_1} = \frac{599.401 \times 1.74 + 487.21}{581.695 \times 1.45} = 1.24$$

When the seismic influence is considered, for I failure plane:

On the right side of pivot O, the horizontal seismic force  $F_{h1}=a_h \times G_1 = 0.127 \times 581.695 = 73.875 \text{ kN}$ , and the arm of force  $L_{h1}$  is 2.53 m.

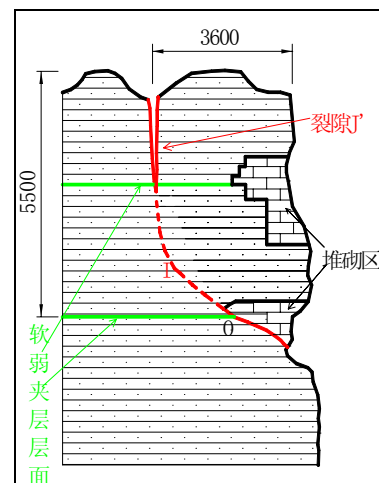


(b) 3号危岩体平面图

(b) Plane View of No. 3 Unsafe Rock



(c)

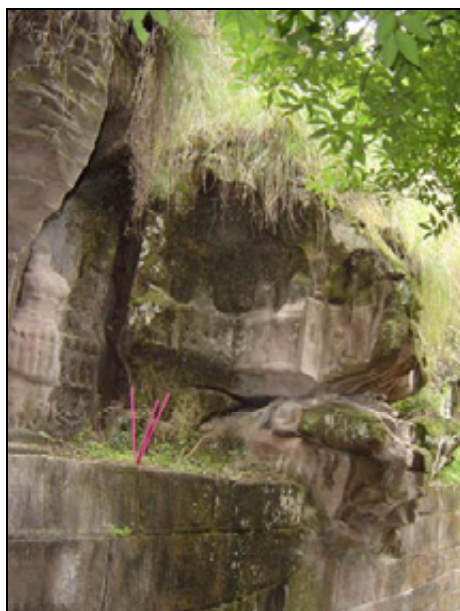


(d)

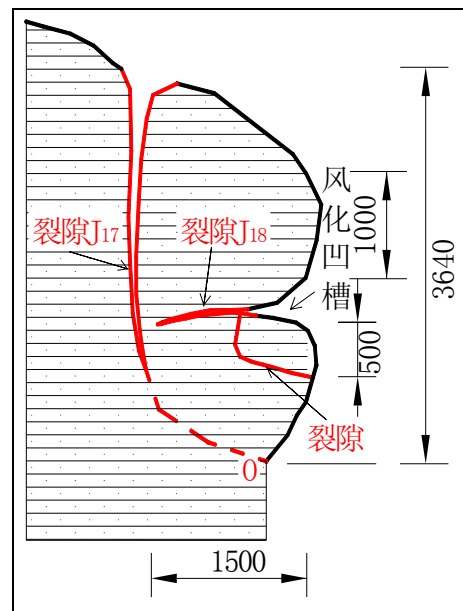
3号危岩体侧面  
Lateral Surface of No. 3 Unsafe Rock

图 6-3 3号危岩体

Fig. 6-3 Dangerous rock mass of No. 3

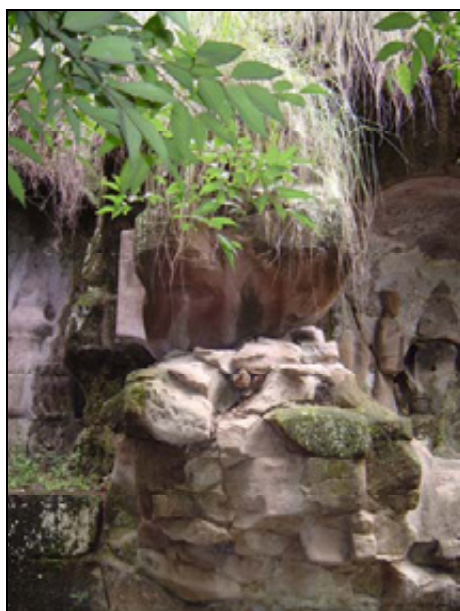


(a)

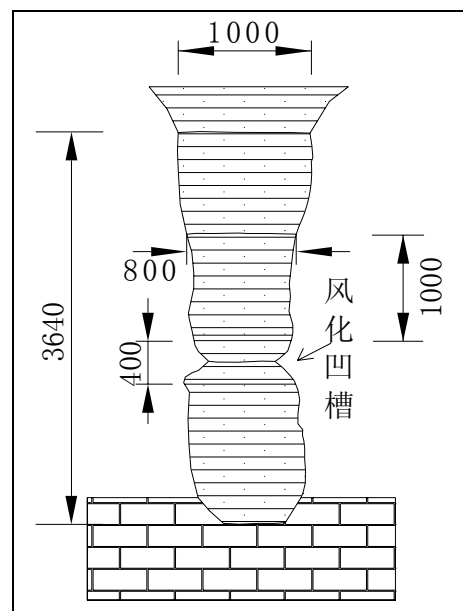


(b)

4号危岩体侧面  
Lateral Surface of No. 4 Unsafe Rock



(c)



(d)

4号危岩体正面  
Front Face of No. 4 Unsafe Rock

图 6-4 4号危岩体  
Fig. 6-4 Dangerous rock mass of No.4

支点 O 左侧, 地震作用力  $F_{h2} = a_h \times$

On the left side of pivot O, the horizontal seismic force  $F_{h2} = a_h \times ( = 0.127 \times 599.401 = 76.124 \text{ kN}$ , and th

$$G_2 = 0.127 \times 599.401 = 76.124 \text{ kN}, \text{ 力臂}$$

$$L_{h2} = 2.48 \text{ m.}$$

将各参数带入式 (6-4) 中, 得:

$$K = \frac{G_2 \times L_2 + M}{G_1 \times L_1 + F_{h2} \times L_{h2} + F_{h1} \times L_{h1}} = \frac{599.401 \times 1.74 + 487.20}{581.695 \times 1.45 + 761.24 \times 2.48 + 738.75 \times 2.53} = 0.86$$

由计算结果可知, 不考虑地震时,  $K=1.24$ , 危岩体为欠稳定状态; 在考虑地震影响情况下, 危岩体可能失稳, 应该进行加固治理。

arm of force  $L_{h2}$  is 2.48 m.

Then, it can be calculated from equation 6-3 that

$$599.401 \times 1.74 + 487.20$$

It can be conclude from the calculation results that  $K$  is 1.24 when the seismic influence is not taken into consideration, which means the unsafe rock is in meta-stable state. And when the seismic influence is taken into consideration, the unsafe rock will be in unstable state, and urgent reinforcement is needed.

## 6.4 4 号危岩体稳定性计算

4 号危岩体位于南壁上层西侧题刻区 63 号龛的左壁。63 号龛的左壁发育两条裂隙  $J_{17}$  和  $J_{18}$ 。裂隙  $J_{17}$  为一条卸荷裂隙, 产状为  $152^\circ \angle 81^\circ$ , 张开度近 20cm, 其中有松散粘土充填。该裂隙构成 4 号危岩体的后缘切割面。在下部发育一条产状为  $0^\circ \angle 20^\circ$  的近水平状裂隙  $J_{18}$ , 此裂隙起伏较大, 隙宽 0~15cm 不等。由于  $J_{17}$  与  $J_{18}$  的切割导致 63 号龛左壁岩体形成危岩体。沿裂隙  $J_{18}$  形成一风化凹槽, 其上部的岩体后缘可能拉裂破坏, 向临空方向发生倾覆, 导致岩体失稳 (图 6-4)。

## 6.4 Stability calculation for No. 4 unsafe rock

No. 4 unsafe rock lies on the left wall of No. 63 Niche, western inscription area of south wall of the mountain. Two fissures  $J_{17}$  and  $J_{18}$  are developed on the left wall of No. 63 Niche.  $J_{17}$  is a relief joint occurs in the angle of  $152^\circ \angle 81^\circ$  with about 20 cm open width, which is filled with loose clay and forms the trailing edge of the cutting plane of No. 4 unsafe rock.  $J_{18}$ , which occurs in the angle of  $0^\circ \angle 20^\circ$ , is developed in the lower part of No. 63 niche, and the width of this fissure ranges from 0 to 15 cm. Because of the intersect of  $J_{17}$  and  $J_{18}$ , the left wall of No. 63 Niche becomes unsafe rock. There is a weathering flute developed along  $J_{18}$  fissure, and the trailing edge of the rock upper than  $J_{18}$  maybe break down to the free face by gravity pulling, which will result in the destabilization of the rock body.

不考虑地震力作用的影响时：

对于 I 破坏面处：砂岩的抗拉强度取  $\sigma_t = 0.28 \text{ MPa}$ ；

设破坏面处砂岩抗拉力对支点 O 的力矩为  $F_s$ ：

支点 O 右侧，危岩体重力  $G_1 = \gamma \times A \times B = 21.86 \times 2.19 \times 0.82 = 39.256 \text{ kN}$ ，力臂  $L_1 = 0.41 \text{ m}$ ；

支点 O 左侧，危岩体重力  $G_2 = \gamma \times A \times B = 21.86 \times 2.81 \times 0.97 = 59.584 \text{ kN}$ ；力臂  $L_2 = 0.33 \text{ m}$ 。

将各参数代入式 (6—3) 中，得：

$$K = \frac{G_2 \times L_2 + M}{G_1 \times L_1} = \frac{59.584 \times 0.33 + 134.4}{39.256 \times 0.41} = 1.23$$

考虑地震力作用的影响，对 I 破坏面：

支点 O 右侧，地震作用力  $F_{h1} = a_h \times G_1 = 0.127 \times 39.256 = 4.986 \text{ kN}$ ，力臂  $L_{h1} = 0.34 \text{ m}$ ；

支点 O 左侧，地震作用力  $F_{h2} = a_h \times G_2 = 0.127 \times 59.584 = 7.567 \text{ kN}$ ，力臂  $L_{h2} = 0.49 \text{ m}$ 。

When seismic influence is not considered:

For I failure plane:

The tensile strength of the sandstone  $\sigma_t$  is  $0.28 \text{ MPa}$

On the right side of pivot O, the gravity of unsafe rock  $G_1 = \gamma \times A \times B = 21.86 \times 2.19 \times 0.82 = 39.256 \text{ kN}$ , and the arm of force  $L_1$  is  $0.41 \text{ m}$ .

On the left side of pivot O, the gravity of unsafe rock

$G_2 = \gamma \times A \times B = 21.86 \times 2.81 \times 0.97 = 59.584 \text{ kN}$ , and the arm of force  $L_2$  is  $0.33 \text{ m}$ .

Then, it can be calculated from equation 6-3 that

When seismic influence is considered, for I failure plane:

On the right side of pivot O, the seismic force  $F_{h1} = a_h \times G_1 = 0.127 \times 39.256 = 4.986 \text{ kN}$ , and the arm of force  $L_{h1}$  is  $0.34 \text{ m}$ .

On the left side of pivot O, the seismic force  $F_{h2} = a_h \times G_2 = 0.127 \times 59.584 = 7.567 \text{ kN}$ , and the arm of force  $L_{h2}$  is  $0.49 \text{ m}$ .

$$\begin{aligned}
 K &= \frac{G_2 \times L_2 + M}{G_1 \times L_1 + F_{h2} \times L_{h2} + F_{h1} \times L_{h1}} \\
 &= \frac{59.584 \times 0.33 + 134.4}{39.256 \times 0.41 + 7.567 \times 0.49 + 4.986 \times 0.34} \\
 &= 0.92
 \end{aligned}$$

由计算结果可知,在不考虑地震影响情况下  $K=1.23$ , 4 号危岩体处于欠稳定状态; 考虑地震影响因素时  $K=0.92$ , 危岩体失稳, 应该对危岩体进行加固治理。

It can be conclude from the calculation results that  $K$  is 1.23 when the seismic influence is not taken into consideration, which means the unsafe rock is in meta-stable state. And  $K$  will be 0.92 when the seismic influence is taken into consideration, which means the unsafe rock will be in unstable state, and urgent reinforcement is needed.

## 第七章 环境地质病害防治对策

根据前述环境地质病害分析，安岳圆觉洞石刻区主要环境地质病害为危岩体崩塌、风化病害和生物病害等。产生这些地质病害的基本原因是遭受各种地质营力及生物覆盖的长期作用。因此，防治措施的基本原则是改造地质环境，提高石刻岩体本身抵抗自然地质营力破坏的能力，消减或消除自然地质营力的破坏作用。现提出各种病害的防治对策如下：

### 7.1 危岩体锚固

安岳圆觉洞石刻区共存在4处危岩体。在考虑地震力作用的影响时，这些危岩体的稳定系数均在1.3以下，处于不稳定状态，时刻威胁着游客及石刻文物的安全。应及时采取措施进行加固处理。

在危岩体加固时，需考虑危岩体的破坏类型选取适当的加固措施。

对于1、2号危岩体，最可能的破坏模式为单面滑动破坏。考虑到这两个危岩体厚度不大（仅为

### Chapter 7 Prevention and Control Countermeasures for the Environmental Geological Diseases

According to the analysis mentioned above, the main environmental geological diseases in Yuanjuedong can be divided into three types, i.e. rock collapse, weathering and biological breakdown, and the key reasons for these diseases are the long term geological and biological influences on the stone carvings. Therefore, the basin principles for the disease prevention and control are to change the geological environment, improve the resistance capacity of the rock to the geological influences, reduce or eliminate the natural geological destroy. The countermeasures for the diseases are as follows:

### 7.1 Anchoring of the unsafe rock

There are four unsafe rock bodies in Yuanjuedong. Take into consideration the influence of earthquake, the stability coefficient of these rock bodies are below 1.3, and they are in unstable conditions, which gives threat to the safety of tourists and cultural relics. Therefore, it is urgent to take measures to reinforce these rock bodies.

The damage type should be considered during the reinforcement of the unsafe rocks, thus to select suitable countermeasures.

The most possible damage type for No.1 and No.2 unsafe rock is single side slide. Since these two unsafe rocks have limited deadweight with only 1 m thick, short anchorage bar is recommended for the

1m) 及自身重量有限, 建议采用短锚杆进行加固处理。同时对软弱夹层处的风化凹槽, 采用充填粘结的方式进行加固。

对于 3、4 号危岩体, 其最可能的破坏模式是危岩体在重力作用下向临空方向产生变形拉裂, 最终导致分离块体在重力作用下朝临空方向发生倾覆崩塌。其加固措施可选取在危岩体下方悬空处进行挡墙支撑的方法。此外, 还可采用锚杆技术, 穿过卸荷裂隙, 将危岩体和山体连接在一起。进行锚固时应采用预应力锚杆, 同时对卸荷裂隙进行灌浆粘结加固, 以增强立壁岩体的整体性。

所有锚固后的岩体均需做旧处理, 尽量保持石刻区岩体的原貌。

## 7.2 风化及生物病害治理

圆觉洞石刻区的风化作用以物理风化和生物风化作用为主。

### 7.2.1 物理风化病害治理

石刻区岩体受温差作用和干湿变化的影响, 使表层变得疏松, 产生大量的风化裂隙, 造成石雕的

reinforcement. On the same time, filling and cementing method will be used to strengthen the weak embedded weathering flute.

The most possible damage type for No.3 and No.4 unsafe rock is as follows: the deformation and pullapart of the unsafe rock to the free face, which is resulted from the influence of gravity, and will finally lead to break down of the separated rock to the free face. The supporting and retaining wall can be constructed in the hanging up area under the unsafe rock to reinforce it. Furthermore, anchorage bar technology, which will penetrate through the relief fissure, can be adopted to connect the unsafe rock and mountain. Prestress bar should be used during the anchoring process, while grouting and cementing reinforcement should be carried out for the relief fissure, thus to increase the integrity of the cliff rock body.

The anchored rock body should be treated in the style and color of the ambient rock and carvings, thus to keep the original appearance of the rock in Yuanjuedong.

### 7.2 Treatment of the weathering and biological

The weathering diseases in Yuanjuedong are mainly in physical and biological type.

#### 7.2.1 Treatment of the physical weathering diseases

Under the influence of temperature and humidity difference, the surface layer of the rock in Yuanjuedong becomes loosening, and plenty of weathering fissures will be generated, which leads to the exfoliation of

鳞片状、片状剥落。这种风化现象主要存在于石刻岩体的周围小石龛中，该类石龛防护结构作用有限，容易受到降水及太阳照射的直接影响，风化比较严重。

凝结水病害加剧了石刻岩体的风化作用。

调查发现，圆觉洞石刻区龛窟的规模不大，龛檐对造像有很好的保护作用。建议恢复各龛原有的龛檐。

### 7.2.2 化学风化病害治理

化学风化主要是水溶液在与石雕中的矿物进行化学反应的过程中，使石雕的结构构造遭到破坏，成分受到改造，并产生一些在地表条件下稳定的新矿物，例如石刻区砂岩中的长石经水解作用形成高岭石、伊利石、绿泥石、氢氧化钾和二氧化硅。水化作用和氧化作用均会在石刻岩体表层产生褐铁矿交代浸染。

本次研究给出了石刻区岩体的矿物成分分析、化学成分分析和地下水化学分析的成果，为风化病害防治提供了基础资料。可针对石刻区的砂岩，采用以甲基三甲氧基硅烷为主剂的有机硅复合材料，在

the stone carvings. The weathering phenomenon mentioned above mainly exists in the peripheral small stone grottoes along the rock body. Such kind of grotto, which has limited protection structure, is subject to the precipitation and solar radiation and in relatively serious weathering condition.

Condensation effect intensifies the weathering of the carving rock body.

According to the investigation, the grotto scale of Yuanjuedong is rather small, and the eaves work well for the protection of the statues. Therefore, it is recommended to restore the original eaves of all grottoes.

#### 7.2.2 Treatment of the chemical weathering

Chemical weathering mainly occurs in the chemical reaction process between the aqueous solution and the minerals in the stone statues, which will destroy the statue structure, change the rock ingredient, and produce stable new mineral under certain ground surface conditions. For instance, under the hydrolytic action, the feldspar in the sandstone of the carving area will form kaolinite, andreatite, chlorite, potassium hydroxide and silicon dioxide. Both hydration and oxidation will generate alternative impregnation of brown hematite on the carving stone surface.

The mineral and chemical ingredient analysis of the rock and the chemical analysis of groundwater in Yuanjuedong were conducted in this research project, which provides fundamental data for the prevention and control of the chemical weathering disease. It is recommended that a representative area near Yuanjuedong should be selected to carry out the in situ

石刻区附近选择一个有代表性的试验点，进行防风化材料的现场试验，为风化病害防治提供依据。

### 7.2.3 生物风化病害治理

石刻区的生物风化主要是构造裂隙中生长的植物根系的根劈作用，使裂隙加宽，岩体破裂。石刻岩体表面生长的苔藓也有腐蚀作用，在岩体表面产生黑色的沉积物。

圆觉洞的苔藓和霉菌十分茂盛，这与其潮湿的环境密切相关。通过建立石刻区排水系统、修建窟檐、封堵裂隙等工程改变圆觉洞石刻的赋存环境，使龛窟保持干燥状态，可以有效的抑制苔菌类的生长。对裂隙充填物中生长的植物要及时清除。

### 7.2.3 环境污染

此类病害属于第二类环境地质病害。由于环境污染产生的酸雨、空气中的二氧化硫、硝酸根离子含量等，对石刻岩体会产生腐蚀作用。

环境污染是一个全社会关注

experiment about the anti weathering material, and the organosilicon composite material mainly composed of methyltrimethoxy silane should be used, thus to provide basis for the weathering prevention and control of the sandstone in Yuanjuedong.

### 7.2.3 Treatment of the biological weathering

Biological weathering in Yuanjuedong is mainly resulted from the split effect of the vegetables root system in the tectonic fissures, which will widen the fissure and break down the rock body. The corrosive influence resulted from moss growing on the stone carving will generate black sediment on the rock surface.

The moss and fungi in Yuanjuedong is very flourishing, which has close relation with the humid circumstance of this area. The existing environment of Yuanjuedong stone carving can be changed through engineering projects as drainage system construction, eave restoration and fissure plugging, thus to keep the dry state of the grotto and to restrain the growth of moss and bacteria efficiently.

### 7.2.3 Environmental pollution prevention and control

The environmental pollution belongs to the second type of environmental geological diseases. The acid rain, sulfur dioxide and nitrate ion in the air, which is resulted from environmental pollution, will corrode the stone carvings.

The influence of environmental pollution,

的问题，其形成和治理的效果都具有滞后性和长期性的特点。建议作好监测，对其发展做出合理预测，通过政府立法治理环境，以利于圆觉洞石刻的长期保护。

which attracts attention from about all society, has the characteristic of chronicity and posteriority. Therefore, efficient monitoring should be carried out to make reasonable prediction about the progress of environmental pollution. The environment quality should be improved through governmental legislation, which is in favor of the long-term protection of the Yuanjuedong stone carving.

## 第八章 结论与建议

圆觉洞石刻区造像均分布在高6~15m的巨厚层状砂岩陡崖之中。砂岩中的粉砂质泥岩夹层抗风化能力低，易形成风化凹槽。日晒雨淋使石刻表面风化病害严重。苔藓、霉菌等生物覆盖腐蚀和植物根系的劈裂作用形成生物病害。圆觉洞石刻区近直立状的宽大裂隙切割形成危岩体，发生崩塌病害。

产生这些地质病害的基本原因是遭受各种地质营力及生物覆盖的长期作用。因此，防治措施的基本原则是改造地质环境，提高石刻岩体本身抵抗自然地质营力破坏的能力，消减或消除自然地质营力的破坏作用。

结论与建议如下：

1、石刻区主要发育构造裂隙、卸荷裂隙及层面裂隙，裂隙切割岩体成块状，是石刻区岩体失稳的主要因素。调查发现圆觉洞石刻区共存在4处危岩体。稳定性计算表明，石刻区4处危岩体均处于欠稳定状态，

## Chapter 8 Conclusion and Suggestions

The statues in Yuanjuedong are all distributed on the sandstone cliff of 6 to 15 m thick. The silty mud interbedding in the sandstone has low weathering resistance capacity, which always leads to weathering flute. The sunshine and rainfall result in serious weathering on the stone carving surface. The corrosion caused by covering of moss and fungi and the split caused by plant root system result in biological diseases. The wide and large fissures, which is almost perpendicular, cut the rocks in Yuanjuedong and make it unstable, thus lead to breakage diseases.

The basic reason for these geological diseases is the long-term influence of different geological process and biological coverage. Therefore, the basin principles for the disease prevention and control are to change the geological environment, improve the resistance capacity of the rock to the geological influences, reduce or eliminate the natural geological destroy.

The conclusion and suggestions are as follows:

1. The fissures developed in Yuanjuedong are mainly tectonic fissure, relief fissure and bedding fissure, which cut the rock into pieces, and they are the key factors for the instability of the rock in this area. It can be concluded from the investigation and calculation that 4 unsafe rocks lie in Yuanjuedong, all of which are in unstable status, and give threat to the safety of the tourists and stone cultural relics in Yuanjuedong. It is recommended to take measures of anchoring bar

时刻威胁着石刻区游客及石刻文物的安全，建议对其采用锚杆加固和砌墙支撑的方法处理。锚固后的岩体均需做旧处理，尽量保持石刻区岩体的原貌。

2、石刻区8号窟圆觉洞由于进深较大，在夏季凝结水现象较为严重，使洞窟潮湿，不利于石刻的保存。建议改善通风条件，在凝结水富集的7、8月间对洞窟进行去湿处理。

3、石刻区的风化作用以物理风化和生物风化作用为主，物理风化作用下，岩体产生大量的风化裂隙，造成石雕的鳞片状、片状剥落。生物风化为裂隙中生长的植物根系的根劈作用、岩体表面苔藓的覆盖及腐蚀作用所产生。建议针对石刻区的砂岩，采用防风化新型材料，选择代表性的试验点，进行现场试验，为风化病害防治提供依据。

4、调查发现，龛檐对圆觉洞石刻区的造像有很好的保护作用。建议恢复各龛原有的龛檐。

5、环境污染对石刻岩体会产生

and supporting wall to reinforce these unstable rocks, and the anchored rock body should be treated in the style and color of the ambient rock and carvings, thus to keep the original appearance of the rock in Yuanjuedong.

The No. 8 Grotto of Yuanjuedong in rock carving area has large depth, which leads to serious water condensation in summer, makes the circumstances very humid and does harm to the preservation of the stone carving. It is suggested to improve the ventilation condition of the grotto, and dehumidification measures should be taken during June and August, when the water condensation is very serous.

The weathering diseases in Yuanjuedong are mainly in physical and biological type. Lots of fissures develop under the influence of physical weathering, which leads to the exfoliation of the stone carvings. Biological weathering is resulted from the split effect of the plant root system in the tectonic fissures and the corrosion and coverage of moss on the stone carving surface. New weathering resistance material is recommended to prevent and control the weathering of the sandstone in Yuanjuedong, and representative area should be selected first to carry out the in situ experiment, which will provide basis for the weathering prevention and control work.

4. It can be concluded from the investigation that the eaves work well for the protection of the Yuanjuedong statues. Therefore, it is recommended to restore the original eaves of all grottoes.

Environmental pollution corrodes the stone

腐蚀作用。建议作好监测，对其发展做出合理预测。通过政府立法进行环境污染治理和监控，以利于圆觉洞石刻的长期保护。

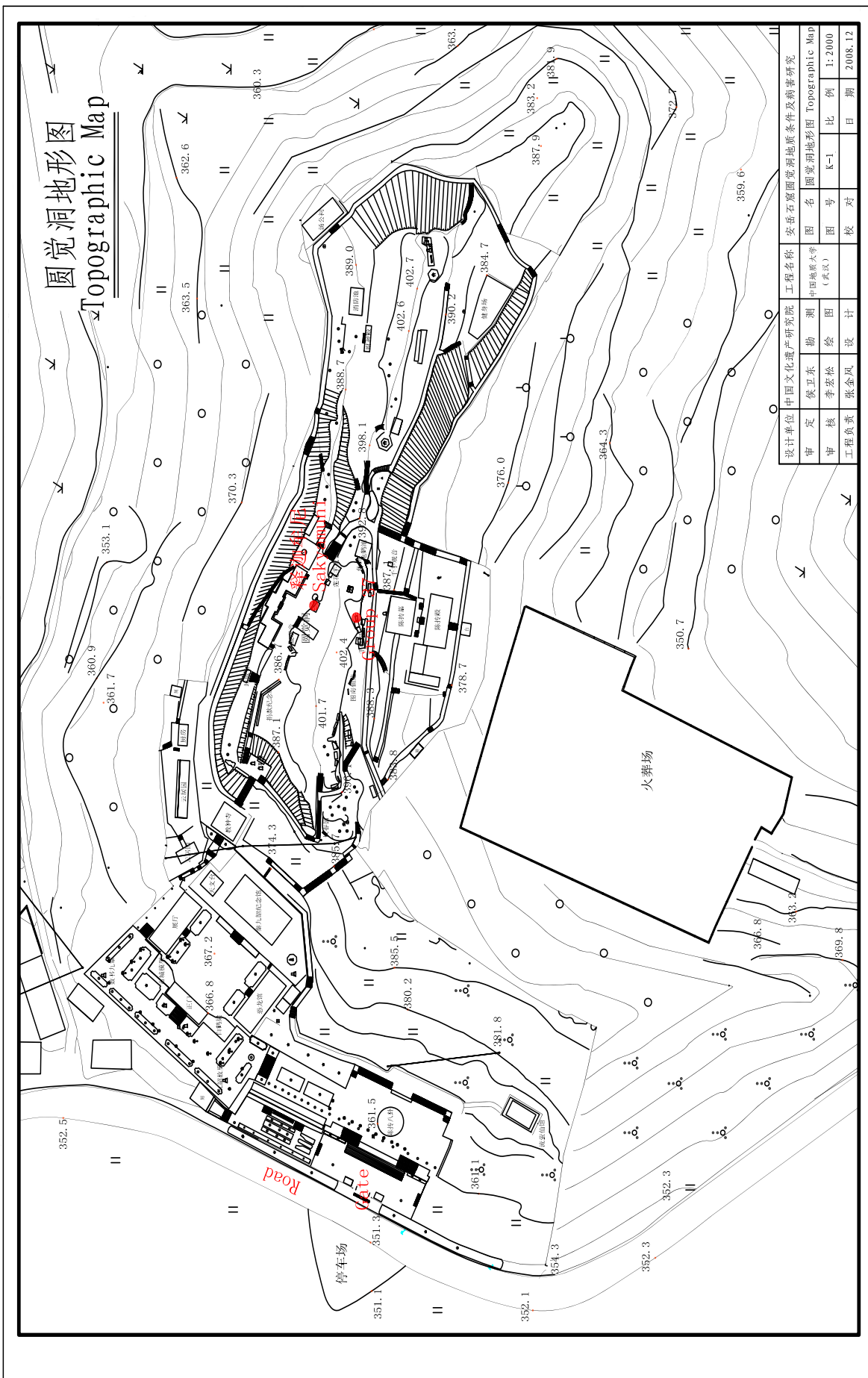
6、建立和加强对石刻区环境地质病害的长期监测，了解各种防治措施的效果和环境变化状况。

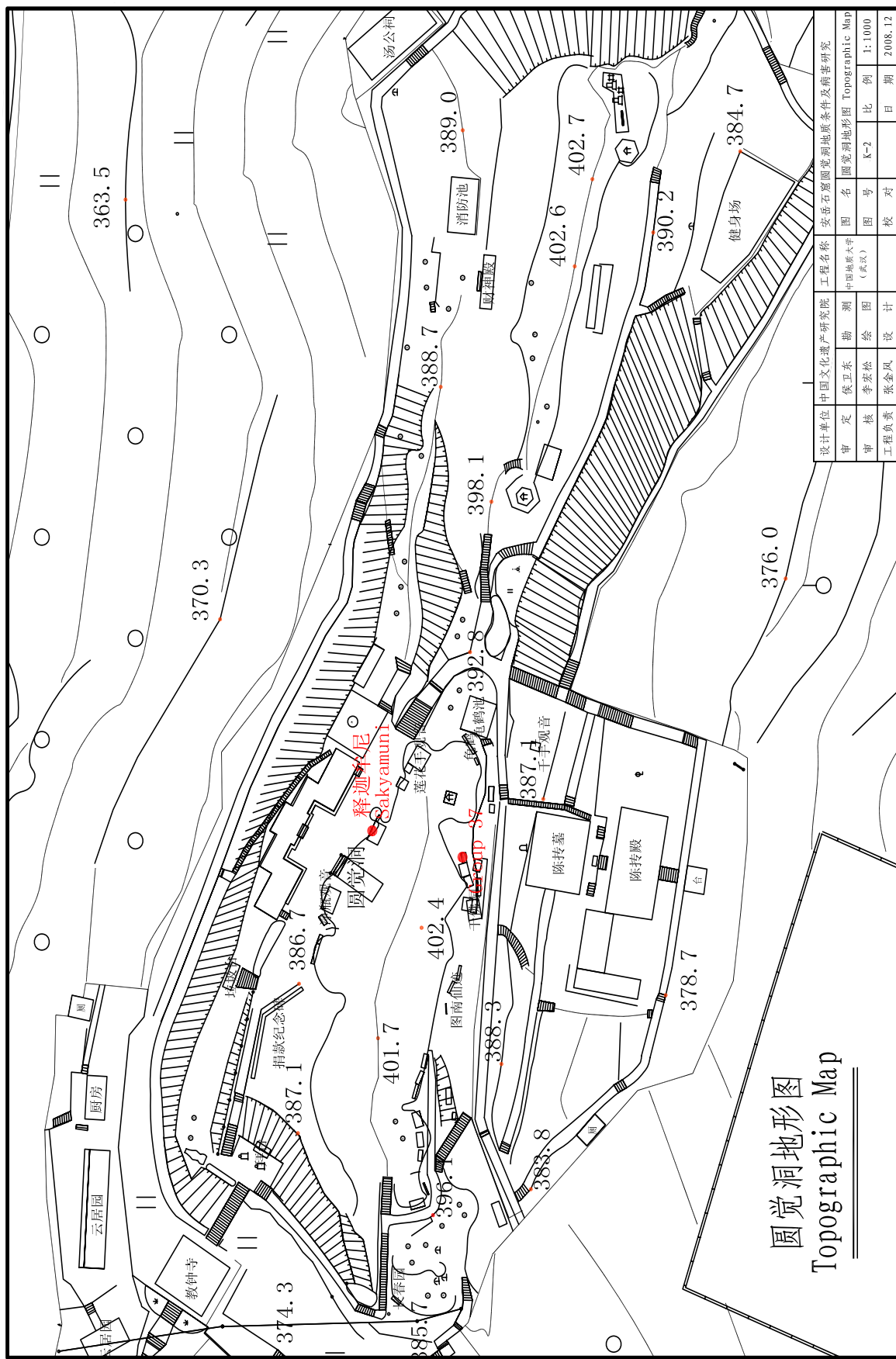
建立和完善防治技术档案，记录和整理各类病害的发生时间、条件和范围，为病害防治积累资料。

carvings. It is suggested to carry out effective monitoring to make reasonable prediction about the progress of environmental pollution, and the environment quality should be improved through governmental legislation, which is in favor of the long-term protection of the Yuanjuedong stone carvings.

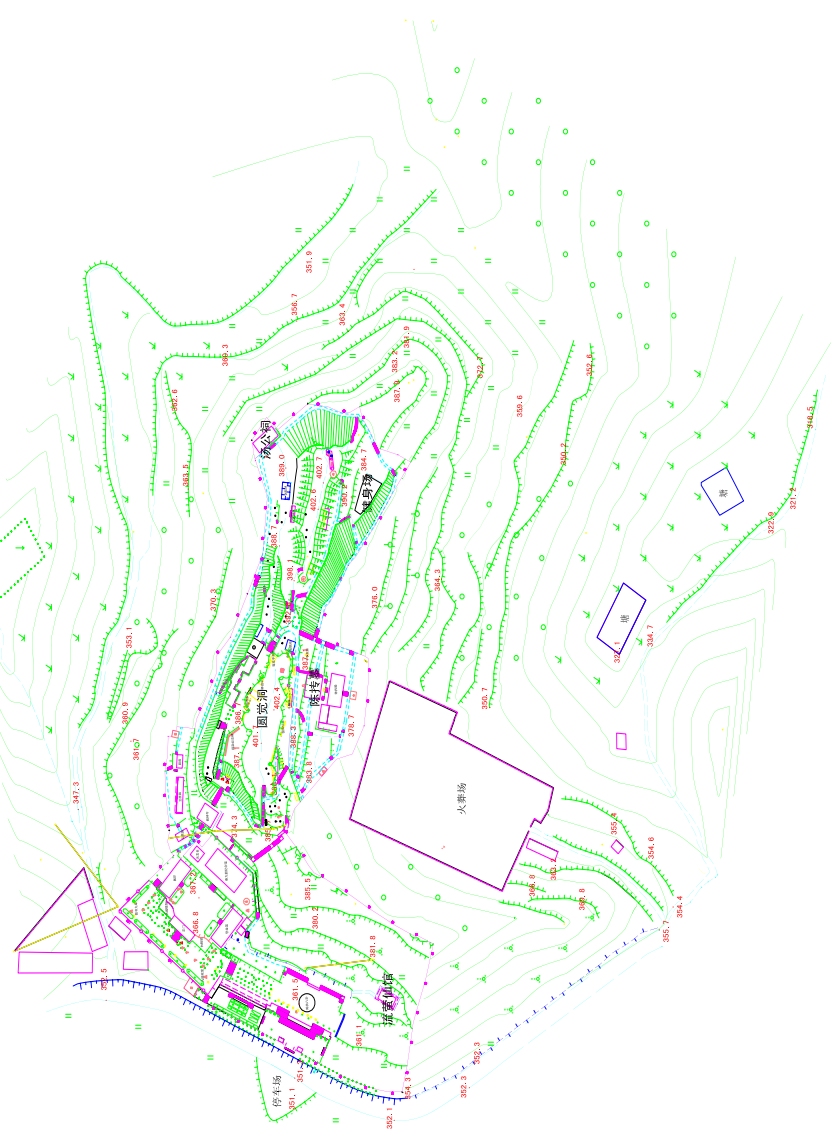
6. Long-term monitoring about the environmental geological diseases should be improved and strengthened, thus to understand and assess the efficiency of preservation measures and the status of environmental changing.

The preservation technology archives should be setup and improved, thus to record and classify the time, condition and scope of all kinds of diseases, which will accumulate and provide data for the prevention and control of the environmental geological diseases.





# 四川安岳圆觉洞石刻保护区地形图 relief map

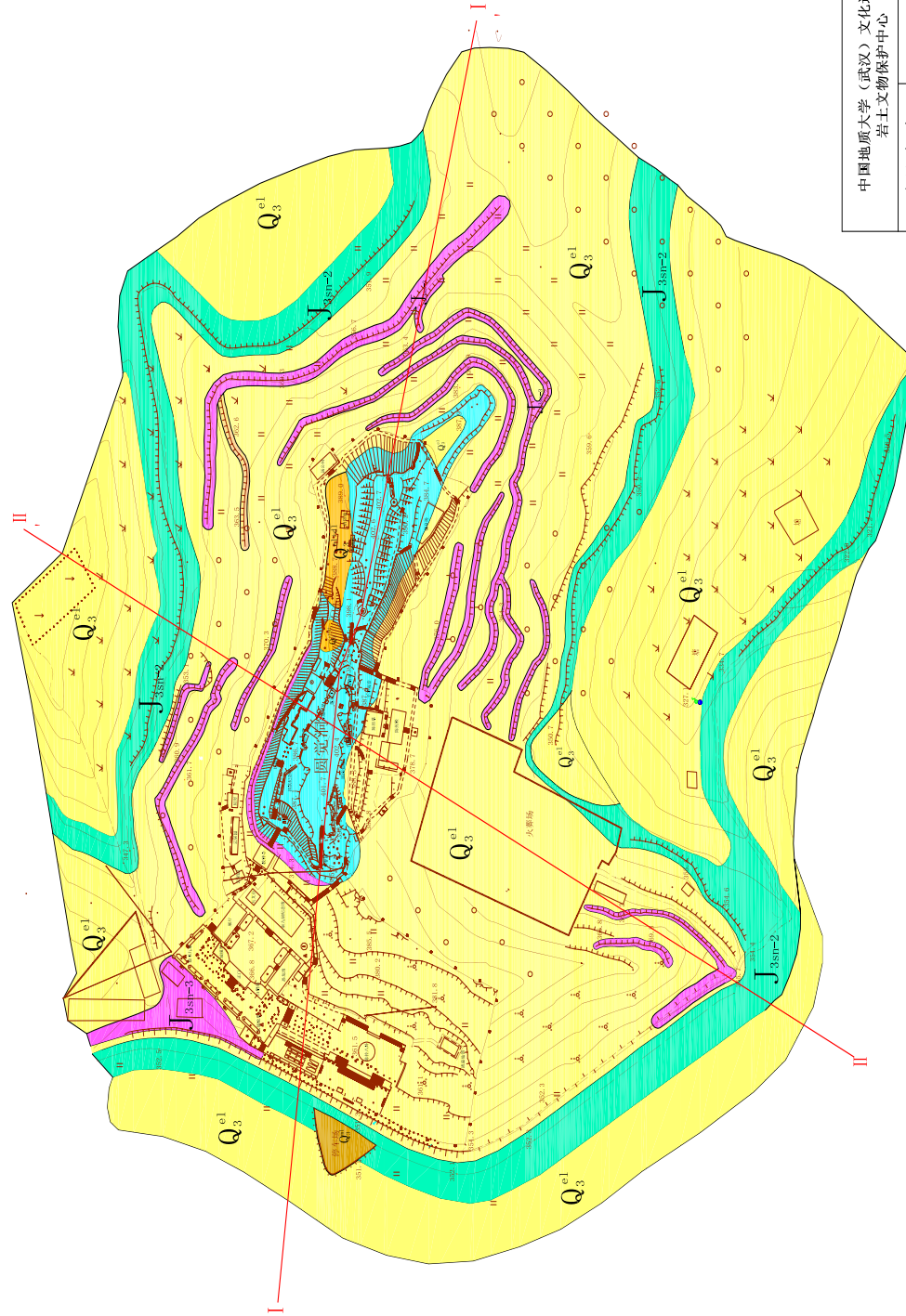
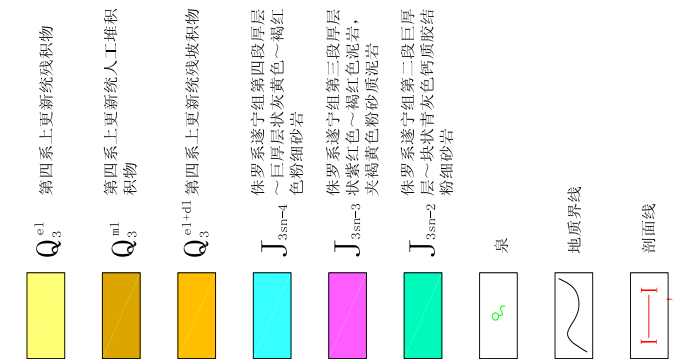


中国地质大学（武汉）文化遗产和 岩土文物保护中心		项目名称	四川安岳圆觉洞石刻区环境地质调查 附图 1 方云	
测绘员：王波斌 绘图员：周光华 检查员：王鹏		图号	1:2000 附图 1 地形图	
制图 朱华 校核 刘建辉 审核		图名	四川安岳圆觉洞石刻保护区地形图 2007.11 期	
2007年10月数字化制图， 1954北京坐标系， 1956黄海高程基准，等高距为1米。 1996年版图式。	2007.11 期	比例尺	1:2000	2007.11 期
2007年10月数字化制图， 1954北京坐标系， 1956黄海高程基准，等高距为1米。 1996年版图式。	2007.11 期	图幅	1:2000	2007.11 期

# 四川安岳圆觉洞石刻保护区地形图

## geological plans

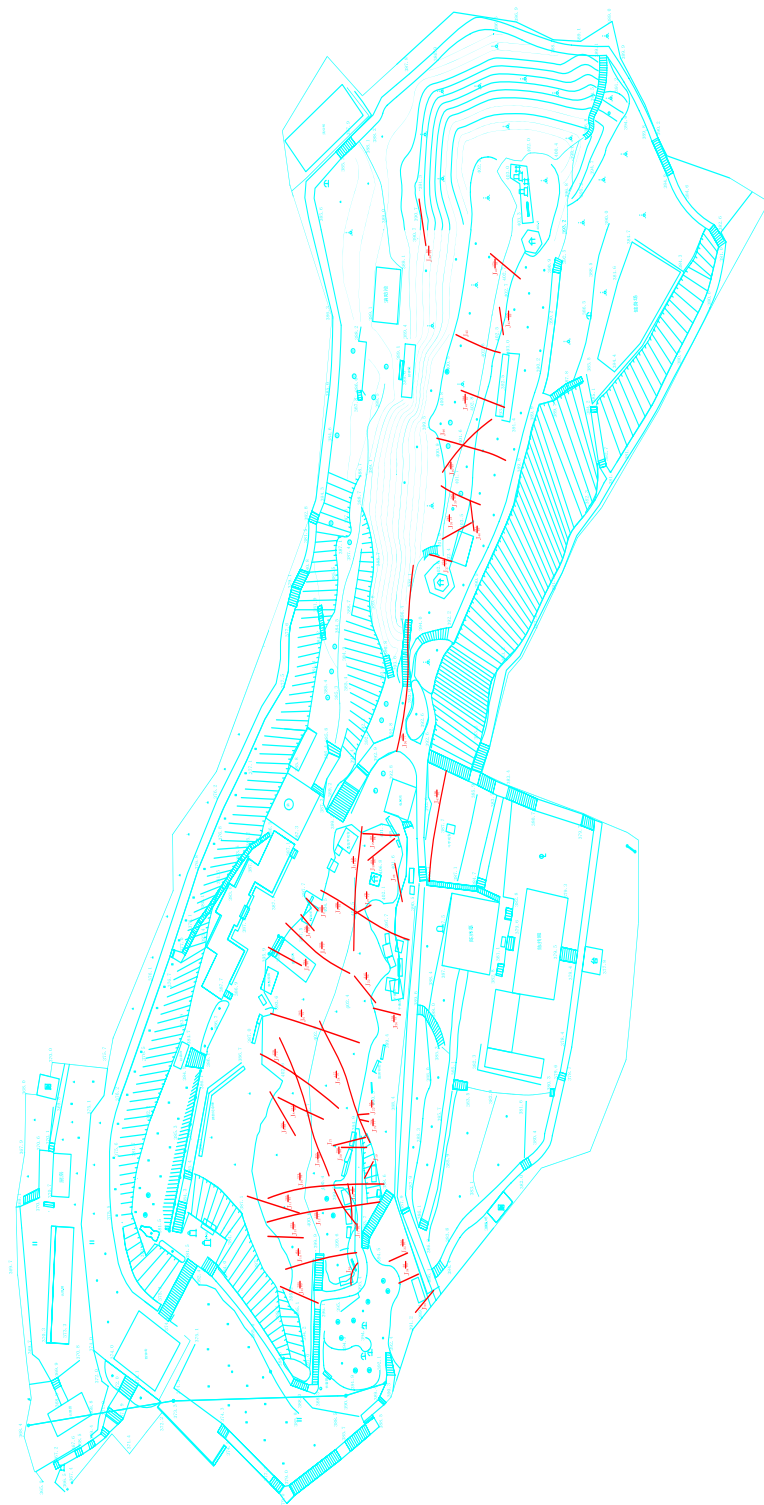
图例:



中国地质大学(武汉)文化遗产和 岩土文物保护中心		项目名称 四川安岳圆觉洞石刻区环境地质调查 附图 1	
项目负责	制图	图名	比例尺
方云	朱华	四川安岳圆觉洞石刻保护区地形图	1:2000
刘建辉	严绍军	审核	日期 2007.11

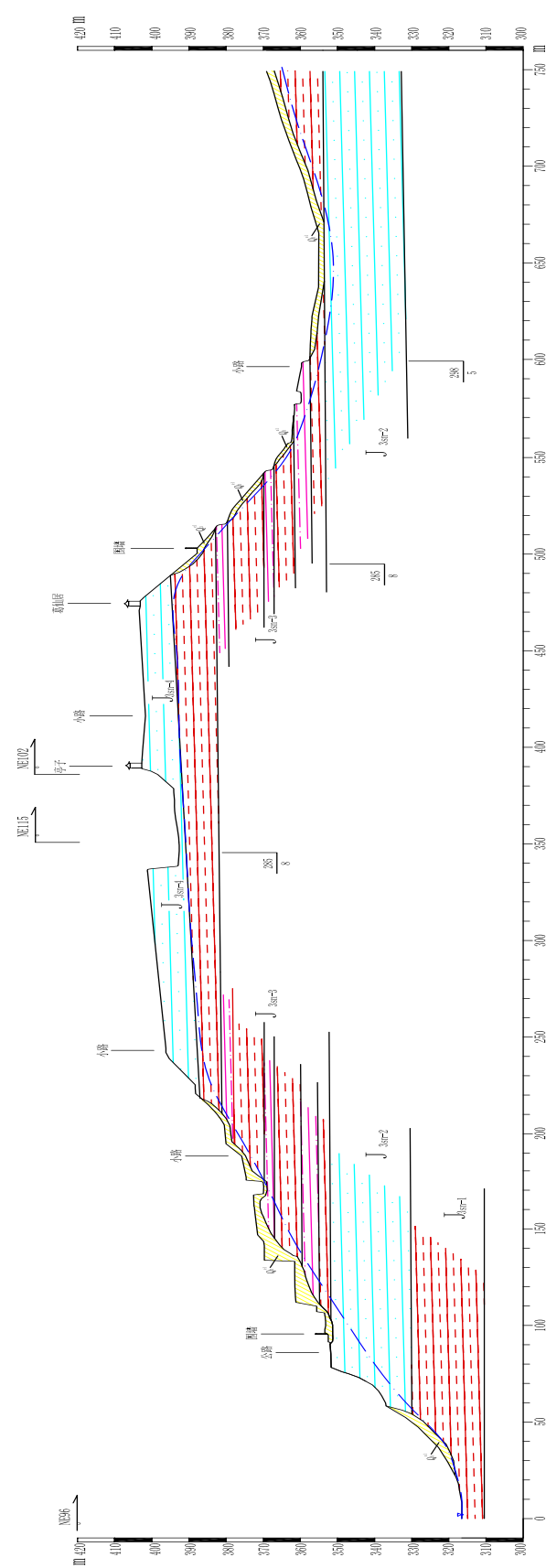
# 圆觉洞石刻保护区裂隙分布图

## Fissure Distribution Map



中国地质大学（武汉）文化遗产和 岩土文物保护中心		项目名称	四川安岳圆觉洞石刻区环境地质病害调查	
项目负责	方云	图号	附图2	比例尺 1:1000
制图 阎波 校核 刘建辉		图名	圆觉洞石刻保护区裂隙分布图	
2007.11	严绍军	审核	日期	2007.11

安岳圆觉洞石刻保护区I-I'地质剖面图  
I-I' Profile Map

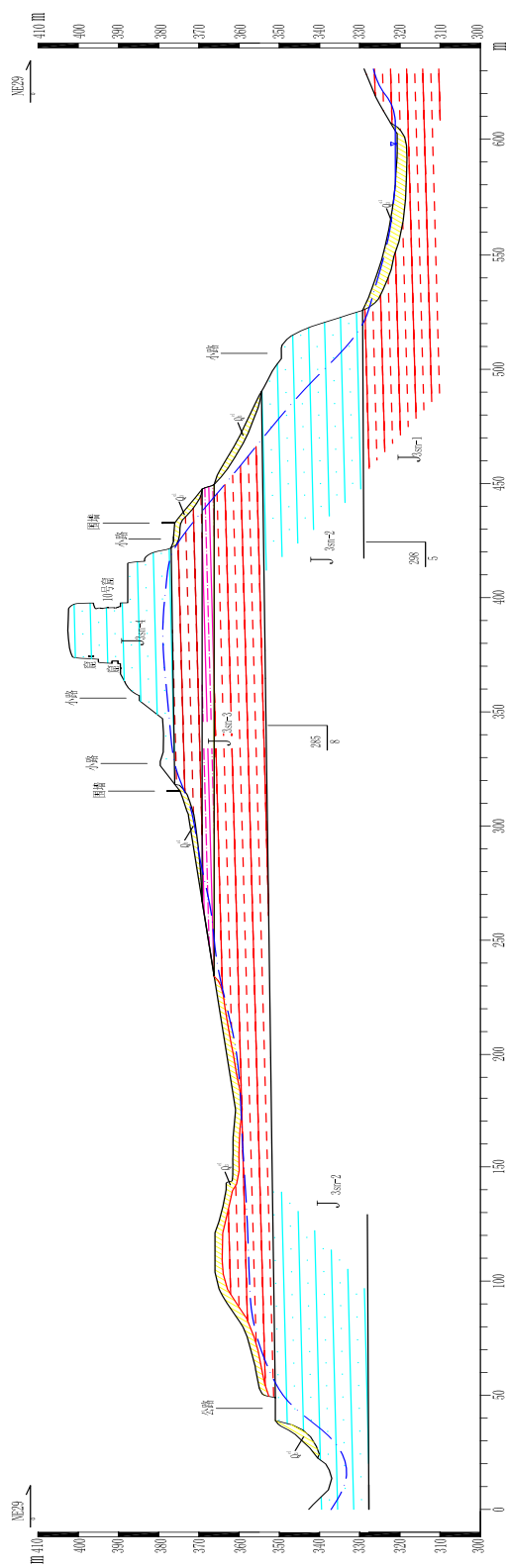


图例:

- $J_{3\text{c}2}$ : 假山系灰岩~页岩互层
- $J_{3\text{c}1}$ : 假山系灰岩~页岩互层
- $J_{3\text{b}2}$ : 假山系灰岩~页岩互层
- $J_{3\text{b}1}$ : 假山系灰岩~页岩互层
- $J_{3\text{a}2}$ : 假山系灰岩~页岩互层
- $J_{3\text{a}1}$ : 假山系灰岩~页岩互层
- $J_{2\text{c}2}$ : 假山系灰岩~页岩互层
- $J_{2\text{c}1}$ : 假山系灰岩~页岩互层
- $J_{2\text{b}2}$ : 假山系灰岩~页岩互层
- $J_{2\text{b}1}$ : 假山系灰岩~页岩互层
- $J_{2\text{a}2}$ : 假山系灰岩~页岩互层
- $J_{2\text{a}1}$ : 假山系灰岩~页岩互层
- $Q_1$ : 风积物

中国地质大学(武汉)文化遗产和 岩土文物保护中心		
项目负责	方云	图号 附图3
制图	黎若普	图名 四川安岳圆觉洞石刻保护区I-I'地质剖面图 审核 李建群 审核时间 2007.11

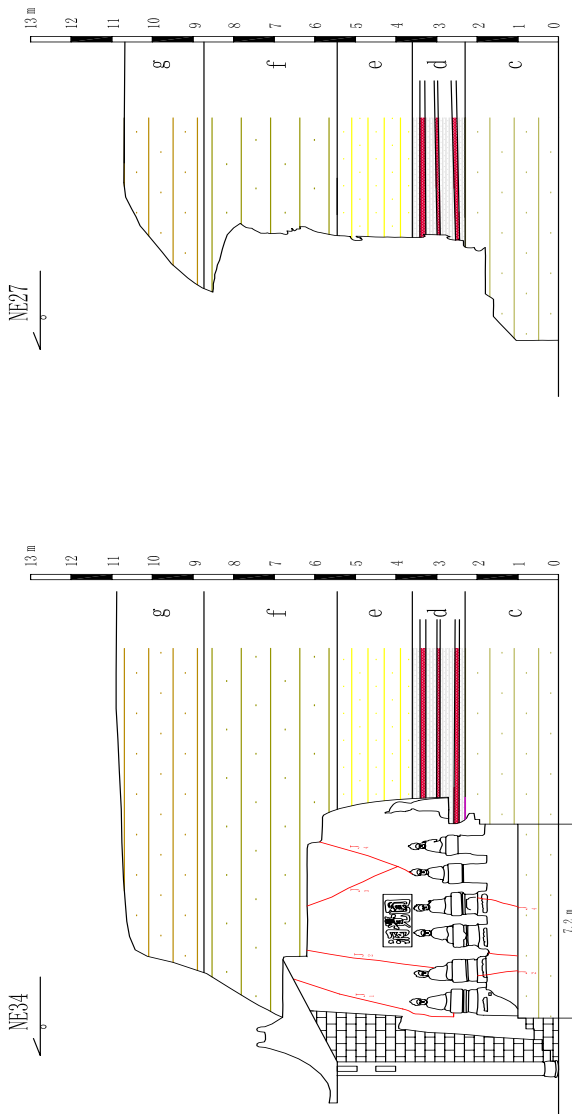
安岳圆觉洞石刻保护区II-II'地质剖面图  
II-II' Profile Map



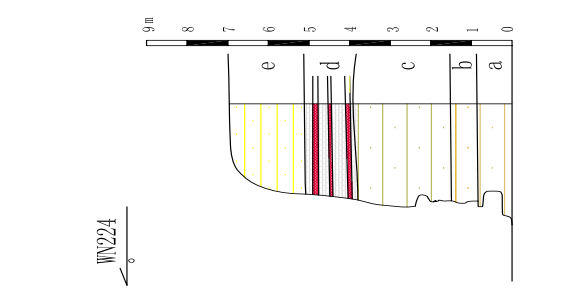
中国地质大学(武汉)文化遗产和 岩土文物保护中心		项目名称	四川省安岳圆觉洞石刻保护区踏查	
项目负责		图号	图名	
制图 朱华 校核 刘建峰 审核 严绍军		图 4	安岳圆觉洞石刻保护区II-II'地质剖面图	

比例尺 1:1000  
日期 2007.11

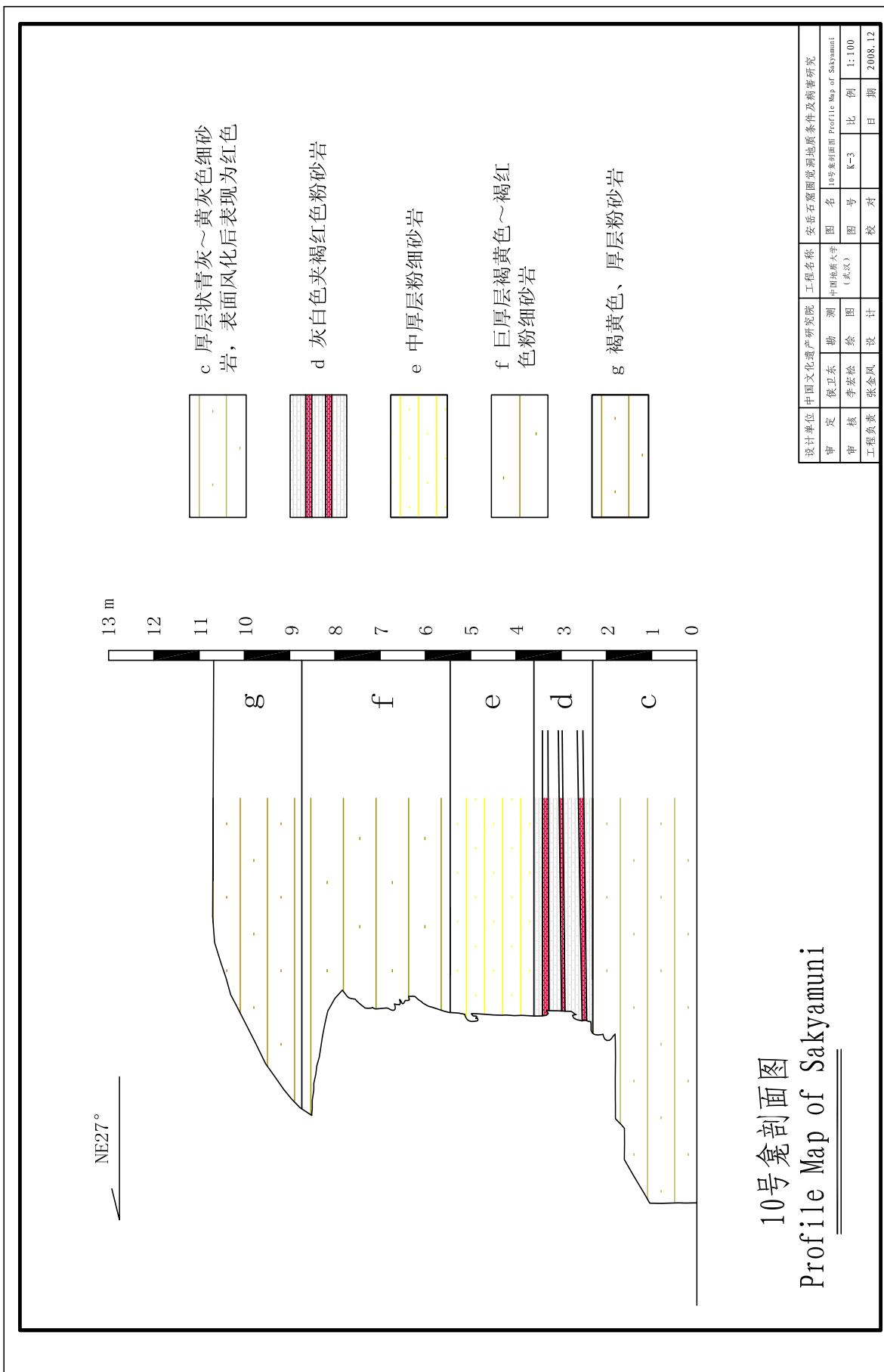
圆觉洞剖面图  
Group 9 Profile Map



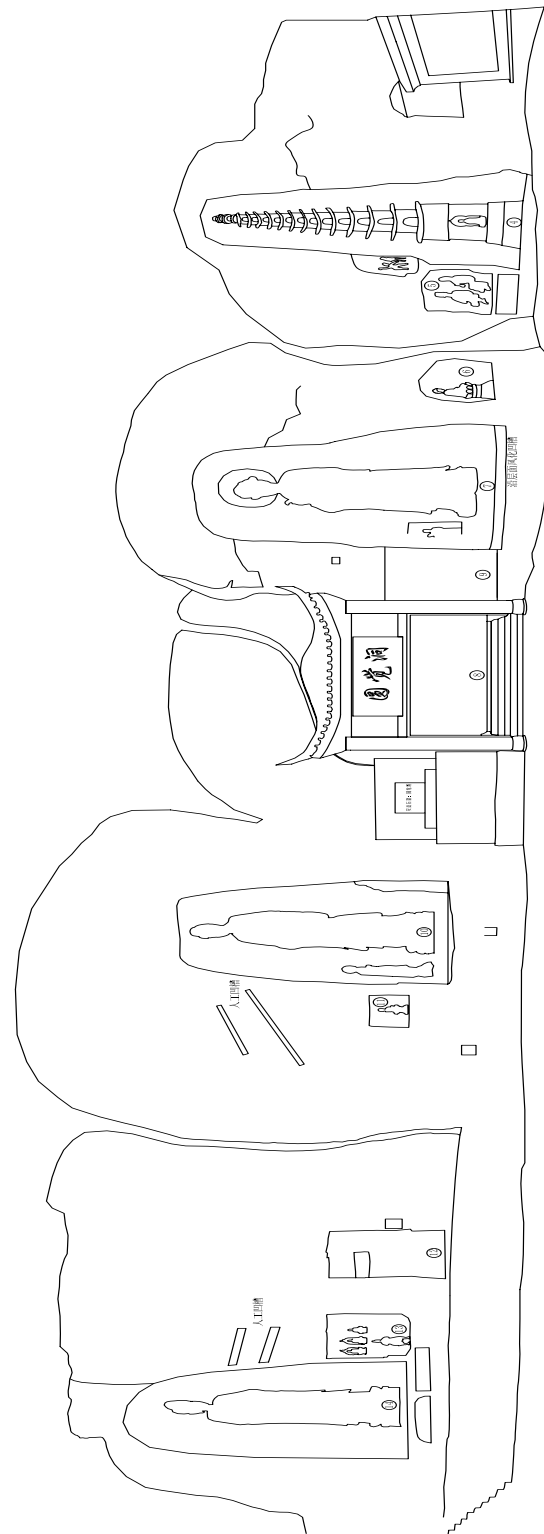
5号窟剖面图  
Group 10 Profile Map



中国地质大学(武汉)文化遗产和 岩土文物保护中心	项目名称	四川安岳圆觉洞石刻区环境地质病害调查
项目负责	图名	附图 5 比例尺 1:100 1. 圆觉洞剖面图 3、10号窟剖面图 2. 5号窟剖面图
制图	审核	刘建辉 审核 严绍军 日期 2007.11



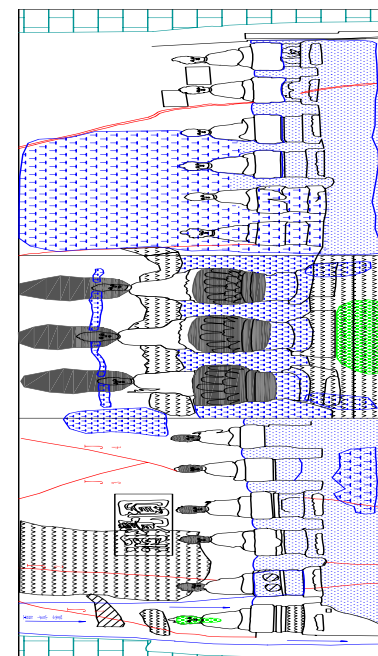
四川安岳圆觉洞石刻保护区北壁立面图  
Northern elevational drawing



中国地质大学(武汉)文化遗产和 岩土文物保护中心	项目名称 四川安岳圆觉洞石刻保护区地质调查 图号	图名 四川安岳圆觉洞石刻保护区北壁立面图	比例尺 1:100
项目负责 方云	审核 刘建辉	日期 2007.11	
制图 朱华	校核 严绍军		

四川安岳圆觉洞窟立壁病害调查图

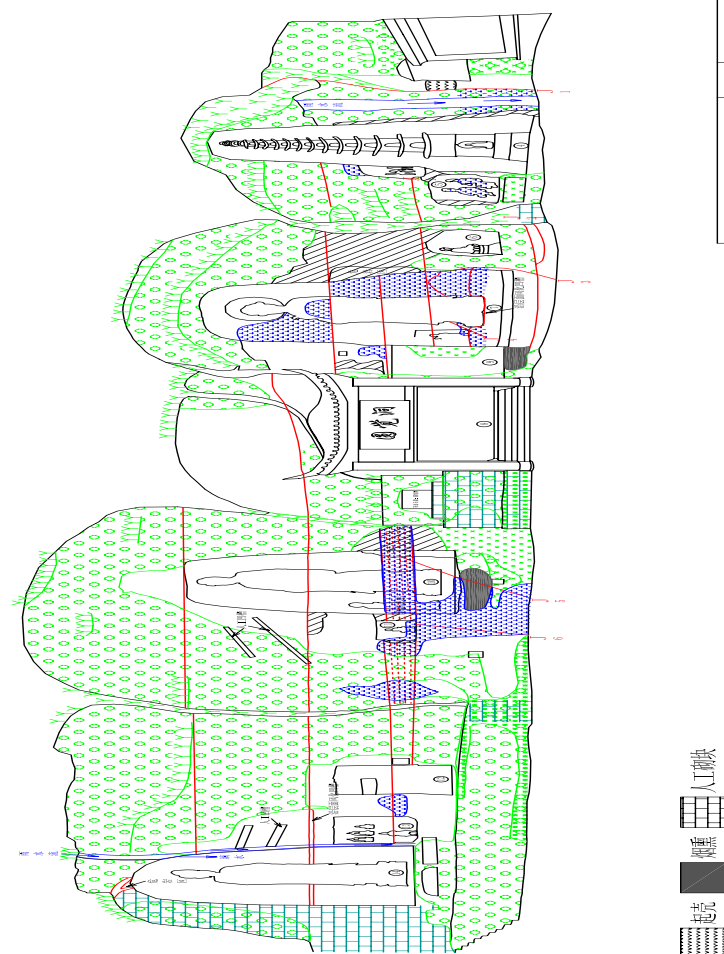
Decay Distribution Map



东壁 南壁 西壁  
左壁 右壁

四川安岳圆觉洞石刻保护区北壁病害调查图

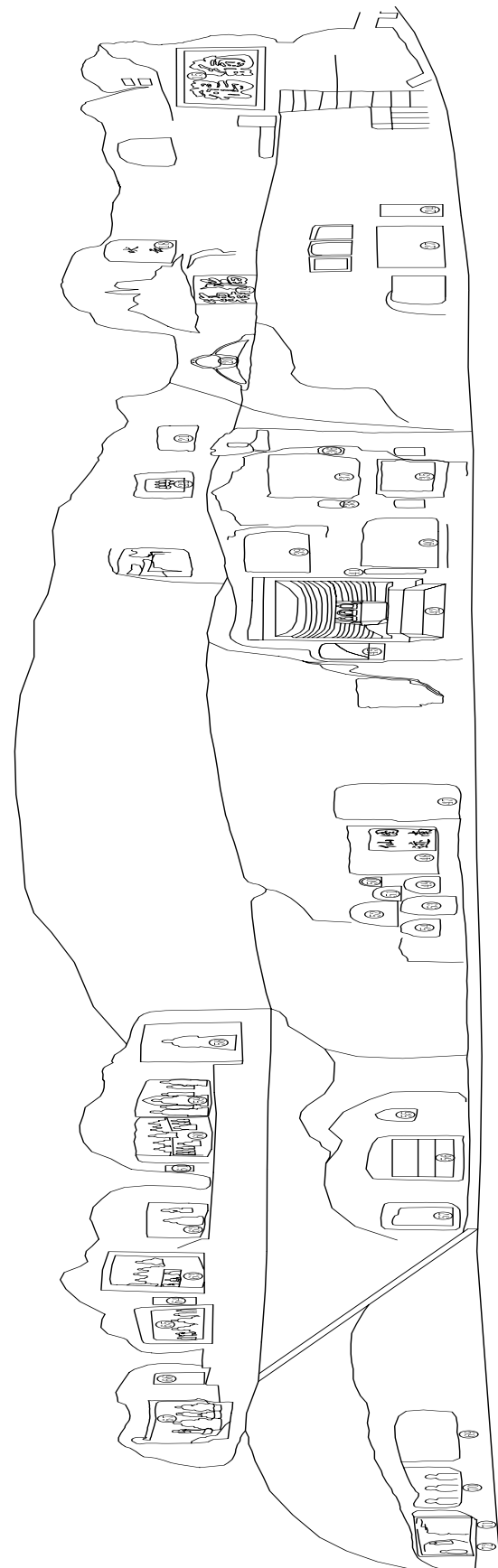
Decay Distribution Map



东壁 南壁 西壁  
左壁 右壁

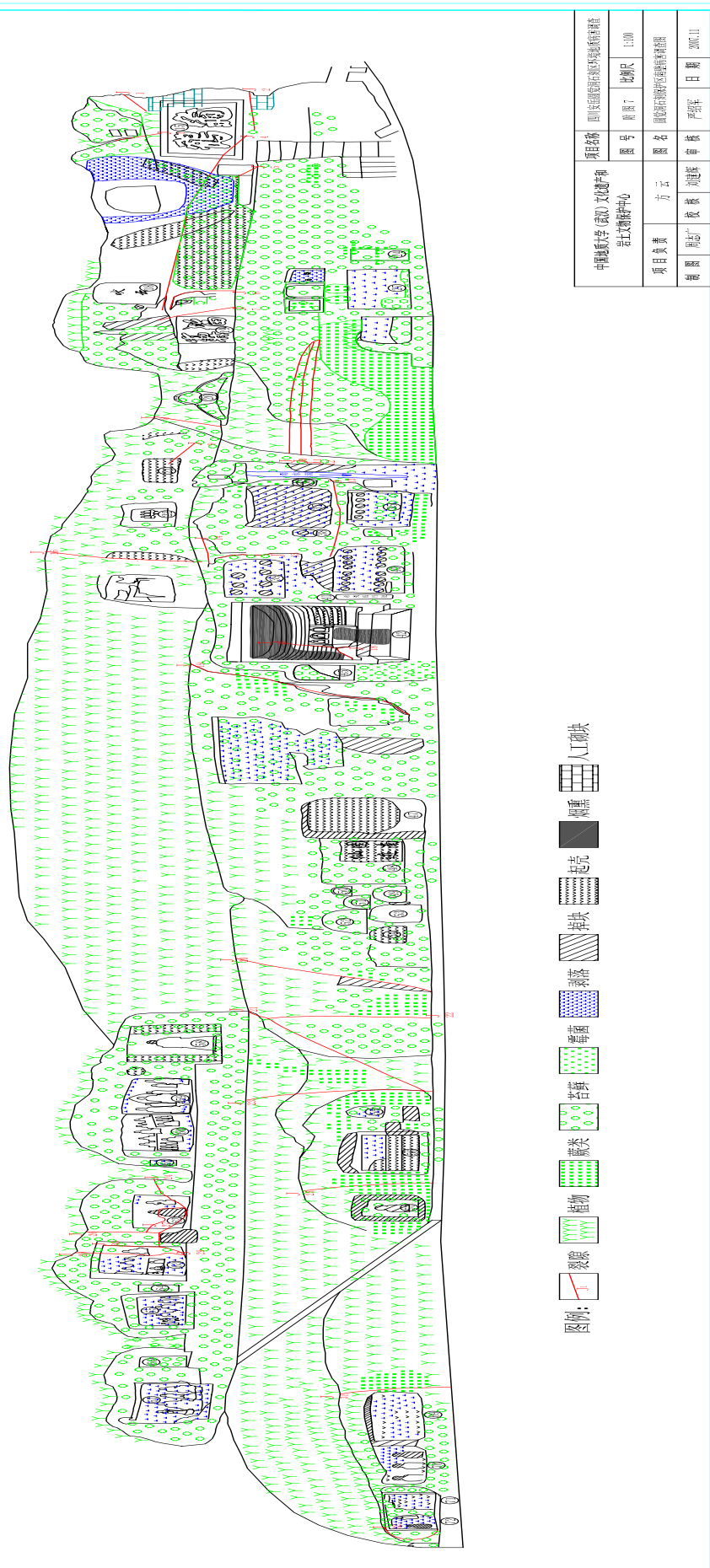
中国科学院成都文物考古研究所 岩土文保中心	领办人	项目名称
	项目负责人	1. 传统洞窟病害调查 2. 岩溶石窟风化病害调查
	方云	图名
	制图 李华	1:50000
	校核 钟伟	2007.11
	审核 严翠平	
	日录	

四川安岳圆觉洞石刻保护区南壁立面图  
Northern elevational drawing



中国科学院成都生物研究所	刘遵海	用途	四川省重点文物保护单位
岩土文物研究中心	方云	图号	1:100
项目负责	方云	图名	四川安岳圆觉洞石刻保护区南壁立面图
制图	朱华	校核	审核
		严翠平	日期
		2007	2009

四川安岳圆觉洞石刻保护区南壁病害调查图  
Decay Distribution Map





**Examination of the stone samples from the Yuanjue  
grottos, Anyue, in the province Sichuan**

**Rolf Snethlage, Erwin Emmerling, Mathias Kocher and  
Melanie Eibl**

**Technische Universität München, Lehrstuhl für Restaurierung,  
Kunsttechnologie und Konservierungswissenschaft**

**Bayerisches Landesamt für Denkmalpflege,  
Zentraallabor**



## Contents

<b>Basics .....</b>	135	<b>Stone Values – Anyue Sandstone .....</b>	146
<i>The Structure of Rocks .....</i>	135		
<i>Weathering .....</i>	135		
<b>Objective of Stone Conservation .....</b>	135	<b>Results of the Treated Samples .....</b>	148
<b>Laboratory Analysis .....</b>	135		
<b>Hygric Values .....</b>	135	<b>Hygric Values .....</b>	148
<i>Porosity .....</i>	135	<i>Water Absorption .....</i>	148
<i>Water absorption .....</i>	136	<i>Isothermal Line of Sorption .....</i>	148
<i>Isothermal Line of Sorption .....</i>	136	<i>Hygric Dilatation .....</i>	148
<i>Hygric Dilatation .....</i>	137		
<b>Thermal Values – Thermal Dilatation .....</b>	137	<b>Thermal Values – Thermal Dilatation .....</b>	149
<b>Mechanical Values .....</b>	137	<b>Mechanical Values .....</b>	149
<i>Bending Tensile Strength .....</i>	137	<i>Bending Tensile Strength .....</i>	149
<i>Drill Resistance .....</i>	138	<i>Drill Resistance .....</i>	150
<b>Consolidation Treatment .....</b>	138	<b>Summary .....</b>	151
<i>Consolidation Products .....</i>	139	<b>Endnotes .....</b>	152
<i>Consolidation Treatment .....</i>	139	<b>Literature .....</b>	153
<i>Parameters .....</i>	139	<b>DIN-Standards (selection) .....</b>	154
<b>Results of the Untreated Samples .....</b>	141	<b>List of Illustrations .....</b>	155
<b>Hygric Values .....</b>	141	<b>List of Tables .....</b>	155
<i>Porosity – Mercury Porosimetry .....</i>	141	<b>Appendix .....</b>	156
<i>Water Absorption .....</i>	141		
<i>Isothermal Line of Sorption .....</i>	142		
<i>Hygric Dilatation .....</i>	142		
<b>Thermal Values – Thermal Dilatation .....</b>	143		
<b>Mechanical Values .....</b>	143		
<i>Bending Tensile Strength .....</i>	143		
<i>Drill Resistance .....</i>	144		



## Basics

### Structure of Rocks

Every rock is made up of various mineral components, which influence the stone structure due to their linkage. The qualitative and quantitative description of stone can be made based on the primary petrographic characteristics like mineralogical composition and structure. Based on these basic characteristics, material specific values like mechanical and thermal features can be derived.

The petrographic characteristics of rocks (minerals, structure and chemism) allow them to be unmistakably classified. The mineral composition provides for a qualitative and quantitative description of the rock's components, in other words a listing of the mineral types and the volume percent of each mineral. Major components are those minerals which comprise more as 10 vol.% of the rock. Minor components comprise less than 10 vol.% and accessory components less than 2 vol.%.<sup>1</sup>

The stone structure is characterised by texture and pore structure, whereby the pore structure is described by pore volume, pore size, pore form, pore distribution and the inner surface of the pores. The identification of these features allows not only classification of the stone but also determination of transport processes of gaseous and liquid phases, weathering processes as well as the stability of the stone. In order to control the consolidation treatment and to prove effectiveness, knowledge about the structure is imperative. The term structure includes all steric aspects of the components and their steric relation to one another. The structure describes the steric aspects of the single mineral grains, whereas the texture describes the steric arrangement of the mineral grains. The structure is described by absolute and relative size of the grains, the habitus of the components and the degree of growth of typical grain shapes.<sup>2</sup>

### Weathering

Every stone, as a natural material, is exposed to factors like climate, biosphere and pollutants. Alteration due to physical, chemical and biological weathering processes result in a modification of the rock's characteristics. Most of these mechanisms occur in the surficial pore space, and so the alteration of a stone is significantly affected by its porosity values. At the same time, every weathering process effects a change in the pore space. Thereby, the stone's structure also affects its durability. In addition, the durability of the single minerals as well as the linkage of the grains are of importance. The state of weathering can be evaluated by determining

the stone parameters, which enables the assessment of changes caused by weathering.

### Objective of Stone Conservation

The goal of stone conservation is to improve the durability of natural stone. Usually the altered stone structure has to be additionally stabilised and the capillary water absorption reduced. The application of the consolidants changes the stone's physical behaviour. Scientific analyses are of great importance, not only to describe the state of weathering, but also to determine the appropriate consolidation products and methods, as well as to document the success of consolidation treatments.<sup>3</sup>

The standard methodology and its significance in the field of stone conservation will be described subsequently, followed by a detailed description of the examination of the Anyue sandstone, including the presentation of the results of the study.

### Laboratory Analysis

#### Hygric Values

With the exception of weathering caused by temperature changes, all the weathering processes within the stone are connected to the presence of water. Every stone has specific hygric parameters which are defined by sorption, desorption and permeation processes. The behaviour of water in stone, which depends upon the pore space, is of significant importance. Different correlations between pore structure and hygric transport exist so that the degree of porosity can be defined according to the amount of water absorption. All hygric transport and hygric expansion values are part of the basic data that must be gathered before consolidation treatment.<sup>4</sup>

#### *Porosity*

All physical and mechanical attributes of the material depend significantly upon the pore system.<sup>5</sup> The pore structure is of central importance regarding weathering processes and consolidation treatments. The pore structure is influenced by the porosity (volume percent of the pores), as well as size and shape of the pore spaces (pore structure).

The pore system is very complex, requiring varying classifications. A basic subdivision can be made by characterising open and closed pores. Open pores interact with the surrounding atmosphere whereas closed pores are completely isolated. Porosity is the ratio of all pores in the stone to its total volume,

whereby the amount of pores ( $n$ ) is the proportion (%) of spaces filled with liquids or gases.<sup>6</sup>

$$n = \frac{V_p}{V_g} \cdot 100 = \frac{V_p}{V_s + V_p} \cdot 100 \text{ [Vol. %]}$$

$V_p$  = pore volume,  $V_s$  = volume of solids,  $V_g$  = total volume

The total porosity includes all pores in a stone regardless of whether they are open or closed pores. Therefore, it is the largest possible porosity value that can be calculated according to the DIN 52501 formula (particle density – bulk density)/particle density. The actual pore space is defined by determining the water absorption in a vacuum.

The various pore types have various sizes. Size is therefore another method of classification. There are various methods of analysing pore spaces. The classic method is microscopic analysis of thin sections of stone. By parallel use of image analysis, pore structure, size and form can be quantitatively determined and statistically interpreted. Only the pores visible under a microscope are taken into consideration. The most frequently used indirect measuring method in this case is the mercury porosimetry; the method which allows the largest amount of pore space in the stone to be determined. The values are calculated using standard pore models, whereby the real pore form cannot be analysed. Using this method, the distribution of pore spaces in relation to certain pore radii ranges can be depicted.

The radius of the pore determines the pressure needed to inject the mercury. Radius and volume of the specific pore group can be determined by the pressure used and the amount of mercury injected.<sup>7</sup> However, it must be taken into account that pore radii are pore penetration radii, so that the measurement may deviate from the actual pore size distribution. A general classification of the pore groups is listed in table 1.

**Table 1:** Classification of pore sizes according to IUPAC, DIN 66131 and architectural literature

Classification	Radius (IUPAC and DIN 66131)	Radius (architectural) <sup>8</sup>
Macropores	> 0,05 µm	> 100 µm
Mesopores	0,002–0,05 µm	0,1–100 µm
Micropores	< 0,002 µm	< 0,1 µm

The classification according to IUPAC and DIN 66131 is not solely used for rocks. Therefore this report uses the architectural method of classification for evaluation of the analytical results.

In addition to the total porosity, the distribution of pore sizes has a significant effect on the physical property of stone. Compression strength, tensile

strength and water absorption of a stone mainly depend upon its absolute porosity, while hygric dilatation for example is more influenced by pore size distribution.

### Water Absorption

Evaluation of water absorption allows determination of the porosity of stone. This evaluation additionally allows determination of how water absorption changes after conservation treatments are applied. Water absorption and porosity are determined using the Archimedes method, for which three different methods of weighing are used.<sup>9</sup>

- 1 Weighing while dry with air in the pores ( $m_1$ )
- 2 Weighing while saturated with water, with pores full of water ( $m_2$ )
- 3 Weighing while saturated with water while under water ( $m_3$ )

The porosity ( $n$ ) can than be calculated using the equation:

$$n = \frac{(m_2 - m_1)}{(m_2 - m_3)} \text{ [Vol. %]}$$

Water absorption under atmospheric pressure is the highest possible water absorption of stone under normal pressure, determined using DIN-EN 13755 (formerly: DIN 52103). A sample, dried at 70 °C and then cooled to room temperature, is immersed in distilled water for 48 hours before the amount of water absorbed is measured in relation to the weight of the dry sample [mass%]. Additionally, the amount of absorption in a vacuum is measured. The dry samples are evacuated and immersed in water for 48 hours before absorption is measured. The value of saturation is the ratio of water absorption under atmospheric pressure to water absorption in a vacuum.<sup>10</sup>

The bulk density [g/cm<sup>3</sup>] is the density of a stone including pore space when completely dry. In accordance with DIN-EN 1936 the buoyancy of the water-saturated specimen of defined volume is weighed after drying at 70°C. The density [g/cm<sup>3</sup>] on the other hand is the density of only the stone substance itself, excluding the pores. DIN-EN 1936 is also used in this case to determine the total porosity [Vol. %], which is the percent of total pore volume to the total volume of the stone. The actual porosity [Vol. %] only includes the pore space in which gases and liquids can interact.

### Isothermal Line of Sorption

The isothermal line of sorption is used to determine why moisture has penetrated a stone. The series

of measurements allow assessment of the rock's water absorption in the hygric range (between 0 and 98% RH) at various constant and defined humidities.

While planning consolidation treatment, knowing the isothermal line of sorption is important in order to define ideal humidity conditions for use during treatment.<sup>11</sup> As a certain amount of water in the pore spaces is necessary in order for the consolidants to harden, the isothermal line of sorption allows for determination of which relative humidity will ensure the necessary water content in the rock.

#### *Hygric Dilatation (swelling due to water absorption)*

Swelling describes the process of solid matter that undergoes a change in volume due to exposure to liquids and gases. The mineral composition of stone does not change during this process. The water intake causes an increase in volume, which in most cases is reversible. The clay mineral content is significant due to the intercrystalline swelling of clay, which causes additional swelling in the stone.<sup>12</sup>

The quantification of swelling can be measured by evaluating the change of length of the sample using distilled water as fluid. The change of length due to hygric dilatation, as regard to time applied, asymptotically approaches a maximum value. Therefore it is necessary to define the end of the experiment, and thus at which point to take the final measurement. Only this method can provide comparable and reproducible values. In general, sandstones reach a 98 % change of length after the first 48 hours. Therefore, the 48-hour-value is used to calculate the hygric dilatation. In practice, the 48-hour value is of significance because it is also used to calculate the water absorption and to determine the degree of swelling and shrinkage. Nevertheless, specification of the interval and the period of measurement is important in order to adjust the results as seen in a greater context.<sup>13</sup>

#### **Thermal Values – Thermal Dilatation**

Most substances react to heat with an increase of volume (expansion) and to cooling with a loss of volume (contraction). In practice, thermal dilatation is important if a stone is exposed to repeated natural temperature variations, which causes stress and damage to the material structure.<sup>14</sup>

The thermal dilatation  $\Delta l$  of a stone is, at moderate temperatures and minor temperature changes, nearly proportional to the original length  $l_0$  and the temperature difference  $\Delta T$ . The formula is:

$$\Delta l = l_0 \alpha T$$

with  $l_0$  length at 0°C and  $\alpha$  as linear dilatation coefficient.

The evaluation of the thermal dilatation coefficient  $\alpha$  [ $\mu\text{m}/\text{m}^\circ\text{C}$ ] is based on DIN-EN 14581. It is the linear dilatation of a specimen related to its length at 20°C per degree temperature increase. In practical laboratory work it is measured by heating the specimen to a defined temperature and measuring the contraction while cooling the sample.<sup>15</sup>

#### **Mechanical Values**

The mechanical characteristics of stone can be described by determining its strength and hardness. The difference between strength as mechanical resistance with which a stone resists its deformation, and hardness as resistance of a stone towards the distortion of its surface must be taken into account.<sup>16</sup>

The strength can be determined by the deformation of a stone specimen placed under pressure, while the pressure at which the fracture occurred is quoted. In physics, a fracture is a complex process involving breaks due to separation, sliding, shearing and shifting. The break begins with micro-fissures between the mineral grains.<sup>17</sup>

#### *Bending Tensile Strength*

Every form of weathering causes loss in strength. Measuring the strength of stone is therefore of great significance especially when planning conservation treatments. Strength can be defined as the sum of bonding energy of a compound.<sup>18</sup> In most cases, there is no pure form of linkage but a coexistence of bonding types (coagulation contact, atomic contact and phase contact) (fig. 1). The strength is influenced by a number of parameters like material composition, form and size of the specimen, alteration and treatment of the samples. Strength is therefore not a value that can be definitely defined physically, and thus testing standards are necessary to guarantee comparability of the results.<sup>19</sup>

According to the standard DIN-EN 14580 the measurement of bending tensile strength has to be performed with slices of stone placed between two steel rings. The stone slice diameter should be a minimum of 50 mm, with the ratio of slice diameter to slice thickness being 1 : 10.

The amount by which a material body is deformed (the strain) is linearly related to the force causing the deformation (the stress) (Hooke's law). With increasing inelastic deformation, the curve's course deviates from that linear curve until the specimens reaches its breaking point. The elasticity of a material is described by Young's modulus (E-modulus), which is determined by the increase of the stress-strain-relation (straight line). A low E-modulus value indicates great strain with low tension differences, and a high E-modulus value indicates low strain with high tension differences.<sup>20</sup>

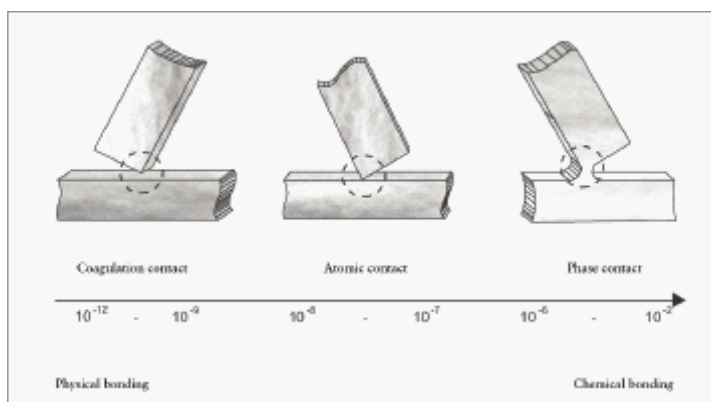


**Fig. 1:** Various contact types with their corresponding bonding strength

### Drill Resistance

The drill resistance measurement is a micro-destructive method, which is used to determine the stone's hardness, whereby obtaining information about the depth profile is also possible. The basic principle here is the correlation between drill resistance and strength of the stone material. The method is based on the characterization of the drilling process by using the values of drill speed, torque and contact pressure. If both the penetration and rotation values are kept constant, both other values can be used to determine the drill resistance.

The drill resistance profile gives values as [mm/min] or ascent angle [ $^{\circ}$ ] of the recorded curve (penetration speed) or, for the DRMS machine from the company Sint which was used for these analyses at the "Bayerisches Landesamt für Denkmalpflege", also the drill resistance [N]. The drill hole with a diameter of two to five millimetres is relatively

small. A depth resolution of one millimetre allows detection of surficial alterations or contour scaling. The drill bits are diamond drill bits, which must be calibrated using a standard material. Every drill bit used must be named and stored for later use to obtain comparable measurements.<sup>21</sup>

### Consolidation Treatment

The loss of bonding force caused by different weathering processes in the stone leads to loss of strength. The need for conservation treatment can be determined by analysing the state of the weathering as well as the parameters of an unweathered stone. The goal of consolidation treatment is to restore the weathered stone's homogenous depth profile, so that it is comparable to the unweathered stone, by use of a binder. The first step is therefore determination of the values of the intact stone. Then, all values of

**Table 2:** Product specification of the three consolidants as indicated by the manufacturer

	<b>KSEOH</b>	<b>KSE100</b>	<b>KSE300</b>
Active ingredients [Mass%]	75	20	99
Catalytic system	neutral	neutral	neutral
Density at 20°C [g/cm <sup>2</sup> ]	0,95	0,79	1,0
Colour	clear, yellow touch	clear, yellow touch	clear, yellow touch
Smell	typical	typical	typical

**Table 3:** Product specification of the three consolidants after application

	<b>KSEOH</b>	<b>KSE100</b>	<b>KSE300</b>
gel deposit [g/L]	300	100	300
reaction-related by-product	ethanol (gaseous)	ethanol (gaseous)	ethanol (gaseous)

the treated samples are again measured, and again compared to the values of the intact stone. Finally, the product most suitable for consolidation treatment is chosen and tested.<sup>22</sup>

### *Consolidation Products*

For these laboratory tests, pre-selected consolidation products from the company Remmers were tested: Funcosil stone consolidant OH (KSEOH), Funcosil stone consolidant 100 (KSE100) and Funcosil stone consolidant 300 (KSE300).<sup>23</sup> These three stone consolidants are, according to the manufacturer's description, suitable for the consolidation of semi-porous, absorbent, unconsolidated mineral materials, especially sandstone.<sup>24</sup> They differ in regards to their active ingredients, density and gel deposit, as shown in tables 2 and 3.

The silicic esters (KSE) used here are orthosilicic acid  $H_4SiO_4$  esters. These compounds result from the chemical reaction of silicon halogenides with alcohols; they are also called ethyl silicates. Due to their ability to produce silicon dioxide through hydrolysis (e.g. humidity) by releasing ethanol, they are used as artificial binders for the consolidation of natural stone. Today tetraethyl-orthosilic esters are predominantly used; their ability to consolidate comes from their formation of amorphous, hydrous  $SiO_2$ -gels that fills the pore spaces of the stones.

The chemically and physically induced hardening process of KSE is a sol-gel process which can be divided into several phases:<sup>25</sup>

1. Evaporation of the solvent without a noticeable increase of viscosity and minor hydrolysis. Only isolated Si-O-Si-clusters are present.
2. After the evaporation of the solvent, sudden gel-formation takes place simultaneous to an increase of viscosity.
3. Inside the gel, further hydrolysis, condensation and polymerization continues to occur, whereby alcohol is produced. The alcohol evaporates and the gel's density increases. Condensation reactions cause inner tension in the gel layers. This tension becomes so strong that it exceeds the inner strength, leading to fissures.
4. The end product of the gel formation is a brittle, hyaline substance whose general formula is  $SiO_2 \times nH_2O$ .

The entire chemical reaction could be described with the following molecular formula:



This molecular formula can be schematically divided into two successive stages:

1. The separation of alkyl groups, called hydrolysis, and the protonation of free oxygen to silanol groups.
2. The condensation and polymerization of  $SiOH-HOSi$ -structures ( $H_2O$  separation) to disordered  $SiO_2$  lattice structures.

These reactions are sensitive to pH-values and temperatures, which influence the gel characteristics in the same way as the presence of salts does in the stone.<sup>26</sup>

### *Consolidation Treatment*

During these laboratory experiments 14 stone slices ( $\varnothing$  76 mm, 8 mm thick) and 2 cubes (50 x 50 x 50 mm) respectively were treated with the chosen consolidation products (KSEOH, KSE100 and KSE300). During treatment the laboratory conditions were kept constant at 50 % relative humidity and 24°C. Before treating the samples with the consolidation products their dry weight was determined. The consolidation product was absorbed by means of capillary immersion: the slices were brought into contact with the consolidation product for three minutes on each side, and the cubes for one minute on each side. The specimens were then weighed after being swabbed on all sides, but before being dried (hardening of the consolidation agent) at 65 % relative humidity and 20°C. After the drying period of about six weeks, the treated samples were again weighed. The values of absorption of consolidation products shown in figure two are based on these differing weights.

### *Parameters*

There are various parameters for assessing the effectiveness of a consolidation product.<sup>27</sup>

In theory, the visual properties of the material should not change as a result of the consolidation treatment. In fact, most consolidation products cause a certain darkening of the stone. The criteria "visual characters" must therefore always be assessed separately for every single case.

Water absorption and penetration should be reduced after the treatment. Both values usually drop due to reduction in the diameter of macro pores capable of absorbing.

The penetration depth of the consolidant must pass by the zone of reduced stability and reach the unweathered zone of the stone. In practice, the desired or necessary penetration depth must be reached in about two to maximum five minutes.

The hygric dilatation – the expansion and contraction of stone due to presence of moisture - must not be modified in a way that results in an increase in the inner tensions of the stone after treatment. In the best-case scenario, the treatment reduces the moisture expansion of a stone.

SNETHLAGE refers to the importance of the relation of strength to the E-modulus, which should only increase in a constant proportion according to the quotient of bending tensile strength and the E-modulus of the unweathered stone.<sup>28</sup>

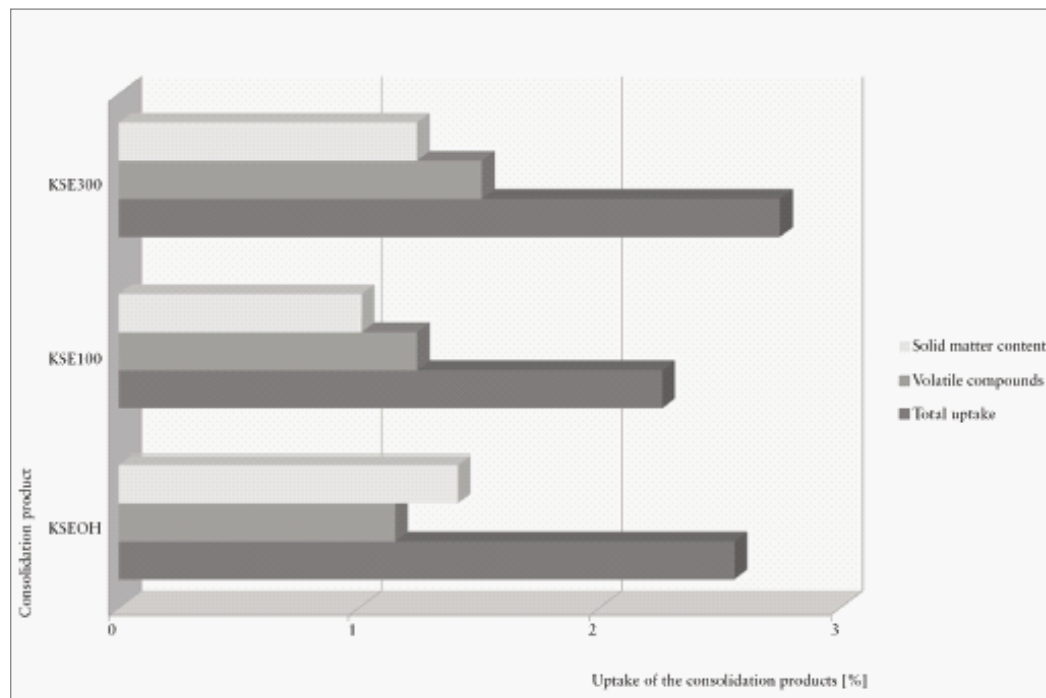


**Fig. 2:** Differing absorption of the consolidation products by the stone slices

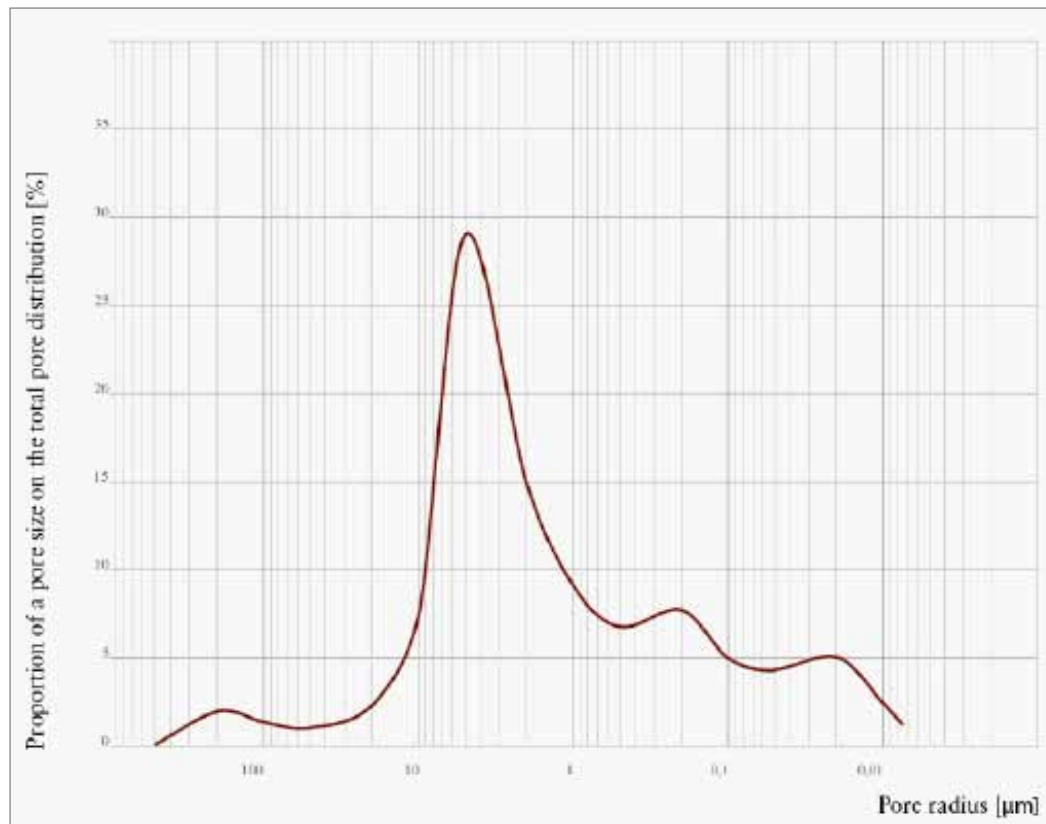


**Fig. 3:** Results of the Mercury Porosimetry

## Results of the Untreated Samples

### Hygric Values

#### *Porosity – Mercury Porosimetry*

The porosity was determined using mercury porosimetry on six untreated samples by the INSTITUT FÜR PALÄONTOLOGIE DER FRIEDRICH-ALEXANDER-UNIVERSITÄT ERLANGEN-NÜRNBERG. The average-value curve in figure 3 was calculated using the single values of all six analyses.

The curve indicates the ratio of the pore radii to the total number of pores. In the case of the Anyue Sandstone, the curve indicates that macropores are nearly nonexistent. Around 70 % of all the pores are mesopores with a radius of between 10 and 1 µm (max. height of curve at 5 µm). Circa 20 % of the pores are micropores, classified according to the architectural method indicated in table 4. The samples from Anyue are therefore fine-pored sandstone.

**Table 4:** Classification of pore sizes according to IUPAC, DIN 66131 and architectural literature

Classification	Radius (IUPAC and DIN 66131)	Radius (architectural) 29
Macropores	> 0,05 µm	> 100 µm
Mesopores	0,002–0,05 µm	0,1–100 µm
Micropores	< 0,002 µm	< 0,1 µm

#### *Water Absorption*

To assess the water absorption of the samples from Anyue, they were placed in a cabinet drier with a temperature of 60°C for 48 hours to reach their constant mass. Before determining the dry weight ( $m_0$ ) the samples were placed in an exsiccator until they reached room temperature.

Determination of water absorption took place under atmospheric pressure (WAa) in a vacuum (WAv). Rock under atmospheric pressure absorbs water through its capillaries. To this end, the samples are immersed in approximately one centimetre of water, and the rock absorbs the water through its capillaries until it reaches the surface of the sample. The samples are then totally immersed in ca. three centimetres of water for 48 hours before the wet weight is determined.

To assess water absorption in a vacuum, the samples are initially placed in an exsiccator for a minimum of five hours. This is subsequently flooded with water until the samples are immersed in around five centimetres of water. Again, the wet weight is determined after 48 hours. Additionally, by weighing under water, the buoyancy (determination of volume) is tested.

Tables 5 and 6 show the resulting values gathered by water absorption, like porosity, saturation, particle density and bulk density. The complete results of the analyses can be found in the appendix, pages 156.

The porosity of the Anyue samples tested is relatively high (20 Vol.%), so that they must be called porous rock. The value of 6,5 Mass% of water absorption under atmospheric pressure is also high.

**Table 6:** Results of water absorption tests on the slice samples

Sample	WAa [Mass%]	WAv [Mass%]	Porosity [Vol.%]	Saturation [-]	Particle Density [g/cm³]	Bulk Density [g/cm³]
W1	6,71	9,38	20,03	0,72	2,67	2,14
W2	6,41	9,25	19,80	0,69	2,67	2,14
W3	6,36	9,64	20,50	0,66	2,67	2,12
W4	6,47	9,31	19,91	0,70	2,67	2,14
W5	6,51	9,69	20,57	0,67	2,67	2,12
Average	<b>6,49</b>	<b>9,45</b>	<b>20,16</b>	<b>0,69</b>	<b>2,67</b>	<b>2,13</b>

**Table 5:** Results of water absorption tests on the cube samples

Sample	WAa [Mass%]	WAv [Mass%]	Porosity [Vol.%]	Saturation [-]	Particle Density [g/cm³]	Bulk Density [g/cm³]
(2)1	6,88	8,96	19,34	0,77	2,68	2,16
(2)2	6,49	9,29	19,91	0,70	2,68	2,14
(2)3	6,76	8,92	19,28	0,76	2,68	2,16
(2)4	6,74	8,50	18,54	0,79	2,68	2,18
(2)5	6,81	8,90	19,24	0,76	2,68	2,16
Average	<b>6,74</b>	<b>8,91</b>	<b>19,26</b>	<b>0,76</b>	<b>2,68</b>	<b>2,16</b>

**Table 7:** Relative humidity with saline solutions

Salt	Relative Humidity at 20°C [%]	Solubility at 20°C [g/100g H <sub>2</sub> O]
Lithium Chloride	12	
Calcium Chloride	32	73,9
Potassium Carbonate	45	110,6
Ammonium Nitrate	63	189,6
Sodium Chloride	75	36,0
Potassium Chloride	86	34,4
Copper Chloride	98	11,1

### Isothermal Line of Sorption

The isothermal line of sorption was determined using the following relative humidity values: 12 % RH, 32 % RH, 45 % RH, 63 % RH 75 % RH, 86 % RH and 98 % RH. To this end, the respective humidity values were generated using saline solutions (table 7) in exsiccators.

Measurement of the isothermal line of sorption was taken for each relative humidity on five slice samples. Before the samples were placed in the exsiccators until they reached their constant weight, their dry weight was determined after being dried in a cabinet drier at 60°C and cooled in an exsiccator. The samples were stored in exsiccators until they reached their constant weight (four weeks). After reaching their constant values, the samples were weighed and the percent of water absorbed determined. Figure 4 shows the average values of the five measurements for the respective humidi-

ties. The moisture content of the samples increased as the humidity increased, as was to be expected.

### Hygric Dilatation

The hygric dilatation of the Anyue Sandstone was determined at 98 % relative humidity and under water in directions x, y and z (fig. 6). The dry weight of the samples (cabinet drier at c. 60°C and subsequent cooling in an exsiccator) was determined before they were mounted in the dial gauge (fig. 5).

The measurement period of the hygric dilatation under water was 48 hours, the hygric dilatation at 98 % RH until the constant value was reached took around four weeks. Table 8 shows the average values of hygric dilatation under water at 98 % relative humidity for all three directions (fig. 6).

As indicated in table 8, the rock reached its greatest dilatation in direction z (right angle ss), while

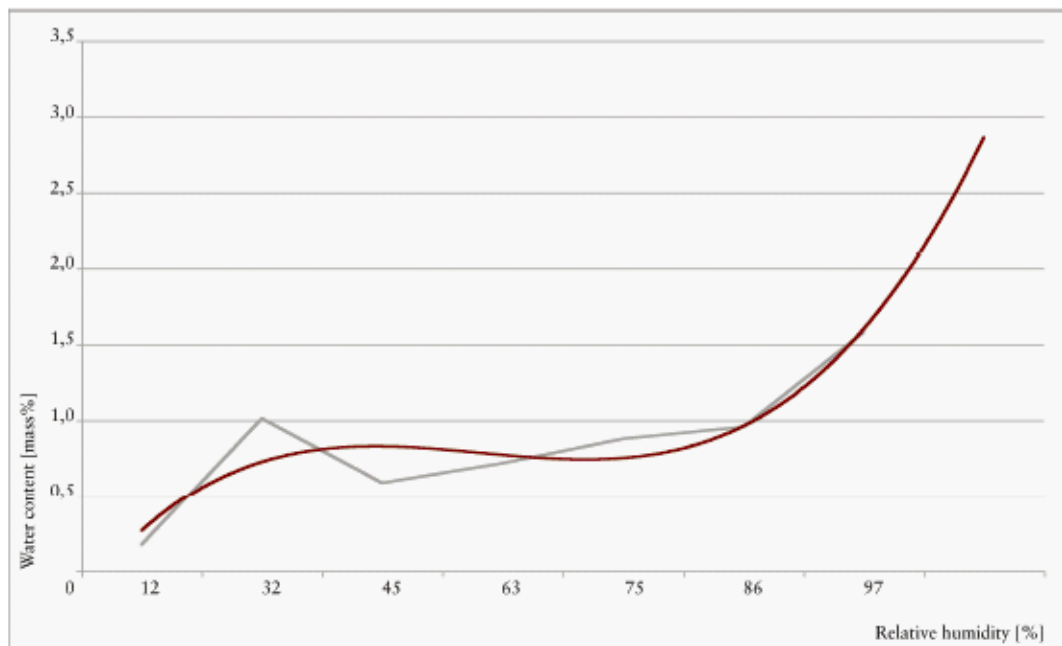
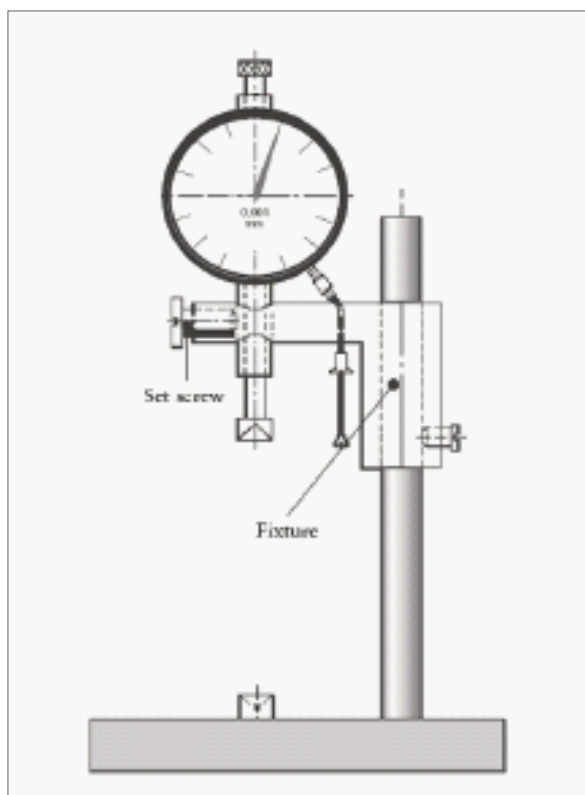
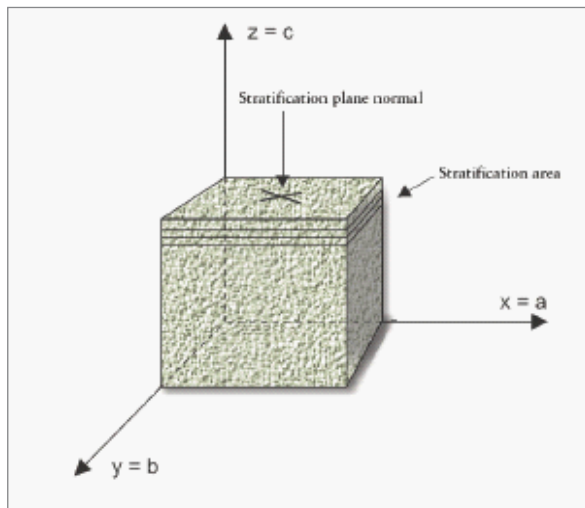


Fig. 4: Course of the isothermal line of sorption (red curve) determined using the measured values (gray curve)



**Fig. 5:** Dial gauge for determining hygric and thermic dilatation



**Fig. 6:** Orientation of the samples in a coordinate system

**Table 8:** Average values of hygric dilatation under water at 98 % RH

Direction	Hygric Dilatation at 98 % RH [mm/m]	Hygric Dilatation Under Water [mm/m]
x (parallel ss)	0,41	1,36
y (parallel ss)	0,38	1,39
z (right angle ss)	0,47	2,13

the values of directions x and y are lower. These results make it quite evident that the rock's change of length is three (directions x and y) to five (direction z) times higher after only 48 hours under water than after four weeks at 98 % RH.

### Thermal Values – Thermal Dilatation

Thermal dilatation indicates how rock either expands or shrinks depending upon temperature. Thermal dilatation is determined in a laboratory by heating the rock up to c. 50°C, mounting it in a dial gauge (fig. 5) and measuring the change in size as it cools. The thermal dilatation was also measured in directions x, y and z. Table 9 shows the average results.

The thermal dilatation is parallel and at a right angle to stratification in a comparable scale.

### Mechanical Values – Bending Tensile Strength

Using the tension-tensile curve from the biaxial bending tensile tests, the biaxial tensile strength and the E-modulus are determined. The biaxial bending

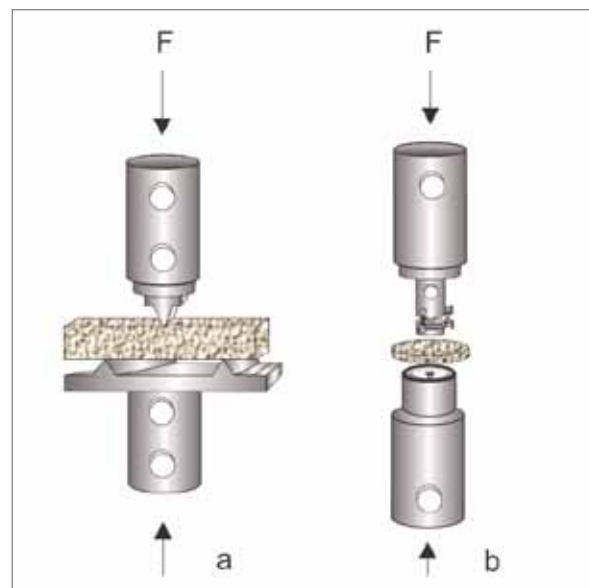


**Fig. 7:** Test structure for determining uniaxial (a) and biaxial (b) bending tensile strength

**Table 9:** Thermal dilatation

Direction	Linear Expansion Coefficient $\alpha$ [μm/m/°C]
x (parallel ss)	11,92
y (parallel ss)	10,63
z (right angle)	12,71

tensile strength is the maximum bending tension that can be reached.

A stone slice is positioned on a bearing ring ( $\varnothing$  39 mm) and put under pressure by a second ring ( $\varnothing$  13 mm) until it breaks. Circular pressure is applied, and the various radii of the rings effect bending tension in the rock. The measurements, the results of which can be found in figure 8, were carried out using the universal testing machine Z010 [10 kN] from the company Zwick. The preliminary test force was 10 Newtons and then additional force was applied in steps of 0,50 mm/min.

As already explained, the E-modulus can be determined using bending tensile measurement. The E-modulus of the untreated Anyue stone sample was 3,5 kN/mm<sup>2</sup>.

#### *Drill Resistance*

Measurement of the drill resistance was carried out with a Sint DRMS Cordless. Diaber diamond bits with a radius of 5 mm were used. The reference material used was Marcor, a homogeneous glass-ceramic.<sup>30</sup>

Before the first drilling in the rock, a drilling was made in the Marcor as a reference. This was repeated after every three drillings in the rock to determine

the percental rise of drilling power needed due to wear on the bit per drilling.<sup>31</sup> The measurements were carried out in directions x and z. Table 10 shows the adjusted averages of the average force [N] used for the three Anyue stone samples.

This weathered sandstone is a very soft stone, which will probably make it quite difficult to test its drilling resistance. Probably, larger drill bits (10 mm) will be necessary.

**Table 10:** Drilling force. Adjusted averages of the force used for the three samples

Sample	Direction X Force [N]	Direction Z Force [N]
W1	2,8	3,6
W2	3,9	4,2
W3	4,3	4,8
<b>Average Force</b>	<b>3,6</b>	<b>4,2</b>

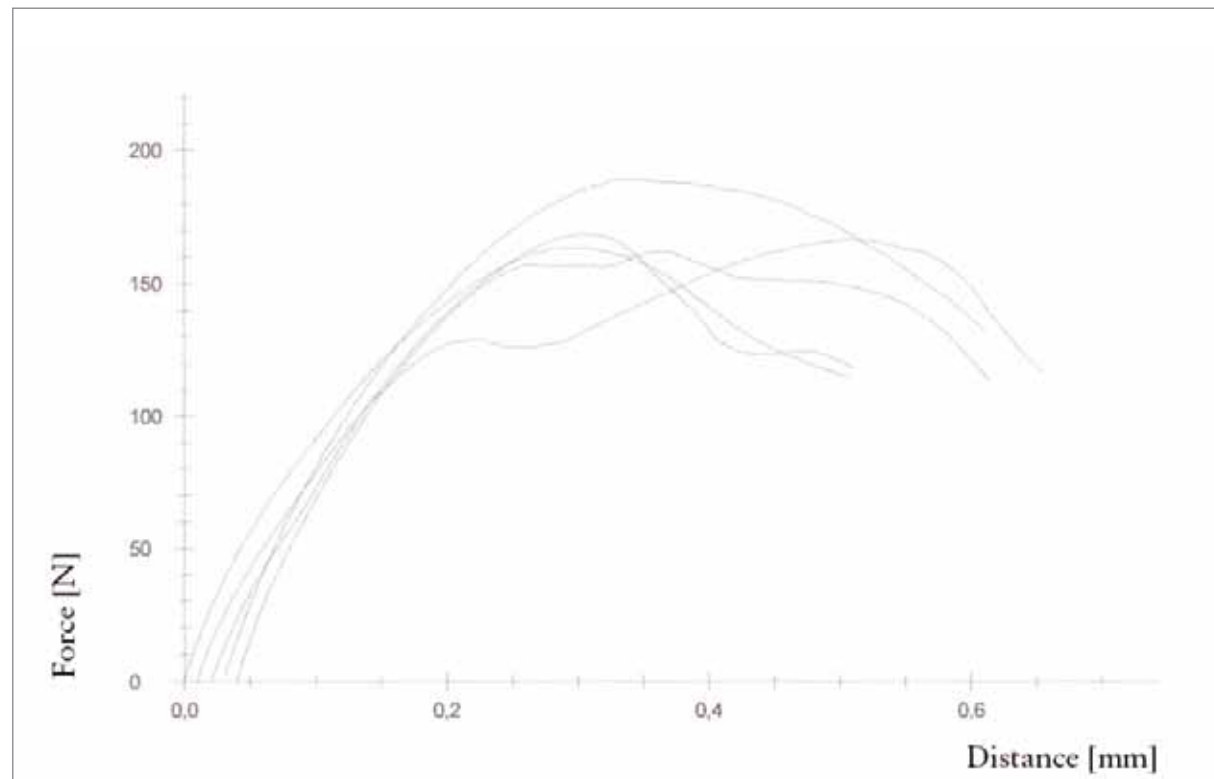


**Fig. 8:** Results of the bending tensile measurements on untreated samples

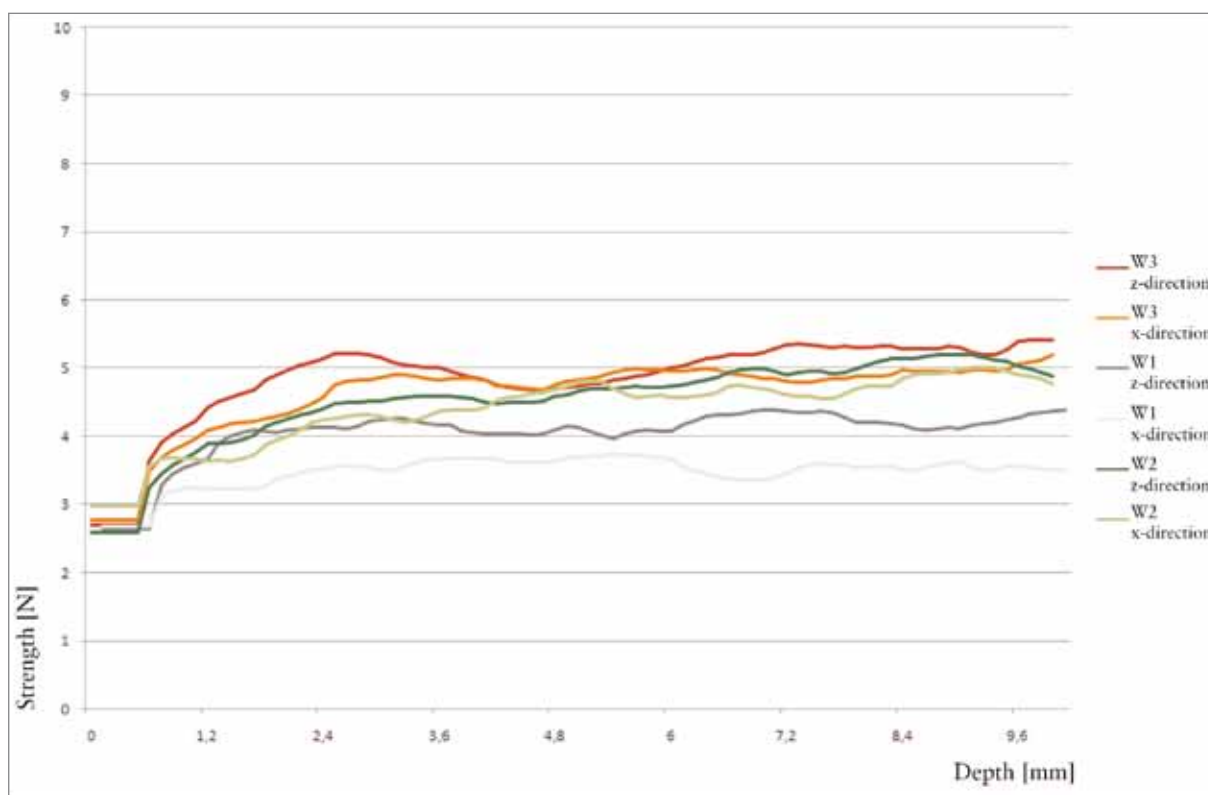


**Fig. 9:** Curve progression of the drill resistance tests in directions x and z

## Stone values – Anyue Sandstone

### Mining Location

China, Sichuan province, city of Ziyang, Anyue district

### Geological Short-Term Description

Reddish to grey-red, fine-grained sandstone

### Petrographic Description

#### Colour

Red with uniform coloration

#### Structure

Fine-grained

#### Texture

Not recognizable

### Microscopy

#### Components

82 % components, 15 % binder, 3 % visible pore space

60 % quartz, 3 % albite, 3 % potashfeldspar, 12 % polycrystal quartz (rock fragments), 5 % clay consisting rock fragments, < 1 % accessory components.

Quartz crystal-clear; Albite with twin-lamella, kaolinized; Potashfeldspar dull, formation of sericite (coarsegrained illite); Polycrystal quartz as fine-grained chert or coarse-grained polyquartz; clay consisting of rock fragments with slately tecture and bunches of chlorite.

Carbonate and clay binder. Calcite as spandrel filling has been formed. Clay minerals with rusty red coloration on the grain surfaces

### Grain Size, Grain Size Distribution and Grain Form

Main grain size between 0,15 and 0,30 mm. Biggest grains up to 0,60 mm, moderately sorted, grain forms angular to subangular, grain contacts mostly along the longitudinal axis, point contacts rare.

### Diagenesis

Formation of calcite in the grain spandrels

### Classification

Carbonatic-clay-bound sandstone with rock fragments

**Table 11:** Stone values

Density		[g/cm <sup>3</sup> ]	2,67
Bulk density		[g/cm <sup>3</sup> ]	2,13
Water absorption (atmospheric pressure)		[Gew.%]	6,46
Water absorption (vacuum)		[Gew.%]	9,57
Porosity		[Vol.%]	20,14
Saturation		[-]	0,69
Hygric dilatation (95%rf) (right angle ss)		[μm/m]	448
	(parallel ss)	[μm/m]	391
Hygric dilatation (H <sup>2</sup> O) (right angle ss)		[μm/m]	2134
	(parallel ss)	[μm/m]	1375
Thermic dilatation (right angle ss)		[μm/°C]	13
	(parallel ss)	[μm/°C]	11
E-modulus		[kN/mm <sup>2</sup> ]	3,45
Bending tensile strength (right angle ss)		[N]	4,2
	(parallel ss)	[N]	3,6



**Fig. 10:** Slice of the Anyue Sandstone

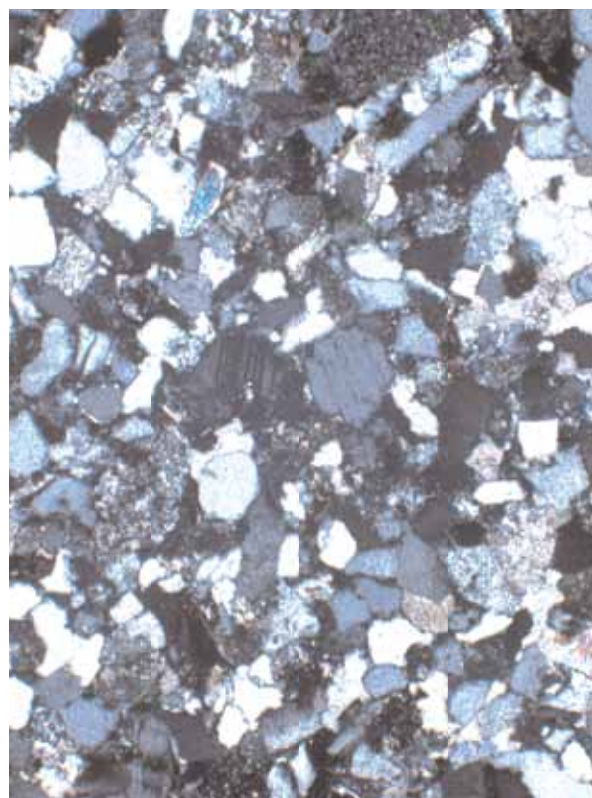


**Fig. 11:** 63 x zoom x polarizers

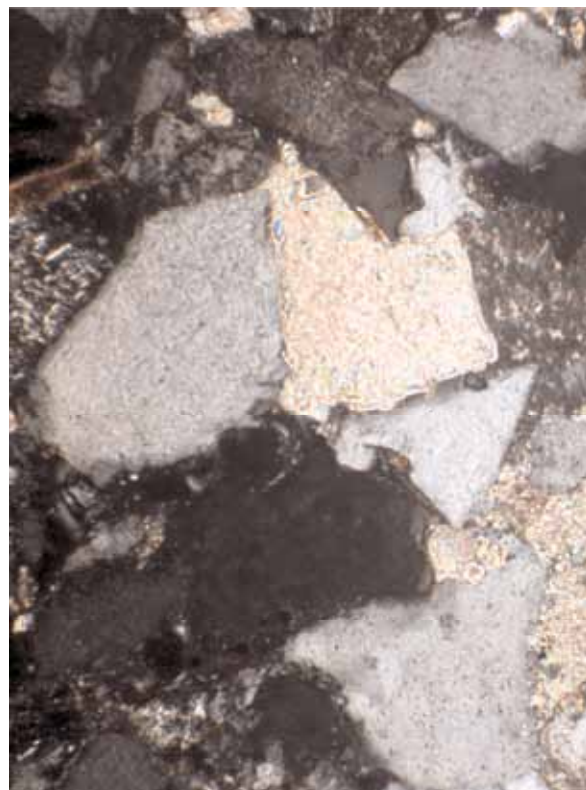


**Fig. 12:** 120 x zoom x polarizers

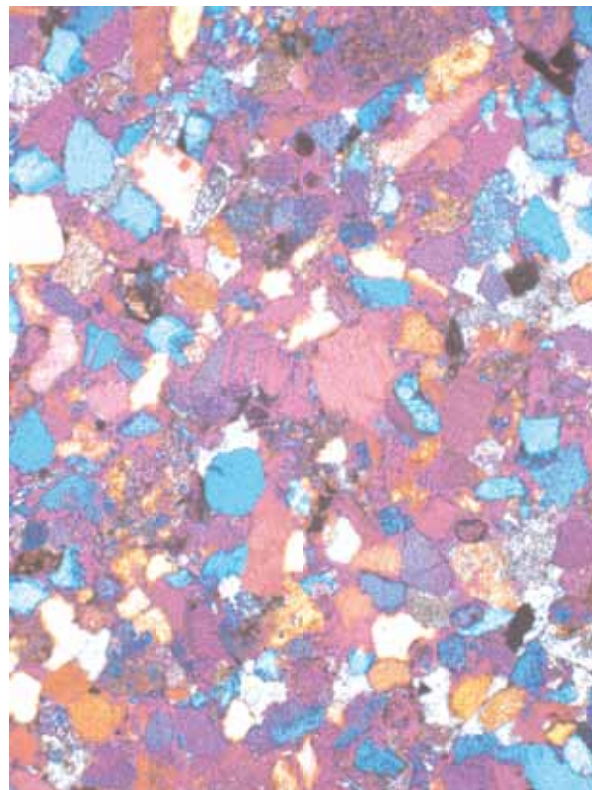


**Fig. 13:** 63 x zoom x polarizers, rotavap

## Results of the Treated Samples

Conclusive analysis of treated and untreated stone can only be reached if the conditions during testing are identical. Therefore, the tests must be carried out in the same way and the stone samples must be the same size.

### Hygric Values

#### Water Absorption

Table 12 shows the definable results of the water absorption assessment of the stone cubes such as porosity, saturation, particle density and bulk density after they were treated with consolidation products (p.139). The complete results of the analyses can be found in the appendix on page 157.

#### Isothermal Line of Sorption

Figure 14 shows the average values of every consolidation product for the respective relative humidities.

Comparison of the three consolidation products (KSEOH, KSE100, KSE300) reveals that the water content in the samples treated with KSEOH is larger than those treated with KSE300. The lowest water content is in the samples treated with KSE100.

#### Hygric Dilatation

The testing period for dilatation under water was 48 hours, the hygric dilatation at 98 % RH was tested until constant values were reached after around four weeks. Table 13 shows the average values at 98 % RH and under water in direction z, as the largest values can be expected in the perpendicular expansion.

**Table 12:** Results of water absorption tests on cube samples

Sample	WAa [Mass%]	WAv [Mass%]	Porosity [Vol.%]	Saturation [-]	Particle Density [g/cm <sup>3</sup> ]	Bulk Density [g/cm <sup>3</sup> ]
WKSEOH	6,31	9,05	19,47	0,70	2,67	2,15
WKSE100	6,42	9,34	19,90	0,69	2,66	2,13
WKSE300	5,90	9,26	19,80	0,64	2,67	2,14

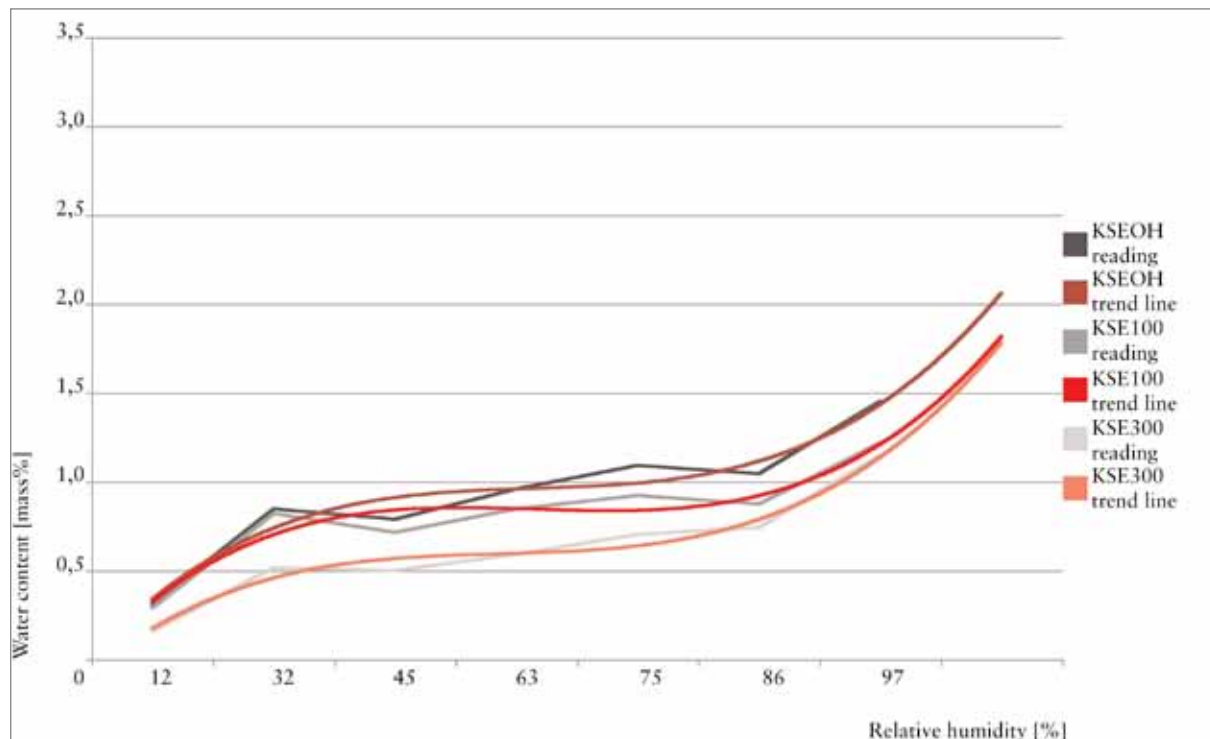


**Fig. 14:** Progression of the isothermal line of sorption (red curves) of the samples treated with three different consolidation products

## Thermal Values – Thermal Dilatation

Thermal dilatation indicates how rock either expands or shrinks depending on temperature. Thermal dilatation is determined in a laboratory by heating the rock up to c. 50°C, mounting it in a dial gauge and measuring the change in size as it cools. The thermal dilatation was measured in directions x, y and z. Table 14 shows the average results.

## Mechanical Values

### Bending Tensile Strength

Tension-tensile curves, determined by testing bending tensile strength, allow conclusions to be made about the tensile strength with specification of the E modulus relating to the respective cross-section up to maximum force.

The biaxial tensile strength is the maximum bending tension reached during the tests. A stone ring is placed on a bearing ring and put under pressure by a second, smaller ring until it breaks. Circular pressure is applied, and the various radii of the rings effect bending tension in the rock. The measurements, the results of which can be found in figure 15, were carried out using the universal testing machine Z010 [10 kN] from the company Zwick.

The preliminary test force was 10 Newtons and then additional force was applied in steps of 0,50.

**Table 13:** Average values of the hygric dilatation under water at 98 % RH for KSEOH, KSE100 and KSE300 in direction z

Test Condition	Hygric Dilatation [mm/m]		
	KSEOH	KSE100	KSE300
98 % RH	0,50	0,58	0,50
Under Water	2,35	2,70	1,92

**Table 14:** Thermal Dilatation for direction z with KSEOH, KSE100 and KSE300

Consolidation Product	Thermal Dilatation [ $\mu\text{m}/\text{m}^{\circ}\text{C}$ ]
KSEOH	14,16
KSE100	16,18
KSE300	17,39

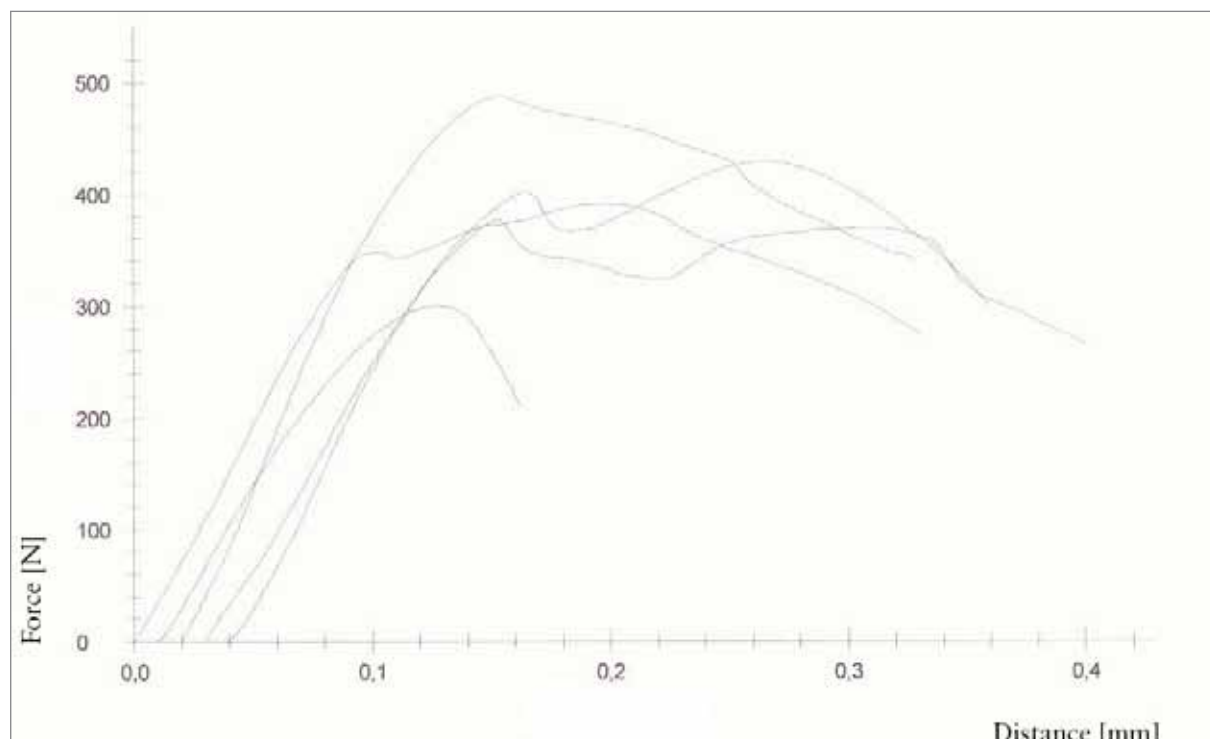


**Fig. 15:** Exemplary results of the bending tensile measurements on samples treated with KSE300

### Drill Resistance

Measurement of the drill resistance was carried out with a Sint DRMS Cordless. Diaber diamond bits with a radius of 5 mm were used. The reference material used was Marcor.

Before the first drilling in the rock, a drilling was made in the Marcor as a reference. This was repeated after every three drillings in the rock to determine the percental rise of drilling power needed due to wear on the bit per drilling.<sup>31</sup> The measurements were carried out in directions x and z. Table 16 shows the adjusted averages of the average force [N] used for the three Anyue stone samples.

**Table 15:** E-modulus determined for KSEOH, KSE100 and KSE300 by bending tensile measurement

	KSEOH	KSE100	KSE300
E-modulus [kN/mm <sup>2</sup> ]	7,54	6,88	12,41

**Table 16:** Adjusted average values of the force used for the three measured samples

Sample	Direction X Force [N]	Direction Z Force [N]
W1KSEOH	2,8	3,3
W2KSE100	3,2	4,7
W3KSE300	3,7	7,2

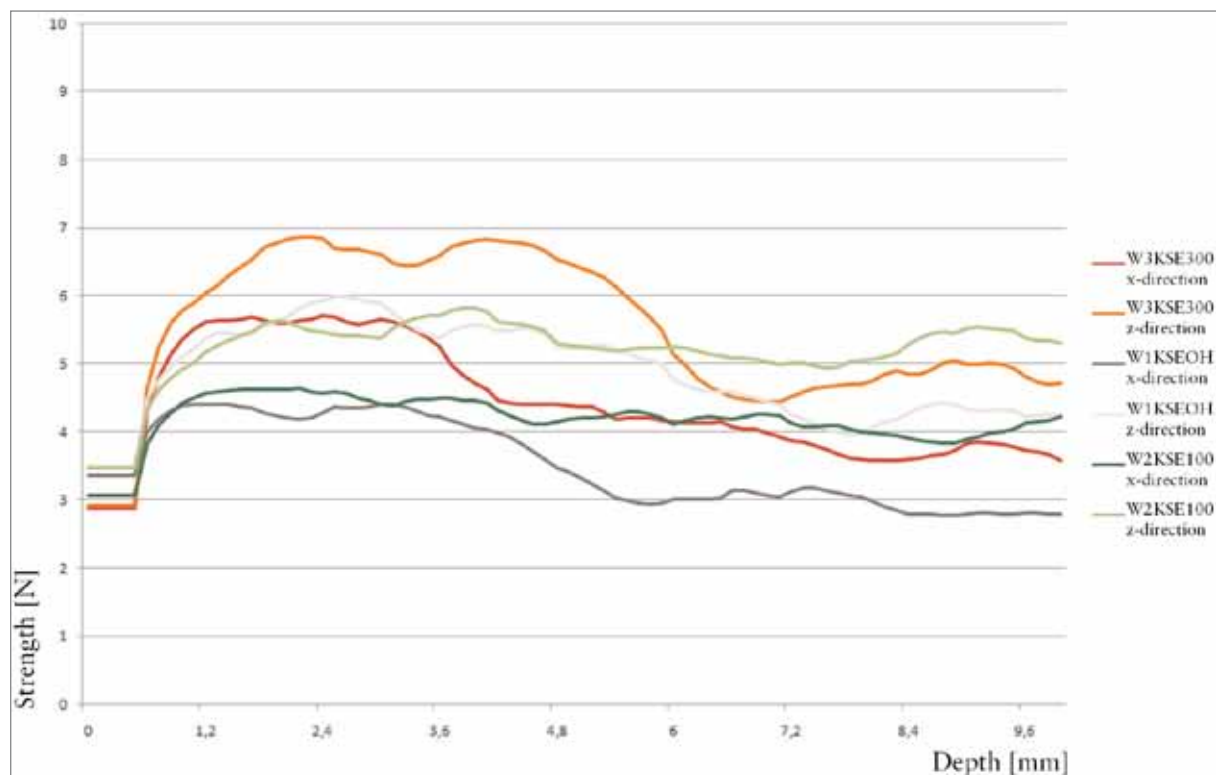


**Fig. 16:** Curve progression of drill resistance tests for KSEOH, KSE100 and KSE300 in direction x and z

## Summary

The research was done to choose a consolidation product for further experiments. Based on the results, as shown in tables 17 and 18, KSE100 should be excluded. A consolidation treatment with this product affects both hygric and thermic dilatation in a negative way. Even the specimen treated with KSE300 shows a noticeable increase

in thermic dilatation, which could be problematic for consolidation treatments in subtropical environments.

Positive values were obtained for the samples treated with KSEOH. With this product, however, health and environment issues must also be considered. While doing treatment, respirators must be worn, and any left-over product must not be allowed to permeate the ground water (WGK2) and therefore disposed of separately.

**Table 17:** Comparison of the values of the untreated sample to the treated samples (KSEOH, KSE100 and KSE300) each in direction z

Results	Original	KSEOH	KSE100	KSE300
Water absorption [mass%]	6,49	6,31	6,42	5,90
Water absorption vacuum [mass%]	9,45	9,05	9,34	9,26
Porosity [vol.%]	20,16	19,47	19,90	19,80
Density [g/cm <sup>3</sup> ]	2,67	2,67	2,66	2,67
Bulk density [g/cm <sup>3</sup> ]	2,13	2,15	2,13	2,14
Hygric dilatation 97% rH [mm/m]	0,47	0,50	0,58	0,50
Hygric dilatation (water) [mm/m]	2,13	2,35	2,70	1,92
Thermic dilatation [ $\mu\text{m}/^\circ\text{C}$ ]	12,71	14,16	16,18	17,39
Young's modulus (Ym) [kN/mm <sup>2</sup> ]	3,72	11,11	7,04	13,05
Bending tensile strength (bts) [kN/mm <sup>2</sup> ]	2,43	5,53	4,16	5,77
Ratio bts/Ym	0,65	0,50	0,59	0,44
Drill resistance [N]	4,2	3,3	4,7	5,4
Health				
Danger symbols		Xi, Xn, F, T	Xn, Xi, T	Xn, Xi, T
Environment				
WGK	2	2	1	1

**Table 18:** Assessment of the consolidation products KSEOH, KSE100 and KSE300

Results	KSEOH	KSE100	KSE300
Water absorption atmosphere	✓	✓	✓
Water absorption vacuum	✓	✓	✓
Porosity	✓	✓	✓
Density	✓	✓	✓
Bulk density	✓	✓	✓
Line of isothermal sorption	✓	✓	✓
Hygric dilatation 97% rFH	✓	--	✓
Hygric dilatation under water	✓	--	✓
Thermic dilatation	✓	--	--
Ratio bts/Ym	✓	✓	--
Health	--	✓	✓
Environment	--	✓	✓

## Endnotes

- 1 REINSCH 1991.
- 2 REINSCH 1991.
- 3 SNETHLAGE 2005.
- 4 SNETHLAGE 2005.
- 5 REINSCH 1991.
- 6 KOCHER 2004.
- 7 REINSCH 1991.
- 8 KLOPFER 1974.
- 9 ANGENHEISTER 1982.
- 10 REINSCH 1991.
- 11 SNETHLAGE 2005.
- 12 KOCHER 2004.
- 13 KOCHER 2004.
- 14 KOCHER 2004.
- 15 KOCHER 2004.
- 16 REINSCH 1991.
- 17 REINSCH 1991.
- 18 KOCHER 2004.
- 19 KOCHER 2004.
- 20 Internal document for the evaluation of mechanical values prepared by TUCIC.
- 21 SNETHLAGE 2005.
- 22 SNETHLAGE 2005.
- 23 The technical datasheets of the consolidants are available in digital form on CD.
- 24 The technical datasheets of the consolidants are available in digital form on CD.
- 25 GRASSEGGER 1992.
- 26 GRASSEGGER 1992.
- 27 SNETHLAGE 2005.
- 28 SNETHLAGE 2005.
- 29 KLOPFER 1974.
- 30 Information from the producer is available in digital form on CD.
- 31 The increase is given as validation [%].

## Literature

- ANGENHEISTER G. ANGENHEISTER (Hrsg.): *Physikalische Eigenschaften der Gesteine*  
Berlin/Heidelberg/New York 1982
- ENGELHARDT Wolf von ENGELHARDT: *Die Bildung von Sedimenten und Sedimentgesteinen*  
Stuttgart 1973
- FÜCHTBAUER Hans FÜCHTBAUER: *Sedimente und Sedimentgesteine*  
Stuttgart 1988
- GRASSEGGER G. GRASSEGGER: *Charakterisierung der Gel-Strukturen von Kieselsäureester-Steinfestigern unter verschiedenen Erhärtungsbedingungen mittels thermodynamischer Methoden (DTA/TG)*  
In: Rolf SNETHLAGE (Hrsg.): *Jahresberichte Steinzerfall – Steinkonservierung 1990*  
Berlin 1992
- KLOPFER H. KLOPFER: *Wassertransport durch Diffusion in Feststoffen*  
Wiesbaden/Berlin 1974
- KOCHER Mathias KOCHER: *Quelldruckmessungen und thermische Druckmessungen an ausgewählten Sandsteinen*  
Dissertation der Fakultät für Geowissenschaften der Ludwig-Maximilians-Universität München  
München 2004
- KRUS Martin KRUS: *Feuchtetransport- und Speicherkoefzienten poröser mineralischer Baustoffe. Theoretische Grundlagen und neue Meßtechniken*  
Dissertation der Fakultät Bauingenieur- und Vermessungswesen der Universität Stuttgart  
Stuttgart 1995
- MENG/SCHISSL B. MENG/P. SCHISSL: *Wechselseitige Beziehungen zwischen Parametern des Porenraumes und des Feuchtetransportes bei Sandsteinen*  
In: Rolf SNETHLAGE (Hrsg.): *Jahresberichte Steinzerfall – Steinkonservierung 1990*  
Berlin 1992
- REINSCH Dietmar REINSCH: *Natursteinkunde*  
Stuttgart 1991
- SCHÖN Jürgen SCHÖN: *Petrophysik*  
Berlin 1983
- SNETHLAGE (Hrsg.) Rolf SNETHLAGE (Hrsg.): *Jahresberichte Steinzerfall – Steinkonservierung 1990*  
Berlin 1992
- SNETHLAGE (Hrsg.) Rolf SNETHLAGE (Hrsg.): *Jahresberichte Steinzerfall – Steinkonservierung 1992*  
Berlin 1994
- SNETHLAGE Rolf SNETHLAGE: *Leitfaden Steinkonservierung*  
Stuttgart 2005
- SNETHLAGE/WENDLER Rolf SNETHLAGE/Eberhard WENDLER: *Chemical Compounds for Conservation of Natural Stone*  
Vorlesungsskript LMU Fakultät Geowissenschaften  
München ohne Jahr

**DIN-Standards (selection)**

DIN 12407	Method of testing natural stone – petrographical test August 2006
DIN EN 13755	Method of testing natural stone– Determination of water absorption under atmospheric pressure, October 2007
DIN EN 14581	Method of testing natural stone – evaluation of the thermal dilatation coefficient March 2005
DIN EN 1926	Method of testing natural stone – Determination of the uniaxial compression strength March 2007
DIN EN 1936	Method of testing natural stone – Determination of density, bulk density, open porosity and total porosity, Februar 2007
DIN 52008	Method of testing natural stone – assessment of resistance to weathering March 2006
DIN 52009	Method of testing stone grains – Determination of water absorption under pressure February 2006
DIN 52100-1	Natural stone – petrographic analyses – general and overview June 2007
DIN 52102	Method of testing stone grains – Determination of bulk density when dry with the measuring cylinder method and calculation of the degree of density February 2006

## List of Illustrations

- Fig. 1 Various contact types with their corresponding bonding strength  
 Fig. 2 Differing absorption of the consolidation products by the stone slices  
 Fig. 3 Results of the Mercury Porosimetry  
 Fig. 4 Course of the isothermal line of sorption (red curve) determined using the measured values (gray curve)  
 Fig. 5 Dial gauge for determining hygric and thermic dilatation  
 Fig. 6 Orientierung of the samples in a coordinate system  
 Fig. 7 Test structure for determining uniaxial (a) and biaxial (b) bending tensile strength  
 Fig. 8 Results of the bending tensile measurements on untreated samples  
 Fig. 9 Curve progression of the drill resistance tests in directions x and z  
 Fig. 10 Slice of the Anyue Sandstone  
 Fig. 11 63x zoom x polarizers  
 Fig. 12 120x zoom x polarizers  
 Fig. 13 63x zoom x polarizers, rotavap  
 Fig. 14 Progression of the isothermal line of sorption (red curves) of the samples treated with three different consolidation products  
 Fig. 15 Exemplary results of the bending tensile measurements on samples treated with KSE300  
 Fig. 16 Curve progression of the drill resistance tests for KSEOH, KSE100 and KSE300 in directions x and z

## List of Tables

- Table 1 Classification of pore sizes according to IUPAC, DIN 66131 and architectural literature  
 Table 2 Product specification of the three consolidants as indicated by the manufacturer  
 Table 3 Product specification of the three consolidants after application  
 Table 4 Classification of pore sizes according to IUPAC, DIN 66131 and architectural literature  
 Table 5 Results of water absorption tests on the cube samples  
 Table 6 Results of water absorption tests on the slice samples  
 Table 7 Relative humidity with saline solutions  
 Table 8 Average values of hygric dilatation under water at 98% RH  
 Table 9 Thermal Dilatation  
 Table 10 Drilling force. Adjusted averages of the force used for the three samples  
 Table 11 Stone values  
 Table 12 Results of water absorption tests on cube samples  
 Table 13 Average values of the hygric dilatation under water at 98% RH for KSEOH, KSE100 and KSE300 in direction z  
 Table 14 Thermal Dilatation for direction z with KSEOH, KSE100 and KSE300  
 Table 15 E-modulus determined for KSEOH, KSE100 and KSE300 by bending tensile measurement  
 Table 16 Adjusted average values of the force used for the three measured samples  
 Table 17 Comparison of the values of the untreated sample to the treated samples (KSEOH, KSE100 and KSE300) each in direction z  
 Table 18 Assessment of the consolidation products KSEOH, KSE100 and KSE300

## Appendix

### Water Absorption of Untreated Samples

#### Sample identification

W1	Anyue sandstone untreated, Water absorption vakuum
W2	Anyue sandstone untreated, Water absorption vakuum
W3	Anyue sandstone untreated, Water absorption vakuum
W4	Anyue sandstone untreated, Water absorption vakuum
W5	Anyue sandstone untreated, Water absorption vakuum
W6	Anyue sandstone untreated, Water absorption atmospheric pressure
W7	Anyue sandstone untreated, Water absorption atmospheric pressure
W8	Anyue sandstone untreated, Water absorption atmospheric pressure
W9	Anyue sandstone untreated, Water absorption atmospheric pressure
W10	Anyue sandstone untreated, Water absorption atmospheric pressure

#### Measurement

Sample	Water absorption vakuum (WA <sub>V</sub> )			Sample	Water absorption atmospheric (WA <sub>A</sub> )	
	Dry weight	Under water	Wet/air		Dry weight	Wet weight
W1	515,64	322,6	563,98	W6	489,5	522,35
W2	574,03	358,99	627,11	W7	544,22	579,08
W3	497,42	311,219	545,37	W8	550,33	585,31
W4	427,76	267,626	467,57	W9	529,16	563,42
W5	539,97	337,845	592,3	W10	572,94	610,26

#### Results

WA <sub>V</sub>	WA <sub>A</sub>	WA <sub>Vol.</sub>	Poros.	Saturation	Buld density	Density
M%	M%	Vol.%	Vol.%	/	g/cm <sup>3</sup>	g/cm <sup>3</sup>
9,375	6,711	14,336	20,027	0,716	2,671	2,136
9,247	6,405	13,714	19,797	0,693	2,669	2,141
9,640	6,356	13,503	20,478	0,659	2,671	2,124
9,307	6,474	13,851	19,911	0,696	2,671	2,139
9,691	6,514	13,823	20,566	0,672	2,671	2,122

## Water Absorption of Treated Samples

### Sample identification

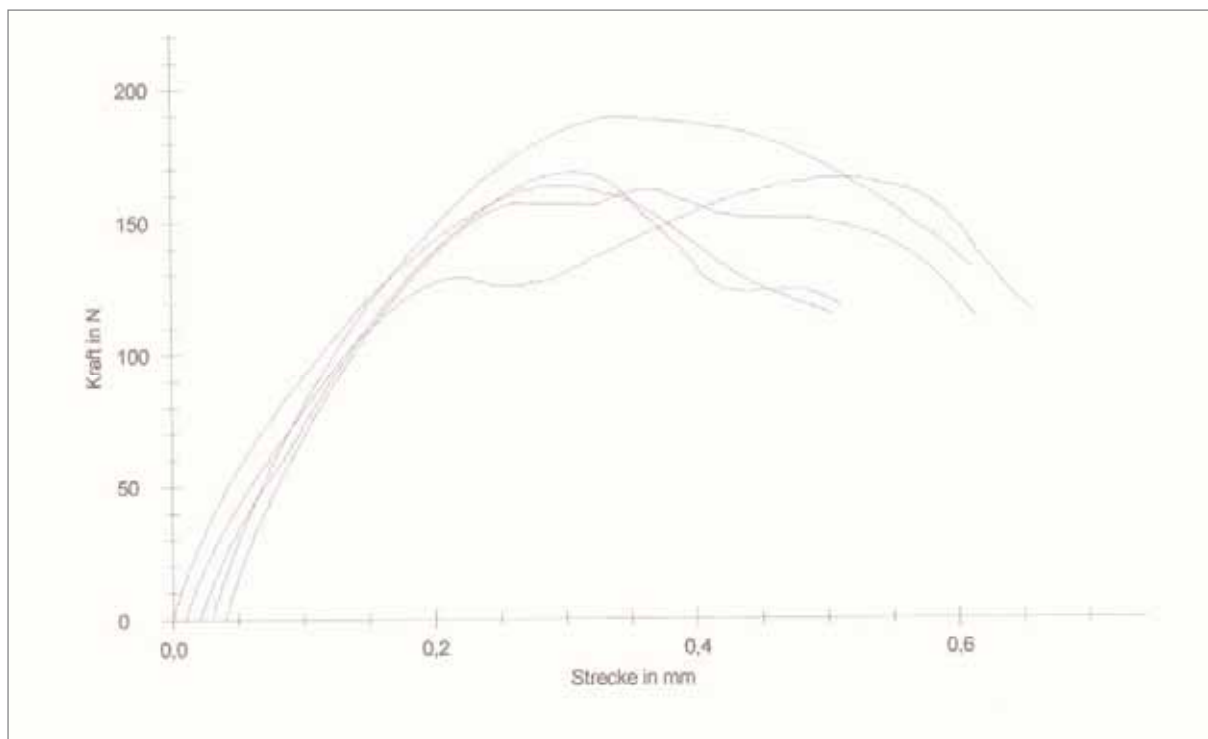
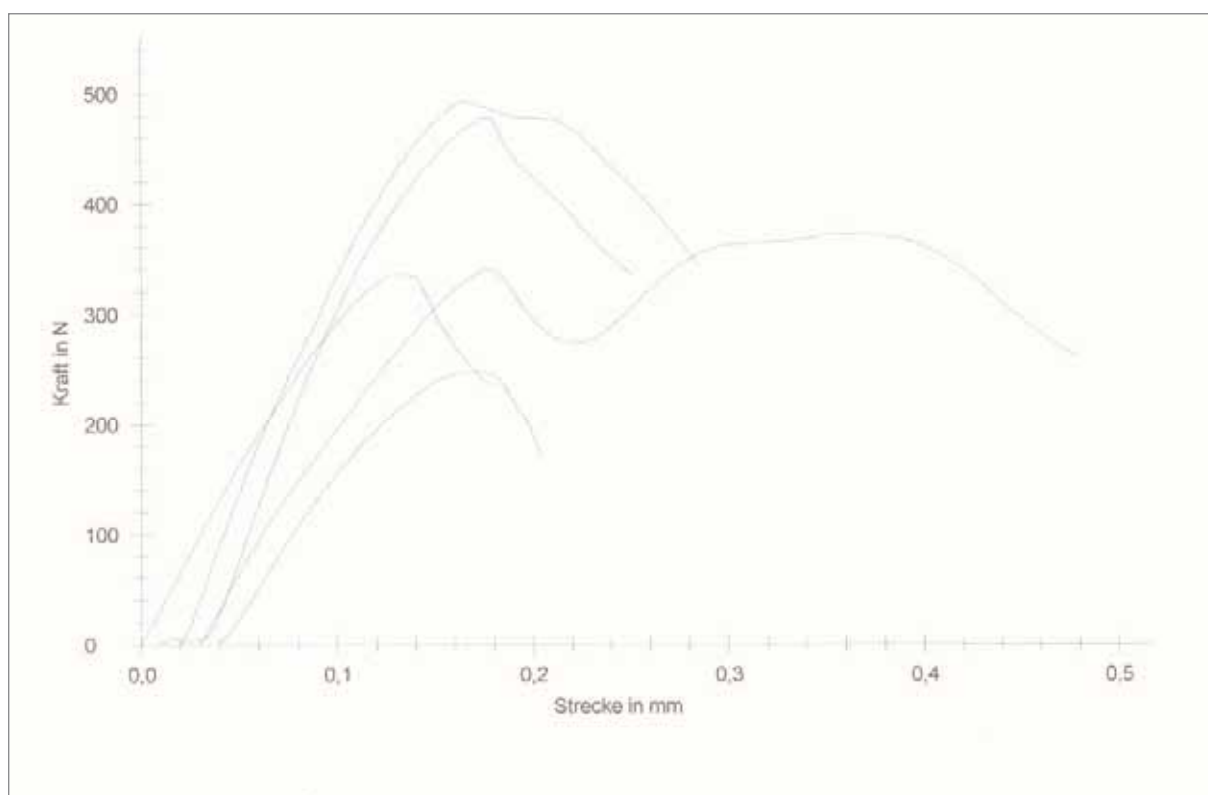
W1KSEOH	Anyue sandstone consolidated KSEOH, Water absorption vakuum
W2KSE100	Anyue sandstone consolidated KSE100, Water absorption vakuum
W3KSE300	Anyue sandstone consolidated KSE300, Water absorption vakuum
W6KSEOH	Anyue sandstone consolidated KSEOH, Water absorption atmospher
W7KSE100	Anyue sandstone consolidated KSE100, Water absorption atmospheric pressure
W8KSE300	Anyue sandstone consolidated KSE300, Water absorption atmospheric pressure

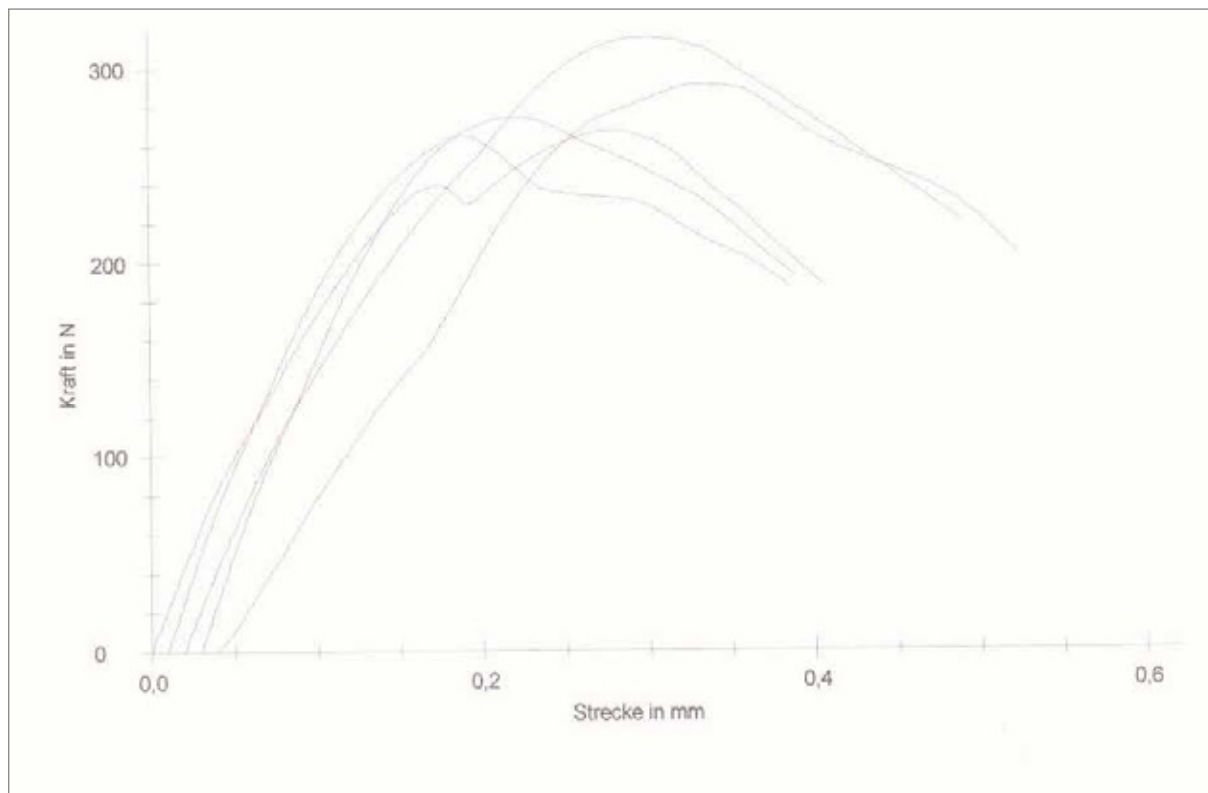
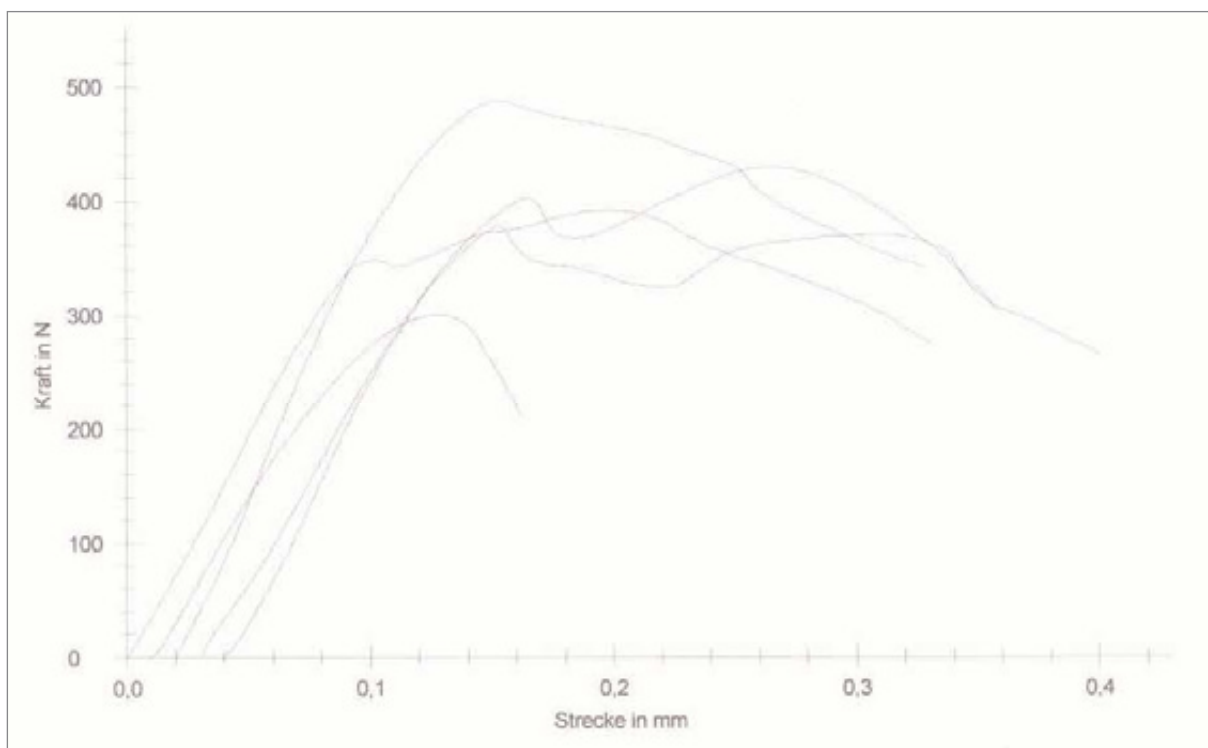
### Measurement

Sample	Water absorption vakuum (WAv)			Sample	Water absorption atmospheric (WAa)	
	Dry weight	Under water	Wet/air		Dry weight	Wet weight
W1KSEOH	515,73	322,72	562,39	W6KSEOH	492,446	523,53
W2KSE100	573,13	357,614	626,67	W7KSE100	546,08	581,14
W3KSE300	497,39	310,881	543,43	W8KSE300	553,35	585,97

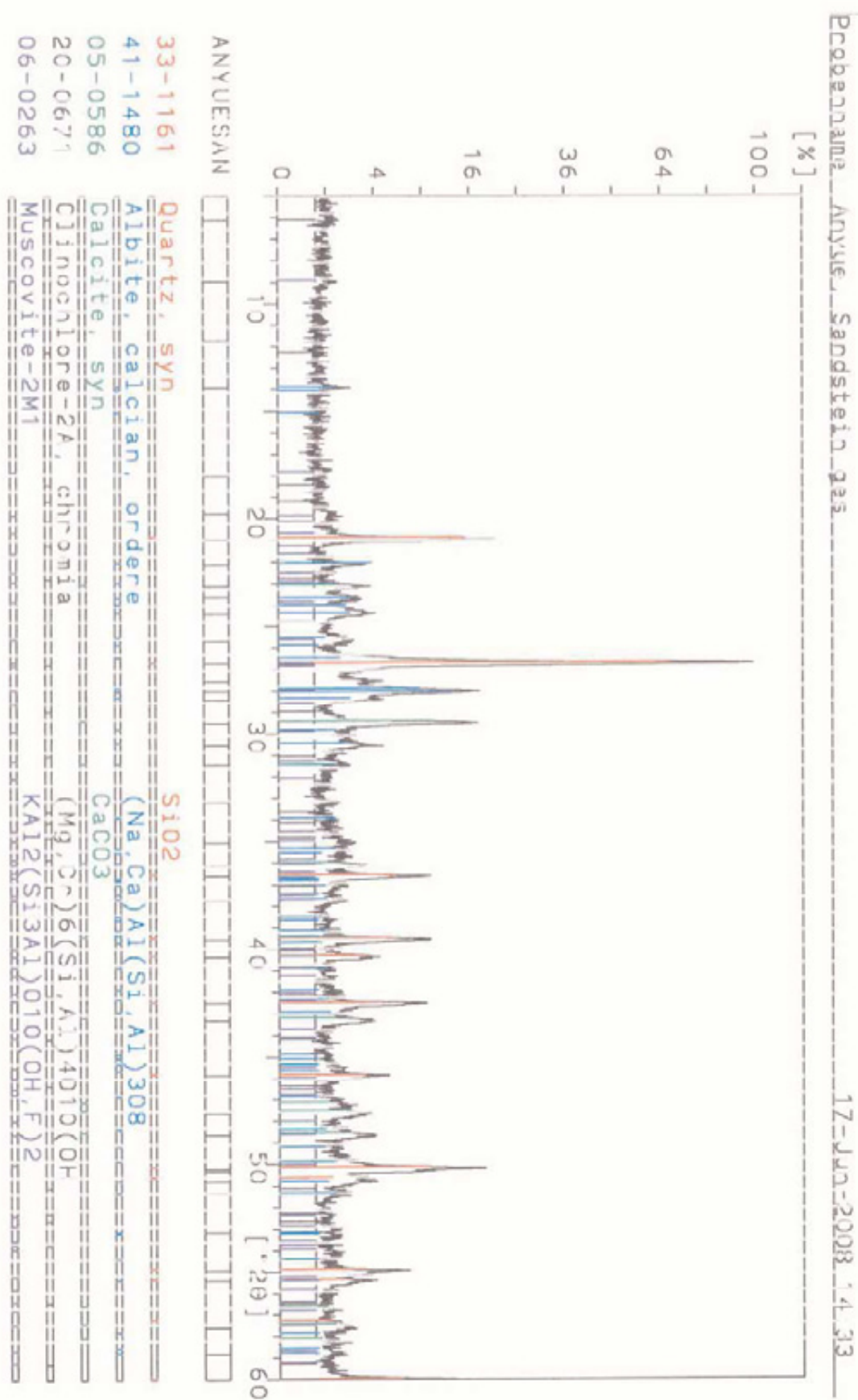
### Results

WAv	WAa	WAvol.	Poros.	Saturation	Buld density	Density
M%	M%	Vol.%	Vol.%	/	g/cm <sup>3</sup>	g/cm <sup>3</sup>
9,047	6,312	13,583	19,468	0,698	2,672	2,152
9,342	6,420	13,676	19,899	0,687	2,659	2,130
9,256	5,895	12,609	19,798	0,637	2,667	2,139

**Bending Tensile Strength of the Untreated Samples****Bending Tensile Strength of the Samples treated with KSEOH**

**Bending Tensile Strength of the Samples treated with KSE100****Bending Tensile Strength of the Samples treated with KSE300**

## Results of the X-ray Crystallography



**3-D-Vermessung und Texturierung der Grotte Nr. 10  
des Buddha Shakyamuni und der Grotte Nr. 37**



# 3-D-Vermessung und Texturierung der Grotte Nr. 10 des Buddha Shakyamuni und der Grotte Nr. 37

Felix Horn

Ziel der Vermessungsarbeiten in Anyue/China war die Vermessung der Grotte Nr. 10 des Buddha Shakyamuni mit 3-D-Laserscanning und Streifenprojektionstechnik sowie digitaler Fotografie und die Überführung in ein hochauflösten, fotorealistisches 3-D-Modell. Das erstellte 3-D-Modell soll später zur 3-D-Dokumentation, Schadenserfassung und als Grundlage für die Erstellung eines Schutzdaches verwendet werden.

Besonderer Wert bei der Erfassung lag dabei auf der Figur des Buddha Shakyamuni selbst, auf den Verzierungen der Rückwand sowie auf den Strukturen in der Felswand. Neben der Erfassung der Grotte Nr. 10 wurde auch die Grotte Nr. 37 erfasst.<sup>1</sup>

## 3-D-Vermessung

*Eingesetzte Messtechnik: 3-D-Laserscanner*

Für die Erfassung der Gesamtgeometrie der Buddhafigur sowie der Felssituation kam der Laserscanner LMS-Z 420i der Firma Riegl-Laser-Measurement-Systems zum Einsatz.

**Tab. 1:** Angaben des Herstellers über Arbeitsbereich und Genauigkeit

Arbeitsbereich (je nach Reflektivität des Ziels)	2 – 1000 m
Maximale Auflösung	0,002°
Genauigkeit einer Einzelstreckenmessung	+/- 5 mm
Genauigkeit bei Mehrfachmessung	4 mm
Horizontaler Arbeitsbereich	0° – 360°
Vertikaler Arbeitsbereich	0° – 80°

Aufgrund seines großen Aufnahmefeldes, der schnellen Datenaufnahme und der hohen Genauigkeit der Entfernung- und Richtungsmessung ist er für die Aufnahme von Bauwerken, Topografie und anderen Objekten in den Bereichen Denkmalpflege, Archäologie und Architektur effektiv einsetzbar.

Während des Messvorgangs werden dreidimensionale Koordinaten des Messobjekts erfasst. Zusätz-

lich werden digitale Bilder über eine Digitalkamera (Nikon D100) aufgezeichnet, sodass eine fotorealistische Darstellung des Objektes möglich ist.

*Eingesetzte Messtechnik:  
Streifenprojektionssystem QT-Sculptor*

Zur Erfassung der komplexen Detailgeometrie und Verzierungen kam das Streifenprojektionssystem PT-M 1280 in Verbindung mit der Software QT-Sculptor zum Einsatz. Der Arbeitsbereich des Systems liegt zwischen 0,5–4 m, seine Genauigkeit bei max. 0,1 mm. Das Gerät arbeitet dabei standardmäßig mit Hochgeschwindigkeitskameras mit einer Auflösung von 1024 x 768 Pixel.

Aufgrund seiner hohen Genauigkeit, der Möglichkeit komplexe Objekte aus wahlfreien Aufnahmerichtungen zu erfassen, die Messdaten in ein fehlerfreies 3-D-Modell zu überführen und das gewonnene Modell fotorealistisch zu texturieren, ist es besonders für die Aufnahme von Skulpturen, baulichen Details und kleineren Einzelobjekten geeignet.



**Abb. 1:**  
3-D-Laserscanner  
LMS-Z 420i der  
Fa. Riegl



**Abb. 2:** Das Messsystem QT-Sculptor PT-M 1280

#### *Allgemeine Bemerkungen zum Messprozess*

Die Vermessungs- und Dokumentationsarbeiten am Buddha Shakyamuni untergliederten sich in folgende Schritte:

- Erfassung der Texturinformation mittels digitaler Spiegelreflexkamera Nikon D 100
- 3-D-Laserscanning der Gesamtgeometrien und der Detailinformationen mit Riegl LMS-Z420 i
- Vermessung der erreichbaren Bereiche mittels Streifenprojektionssystem QT-Sculptor PT-M 1280 in maximal möglicher Auflösung



**Abb. 3:** Vermessung der Grotte Nr. 10 mit dem Riegl-Laserscanner auf dem fahrbaren Gerüst mit Stützkonstruktion



**Abb. 4:** Vermessung der Grotte Nr. 10 mit dem Riegl-Laserscanner



**Abb. 5:** Messungen innerhalb der Grotte Nr. 10 mit dem Riegl-Laserscanner

Aufgrund der Höhe und der Tiefe der Grotte war bereits im Vorfeld abzusehen, dass bestimmte Bereiche nicht zu erfassen sein würden. Dies betraf vor allem die Haube des Buddhas sowie verdeckte Bereiche am Kopf und den Schultern. Außerdem war am aufsteigenden Wandabschluss wegen zu steiler Zielungen und in den Bereichen hinter den seitlich angeordneten Figuren wegen zu geringem Aufnahmeabstand mit Aufnahmelücken zu rechnen.

Für die Vermessungs- und Fotografiearbeiten stand ein fahrbares Gerüst zur Verfügung. Dies musste für ein stabiles und sicheres Arbeiten mit Stangen am Boden abgestützt werden.

#### *Erfassung der Objekte mittels 3-D-Laserscanning*

Die dreidimensionale Vermessung der Gesamtsituation der Grotte mit dem Laserscanner Riegl LMS-Z 420i erfolgte von mehreren Positionen aus. Dabei wurde der Laserscanner zuerst in einem Abstand von 20–30 Metern aufgestellt, um die Gesamtsituation von Felsen und Grotte zu erfassen. In einem nächsten Schritt entstanden in der Grotte Nahaufnahmen, um Scannerschattenbereiche zu minimieren. Abschließend erfolgten Aufnahmen vom Gerüst. Durch die Drehung des Scanners innerhalb

**Tab. 2:** Aufnahmekonfiguration der Digitalisierung von Grotte Nr. 10

<b>Aufnahmekonfigurationen für Grotte Nr. 37</b>	
Auflösung Grottenbereich:	2–5 mm
Auflösung Felsenbereich:	5–10 mm
Anzahl Scanpositionen:	10
Genauigkeit (gemittelt):	5 mm

**Tab. 3:** Aufnahmekonfiguration der Digitalisierung von Grotte Nr. 37

<b>Aufnahmekonfigurationen für Grotte Nr. 37</b>	
Auflösung Grottenbereich:	3–5 mm
Anzahl Scanpositionen:	4
Genauigkeit (gemittelt):	5 mm

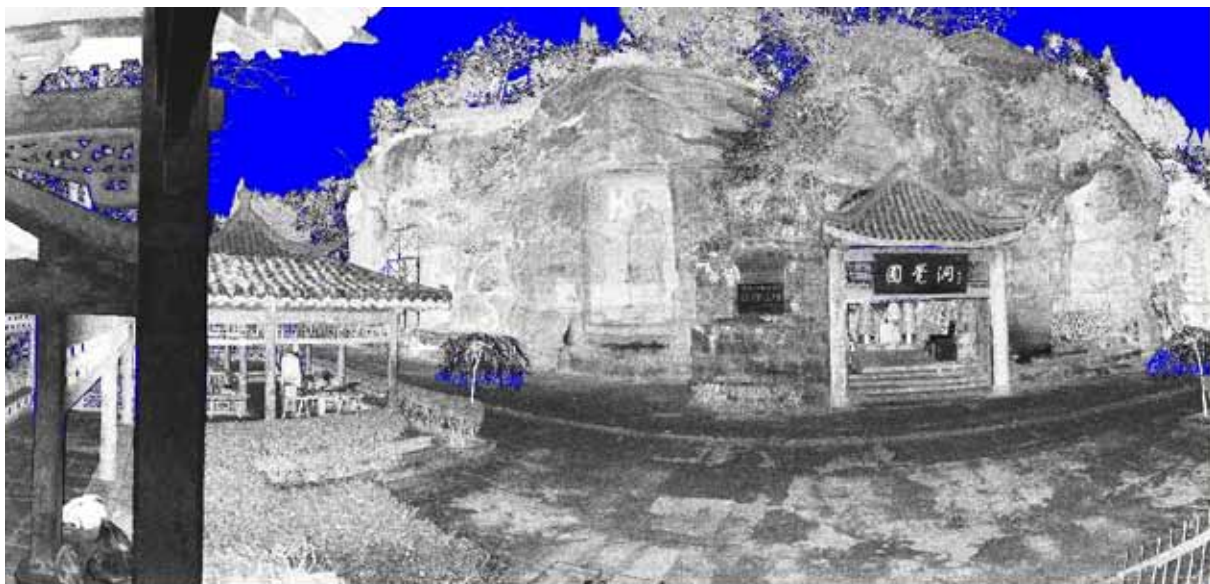


**Abb. 6:** 2-D-Ansicht einer Scanposition (links) und 3-D-Punktwolke mit Scannerstandpunkt

seiner Kippvorrichtung konnten auch schwierig zu erfassende Bereiche vermessen werden.

Während der Aufnahmen wurden größtenteils Scansequenzen, d.h. Mehrfachaufnahmen der Bereiche mit anschließender Mittelung zur Genauigkeitssteigerung der Daten durchgeführt, um eine optimale Erfassung aller Merkmale zu gewährleisten. Eine Überlappung einzelner Messzonen wurde zugelassen.

Für die Visualisierung der Grotte in ihrer Gesamtsituation wurde in einem letzten Schritt die gesamte Felswand mit den benachbarten Grotten und Figuren mit 3-D-Übersichtsaufnahmen und kombinierter Fotografie mit dem Laserscanner erfasst.

#### *Erfassung der Objekte mittels Streifenprojektion*

Die Vermessung der Gesamtgeometrie des Buddha Shakyamuni sowie der Detailgeometrien und Verzierungen im Grottenbereich – besonders der Verzierungen an der Rück- und Seitenwand – erfolgte nach Einbruch der Dämmerung am frühen Abend bis spät in die Nacht hinein mit einer höheren Auflösung. Die zu erfassenden Bereiche wurden dabei mit strukturiertem Licht beleuchtet und mit Hochgeschwindigkeitskameras aufgezeichnet. Aus der bekannten Aufnahmekonfiguration des Messsystems und den Messbildern lassen sich in Echtzeit 3-D-Koordinaten der Objekte ableiten.

Wegen der tiefen Position der Buddhafigur in der Grotte (2–4 m), der Höhe der Grotte und den eingeschränkten Positionierungsmöglichkeiten des Gerüstes vor der Grotte gestalteten sich die Aufnahmen schwierig.

Das Messsystem QT-Sculptor wurde daher auf den maximal möglichen Aufnahmebereich konfiguriert, um überhaupt eine Datenerfassung möglich zu machen. Um eine annähernd lückenlose Aufnahme zu gewährleisten, wurde ein Großteil der Aufnahmen bereits vor Ort registriert. Somit konnten Aufnahmelücken weitestgehend ausgeschlossen werden.

**Tab. 4:** Aufnahmekonfiguration der Vermessung des Buddha Shakyamuni in Grotte Nr. 10

<b>Aufnahmekonfigurationen für Grotte Nr. 37</b>	
Messentfernungen:	3,3–4,1 m bzw. 0,9–1,4 m
Max. Aufnahmefenster:	1,5 x 1,5 m bzw. 0,5 x 0,5 m
Auflösung:	1 mm
Mittlere Messgenauigkeit:	0,5 mm
Anzahl der Aufnahmen:	380



**Abb. 7:** Tiefenbild einer Scanposition (2-D)



**Abb. 8:** Ansicht der beim Scannen entstandenen Punktwolke, Aufnahme mit QT-Sculptor

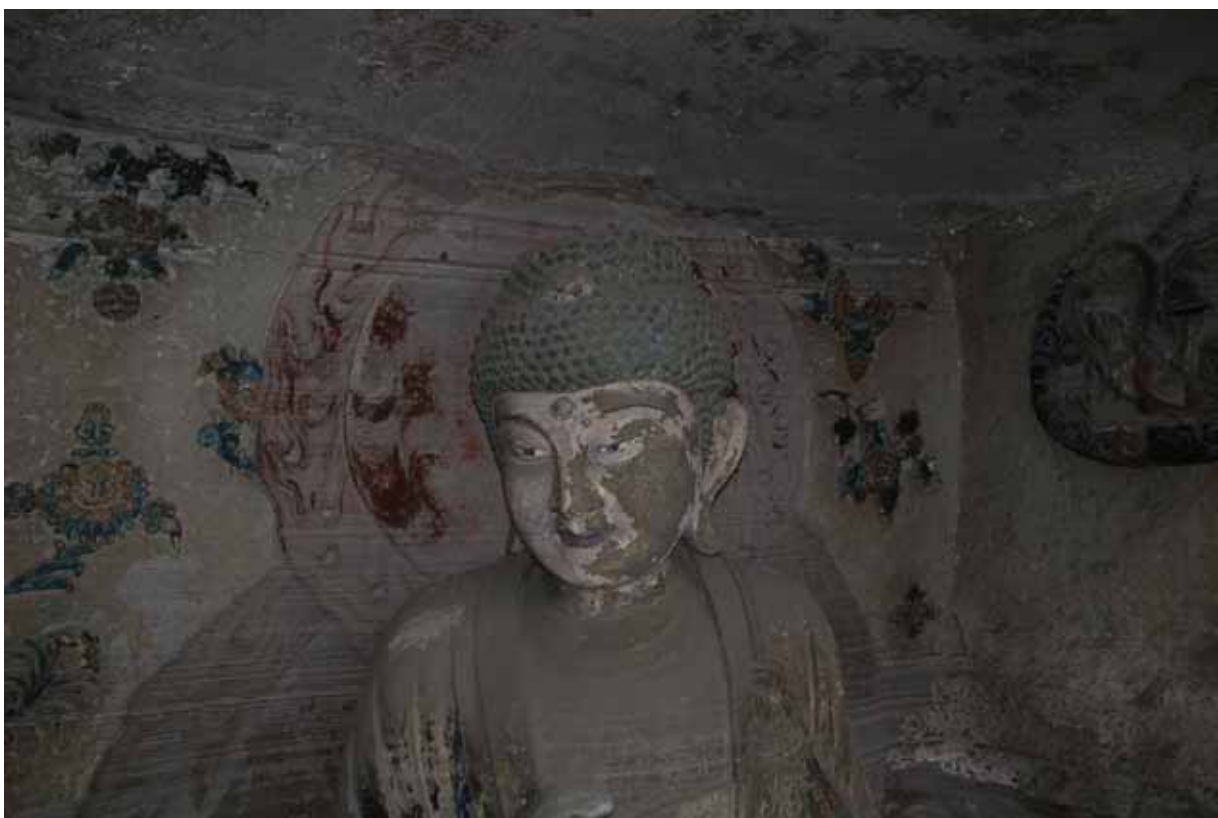


**Abb. 9:** Beispiel für ein Texturbild mit Blitzlicht



**Abb. 10:** Beispiel für ein Texturbild ohne Blitzlicht

## Aufnahme digitaler Bilder

Um fotorealistisch texturierte 3-D-Modelle der Grotte zu erzeugen, war eine besonders sorgfältige Aufnahme digitaler Bilder notwendig. Die Texturbildaufnahme erfolgte dabei mit der Digitalkamera Nikon D100 (Auflösung 6,1 Megapixel). Bestimmte Teilbereiche, besonders an den nicht erreichbaren Regionen am Kopf des Buddhas, konnten nicht vollständig mit Fotoaufnahmen erfasst werden. Hier erfolgt im Texturierungsprozess eine Interpolation der Farbwerte.

Voraussetzung für die Aufnahme von Texturbildern sind gleichbleibende Beleuchtungsverhältnisse bzw. keine direkte Sonne. Für gleichmäßige Texturaufnahmen waren die Lichtverhältnisse in der Grotte an den meisten Tagen eher zu dunkel, sodass alle Bilder von der Buddhafigur und den Grottenwänden mit Blitzlicht aufgenommen werden mussten. Die Aufnahmen der Felsen erfolgten ohne zusätzliches Blitzlicht. Die Anzahl der aufgenommenen Digitalbilder für die Texturierung des 3-D-Modell betrug etwas 600 Stück.

## Auswertung

### Grundlegender Arbeitsablauf

Von den aufgenommenen Messdaten bis zum fotorealistisch texturierten 3-D-Modell ist ein komplexer Arbeitsablauf zu absolvieren, der die reine Messzeit vor Ort um ein Vielfaches übersteigen kann. Im Rahmen des Verarbeitungsprozesses werden dabei die Messdaten registriert, überflüssige Punkte eliminiert, ein konsistentes dreidimensionales Dreiecksnetz erzeugt und dieses über aufgenommene digitale Bilder fotorealistisch texturiert. Danach sind vielseitige Visualisierungs- und Darstellungsmethoden möglich.

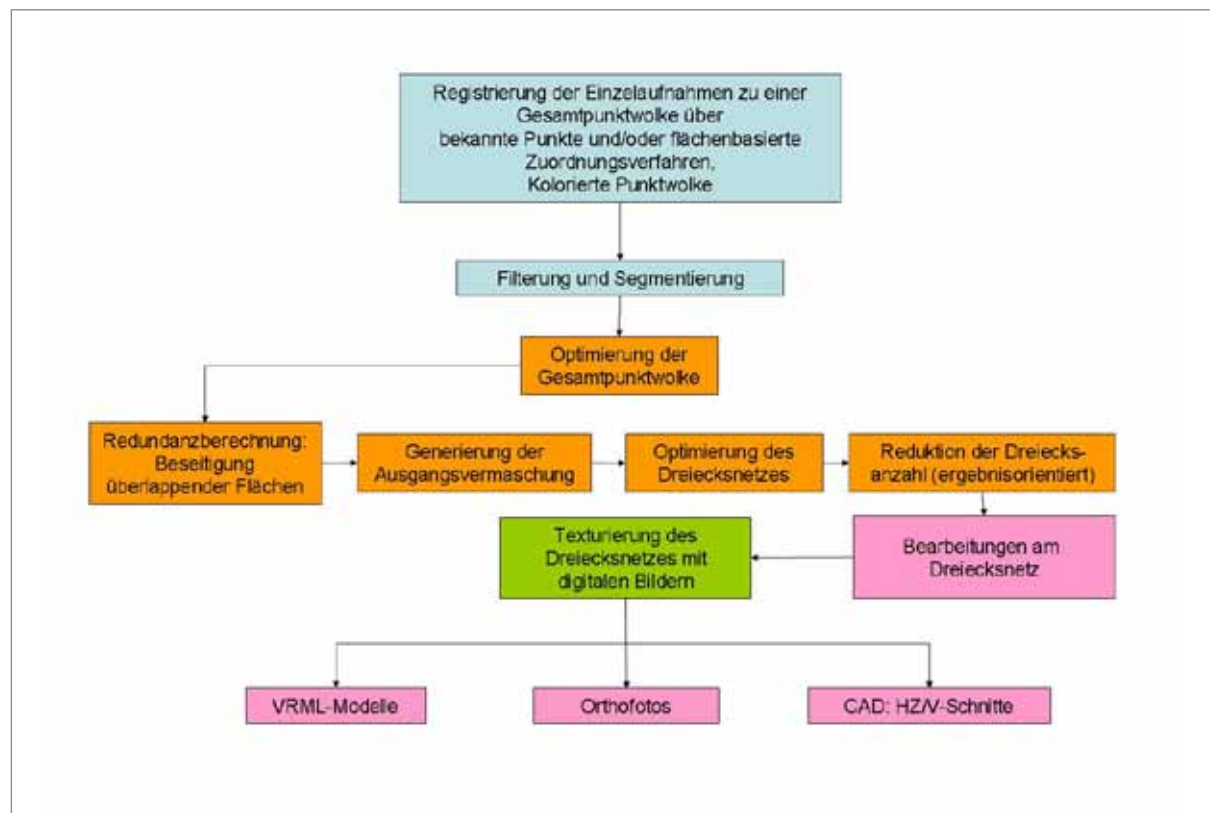


Abb. 11: Schematisierter Arbeitsablauf

## Registrierung der Einzelaufnahmen und 3-D-Modellierung

### Buddha Shakyamuni

Zur Nachbearbeitung der gewonnenen Messdaten zu hochauflösenden 3-D-Modellen kam die Software QT-Sculptor zum Einsatz. Mit ihr wurden auch die Daten des Riegl-Laserscanners über eine spezielle Konvertierungsschnittstelle weiterverarbeitet (Abb. 10).

Die Panorama- und Detailaufnahmen der Aufnahmen aller Standpunkte des Laserscanners wur-

den im ersten Schritt zu einer Gesamtpunktwolke registriert. Außerdem erfolgte eine Registrierung der Streifenlichtscans zueinander. Danach wurden die Aufnahmen der komplexen Detailgeometrie und Verzierungen der Grotte Nr. 10 zusammen mit den jeweiligen Bereichen der Laserscanneraufnahmen über eine Best-Fit-Ausrichtung aneinander angepasst (Abb. 11). Durch die Registrierung entstandene Überlappungsbereiche konnten im Folgeprozess beseitigt werden, sodass eine eindeutig definierte Oberfläche bestimmt wurde. Über diese Objektoberfläche wurde eine hochauflösende Dreiecksvermaschung berechnet (Abb. 12).

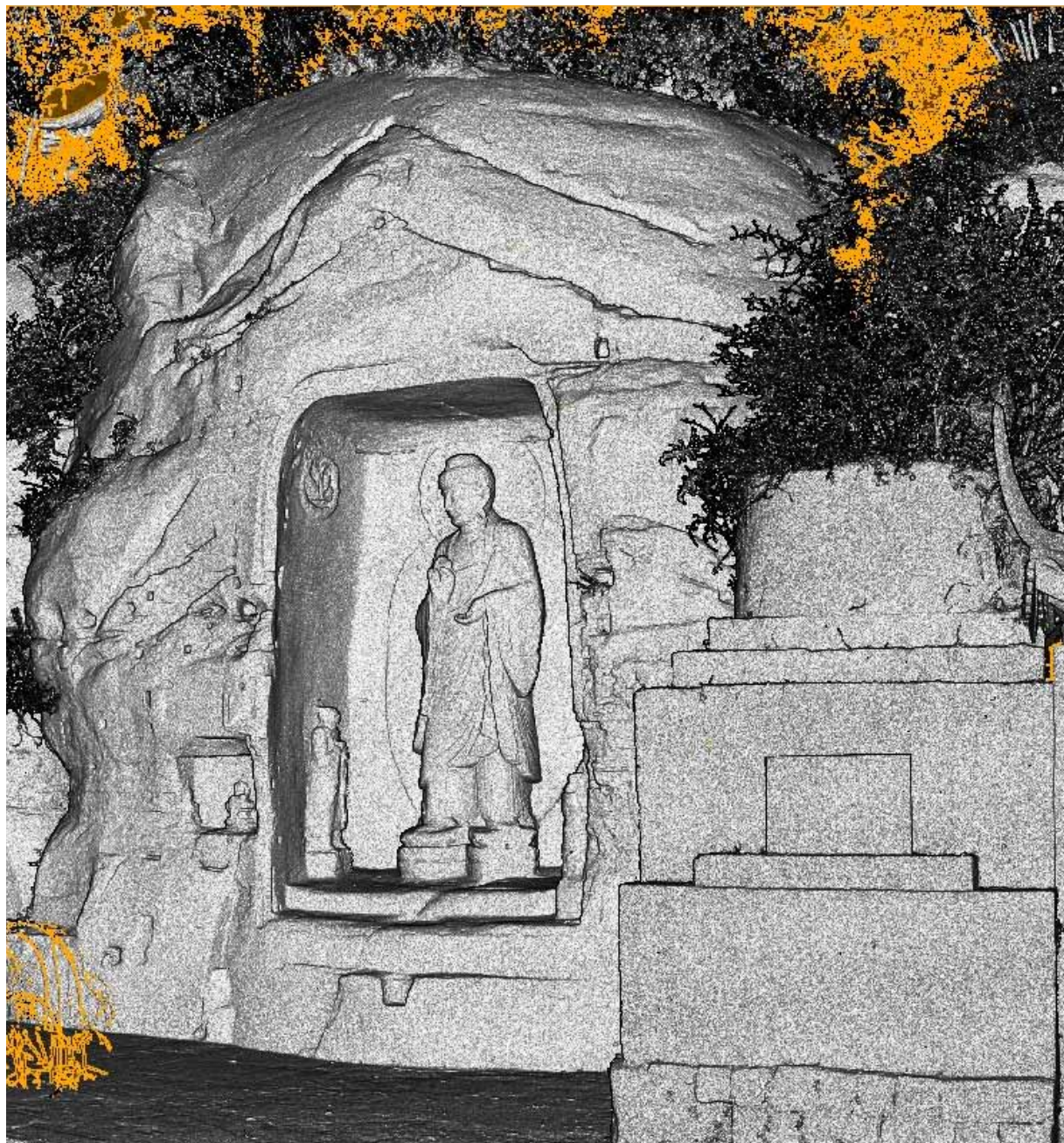


Abb. 12: Konvertierte 3-D-Laserscannerdaten in QT-Sculptor



**Abb. 13:** Kolorierte Gesamtpunktwolke aller Standpunkte des Laserscanners



**Abb. 14:** Gesamtpunktwolke: Kombination der Laserscanner- und Streifenlicht-Aufnahmen mit QT-Sculptor an Grotte Nr. 10

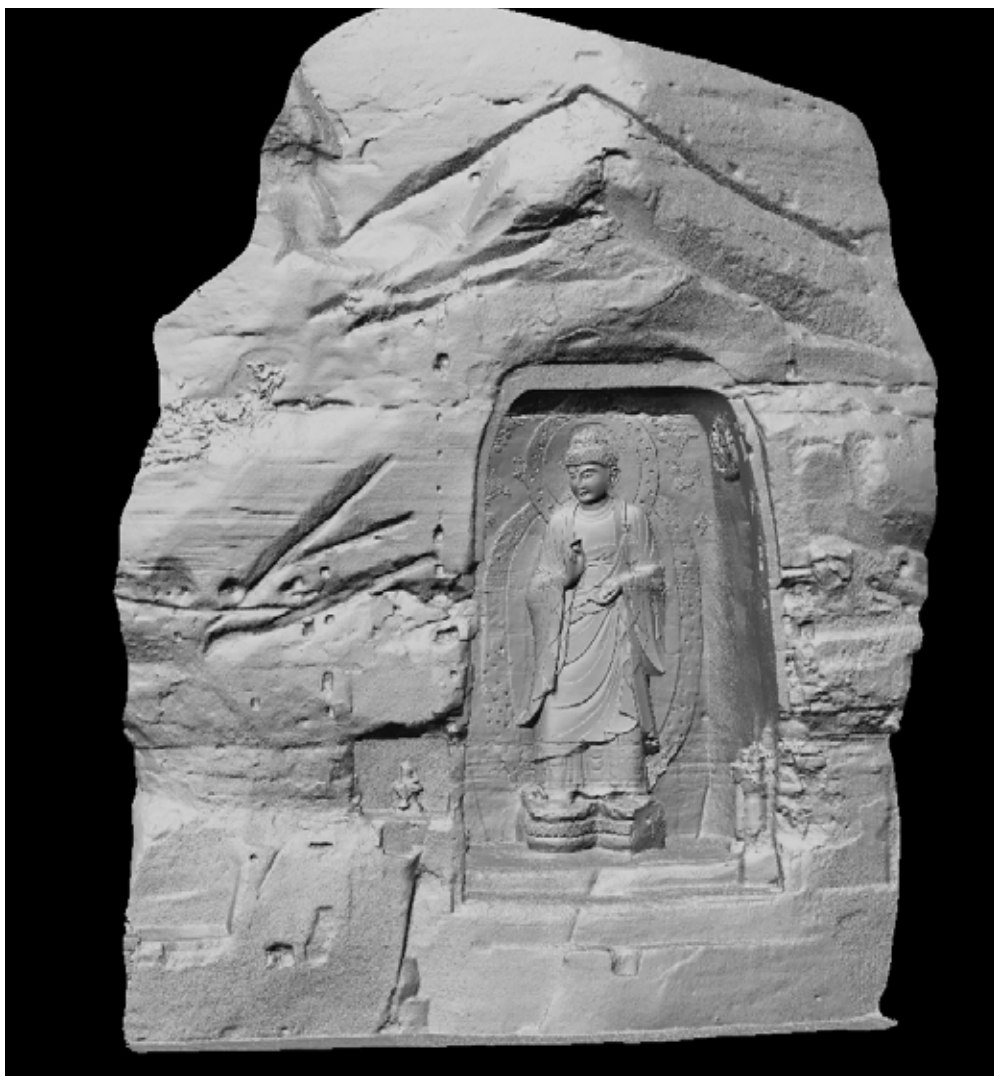


**Abb. 15:**  
Gesamtansicht  
des 3-D-Modells  
(schattiert)

**Tab. 5:** Projektparamenter für Grotte Nr. 10 des Buddha Shakyamuni

<b>Projektparamenter für Grotte Nr. 10 des Buddha Shakyamuni</b>	
Anzahl Laserscans:	60
Anzahl Streifenlichtscans:	378
Gesamtpunktanzahl:	ca. 25 Millionen
<b>Registrierungsgenauigkeit</b>	
Laserscannerdaten:	5,6 mm
Streifenprojektionsdaten:	0,6 – 1 mm
Best-Fit-Optimierung aller Daten:	4,0 mm

Um für die verschiedenen Objektbereiche einen optimalen Kompromiss zwischen Auflösung und Speicherplatz zu erreichen, wurde die Dreiecksberechnung, -optimierung und -reduktion in zwei Objektbereiche untergliedert:

**Tab. 6:** Optimierung und Reduktion der Daten für Grotte Nr. 10 des Buddha Shakyamuni

<b>Auflösung der Ausgangsdreiecksvermaschung</b>	
Modell Buddha mit Rückwand:	1 – 5 mm
Modell Grottenwände und Felsen:	5 – 10 mm
<b>Ergebnis der Dreiecksoptimierung und -reduktion</b>	
Modell Buddha mit Rückwand:	ca. 2 Millionen Polygone
Modell Grottenwände und Felsen:	ca. 2 Millionen Polygone

Einige Bereiche am Kopf des Buddha, hinter der rechten Hand und im Schulterbereich sowie die rechte Seite des Mönches an der linken Grottenwand, konnten nicht erfasst werden. Hier entstanden im 3-D-Modell Fehlvermaschungen, die im Nachhinein manuell beseitigt werden mussten. Das Modell wurde an diesen Stellen vereinfacht geschlossen, um Löcher zu vermeiden. In diesen Bereichen muss mit Abweichungen vom Originalzustand gerechnet werden.



**Abb. 16:** Dreiecksvermaschung aus Laserscanner- und Streifenlichtdaten im Detail (schattierte Ansicht oben und Gitternetz unten)

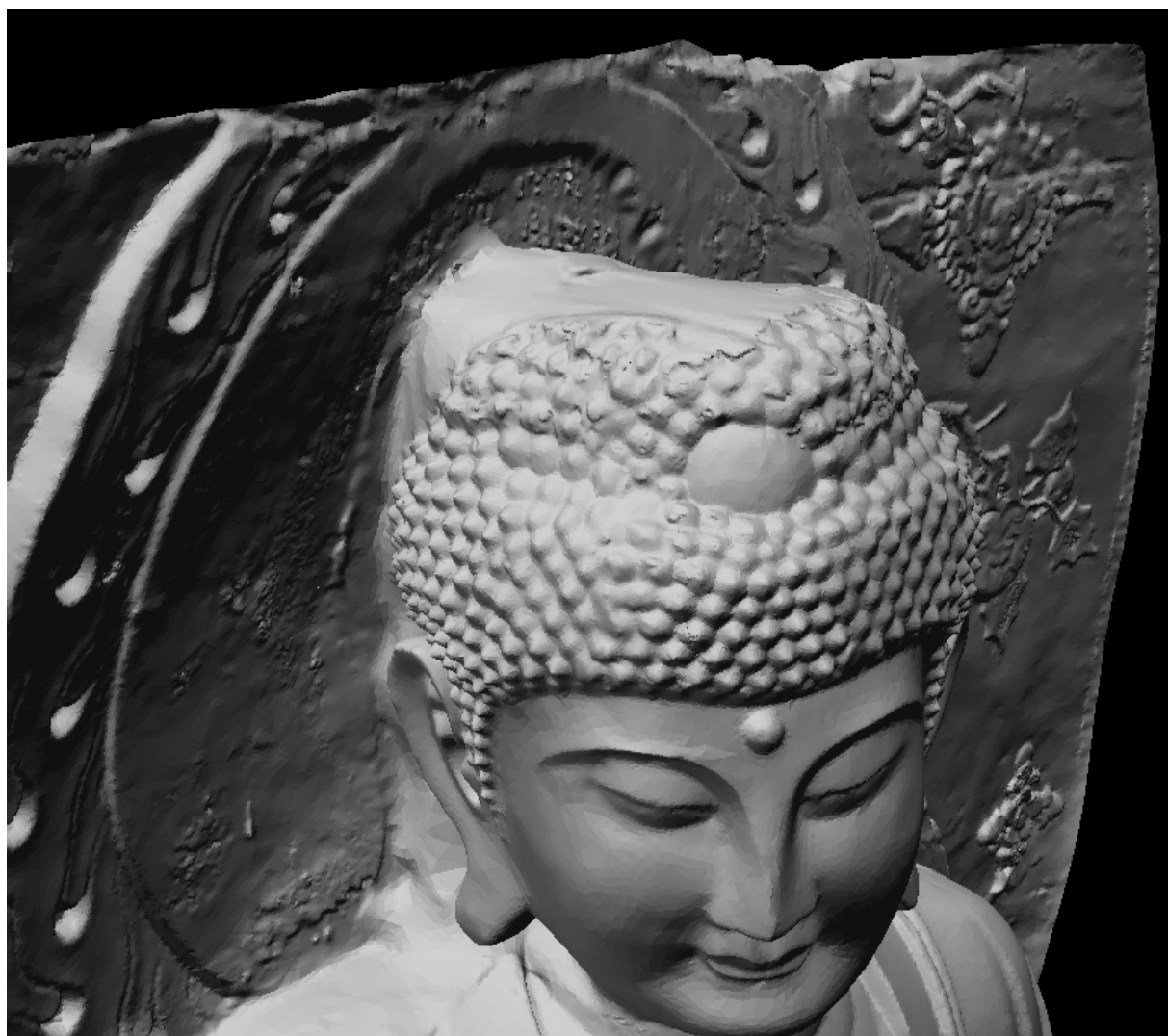


**Abb. 17:** Nicht erfasste Bereiche und dadurch manuell geschlossene Bereiche am Kopf des Buddhas

Für die Weiterverarbeitung im Texturierungsprozess sowie die Verwendung in gängigen 3-D-Programmen liegen nun folgende Modelle im Format STL vor:

**Tab. 7:** Anzahl der Polygone der 3-D-Modelle (LOD1 und LOD2)

Modell Grotte Nr. 10	Detailstufe 1 (LOD1): 100 %	Detailstufe 2 (LOD2): 50 %
Gesamtmodell	4 Millionen	2 Millionen
Teilmodelle		
<i>Buddha mit Rückwand:</i>	2 Millionen	1 Million
<i>Grotte Seite links:</i>	356 000	180 000
<i>Grotte Seite rechts:</i>	375 000	193 000
<i>Boden:</i>	183 000	98 000
<i>Decke:</i>	141 000	74 000
<i>Felsen:</i>	1,2 Millionen	600 000

### *Grotte Nr. 37*

Zusätzlich zu Grotte Nr. 10 mit der Figur des Shakyamuni Buddhas wurde auf der Süd-West-Seite des Felsmassivs die Grotte Nr. 37 zu einem 3-D-Modell ausgearbeitet.

**Tab. 8:** Projektparameter für die Grotte Nr. 37, Süd-West-Wand des Felsmassivs

<b>Projektparameter für Grotte Nr. 37</b>	
Anzahl Laserscans:	9
Gesamtpunktzahl:	5,4 Millionen
<b>Registrierungsgenauigkeit</b>	
Laserscannerdaten:	3 mm
<b>Auflösung der Ausgangsdreiecksvermaschung</b>	
Modell Grotte Nr. 37:	2–5 mm
<b>Ergebnis der Dreiecksoptimierung und -reduktion</b>	
Modell Grotte Nr. 37 und umliegende Bereiche:	ca. 770 000 Polygone
Modell Grotte Nr. 37:	390 000

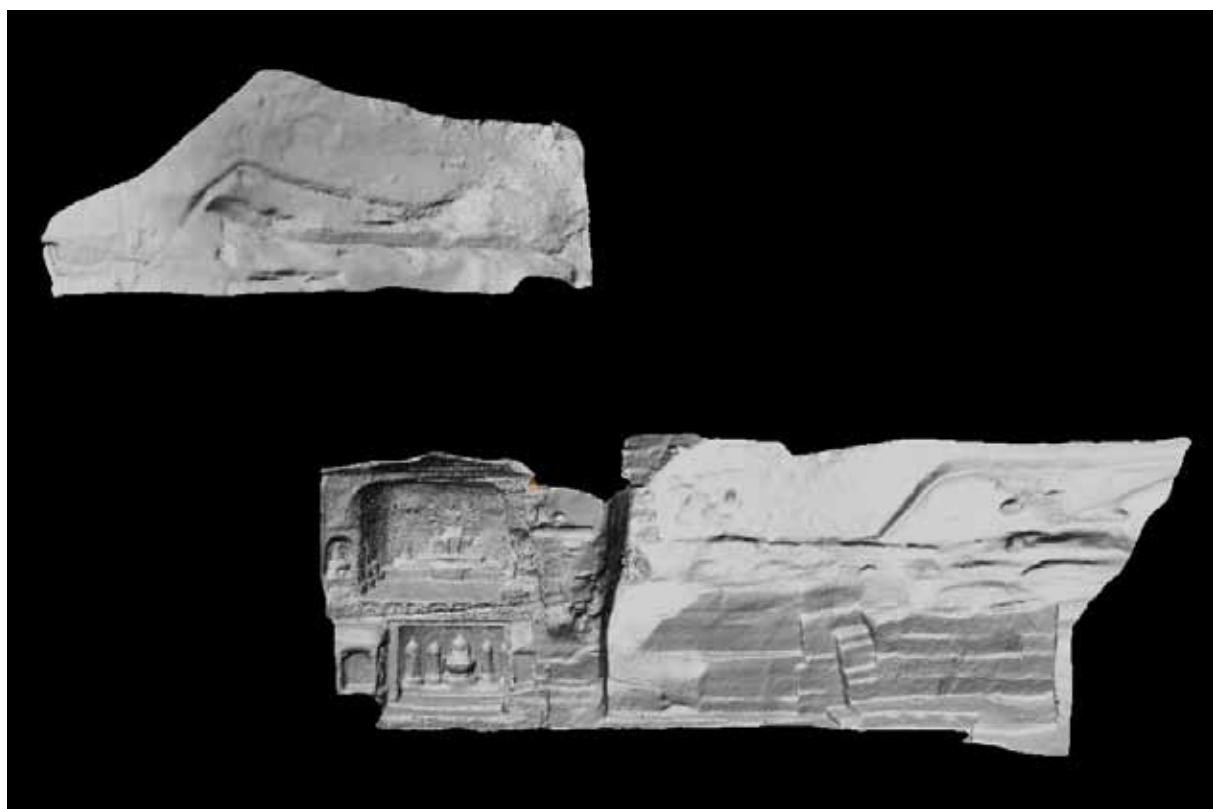


**Abb. 19:** Gesamtansicht des 3-D-Modells Grotte Nr. 37 (schattiert)

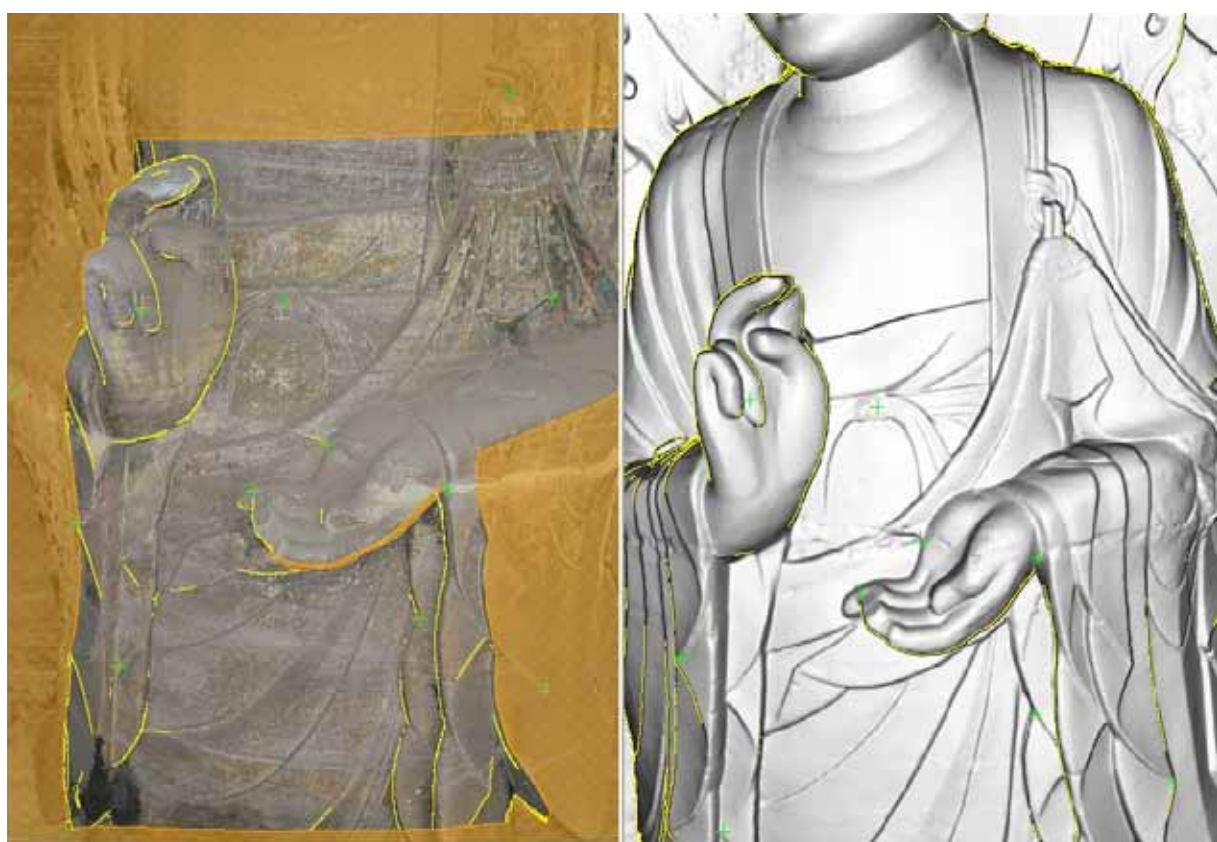


**Abb. 20:** Texturierung am Buddha Shakyamuni mit digitalen Bildern über markanten Punkten

## Texturierung der Einzelmodelle

Durch die Kombination digitaler Bilder mit den 3-D-Modellen können fotorealistisch texturierte Modelle erstellt werden. Dies erfolgte durch differentielle Entzerrung der Digitalbilder über markante Punkte auf dem 3-D-Modell bzw. über Mapping-Verfahren. Zur Anwendung bei der Texturierung kam hierbei ebenfalls die Software QT-Sculptor. Die Fotoaufnahmen mussten aufgrund der teilweise wechselnden Lichtverhältnisse farblich angepasst werden, um eine einheitliche Texturqualität zu erreichen.

Als Ergebnis der Texturierung liegen fotorealistisch texturierte 3-D-Modelle vor, die für die Betrachtung in gängigen VRML-Viewern geeignet sind und für die Dokumentations- und Kartierungsarbeit verwendet werden können.

Bereiche des Kopfes, der rechten Hand und der Schultern sind mit Farbwerten interpoliert worden, die nicht der originalen Farbgebung entsprechen. Hier kann in einer manuellen Nacharbeit eine Verbesserung erreicht werden.

Zur Betrachtung der Daten und der Überführung in einen Digitalisierungsprozess, z. B. für eine Schadenskartierung direkt am Objekt, stehen die Daten im ALO-Format zur Verfügung. Für eine Bearbeitung dieser Daten wird die Software aspect3D eingesetzt. Sie ermöglicht es, Dokumentations- und Kartierungsarbeiten direkt am 3-D-Modell auszuführen und ist mit einer Datenbank verbunden. Dadurch lassen sich die eingegebenen Daten filtern, d. h. nach gewünschten Merkmalen sortieren und entsprechend in Listen ausgeben.

## Orthofotos

Aus den texturierten 3-D-Modellen und den kolorierten Punktfolgen lassen sich schnell und einfach maßstäblich entzerrte Orthofotos ableiten. Dazu wurde die Software aspect3D verwendet. Nach Definition der Orthofotoebene und der Wahl der maximal möglichen Auflösung (hier: 300 dpi) wurden für einzelne Ansichten Orthofotos in verschiedenen Maßstäben berechnet. Sie liegen in den Formaten BMP, PDF, sowie eingebunden in eine AutoCAD-Zeichnung vor.

Folgende Orthofotos wurden erstellt und liegen als Übersichtsplan vor:

- Gesamtansicht der Felswand mit allen Buddhafiguren
- Buddha mit Rückwand
- Felsen von Grotte Nr. 10
- Grottenseiten

## Endnoten

1 Die Vermessung der Grotte Nr. 10 des Buddha Shakyamuni und der Grotte Nr. 37, die Erzeugung der 3-D-Modelle und ihre Texturierung wurde von der Fa. ArcTron in Auftragsarbeit ausgeführt.

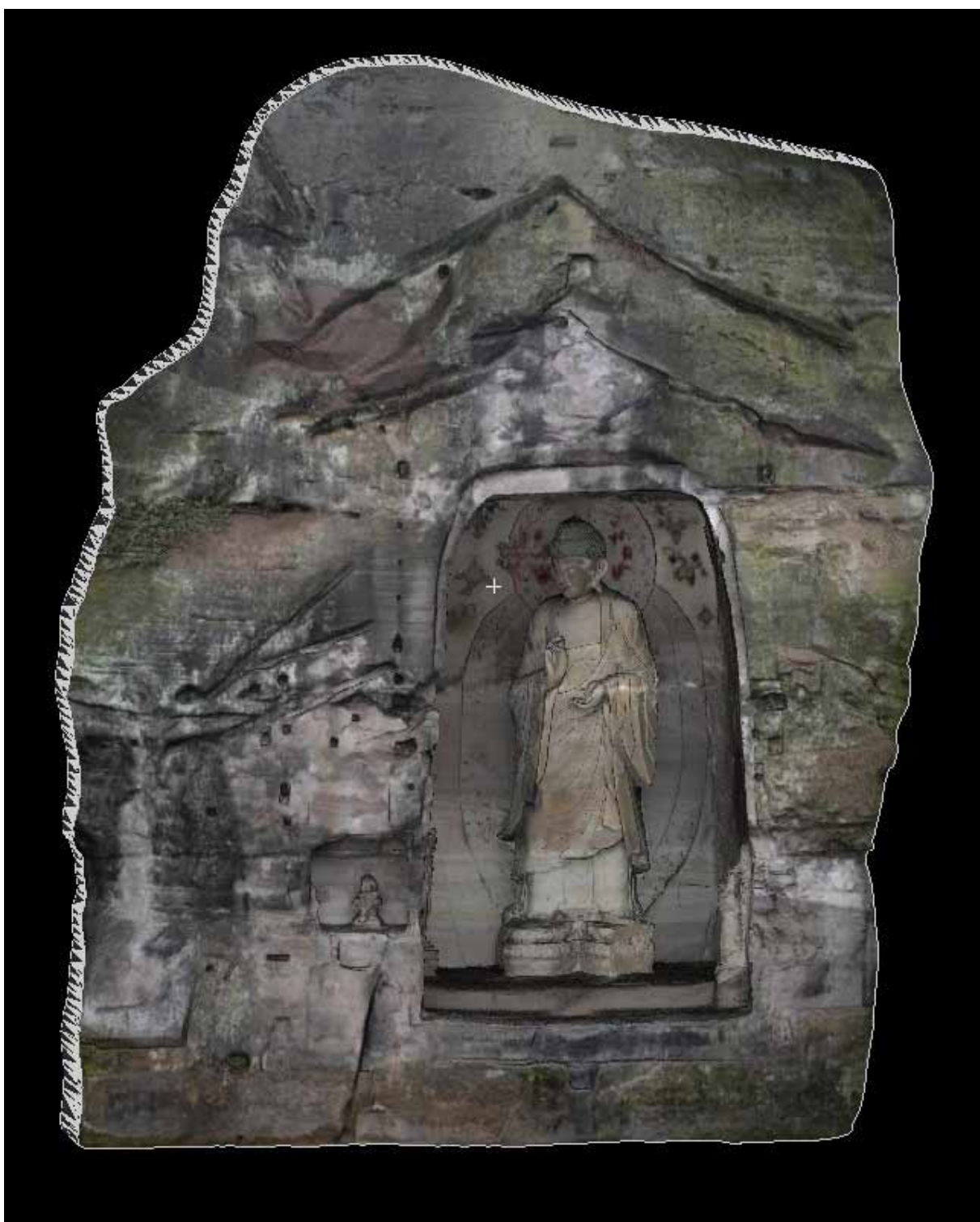


**Abb. 21:** Texturiertes 3-D-Modell der Grotte Nr. 10



### **3-D-Dokumentation der Grotte Nr. 10 des Buddha Shakyamuni**



## 3-D-Dokumentation der Grotte Nr. 10 des Buddha Shakyamuni

Felix Horn

Zur Dokumentation der Grotte Nr. 10 wurden unterschiedliche Methoden eingesetzt: Digitalfotografie, Videoaufnahme, Zeichnungen und 3-D-Scanning. Die Digitalisierung der räumlichen Form von Grotte Nr. 10 erfolgte mit 3-D-Scanning. Ziel der Vermessungsarbeiten in Anyue war die Vermessung der Grotte Nr. 10 des Buddha Shakyamuni mit

3-D-Laserscanning und Streifenprojektionstechnik sowie digitaler Fotografie und die Überführung in ein hoch auflösendes fotorealistisches 3-D-Modell. Das erstellte 3-D-Modell dient dabei als Grundlage für die 3-D-Dokumentation und kann später u. a. zur Befunddokumentation oder für die Bauforschung genutzt werden.



**Abb. 1:** Buddha Shakyamuni,  
Grotte Nr. 10, Grottenanlage  
Yuanjuedong

## Dokumentation am 3-D-Modell

Die visuelle Wahrnehmung des Menschen ermöglicht Tiefenwahrnehmung und erlaubt dadurch räumliches Sehen von Gegenständen. Verdeckte Teile, Hinterschneidungen und Rückseiten einer Skulptur sind in einem Foto nicht, in einer Zeichnung nur bedingt darstellbar. Entsteht bei klassischen Abbildungsverfahren ein zweidimensionales Abbild der dreidimensionalen Wirklichkeit, ist es mit Hilfe von 3-D-Modellen möglich, von Kunstgegenständen ein virtuelles dreidimensionales Abbild zu erzeugen.

Die 3-D-Dokumentation an dreidimensionalen Modellen bietet hier neue Möglichkeiten, da statt auf vielen unterschiedlichen 2-D-Ansichten direkt mit und auf dem 3-D-Objekt gearbeitet werden kann.

Zur 3-D-Dokumentation wird die Software aspect3D eingesetzt. Sie ermöglicht es, Dokumentations- und Kartierungsarbeiten direkt am 3-D-Modell auszuführen und ist mit einer Datenbank verbunden. Dadurch lassen sich die eingegebenen Daten filtern, d. h. nach gewünschten Merkmalen sortieren und entsprechend in Listen ausgeben. So kann man in der Datenbank gezielt nach gewünschten Attributen wie z. B. Rissen oder Bauteilen suchen und sich diese dann gleichzeitig anzeigen lassen. Zur Betrachtung der Daten steht ein kostenloser aspect3D-Viewer zur Verfügung, sodass zur Nutzung der Modelle keine spezielle 3-D-Software angeschafft werden muss.

## Auswertung von 3-D-Modellen

Neben einem Soll-Ist-Vergleich zweier ähnlich geformter 3-D-Modelle lassen sich bei der Auswertung und Vermessung eines Modells Maße und Flächen ermitteln. Auch ist es möglich beliebige Schnitte durch den dreidimensionalen Körper zu legen. Eine Entnahme von Maßen kann jedoch nicht nur am 3-D-Modell erfolgen, ebenso können mit gewissen Einschränkungen dafür Orthofotos verwendet werden.

## Orthofotos

Ausgehend von den texturierten 3-D-Modellen und den kolorierten Punktwolken lassen sich schnell und einfach maßstäblich entzerrte Orthofotos berechnen. Dazu wurde die Software aspect3D verwendet. Nach Definition der Orthofotoebene und der Wahl der maximal möglichen Auflösung (hier: 300 dpi) wurden für einzelne Ansichten Orthofotos in verschiedenen Maßstäben berechnet. Sie liegen in den Formaten BMP, PDF sowie eingebunden in eine AutoCAD-Zeichnung (Abb. 2) vor.

Folgende Orthofotos wurden erstellt und liegen als Übersichtsplan vor:

- Gesamtansicht der nördlichen Felswand der Grottenanlage
- Frontalansicht des Buddha Shakyamuni mit Grottenrückwand
- Umgebendes Felssubstrat von Grotte Nr. 10
- Seitenwände sowie Boden und Decke der Grotte Nr. 10

Diese hoch aufgelösten Orthofotos bieten die Möglichkeit, Masse aus dem Bild zu entnehmen, da Felskanten oder Strukturen, die parallel zur Projektionsebene verlaufen, in wahrer Größe wiedergegeben werden. Verlaufen die Strukturen jedoch schräg zur Projektionsebene werden sie verkürzt wiedergegeben.

Mit Bildverarbeitungs-Software können somit die Orthofotos des Buddha Shakyamuni vermessen werden. So ist es z. B. mit Adobe Photoshop CS 3 Extended möglich, Maße aus den Orthofotos zu extrahieren. Dazu muss in Photoshop zunächst die Messskala anhand einer im Bild bekannten Messstrecke definiert werden. Ist dies erfolgt, können mit Hilfe des Messwerkzeuges Entfernungsmessungen entnommen werden.

Auf diese Weise erfolgte die Vermessung der Balkenlöcher und anderen künstlich geschaffenen Aussparungen in der Außenwand des die Grotte Nr. 10 umgebenden Felssubstrates (siehe Tab. 1 und 2). Als Basis für die Vermessung wurden eine zur Figur des Buddhas mittig verlaufende vertikale Mittelachse und eine auf Niveau des ursprünglichen Bodenhorizontes verlaufende horizontale Achse angelegt. Die Aussparungen im Felsen wurden durchnummiert (A1 bis A38) und mit einem umhüllenden Rechteck versehen (Abb. 3).

### *Horizontale Strecke (Strecke a)*

Gemessen wird hier vom Schnittpunkt der Diagonalen des Rechtecks, welches die Aussparung (Abb. 3) umfängt, bis zur vertikalen Mittelachse. Die Aussparung ist dem Rechteck sozusagen eingeschrieben.

*Beispiel:* Für die Aussparung A16 beträgt die Strecke  $a = 2,23 \text{ m}$  (siehe Abb. 4, Tab. 1 und 2).

### *Vertikale Strecke (Strecke b)*

Die vertikale Strecke wird vom Schnittpunkt der Diagonalen zur horizontalen Achse (entspricht etwa dem Niveau des ursprünglichen Bodens) gemessen.

*Beispiel:* Für die Aussparung A16 beträgt die Strecke  $b = 2,79 \text{ m}$  (siehe Abb. 4, Tab. 1 und 2).

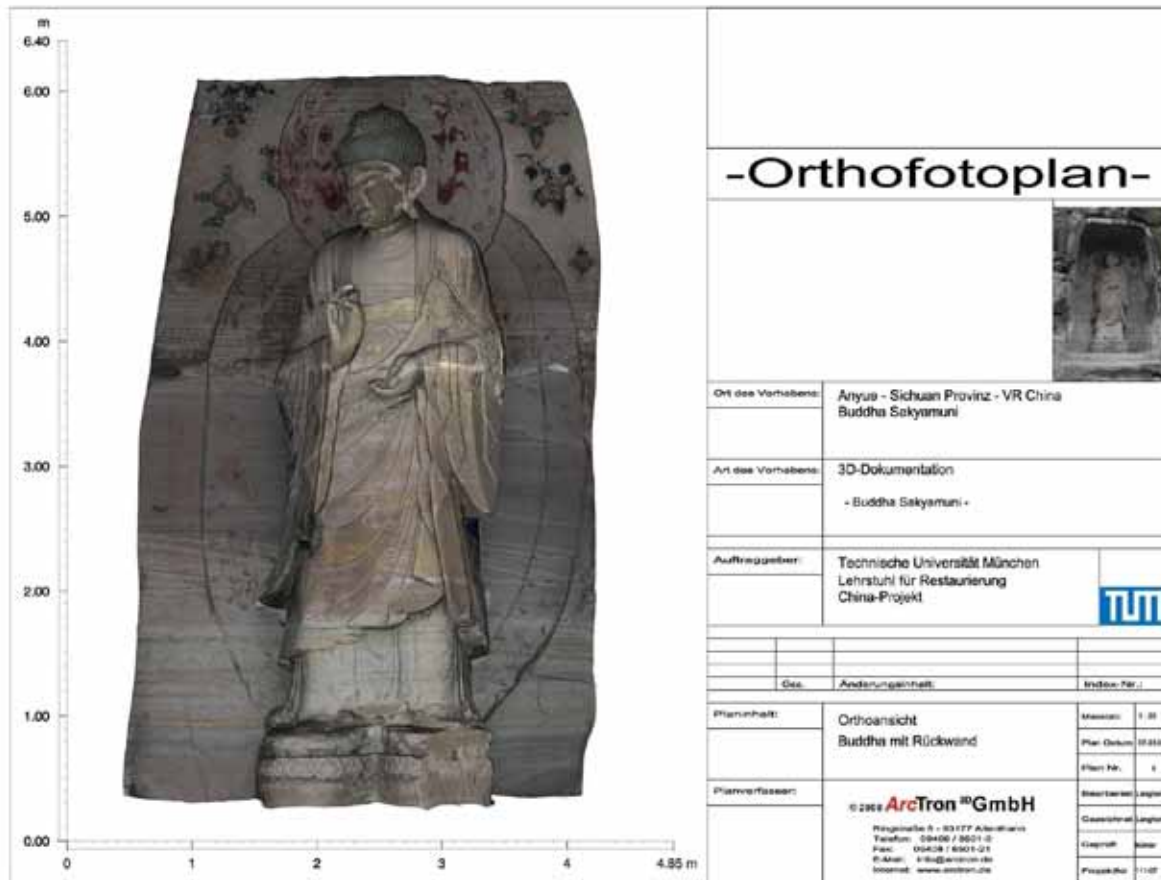


Abb. 2: Orthofotoplan der Grotte Nr. 10 des Buddha Shakyamuni

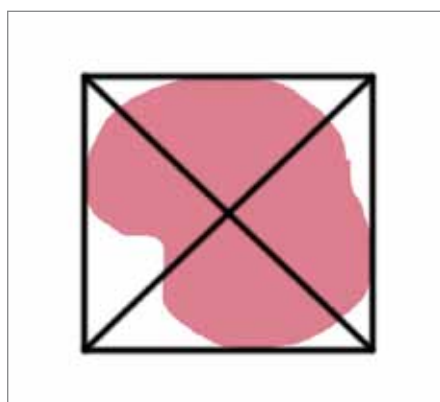


Abb. 3: Schnittpunkte der Diagonalen

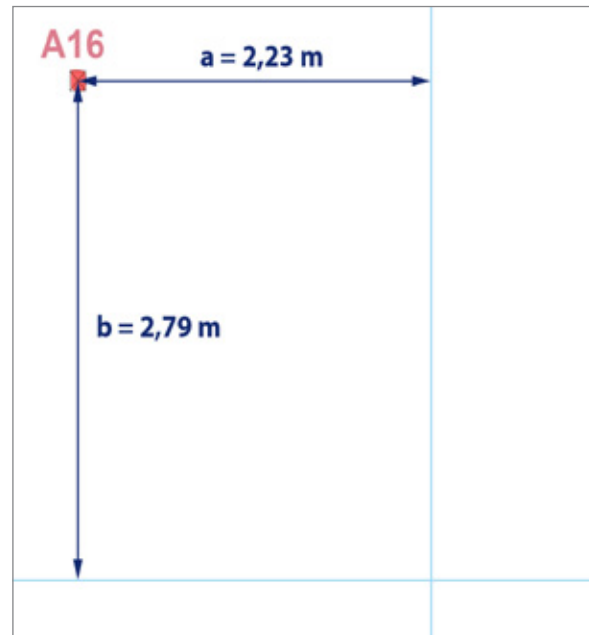


Abb. 4: Vermessung der horizontalen und vertikalen Strecke der Aussparungen

**Distanzen der Aussparungen  
(Balkenlöcher) in der Fassade der  
Außenwand des Felsmassivs (A1–A20)**

**Tab. 1:** Grotte Nr. 10, Distanzen der Aussparungen  
(Balkenlöcher)

Messstrecke	Distanz
A1 – Mittelachse (vertikal)	0,20 m
A1 – Achse (horizontal)	11,39 m
A2 – Mittelachse (vertikal)	1,27 m
A2 – Achse (horizontal)	10,76 m
A3 – Mittelachse (vertikal)	0,06 m
A3 – Achse (horizontal)	9,87 m
A4 – Mittelachse (vertikal)	1,69 m
A4 – Achse (horizontal)	9,79 m
A5 – Mittelachse (vertikal)	0,30 m
A5 – Achse (horizontal)	9,19 m
A6 – Mittelachse (vertikal)	2,27 m
A6 – Achse (horizontal)	7,26 m
A7 – Mittelachse (vertikal)	2,26 m
A7 – Achse (horizontal)	7,36 m
A8 – Mittelachse (vertikal)	2,32 m
A8 – Achse (horizontal)	6,68 m
A9 – Mittelachse (vertikal)	2,33 m
A9 – Achse (horizontal)	6,21 m
A10 – Mittelachse (vertikal)	2,35 m
A10 – Achse (horizontal)	5,78 m
A11 – Mittelachse (vertikal)	2,36 m
A11 – Achse (horizontal)	5,18 m
A12 – Mittelachse (vertikal)	2,34 m
A12 – Achse (horizontal)	4,76 m
A13 – Mittelachse (vertikal)	2,32 m
A13 – Achse (horizontal)	4,42 m
A14 – Mittelachse (vertikal)	2,27 m
A14 – Achse (horizontal)	3,91 m
A15 – Mittelachse (vertikal)	2,21 m
A15 – Achse (horizontal)	3,43 m
A16 – Mittelachse (vertikal)	2,23 m
A16 – Achse (horizontal)	2,79 m
A17 – Mittelachse (vertikal)	2,19 m
A17 – Achse (horizontal)	4,69 m
A18 – Mittelachse (vertikal)	2,32 m
A18 – Achse (horizontal)	4,46 m
A19 – Mittelachse (vertikal)	2,07 m
A19 – Achse (horizontal)	4,04 m
A20 – Mittelachse (vertikal)	2,32 m
A20 – Achse (horizontal)	3,91 m

**Distanzen der Aussparungen  
(Balkenlöcher) in der Fassade der  
Außenwand des Felsmassivs (A21–A38)**

**Tab. 2:** Grotte Nr. 10, Distanzen der Aussparungen  
(Balkenlöcher)

Messstrecke	Distanz
A21 – Mittelachse (vertikal)	2,11 m
A21 – Achse (horizontal)	3,51 m
A22 – Mittelachse (vertikal)	3,64 m
A22 – Achse (horizontal)	4,68 m
A23 – Mittelachse (vertikal)	3,65 m
A23 – Achse (horizontal)	4,20 m
A24 – Mittelachse (vertikal)	4,92 m
A24 – Achse (horizontal)	4,53 m
A25 – Mittelachse (vertikal)	4,11 m
A25 – Achse (horizontal)	4,63 m
A26 – Mittelachse (vertikal)	3,77 m
A26 – Achse (horizontal)	4,75 m
A27 – Mittelachse (vertikal)	5,60 m
A27 – Achse (horizontal)	3,95 m
A28 – Mittelachse (vertikal)	3,99 m
A28 – Achse (horizontal)	4,02 m
A29 – Mittelachse (vertikal)	3,72 m
A29 – Achse (horizontal)	4,13 m
A30 – Mittelachse (vertikal)	2,87 m
A30 – Achse (horizontal)	4,27 m
A31 – Mittelachse (vertikal)	3,15 m
A31 – Achse (horizontal)	3,98 m
A32 – Mittelachse (vertikal)	3,77 m
A32 – Achse (horizontal)	3,35 m
A33 – Mittelachse (vertikal)	3,74 m
A33 – Achse (horizontal)	3,00 m
A34 – Mittelachse (vertikal)	4,65 m
A34 – Achse (horizontal)	3,09 m
A35 – Mittelachse (vertikal)	3,86 m
A35 – Achse (horizontal)	1,29 m
A36 – Mittelachse (vertikal)	4,37 m
A36 – Achse (horizontal)	0,00 m
A37 – Mittelachse (vertikal)	3,98 m
A37 – Achse (horizontal)	0,01 m
A38 – Mittelachse (vertikal)	0,12 m
A38 – Achse (horizontal)	- 0,13 m

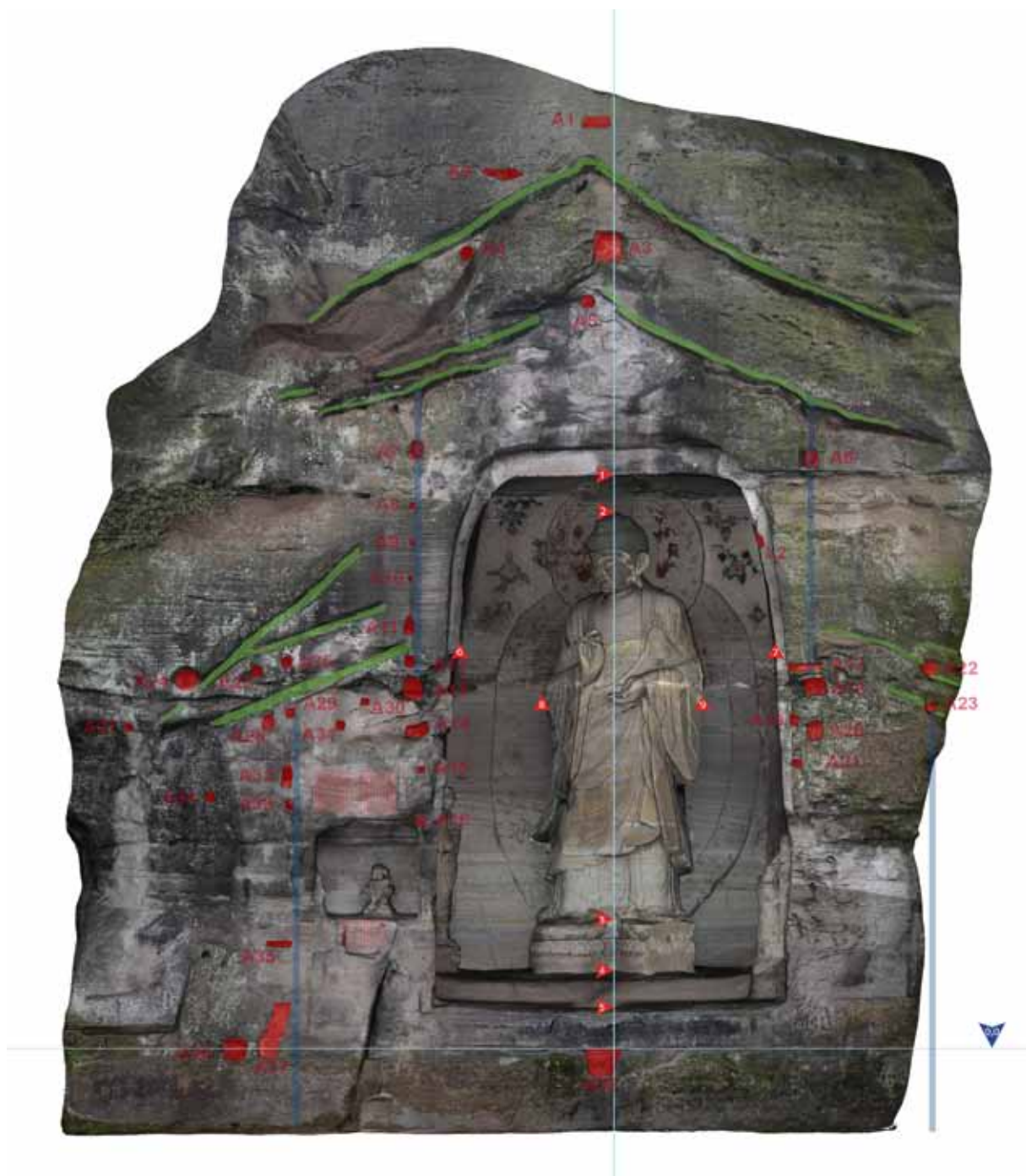


**Abb. 5:** Kartierung und Vermessung der Grotte Nr. 10 des Buddha Shakyamuni

### Bearbeitungsspuren in Form von Balken- oder Pfostenauflager

**Tab. 3:** Buddha Shakyamuni, Grotte Nr. 10, Bearbeitungsspuren

Nr.	Lage	Beschreibung	Abmessungen
A1	befindet sich auf Mittelachse von Grotte und Buddha, ca. 4,2 m über Level Grottendecke	stufenförmige Aussparung im Fels	Höhe ca. 9 cm, Breite ca. 36 cm, Tiefe ca. 12 cm
A2	ca. 0,8 m rechts von Mittelachse (ausgehend vom Buddha), ca. 3,6 m über Level Grottendecke	stufenförmige, durchgebogene Aussparung im Fels	Höhe ca. 9 cm, Breite ca. 54 cm, Tiefe ca. 17 cm
A3	befindet sich auf Mittelachse der Grotte, ca. 2,6 m über Level Grottendecke	nicht sehr tiefe Aussparung mit oben ausgerundeten Ecken, nach unten frei auslaufend; Balken- oder Pfostenloch?; Aussparung für Giebelanschluss?	Höhe ca. 35 cm, Breite ca. 30 cm, Tiefe ca. 17 cm
A4	ca. 1,6 m rechts von Mittelachse, ca. 2,6 m über Level Grottendecke	ovale, trichterförmige und nicht sehr tiefe Aussparung	Höhe ca. 20 cm, Breite ca. 18 cm, Tiefe ca. 8 cm
A5	befindet sich etwa auf Mittelachse der Grotte, ca. 2 m über Level Grottendecke	runde, nicht sehr tiefe Aussparung	Höhe ca. 16 cm, Breite ca. 17 cm, Tiefe ca. 10 cm
A6	ca. 2,2 m links von Mittelachse, ca. 0,01 m über Level Grottendecke	hochrechteckige Aussparung, vermutlich Balkenauflager	Höhe ca. 23 cm, Breite ca. 16 cm, Tiefe ca. 21 cm
A7	(wird fortgesetzt)		

### Dimensionen des Buddha Shakyamuni

**Tab. 4:** Vermessung des Buddha Shakyamuni, Grotte Nr. 10

Messstrecke	Distanz	Nr. Photoshop	Messung Zählpunkt–Zählpunkt
Höhe Grotte (max.)	6,53 m	0001 (Lineal 13)	1–5
Höhe Buddha (ohne Sockel)	5,03 m	0007 (Lineal 19)	2–3
Höhe Buddha (mit Sockel)	5,64 m	0002 (Lineal 14)	2–4
Höhe Sockel	0,61 m	0005 (Lineal 17)	3–4
Breite Grotte (auf Höhe der rechten Hand)	3,64 m	0006 (Lineal 18)	6–7
Breite Buddha (auf Höhe der Ellenbogen)	1,85 m	0003 (Lineal 15)	8–9

## **Biological Investigations of Grotto No. 37**



# Biological Investigations of Grotto No. 37

Ursula G. Drewello, Mathias Kocher

## Results of the Analysis: AN 1994

<b>Location, Object:</b>	China, Szechuan Province, Anyue Grotto, sandstone construction. Written by Prof. Dr. R. Snethlage on 11.12.2008
<b>Test Material,</b> labels	<b>Sample 1a:</b> dark green moss, above no. 38; <b>Sample 1b:</b> stone test with moss (dark green, dry und light green, dry), <b>Sample 2a:</b> dark green moss, leafy, upper right side; <b>Sample 2b:</b> stone test with moss (dark green, non-vascular leaves), <b>Sample 3a:</b> light green moss, dry, lower right; <b>Sample 3b:</b> stone test
<b>Research Questions:</b>	What species can be found on and in the stone substrate? How far has the biogenic covering penetrated the stone? What methods should be used to remove it?
<b>Methods of Identification:</b>	Lichtmikroskopie (LM); Fluoreszenzmikroskopie, Rasterelektronenmikroskopie (REM);
<b>Botanical Examination:</b>	<p><b>Treatment and Evaluation of Materials:</b> Dipl.-Biol. Ursula G. Drewello Labor Drewello &amp; Weißmann GmbH Geyerswörthstraße 6b 96047 Bamberg</p> <p><b>Lichen Identification:</b> Prof. Dr. Rosmarie Honegger Institut für Pflanzenbiologie Universität Zürich Zollikerstrasse 107 CH-8008 Zürich</p> <p><b>Moss Identification:</b> Dr. Edi Urmí Institut für Systematische Botanik dto.</p>

## Results of the Analysis:



Sample 1a, b:

This sample is a piece of red sandstone on which a moss with small, nonvascular leaves have grown. On the outermost layer of stone, the moss has built up a 1<sup>+</sup>-millimetre thick layer of humus. In the mean time, it has dried out and is easily removed from the stone. On the layer of humus, there appears to be an optically light, damaged biogenic area that goes approximately one to two millimetres into the stone. In the layer of humus, the thick, brown rhizoids of the moss and the fine hypomyces mycelium creates a covering that extends into the biogenic layer. As the moss' rhizoids thin out over the intact stone area of the sample (up to 1,5 cm) and are able to penetrate the stone, the fine, transparent fungal hyphae can be found throughout the entire sample. In the sample, there is the typical musty to earthy smell of mold, which is a by-product of metabolic processes. A complex mixture of volatile organic compounds belonging to the material classes of the alcohols, ketones, terpenes, and aromatic compounds are responsible for this.

The overdeveloped biogenic area is evident because of its visibly thickened outer layer. The plentiful residue of crystallized compounds have materialized because of microbially induced precipitation. It has created a layer over the main part of the sample that is visible under a light microscope.

The species and genus of the moss cannot be precisely classified. A conservative assessment is that there are characteristics specific to the species *Gyroweisia sp.* from the Pottiaceae family. In Bryopsida flora from China, there is only one type of this and this is *not* it, so if it is a type that has not yet been described, it is definitely new to China.

There is also growth of the moss species *Gyroweisia* on shady stone walls in our area.<sup>1</sup> *Gyroweisia* Schimp. is one type present in Baden-Württemberg; worldwide there are about 10 types.<sup>2</sup>

In the corresponding thin section (< 20 µm), the inspection of a cross-section of up to 7 mm located over the stone matrix confirms the penetration of moss rhizoids through the test sample. Decomposing biogenic material collects in its many pores and appears to be a diffused brown mass. The intact moss rhizoids appear to be fibrous, structured plant pieces.



Sample 2a, b:

Just as in Sample 1, there is a piece of red sandstone, on which a piece of moss with wide, non-vascular leaves has grown. In this sample, a 1<sup>+</sup>-millimetre thick layer of humus has built up under the layer of moss. The thicker this layer is, the more easily it can be removed. In this sample, the layer of humus has dried out.

Just as in Sample 1, the layer of humus had been penetrated with moss rhizoids and fungus mycelia. This layer microbial area under the layer of humus is less distinctive than in Sample 1. The typical moldy smell is more noticeable in this sample.

The Marchantiophyta is a *Plagiochasma appendiculatum*/Lehm. et Lind. Order: Marchantiales, Family: Aytoniaceae (although the material is sterile, an exact identification cannot be made, because this genus is being revised).

The moss is covered with a number of white rhizoids that, from the bottom of the thallus, appear to be flat. It is located on the outermost layer of stone and penetrates through the sandstone. The dark brown rhizoids in the layer of humus as well as in the stone have resulted from a previous moss growth; under the Marchantiophyta, there is a dead layer of gametophytes, consisting of a small stem made up of small, curly nonvascular leaves, pointing to a Bryopsida.

In the related area (< 20 µm) is to be detected, that before all things the dark brown rhizoids of the preceding Bryopsida colony over the entire area went up to 1,3 cm in the sandstone. The pores are filled with biogenic metabolic products, dead biomasses, a rich microbe population and sporadically also with algae colonies.

Special features of *Plagiochasma appendiculatum*/Lehm. et Lind.: *Plagiochasma appendiculatum* allows for specific biomonitoring of the bodies of water with mercury and copper, as these elements cause damage to the thallus and chlorophyll production. However, zinc, chrome and lead barely harm *Plagiochasma appendiculatum*, if at all.<sup>3</sup>

In addition, because of antimicrobial properties, there is evidence that *Plagiochasma appendiculatum* appears to be able to help heal wounds and has an antioxidant effect as well. In some tribes, pastes from this moss are used for the treatment of skin ailments.<sup>4</sup>



Sample 3a, b:

The red sandstone, as in Samples 1 and 2, is covered with a white-green lichen. Under this layer of lichen is a moss growth that has already been largely displaced from the lichen. The Bryopsida can only sporadically be identified.

By the grown crust of the layer, it is a question of *Lepraria* sp. (testing could not determine the exact type)<sup>5</sup>

There are two clearly identifiable areas in the lichen layer. In the outer layer, the algae partner (photobiont), which is responsible for the light green appearance of the lichen, has become integrated into the white mycelium of the mushroom partner (mycobiont). In contrast, the other layer of lichen consists almost entirely of the mycobionts' white mycelium.

The lichen thallus of this species is typically powdery (leprosous) and consists of small particles, which can be anywhere in shape and size between small and fine to large and almost cotton-like. From these particles, which make up the thallus, the mycel filaments stick out in all directions, like a hedgehog.

In contrast to Samples 1 and 2, in which a multi-millimetre thick layer of humus could build up on the stone, here, there is a visible, thin layer of moss rhizoids adhering to the stone. There is a microbial area that has affected the stone and, as described in Sample 1, appears to be lighter and goes 1–2 mm into the stone.

On the other hand, the stone matrix is infiltrated by metabolic products, which appears to be more finely structured lets the layer. The large variety of metabolic products, which are being disposed of in the form of crystalline phases of the microorganisms and surrounded the hyphen of the mushroom partner, are clearly visible in the raster electron microscope.

There are a number of additional microbes to be identified by the raster electron microscope, creating the impression that there is a complex biological environment. Aside from the lichen, there are, among others, additional fungi, bacteria, and actinomycetes, and diatoms (brown algae).

In comparison to Samples 1 and 2, there is almost no noticeable moldy smell.

In the accompanying thin section (< 20 µm) it is noticeable that the moss rhizoids over the entire cross section go up to 0,7 cm into the sandstone and the

few dense sandstone structures within it are filled with biomass and metabolic products.

### Cleaning, Removal:

The removal of moss from the outer layer of stone should be relatively simple if the layer of humus on top of the stone is also removed.

In order to prevent moss growth over the long term, the conditions of the area must be changed over the long term, too, keeping moisture at a minimum. Then it is important to pay attention, that the moisture in the stone substrate plays a lesser role than humidity. This is not because mosses do not absorb water through their rhizoids but instead through their nonvascular leaves and thalli. Maintaining a dry environment with lots of sunlight is helpful in drying out existing colonies and preventing the growth of new ones.

At the moment, it is unclear if it would be beneficial to remove mosses and lichens from the stone.

The following issues should be considered:

- The removal of the moss always leads to a removal of the outermost layer of the stone.
- The moss rhizoid growth goes deep into the stone, so a complete removal is impossible.
- Endolithic lichens that have grown into the stone can only be removed at the surface layer.
- Because the partner fungi deeply penetrates the stone, a mechanical removal is not going to be able to completely remove the growth, either. The lichens regenerate themselves in many cases, so that a removal merely leads to a loss of the outermost layer of stone.
- In addition, the method of burning off lichens and/or using biocides is not recommended, because the lichen population will surely be affected, and because it is highly likely a new colony will grow. There is the danger that because of the slight competitive pressure, a quickly-growing lichen will grow in a species-poor population, leading to a significantly thicker settlement in the outermost layer of stone which can even begin to grow before treatment is over.
- A species-rich lichen and moss population on the outermost layer of stone is actually better to have than a new growth of a species-poor population after a cleaning.

- As a rule, mosses and lichens are typically more protective of than damaging to the stone. The sandstone that is present here has over a loose, very porous structure, through which moss rhizoids easily grow. Their growth can also help to consolidate and strengthen the sandstone structure.
- There are negative consequences of the removal of the green moss thallus. As a result of its removal, the rhizoids dry out, and the exposed outer layer of stone can weather more quickly.
- The subtropical weather in Szechuan Province means that, year-round, there is relatively high humidity in the Anyue grotto. This, and the low number of sunny days in the province, leads to the rapid moss, lichens and microbe re-colonization after of virtually every method of stone cleaning.
- In addition, the fact that the *Gyroweisia sp.* moss found in Sample 1 has not yet been seen in China. In this instance, it is possible that it is a type that has not yet been discovered! If circumstances allow, this biodiversity-enriching new moss should be left in place.

The identification of other microflora, which consists of a number of different types of bacteria and fungus, has been made. It can be completed by additional surveys.

## Endnotes

- 1 Werner, J. (1985): Einige bemerkenswerte Moose an der Dreiländerecke bei Schengen, Bull. Soc. Nat. Lux. 85 (1980–82), p. 77–81.
- 2 Nebel, M., G. Philippi (Ed.) (2000): Die Moose Baden-Württembergs, Vol. 1, p. 329.
- 3 S. Ghate and S. B. Chaphekar (2000): *Plagiochasma appendiculatum* as a biotest for water quality assessment. Environmental Pollution, Vol. 108, Issue 2, p. 173–181.
- 4 M. Singh, R. Govindarajan, V. Nath, A. Kumar, S. Rawat, A. Kumar and S. Mehrotra (2006): Antimicrobial, wound healing and antioxidant activity of *Plagiochasma appendiculatum* Lehm. et Lind. Journal of Ethnopharmacology, Vol. 107, Issue 1, p. 67–72.
- 5 A monograph of the genus is currently being put together. The author of this monograph has offered assistance to this project.
- 6 Brickwedde, F., Carl Beierkuhnlein, Rainer Drewello (Ed.) (2009): Leitfaden zur naturverträglichen Restaurierung von historisch bedeutsamem Mauerwerk aus Sand- und Kalkstein. Berlin, Erich Schmidt Verlag (in press).
- 7 The lightmicroscope photos have been taken by Ursula G. Drewello.
- 8 The images from the raster electron microscope were taken by Prof. Dr. R. Honegger.

**PHOTO DOCUMENTATION Sample 1<sup>7</sup>**

**Image 1:** Overview of Sample 1: Sandstone with vigorous moss growth (LM, approx. 16x).

**PHOTO DOCUMENTATION Sample 1**

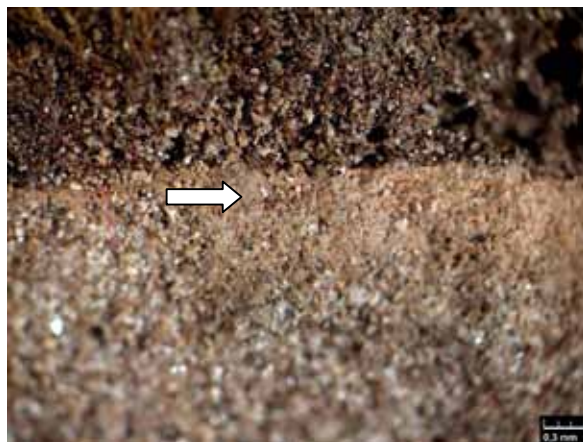
**Image 2:** Detail of Sample 1: The small, non-vascular Bryopsida appears to be *Gyroweisia* sp. (LM, ca. 40x)



**Image 3:** Overview of the Sample: In this photo, the different layers of humus and the original layer of sandstone are visible (LM, approx. 11x)



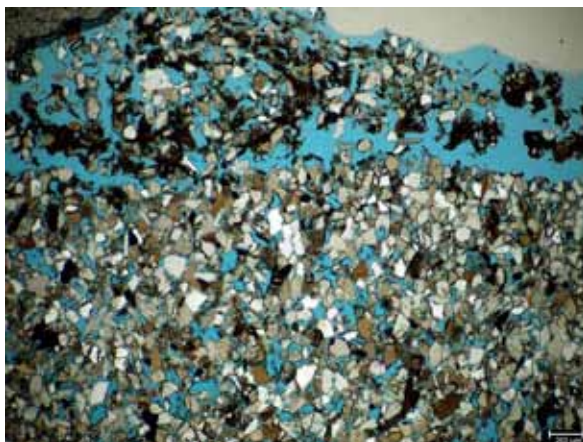
**Image 4:** Detail: Under the moss, a layer of humus about 1 mm thick has built up and is easily removed from the outer layer of the stone (LM, approx. 20x)



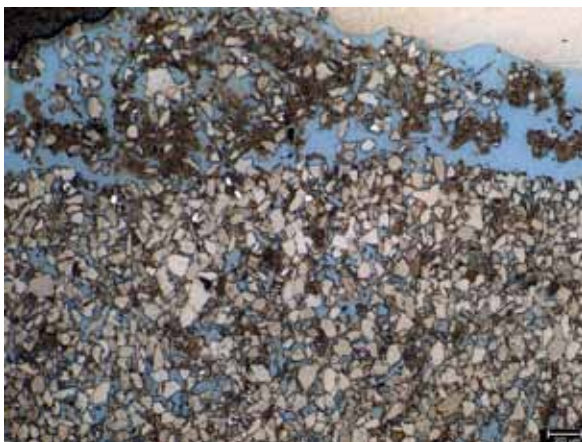
**Image 5:** Detail: The biogenic area seems to be more grainy than the stone that lies underneath it (LM, approx. 40x)



**Image 6:** Detail: Moss rhizoids (red brown) have completely grown through the layer of humus (LM, approx. 50 x)

**PHOTO DOCUMENTATION Sample 1**

**Image 7:** Thin Section/Cross Section: Moss rhizoids under the layer of humus mixed with particles from the outermost layer of stone (LM/POL, approx. 50x)

**PHOTO DOCUMENTATION Sample 1**

**Image 8:** Thin Section/Cross Section: In unpolarized light, the dark-colored amorphous biogenic components in the stone matrix stand in contrast to the light-colored layer of particles in the sandstone (LM, approx. 50x)

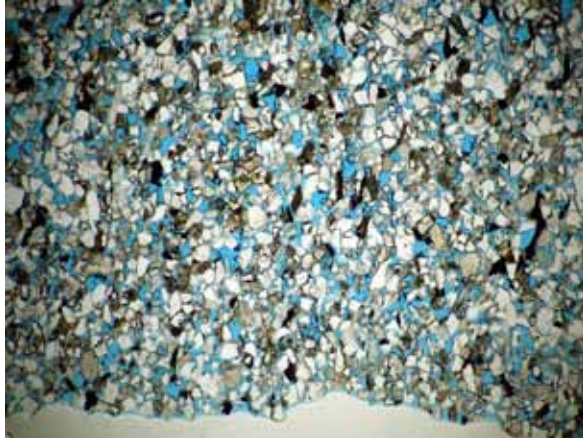


**Image 9:** Thin Section/Cross Section: In the lower portion of the 7-mm-thick cross section, a similarly-sized moss rhizoid growth is present and the biogenic component is recognizable (LM/POL approx. 50x)

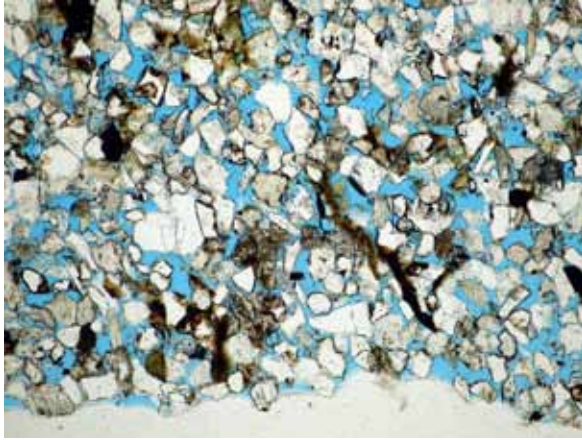


**Image 10:** Thin Section/Cross Section: Moss rhizoids and additional biogenic material that has been stored in the porous stone matrix are recognizable (LM/POL approx. 100x).

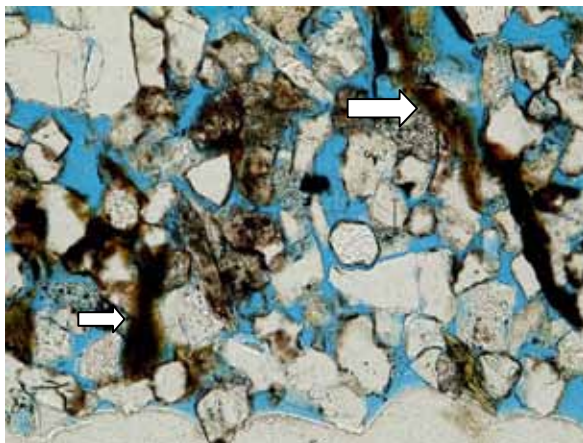


**Image 11:** Thin Section/Cross Section: In the detail, lower portion: dark brown moss rhizoids (arrow) grow up to 7 mm through the stone matrix (LM/POL approx. 200x)

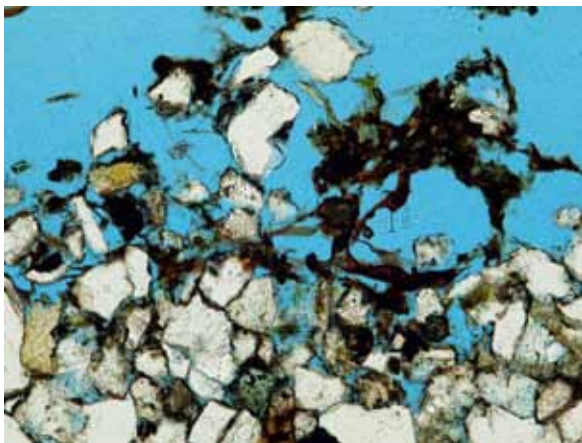


**Image 12:** Thin Section/Cross Section: In the detail above section: moss rhizoids are growing through the porous sandstone (LM/POL approx. 200x)

**PHOTO DOCUMENTATION Sample 2**

**Image 1:** Overview of Sample 2: Sandstone with moss, whose green wide thalli are curling up because of dry local conditions (LM, approx. 11x)

**PHOTO DOCUMENTATION Sample 2**

**Image 2:** Overview of Sample 2: In some spots, there are traces of a previously existing moss colony. Here is the dead stem with small pieces of a Bryopsida (LM, approx. 11x)



**Image 3:** In the cross section The light Marchantiophyta rhizoids, which are one-celled and more delicate than the dark brown rhizoids of the previously existing moss colony (LM, approx. 20x)



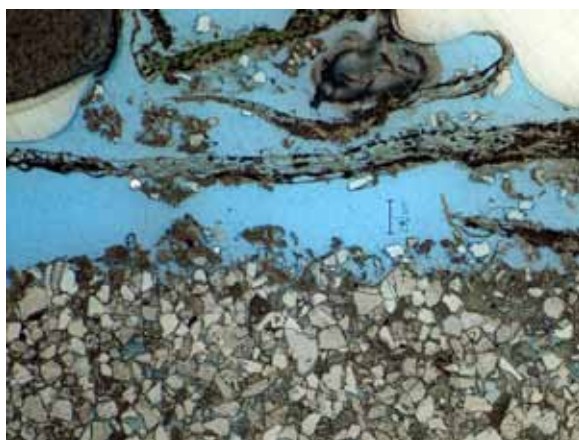
**Image 4:** Overview of the outer layer of stone after removal of the moss growth, with the light rhizoids of the Marchantiophyta and the dark brown rhizoids of the Bryopsida (LM, approx. 40x)



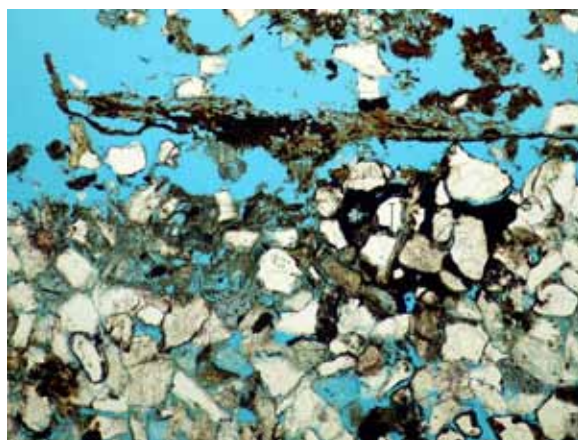
**Image 5:** Cross section of Sample 2: In this probe, it is remarkable that there is a barely noticeable or missing biogenic layer (LM, approx. 11x)



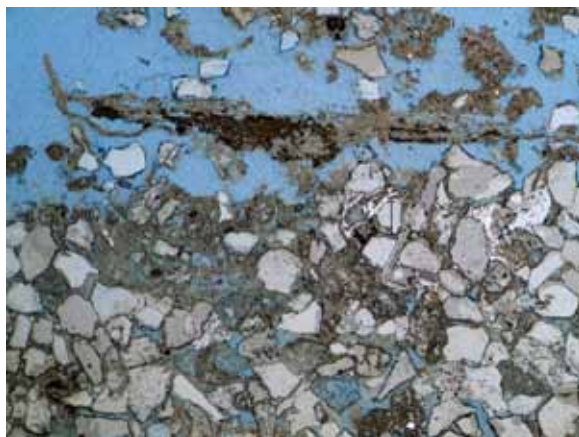
**Image 6:** Cross Section of Sample 2: In the layer of humus, pieces of higher-order plants can be found, just as in layers where germination can occur (LM, approx. 32x)

**PHOTO DOCUMENTATION Sample 2**

**Image 7:** Thin Section/Cross Section: The wide Marchantiophyta thallus has become separated from the stone (LM, approx. 50x)

**PHOTO DOCUMENTATION Sample 2**

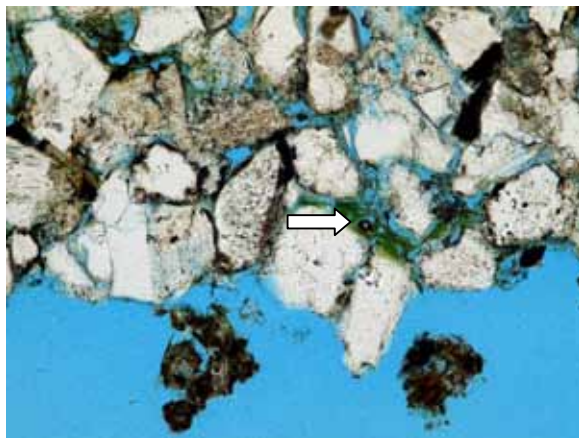
**Image 8:** Thin Section/Cross Section: In the detail, the "holes" filled with biogenic material are visible (LM/POL, approx. 100x)



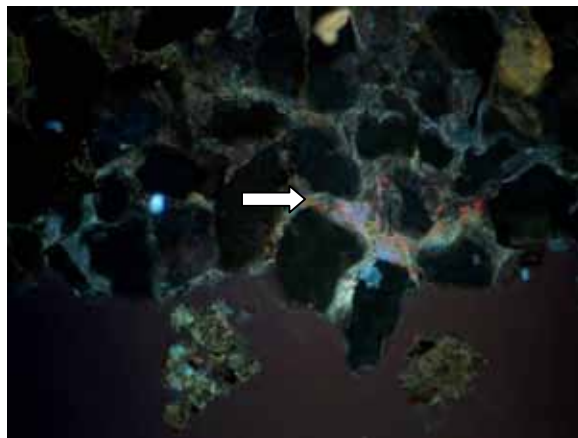
**Image 9:** Thin Section/Cross Section: In unpolarized light, the dark-colored amorphous biogenic components of the stone matrix are seen in contrast to the light-colored stone particles (LM, approx. 100x)



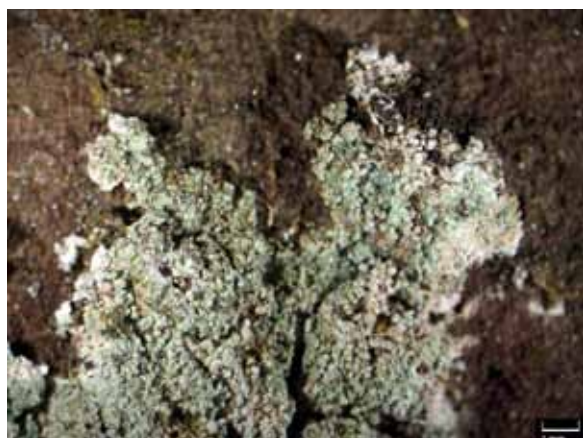
**Image 10:** Thin Section/Cross Section: Here in detail, the structure of the rhizoids and the amorphous material of dead biomasses, with its own microbial colony and stored metabolic processes, can be distinguished from each other (LM/POL, approx. 100x)



**Image 11:** Thin Section/Cross Section: In the lower area of the 13-mm-wide stone cross section, biomasses are also recognizable in the pores



**Image 12:** Analog Image 11 under UV light: there are algae that fluoresce red in this layer of stone (LM/UV, approx. 500x)

**PHOTO DOCUMENTATION Sample 3**

**Image 01:** Overview of Sample 3: Sandstone with the lichen *Lepraria* spec., whose name already hints at its “leprous,” powdery form (LM, approx. 11x)



**Image 03:** Detail: The lichen *Lepraria* spec. has a relatively simple construction. Cotton-like particles break down the thallus into fine particles (LM, ca. 64x)



**Image 05:** Overview of Sample 3: On the outermost layer of the stone, rhizoids from a previous moss growth are visible (LM, approx. 32x)

**PHOTO DOCUMENTATION Sample 3**

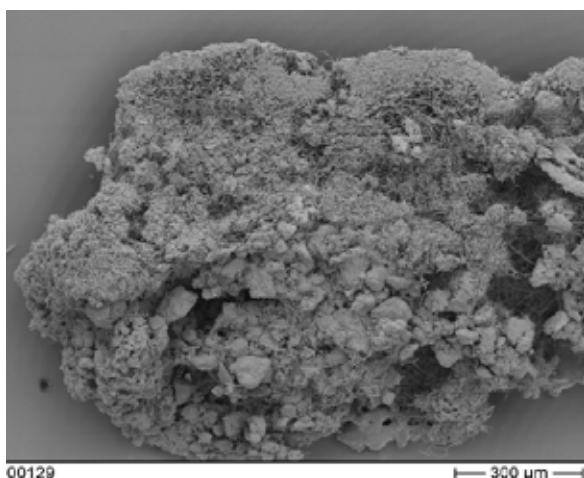
**Image 02:** Detail: *Lepraria* spec. can establish itself on a bryopsida. The lichen growth has almost completely pushed back the moss. In addition, the green, algae-rich area is present in the outer area of the lichen thallus (LM, approx. 20x)



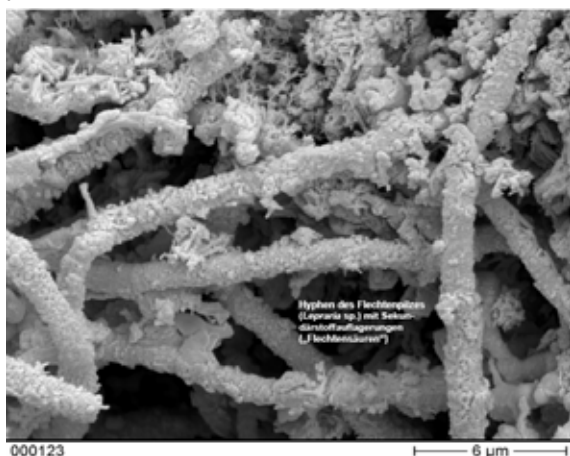
**Image 04:** Detail: Green algae is imbedded into the small pieces which make up the white fungus mycelium (LM, approx. 144x)



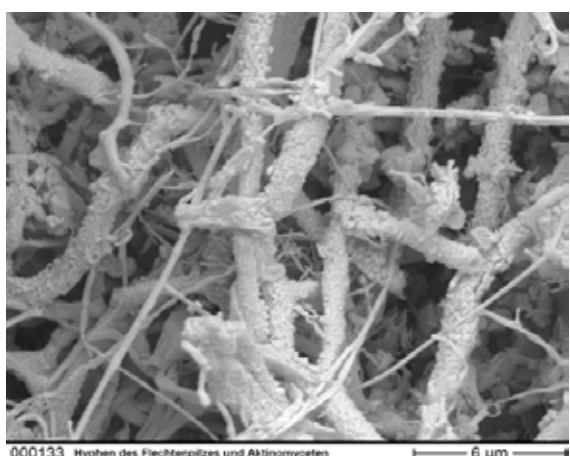
**Image 06:** Overview of Sample 3: There are also moss protonemata next to the rhizoids (LM, approx. 40x)

**PHOTO DOCUMENTATION Sample 3<sup>a</sup>**

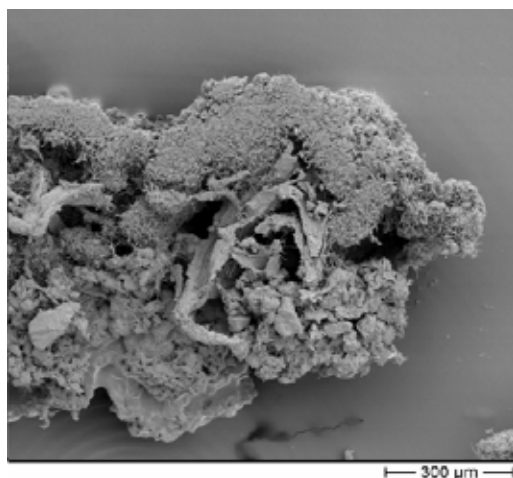
**Image 13:** Cross Section of Probe 3 with lichen thallus over the moss growth, into which pieces of humus and stone have been baked in



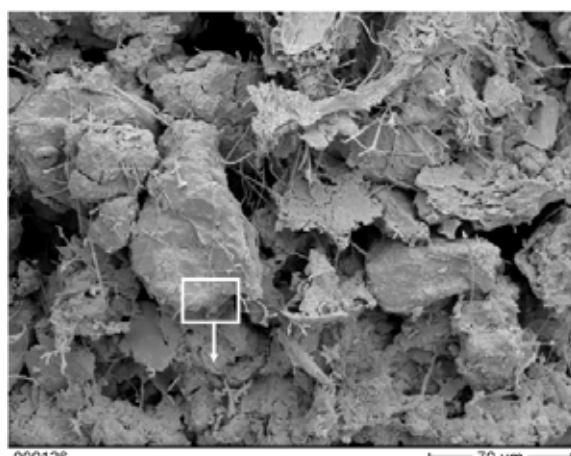
**Image 15:** Detail: Hyphae of the lichen *Lepraria* spec., with residue from secondary material



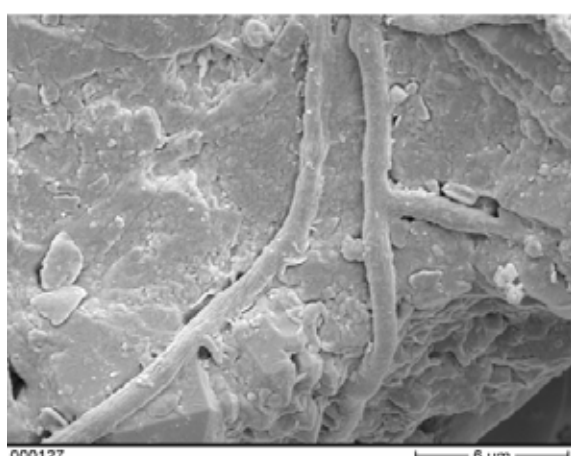
**Image 17:** Detail from Image 13: A thick webbing made up of other mold mycelium and actinomycetaceae has built up on the lichen mycelium

**PHOTO DOCUMENTATION Sample 3**

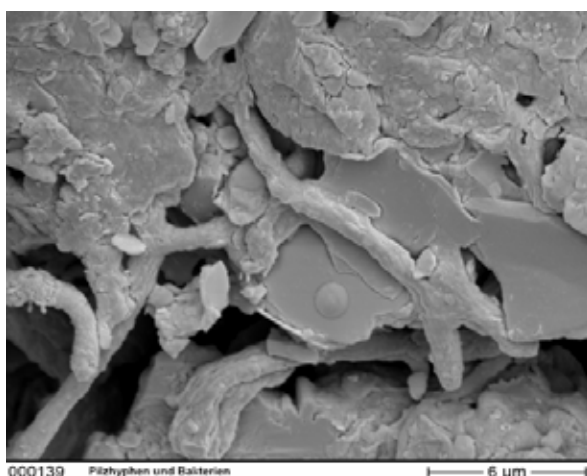
**Image 14:** Cross Section of Sample 3: Continuation of Image 13



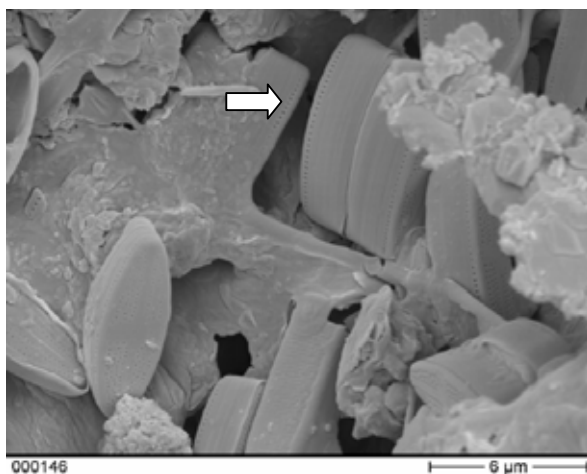
**Image 16:** Detail from Image 13: A matrix that has grown from the mycelium out of pieces of stone and humus



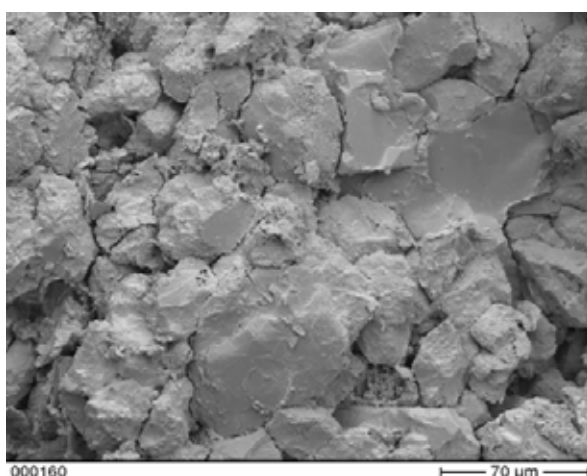
**Image 18:** Detail from Image 16: The lichen neutralizes acids, such as chalk particles that have become cauterized in the stone matrix

**PHOTO DOCUMENTATION Sample 3**

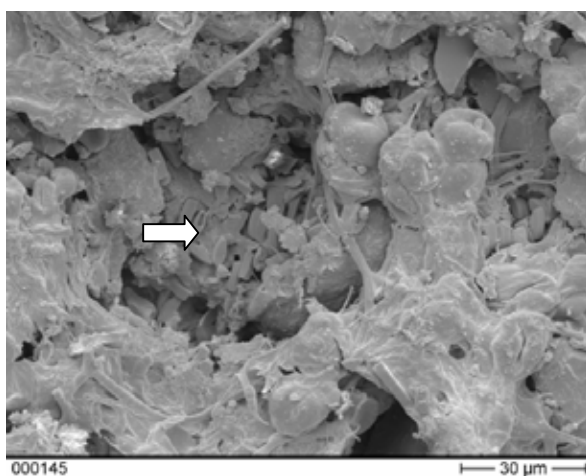
**Image 19:** Detail: The lichen fungus is infested with bacteria



**Image 21:** Detail of Image 20 with diatoms



**Image 23:** Cross Section of Sample 3 in the intact stone structure

**PHOTO DOCUMENTATION Sample 3**

**Image 20:** Detail: In addition, diatoms have been imbedded in the biogenic covering

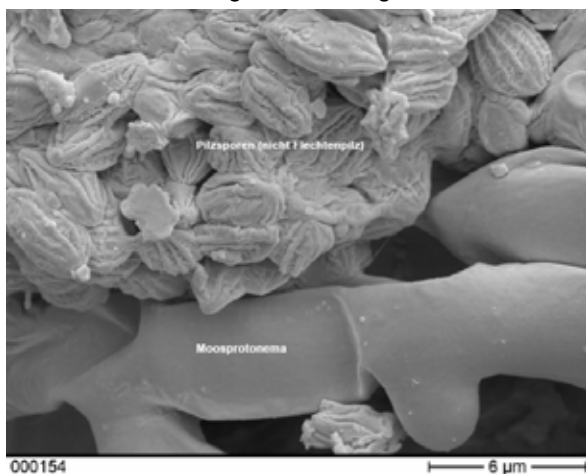


**Image 22:** Detail. Moss protonemata and mold spores that are not from the lichen mycobiont

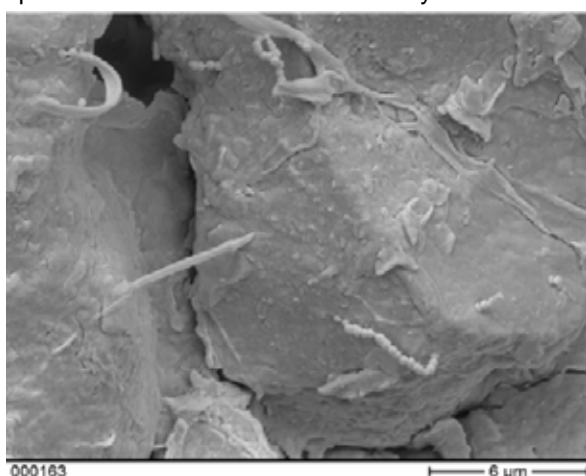


**Image 24:** Detail of Image 23: In the intact stone there are fungus hyphae, bacteria, and actinomycetaceae as well, but in fewer quantities



## **Garden maintenance- and Landscape management plan**





**Fig. 1:** Situation in the 1980's, begin of the reforestation

## Garden maintenance- and Landscape management plan

**Zhang Jinfeng, Mathias Kocher, Melanie Eibl, Felix Horn**

One significant damaging factor concerning the stone of the grottoes of Yuanjuedong is the vegetation. Vegetation in this context refers to plant life like trees, bushes, ferns and moss, but also the colonization of the stone surface through microorganism.

### Actual situation

#### *Tree Population*

According to the image (fig. 1), at the beginning of reforestation in the 1980's, there were comparatively few trees. There are two possibilities: there were always only a few trees before 1980's, or there were a lot of trees before 1960's, because there exists a period to cut down wildly tree in 1960's in the Chinese history and the grottoes usually were built in the mountains with lush trees in ancient China, which is related closely to the Buddhism doctrine, if it is suitable to trees. There is no document to verify which possibility is reality. During reforestation steps in the 1960's and 1980's the population of trees was raised enormously. This dense vegetation causes shadow, which – in combination with the high relative humidity – leads to an increased growth of

moss, ferns and microorganisms. Furthermore the trees have developed a deep entering system of roots, which destroys the stone substance.

Moss and ferns, which are covering the grottoes in part flat, are able to store humidity. This leads to a permanent raise of the stone moisture onto and within the covered area, with the long term consequence of a considerable structural damage of the stone.



**Fig. 2:** Today's situation, peak of hill Yunju

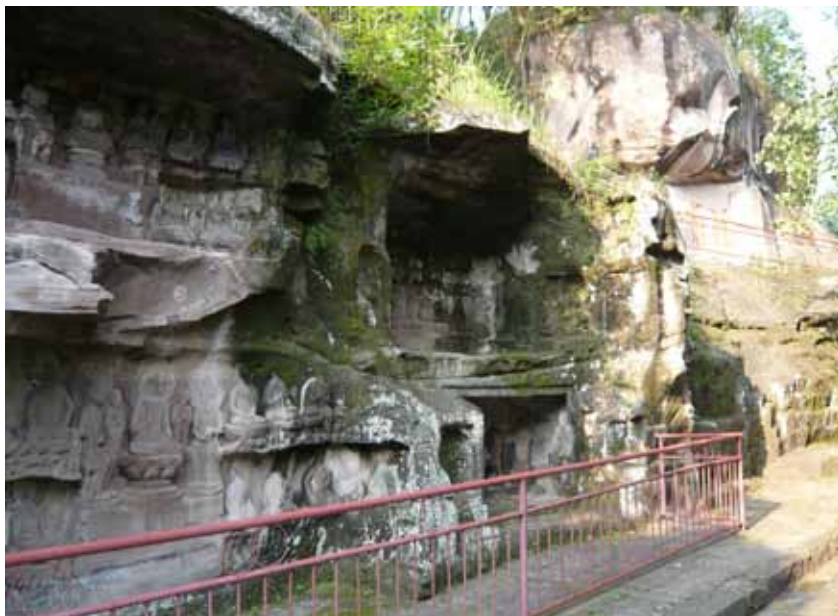


**Fig. 3:** Lush natural cover of moss, predominant at the south side of the grottoes no. 35–40



**Fig. 4:** Scaling as a reason of permanent moisture penetration



**Fig. 5:** Example of discoloured surface areas as a reason of biological colonisation, grotto no. 10, upper left hand side corner

### *Microfauna, Microflora*

Because of the climatic and therefore optimum growth conditions, the grottoes are colonized by a rich microflora. Biofilm-building took place onto the stone surface and a biofilm supports intensively the growth of complex communities of different microorganisms, like fungi, bacteria or lichen. On the other hand biofilms possesses a great capacity to store humidity, which causes problems comparable to that of moss growth. Moreover the secreted by-products of microorganisms metabolic activities are also an important damaging factor.

Some stone surfaces had been darkened because of the presence of the microflora, which can probably cause problems, if the stone is exposed to direct radiation of the sun. By the solar radiation the darker fields warmed up faster than the surrounding undyed stone surface, resulting in tensions within the stone matrix which leads consequently to a crack formation.

## **Package of measures**

### *Tree population*

The specific cut down of the plant life is urgently necessary. The botanic definition of the vegetation would be a support concerning the criteria because of which trees are to be chosen for cutting down. In case of existing botanic definition through a botanist

within the scope of creating the protection plan for the grottoes of absolute enlightenment, it would be useful to supplement the protection plan with the Latin botanic terms of the plant species.

Along the paths the cut-down of trees could be carried out without hesitation. But in the direct surroundings of the grottoes the cutting of the trees should be performed gently because of the fact that the existing trees are protecting the grottoes against the sun radiation. In this context it would be useful to guarantee the shadow for the grottoes until measures against the microorganisms are carried out.

Contrary to that, it is necessary to remove moss, ferns and sprouts, which are growing onto the stone of the grottoes within a radius of about one meter. The therefore required measures, like mechanic and/or chemo-physical methods should be performed exemplary on one selected grotto.

### *Microfauna, Microflora*

As to decide which steps are the most effective and safe to remove microorganisms, the existing microflora should be determined. The characterization of the microflora could be performed with non destructive-techniques like batch-sampling, ATP-measurement and microscopically analyses. Corresponding to the results of microbial investigation, the next step would be to create concrete strategies against growth and damage through the microbiological impact.



## **Die Kunst der Grotte Nr. 10 in der Grottenanlage Yuanjue**



# Die Kunst der Grotte Nr. 10 in der Grottenanlage Yuanjue

Lin Chunmei

Die vom 8. bis zum 12. Jahrhundert gefertigte Grottenanlage Yuanjue liegt auf dem Hügel Yunju, etwa zwei Kilometer östlich der Kreisstadt Anyue in der Provinz Sichuan, China.

Es gibt dort 103 Grotten mit insgesamt 1933 Figuren<sup>1</sup>, die teils vollplastisch oder in Hochrelief gearbeitet sind. Die dargestellten Figuren präsentieren sich mit folgenden Themen: Buddhas in drei Generationen; Sieben Buddhas; Reines Land im Westen; Der Nördliche Himmelskönig Bishamen-tian; 16 Arhats; Kshitigarbha (Dizang) mit zehn unterirdischen Richtern; Avalokiteshvara; Ava-lokiteshvara mit Tausenden Händen und Augen; Buddha Shakyamuni beim Halten einer Blume und Daoistische Gottheiten u.a.

Vor allem die Darstellung des Buddha Shakyamuni beim Halten einer Blume ist ein völlig neues Thema, das die zeitliche Entwicklung des buddhistischen Glaubens widerspiegelt und auch Einfluss in der Umgebung des Kreis Anyue ausübt<sup>2</sup>. Gerade die Grotte dieses Buddha Shakyamuni ist durch eindringendes Wasser gefährdet. Die Begleitfigur des Shakyamuni und das Stifterehepaar darin leiden unter der Verwitterung – so sind die beiden Stifter nur durch ihre Haltung und noch vorhandene Gewandpartien zu identifizieren.

Die Grotte Nr. 10 (Abb. 1) wurde deswegen zur Konservierungsforschung ausgewählt. Im Folgenden wird diese Grotte beschrieben und die Ikonographie der dargestellten Figuren und ihr Stil vorgestellt.

## Beschreibung der Grotte Nr. 10

Die Grotte ist 6,40 Meter hoch, 4 Meter breit und 3 Meter tief. Der nach rechts blickende Buddha steht aufrecht in der Mitte. Neben dem Buddha befinden sich seine Begleitpersonen: unten in der Grotte links ist ein Mönch dargestellt, den Kopf zum Buddha erhoben.

Rechts findet sich das Ehepaar, das den Grottenbau gestiftet hat. Oben, in Gesichtshöhe des Buddha, ist je ein himmlisches Wesen dargestellt. Hinter dem Buddha ist die Rückwand mit Aureolen und Blumen geschmückt.

Abb. 1: Der Buddha Shakyamuni in Grotte Nr. 10

## *Der Buddha Shakyamuni und sein Schüler Mahakasyapa*

Der sechs Meter hohe Buddha wendet sich mit lächelndem Gesicht nach rechts, seine rechte Schulter ein wenig in die gleiche Richtung neigend. Der frontale Betrachter blickt auf ein Zweidrittel-Profil des kantigen Gesichts. Buddha hält seine Arme vor der Brust: Seine rechte Hand mit der Geste des Lehrens streckt sich nach oben und hält dabei eine Blume mit dem Daumen. Seine linke Hand ruht horizontal mit der Handfläche nach oben. Über dem linken Unterarm hängt ein Zipfel des Obergewandes (jiasha). Besonders bemerkenswert ist das nicht frontal dargestellte Gesicht. Die Gewandfalten kennzeichnen sich dadurch, dass die Falten der über den Arm fallenden langen breiten Öffnungen der Ärmelpartien in Dreiecksform fast parallel drapiert sind.





**Abb. 2:** Kasyapa in der Grotte Nr. 10

Die teils verwitterte Figur im Mönchsgewand unten links in der Grotte richtet den Blick nach oben zum Buddha und legt die Hände anbetend zusammen. Trotz der Verwitterung des Kopfteils sind die bis auf die Wangen fallenden langen Augenbrauen und die Falten um die Mundpartie noch zu erkennen – die Figur ist als Kasyapa (Abb. 2) zu interpretieren.

Kasyapa ist einer der zehn berühmten Schüler des Buddha Shakyamuni und wird oftmals als ältere und erfahrungsreiche Gestalt zusammen mit einem anderen Schüler, Ananda d.J., als Vertreter der Schüler des historischen Buddhas dargestellt. Nach Buddhas Eingehen ins Nirwana hatte er 500 Arhats gesammelt und die Reden des Buddha in Form der Sutren dokumentiert.

Der historische Buddha war der Prinz Siddharta Gautama. Er wird von den chinesischen Buddhisten Buddha Shakya oder Shakyamuni („Einsiedler der Shakya“) genannt. Er lebte etwa im 6. bis 5. Jahrhundert v. Chr. in Nordindien. Sein Vater war das Oberhaupt der Adelsfamilie der Shakya. Nach Erlangung der Erleuchtung begann er alle Menschen an seiner Lehre teilhaben zu lassen. Er predigte, wie man durch rechtes Wissen vom leidvollen Leben und durch rechtes Tun, die Sinnesreize zügeln kann, um den Weg zur Aufhebung des Leidens zu erlangen und zur Ruhe zu kommen.

Buddha Shakyamuni beim Halten einer Blume und der zum Buddha blickende Kasyapa lässt erkennen, dass es sich bei dieser Darstellung um das Lehren durch das Halten einer Blume handelt:

Als Buddha Shakyamuni vor einer großen Schülerschar auf dem Geierberg lehrte, hielt er dabei schweigend eine Blume, um seine Lehre, den Dharma, darzustellen. Während alle anderen Schüler nicht begriffen, was er damit aussagen wollte, verstand ihn nur sein Schüler Kasyapa und lächelte.

Daraufhin sagte der Buddha: *Ich habe den Augen-Schatz des wahren Dharma, das wunderbare Nirvana-Bewusstsein, die wahre Form der Nicht-Form, das geheimnisvolle Tor des Dharma. Kashyapa, Du wirst betraut, diese Lehre weiter zu verbreiten und nicht unterbrechen zu lassen.*

Kasyapa, der auf dieser Weise durch den Buddha den Namen Mahakasyapa erhalten hatte, wurde so der erste Patriarch in der indischen Übertragungslinie des Chan, das lautlich aus dem Sanskrit Dhyana stammt und bezeichnet in der indischen Yoga-Philosophie die höheren Bewusstseinszustände der Meditation oder der Versenkung.

#### *Fliegende himmlische Wesen, Gandharva und Kinnara*

Oben an beiden Grottenwänden fliegt je eine Figur, eine Blumenschale haltend, auf Wolken nach innen. Diese fliegenden Wesen tragen einen mit einer kleinen Blumenkrone geschmückten Dutt. Der Oberkörper ist nackt, der Unterkörper in einen langen Rock gewickelt. An der Taille ist ein Schutzteil mit einem Gürtel in zwei Stufen umgeschlagen und darauf noch ein kurzes Schmuckstück unter dem Gürtelband verziert. Ein Rockteil flattert zwischen den Beinen nach oben wie das himmlische Gewand, das, durch ein langes Band verkörpert, sich hinter dem Kopf und unter den Armen in zwei Teilen nach oben schlängelt. Die volutenförmig abstrahierten Wolken reihen sich aneinander wie eine Hängematte (Abb. 3) zum Halt der fliegenden Wesen. Zu Beginn der Christianisierung erscheinen solche „wehenden Wolken“ häufig – als Symbol für einen Glückwunsch – mit dem Drachenmotiv. All-



**Abb. 3:** Das himmlische Wesen an der linken Wand von Grotte Nr. 10

mäßig begleiten diese Wolken die buddhistischen himmlischen Figuren beim Fliegen. Sie stellen sich im 6. Jahrhundert in einer länglichen Form dar und später, ab dem 7. bis zum 9. Jahrhundert, in bunt bemalter Schneckenform.

Das fliegende Wesen an der linken Grottenwand hält mit zwei Händen eine Schale mit Blumen, während das himmlische Wesen an der Gegenwand (Abb. 4) mit jeder Hand je eine Schale mit einem vollerblühten Lotus und eine Lotusknospe trägt.

Fliegende himmlische Wesen, Gandharva und Kinnara, sind himmlische Musiker und Beschützer der buddhistischen Lehre, um einerseits die Götter und Göttinnen zu unterhalten und andererseits die buddhistische Lehre zu schützen. Im Buddhismus spielen sie meist nur eine untergeordnete Rolle. Wo Buddha erscheint, tanzen sie am Himmel und streuen frische Blumen. Beschützend dienen sie dem Buddha mit Musik, Tanz, frischen Blumen und Essen. Sie leben im Bereich der Götter (Devas), einer glücklichen Sphäre, sind aber noch – genauso wie Menschen und andere Lebewesen – dem Kreis-



**Abb. 5:** Ehepaar, Stifter der Grotte Nr. 10



**Abb. 4:** Das himmlische Wesen an der rechten Wand der Grotte Nr. 10

lauf des Geborenwerdens, Alterns und Sterbens unterworfen.

Links und rechts oben an der Rückwand, wo sich die Aureolen des Buddha Shakyamuni befinden, sind je drei oder vier Blüten zu sehen, die von den beiden fliegenden Wesen verehrend zum Lehren des Buddha unterzustreuen sind. Diese beiden Darstellungen im Hintergrund des Buddha bekräftigen den Akt des Belehrens.

#### *Stifter*

Die zwei stark verwitterten Figuren (Abb. 5) unten vor der rechten Grottenwand sind von Handhaltung und Gewandung als Stifter und Stifterin zu identifizieren. An der Figur innen sind noch die Ärmel und der untere Teil des Gewandes zu erkennen.

Da der rechte Ärmel ein wenig höher liegt, könnte es sein, dass ehemals ein Räuchergerät vorhanden war, das völlig verwittert ist. Der Seitenschlitz mit den angedeuteten Falten rechts am Unterteil des Gewandes belegt einen Männerkaftan.

Die Figur außen lässt sich von Handhaltung und Faltenrock als weibliche Figur identifizieren. Zwischen ihren Händen ist noch eine kleine dreieckige Decke für die Opfergabe zu erkennen. Ein gutes Vergleichsbeispiel liefert das Ehepaar in der Grotte Nr. 14 (Abb. 6). Hier trägt die weibliche Figur ein langes Tuch für die Opferschale.



**Abb. 6:**  
Ehepaar,  
Stifter der  
Grotte Nr. 14

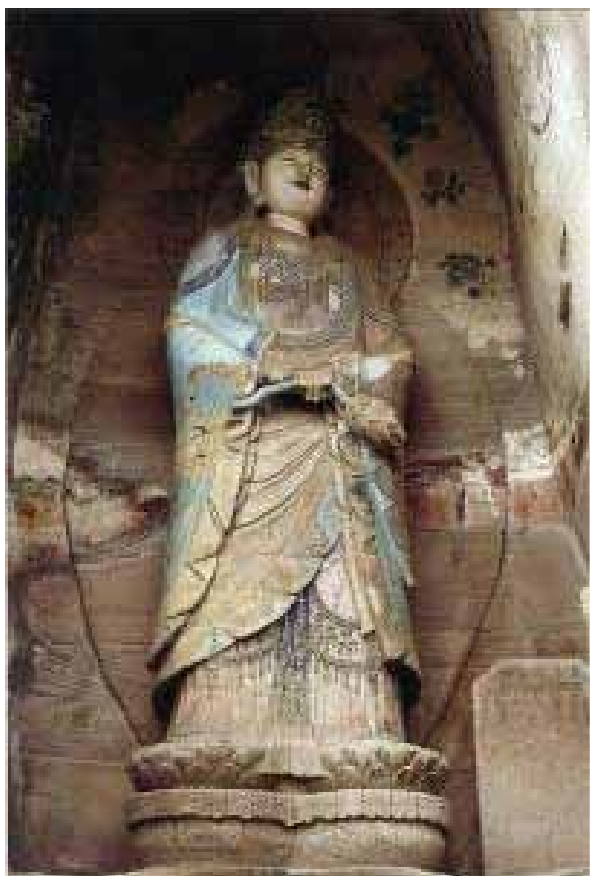


**Abb. 7:** Der Bodhisattva Avalokiteshvara in Grotte Nr. 14

In der Grottenanlage Yuanjue finden sich noch zwei Grotten in ähnlicher Größe. In beiden ist je ein Bodhisattva Avalokiteshvara dargestellt: Der eine hält seine Hände gekreuzt vor dem Bauch. Ein Lotusknospenzweig (Abb. 7) wird in der rechten Hand gehalten, mit der Knospe nach unten. Dieser Avalokiteshvara ist stilistisch noch deutlich der Zeit der Fünf Dynastien (907–960) verhaftet: voll gerundetes Gesicht, dekorative Darstellung der Wolken in Voluten- oder Wirbelform, eng an den Körper gelegte Gewandung, Lotussockel mit geometrischem Blumenblatt. Die von himmlischen Wesen verstreuten Blumen ähneln sehr denen in der Grotte Nr. 10. Die Grotte Nr. 14 ist durch die Inschrift der Stifter auf 1108 datiert.

Der andere Bodhisattva Avalokiteshvara (Abb. 8), mit einem kurzen Weidenzweig in der rechten Hand und mit einer Wasserflasche in der Linken, gehört zu der in das Jahr 1153 datierten Grotte Nr. 7. Im Vergleich mit dem Buddha Shakyamuni und dem Avalokiteshvara mit der Lotusknospe ist die Faltendarstellung des oberen Gewandes wesentlich schlichter aufgelockert. Zum Beispiel sind an der über die Hand mit der Vase herunterhängenden Ärmelpartien drei Schichten zu erkennen. Unten neben dem Handgelenk ist eine gerade Linie, die äußere daneben läuft in drei Falten und oben, nah

zum Ellbogen in zwei, während die Ärmelpartien des Buddha Shakyamuni und des Bodhisattva von Grotte Nr. 14 mit mehr Falten und schärferen Konturen dargestellt sind: die Faltenanzahl bei den Ärmelpartien des Buddha ist geringer als bei den des Avalokiteshvara mit der Knospe. Auch wird die Gestaltung des Flammenmotivs auf der Aureole bzw. des Wolkenmotivs in der Zeit immer abwechslungsreicher. Die Flammen in Grotte Nr. 7 zum Beispiel sind aus zwei bis vier einzelnen Haarnadel-Formen mit unregelmäßigen, breitgerundeten Nadelkurven gruppiert. Die früheren Darstellungen haften noch deutlich dem Stil der Flammendarstellung seit den Fünf Dynastien (907–960) an: Sie präsentieren sich vereinzelt nebeneinander auf der Randpartien der Aureole. Die Flammendarstellung in der Grotte Nr. 10 neigt zur Auflockerung, indem ihre Haarnadelstäbchen kurviger eingeritzt und ihre Länge nicht gleich sind.

Aus den genannten Vergleichspunkten lässt sich sagen, dass die Grotte Nr. 10 zwischen den beiden Grotten für die Avalokiteshvara erstellt wurde, also zwischen 1108 und 1153.

### Vergleichsbeispiele

Interessanterweise gibt es in der Nähe der Kreisstadt Anyue noch zwei Buddhas in ähnlicher Haltung: Der eine liegt in dem Dorf Yunguang des Bezirks Gaosheng in Kreis Anyue und ist durch eine Inschrift auf das Jahr 1193 datiert. Der andere liegt in dem Dorf Luohan des Bezirks Gutian (Abb. 9) in dem Nachbarkreis Zizong und ist ebenfalls



**Abb. 8:** Der Bodhisattva Avalokiteshvara in Grotte Nr. 7

durch Inschriften der Besucher in die Ära Zhenghe (1111–1118) datiert. Im Folgenden wird die Grotte in Zizong zur genaueren Datierung der Grotte Nr. 10 in Yuanjue stilistisch analysiert.

#### *Die Grotte Nr. 2 im Dorf Luohan des Bezirks Gutian-Zizong*

Die Konstruktion der Grotte Nr. 2 im Dorf Luohan ähnelt zwar der in der Grotte Nr. 10 der Grottenanlage Yuanjue in Anyue, Abweichungen sind jedoch zu erkennen:

- Kasyapa steht nicht rechts vom Buddha. Der Buddha wendet seinen Blick über seine linke Schulter zum Kasyapa.
- Die Anzahl der kurvigen Falten des Obergewandes sind geringer, aber im Vergleich zu Grotte Nr. 7 in der Grottenanlage Yuanjue ist die gerade Linie unter der Öffnung der linken Ärmelpartie noch mit zwei kleinen Kurven geziert.
- Der Stil der Ziermotive ist aufgelockerter: Die von himmlischen Wesen gestreuten Blumen verteilen sich nicht mehr symmetrisch, sie finden sich sogar an der Wand Shakypa gegenüber und sind naturhafter dargestellt.

Die genannten stilistischen Analyse belegen, dass die Grotte Nr. 10 mit den Figuren in der Grottenanlage Yuanjue früher als die Grotte Nr. 2 (zwischen 1111–1118) im Dorf Luohan gefertigt worden ist.

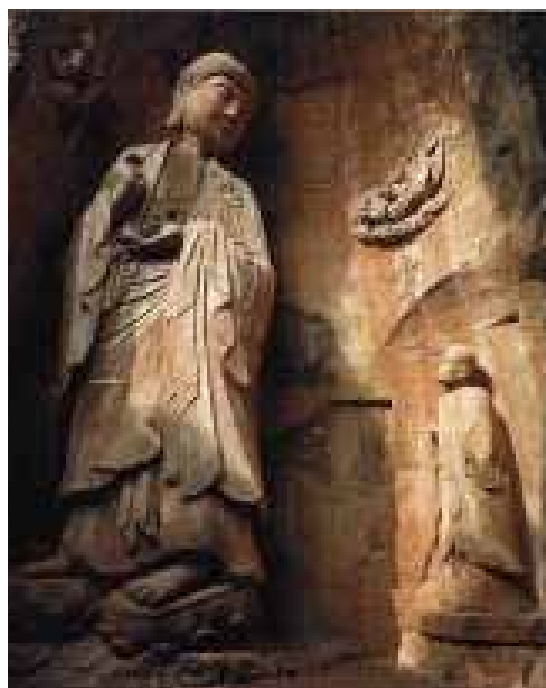


**Abb. 9:** Buddha Shakyamuni und Kasyapa im Kreis Zizong

#### Schlussfolgerung

Die Entwicklung der Chan-Buddhismus in der Nördlichen Song-Dynastie liefert auch die Datierungsmöglichkeit für Grotte Nr. 10. Vorab musste die Entstehung der Geschichte über Buddhas Lehre durch das Halten der Blume geprüft werden.

Nach den buddhistischen Meistern<sup>3</sup> beginnt diese Geschichte erst in der Nördlichen Song-Dynastie (960–1127). Meister Yinshun<sup>4</sup> weist darauf hin, dass der große Chan-Meister Qi Song (1007–1072) in seinem zwischen 1049 und 1053 verfassten Buch *Authentische Biographien der Chan-Meister* die Authentizität dieser Geschichte in Frage gestellt habe. Nach dieser Untersuchung fällt die früheste Erzählung dieser Geschichte in das erste Jahr der Ära Tiansheng (1023) und wird geschildert in dem Werk<sup>5</sup> der *Erweiterten Biographien der Chan-Meister*.

Dass diese zu Beginn des 11. Jahrhunderts beliebten Geschichten nach knapp hundert Jahren in der ersten Hälfte des 12. Jahrhunderts in Anyue als szenische Darstellung in den Felsen geschlagen wurden, hängt wahrscheinlich mit dem berühmten Chan-Meister Yuanwu Keqin (圜悟克勤, 1063–1135)<sup>6</sup> zusammen, der aus dem Kreis Pixian, nordwestlich der Stadt Chengdu in Sichuan stammte, und etwa ab dem Jahr 1104 als Oberbonze am Tempel Zhaojue und dem Tempel Baoguang der Stadt Chengdu tätig war. Im ersten Jahr der Ära Zhenghe (1111–1118) dankte er von dieser Tätigkeit ab und fuhr nach der Provinz Hunan. Er traf in Jiangling den Kanzler Zhang Shangying (1043–1121), der ihn als Chan-Meister hoch verehrte und ihm die Position des Abtes am Kloster Lingquan im Kreis Lixian anbot. Dort begann Yuanwu Keqin die knappen Dialoge der früheren berühmten Chan-Meister zu interpretieren und erhielt vom Kaiser Huizong die Auszeichnung Chan-Meister „Buddhafrucht“ und ein purpurnes Gewand geschenkt. Zwischen 1119 und 1125 wurde er vom Kaiser zum Oberbonzen des Tempels Tianning in der Hauptstadt Kaifeng berufen. Wegen des Krieges kehrte er danach wieder in die Stadt Chengdu zurück und blieb bis zu seinem Tod im Jahre 1135 im Tempel Zhaojue.

Aus dem Lebenslauf des berühmten Chan-Meisters Yuanwu Keqin kann man die Schlussfolgerung ziehen, dass die Bauzeit der Grotte Nr. 10 mit seiner Tätigkeit in Chengdu zu tun hat und vermutlich zwischen 1108 und 1111 entstanden ist. Um die Darstellung dieser Grotte zu interpretieren, ist die Entwicklung des Chan-Buddhismus von den Fünf Dynastien bis zur Nördlichen Song-Dynastie weiter zu untersuchen.

## Endnoten

1 Nach Liu Changjiu, S. 7; Hu Wenhe hat 1931 Figuren angegeben: S. 180.

2 In dem Bezirk Gaosheng des Kreises Anyue und in Dongyan des Kreises Zizong befindet sich je ein seitlich blickender Buddha Shakyamuni.

3 Meister Shengyan: Der Buddha hält eine Blume und der Kashyapa lächelt. Taibei: Fagushan Wenhua Shiye, 1999, S. 185–186.

4 <http://a112.com/0207/0-a2/b3.htm>: 拈華微笑 (Der Buddha hält eine Blume und der Kashyapa lächelt); 29.12.2007.

5 Erweiterte Biographien der Chan-Meister. Juan 2, Z135-612a1–3 (天聖廣燈錄卷第二), aus CBETA 電子佛典 V1.33 普及版.

6 Wei Daoru (魏道儒, 1990): Die Geschichte des Chan-Buddhismus in der Song-Dynastie (宋代禪宗史). Gaoxiong: Foguangshan Wenjiao, 2001, S. 88–118.

## Abbildungsnachweis

Nach Liu Changjiu: Zhongguo shiku quanji : Sichuan. Chongqing, Bd. 8, 2000: Abb. 4: Abb. 113; Abb. 7: Abb. 114; Abb. 8: Abb. 109; Abb. 9: Abb. 200

---

**Kunsthistorische und religionshistorische Grundlagen  
der Restaurierung buddhistischer Kulthöhlen in China**



# Arbeitsbericht 2008 des BMBF-Forschungsprojektes „Deutsch-chinesische Zusammenarbeit im Kulturgüterschutz“

Zhao, Zhou M.A.

Dem Arbeitsplan von 2007 nach (zugestimmt von dem Projektleiter Prof. Ledderose) sollte ich mich für 2008/09 unter anderen auf zwei Themen konzentrieren, nämlich

- die Bearbeitung des Grottenvorbaus sowie die historische Forschung und
- die kunsthistorische Forschung für die Kulthöhlen/-nischen in Sichuan mit dem Shuili Ritual als Schwerpunkt.

Für 2008 besteht der Schwerpunkt der Arbeit in der Bearbeitung des Grottenvorbaus sowie der historische Forschung, von denen die folgenden Vorhaben durchgeführt sind:

- Diskussionen und Gespräche mit dem beiden führenden japanischen Architekturhistorikern Prof. Tanaka Tan und Associate Professor Funayama Toru vom Institute for Research in Humanities, Kyoto University zum Thema „Schutzbauten“, bei den Veranstaltungen „Principle of Japanese Architecture“ und „Restaurierung der historischen Architektur in Japan“.
- Teilnahme am Workshop „Authenticity What? – Concepts of Authenticity in Architectural Heritage Preservation. An international Workshop of the Cluster of Excellence: Asia and Europe in a Global Context.“ mit dem Vortrag „The Construction of a Porch to the Cave no. 10 at Yuanjuedong in Anyue County.“ Dazu Meinungsaustausch mit den Professoren des Exzellenzclusterprojekts der Universität Heidelberg sowie weiteren europäischen Architekten und Denkmalpflegern in Europa.
- Organisation des Workshops „Before and Behind the Great Buddha“ an der Universität Heidelberg mit dem Vortrag „The Wooden Porch and the Shuili rite in Sichuan“. Beim Workshop waren Projektteilnehmer aus Beijing, Sichuan, Taiwan und München versammelt, es wurden Meinungen ausgetauscht und das Projekt diskutiert.

- Gemeinsame Feldforschung mit Kollegen der Technischen Universität München im Oktober. Untersuchung und Diskussion vor Ort mit den lokalen Denkmalpflegern, um die Fragestellungen der Form und des Stils für den Schutzbau zu beantworten. Untersuchung der Kultstätten mit hölzernen (Schutz-)Vorbauten aus der Qing-Zeit im Kreis Anyue, die für die Bearbeitung eines Schutzbau für die Grotte Nr. 10 beispielhaft sein können.
- Bericht über die historische Forschung der Grottenvorbauten in Sichuan sowie die Bearbeitung und Planung eines hölzernen Schutzbau für die Grotte Nr. 10 und eventuell eines 3-D-Models (in Arbeit).

Die kunsthistorische Forschung ist der Arbeitsschwerpunkt für das Jahr 2009, folgende Forschungen sind bereits im Jahr 2008 erfolgt:

- Übersetzung der Inschrift über ein im Jahr 1107 abgehaltenes *Shuili* Ritual aus der Grotte Nr. 13, Yuanjuedong; Erwerbung und Erforschung eines historischen Manuals für *Shuili* aus der Princeton University; Studie über das Verhältnis zwischen dem Wasser-und-Land-Ritual und der Ikonographie der Felsenskulpturen in Sichuan (in Vorbereitung).
- Vortrag: „The Three Teachings in the Rock Carvings“ beim Symposium „Buddhist Epigraphy in China, State of the Field and New Methodologies“ vom 3. bis 6. Juli 2008 in Heidelberg.
- Vortrag: „Gipfel der Schätze – Buddhistische Skulpturenkunst in Sichuan und Chongqing“ im Deutsch-Amerikanischen Institut Heidelberg, August 2007.
- Erforschung der relevanten, für die kunsthistorische Forschung der Region wichtigen historischen Kultstätten mit buddhistischen Skulpturen (Feldforschung in Zusammenarbeit mit den chinesischen Kollegen, Oktober 2008).

- Arbeit an der Dissertation „Three Teachings in the Rock Carvings of the Song Dynasty in Chongqing and Sichuan“, die sich mit der spezifischen Ikonographie der Felsenskulpturen beschäftigt (in Arbeit).

Im Herbst 2008 hat von chinesischer Seite der Kunsthistoriker Dr. Lei Yuhua die Verteilung und Arbeitsabfolge der Grotten und Nischen auf den Felswänden in Yuanjuedong untersucht, um diese zu datieren. Gemeinsam mit den deutschen Kollegen erfolgten an anderen Kultstätten des Kreises Anyue Feldforschungen, u. a. in Antangsi und Kunfosi, die gleichzeitig und kunsthistorisch relevant mit den Nischen in Yuanjuedong sind. Ein Untersuchungsbericht für Antangsi wurde verfasst.

## **Frontal Buildings and Niche No. 10 at Yuanjuedong in Anyue County**



# Frontal Buildings and Niche No. 10 at Yuanjuedong in Anyue County

Zhao, Zhou M.A.

Located about 2 kilometres southeast of the county town of Anyue County and distributed mainly on the north and south side of a hill called Yunjushan, the rock carvings at Yuanjudong ( $30^{\circ}05'21.50''\text{N}$   $105^{\circ}20'35.10''\text{E}$ ) are altogether 103 numbered niches and grottoes carved between the 8<sup>th</sup> and 12<sup>th</sup> century.<sup>1</sup>

Carving no. 10<sup>2</sup> is a large niche – 6.53 metres high and 3.64 metres wide – enshrining a standing Buddha of 5.64 metres height with assistant figures.<sup>3</sup> Finished in the years between 1108 and 1153, the standing Buddha Shakyamuni holding a flower in his hand and smiling at his disciple Kasyapa is iconologically related with Chinese Chan Buddhism.<sup>4</sup>

The niche is chosen as an example of protection, as the lower part of the Buddha statue is heavily weathered and it is commonly agreed by all the experts of the project that constructing a frontal building for the niche would be an effective measure for the protection of the statue. This article looks into the historical and present situation of the frontal buildings to Buddhist grottoes and niches in North China and the Sichuan region and thereupon makes a preliminary plan of the protective building for the niche no. 10, especially from a viewpoint of art history.

## Frontal Buildings of the Buddhist grottos and niches in North China and the Sichuan region

On the facades of the Buddhist grottoes in India the elements of wooden architectures were imitated in stone, which granted the grottoes in mountains an architectural appearance.<sup>5</sup> As Buddhism was introduced into China, the tradition of building grottoes was continued. Since in some places in Central Asia the sandy mountains were not suitable for carving, certain wooden structures were built as the facades of the grottoes. The earliest extant wooden frontal buildings of Buddhist grottoes in China were found in Dunhuang, with a total of five buildings dating from the 9<sup>th</sup> to the 11<sup>th</sup> century.<sup>6</sup>

Traditionally, the wooden constructions added to the Buddhist grottoes are called “roof of the grotto”, in Chinese *Kuyan* 窟檐, and they appear similar to the porches in European architecture.<sup>7</sup>

The archaeological research shows that nearly all the grottoes in Dunhuang were built with wooden frontal buildings as the transition from outer to the inner space.<sup>8</sup> Actually, the frontal buildings in Dunhuang were indivisible parts of Buddhist grottoes and served important religious functions. Though the frontal buildings in the grottoes in North China are mostly destroyed, it is known that their architectural forms and styles were usually in accordance with local and contemporary architecture.<sup>9</sup>

The size and form of the Buddhist grottoes and niches in the Sichuan<sup>10</sup> region differ from those in North China. In the North, the prominent Buddhist grottoes are normally large in scale with a deep space, which form mostly the Buddha halls together with the frontal buildings. In Sichuan, the Buddhist statues were principally made within small or medium-sized niches (therefore called “rock carvings”), to which usually no wooden frontal buildings were built. However, the fieldwork of the project has uncovered traces around the entrances of large grottoes or niches in Yuanjuedong and confirmed that there definitely had been frontal buildings, but regrettably none of the original ones from the Song Dynasty (960–1279) still exist.<sup>11</sup>

In the Sichuan region, the earliest extant frontal buildings to the Buddhist rock carvings are dated to the late 19<sup>th</sup> century and found among others in the three counties of Anyue (Huayandong), Dazu (Thousand-armed-and-eyed Guanyin) and Hechuan (Erfosi), where they were built with statues or caves in large scale. Those wooden structures are functionally similar to those in the north and they form the Buddhist sanctuaries together with the statues. In Dazu it is a wooden hall built before the huge Guanyin statue; in Hechuan the wooden structures shelter the large and small Buddhist statues carved alongside a hill; and in Anyue the frontal buildings are added directly to the grottoes. Both grottoes at Huayandong in Anyue County (Fig. 1) are deep and almost form two halls; the frontal buildings function as transitional parts from the outside to the inside as well as protection for the exquisite statues in the grottoes.

As the best preserved ones from the Qing Dynasty in Anyue County, both frontal buildings at Huayandong are important references for the one to the niche no. 10 at Yuanjuedong.



**Fig. 1:** Two grottoes with frontal buildings at Huayandong in Anyue County

The modern protective buildings are built in the sites with numerous small and medium-sized niches, such as in Beishan (Fig. 2) and Shizhuanshan in Dazu, and Xiyan in Zizhong, etc., protecting the

statues in niches from further weathering. They are also built in the style of the traditional local architecture and appear stylistically consistent with the rock carvings.<sup>12</sup>



**Fig. 2:** Protective structure at Beishan in Dazu County



**Fig. 3:** Two grooves above no. 10 at Yuanjuedong

### Constructing a frontal building to the niche no. 10

#### *Present situation*

Generally speaking, Buddhist grottoes are large and deep caves carved in mountains for monks to live, meditate or carry rituals before Buddha statues; niches are mostly small and shallow concaves in walls that only enshrine holy statues. Although niche no. 10 at Yuanjuedong is in huge scale, it is shallow and does not form a cave; rather, it resembles more a greatly enlarged niche. Therefore, the architectural form of no. 10 at Yuejuedong is a niche, not a grotto, as properly named by a historical inscription thee.

Those types of constructions forming Buddha halls with statues in grottoes are not applicable for the huge niche no. 10 and no historical frontal buildings for niches exist in Sichuan. However, the traces outside the niche itself offer a large amount of information about the former wooden frontal buildings.

The traces show that there has been more than one wooden construction built in front of the niche, of which two constructions could be identified according to the grooves above the niche (Fig. 3). The grooves in the reversed V-form were chiselled into the rock and supported the roofs of the frontal buildings. Of the two groups of traces and grooves, the higher one has been more weathered and would have been the earliest one, properly sized and larger than the second one. The lower and smaller one

seems to be less weathered and thus carved later, presumably after the old one was destroyed. The modern protective frontal building should be built on the basis of the oldest traces, since it assures better lighting and ventilation for the statue in the niche.

Halfway up the niche on both sides there are also many traces and grooves, of which those on the left side of the niche are heavily weathered and have mostly fallen off. On the right side at the same height, several grooves are found corresponding to the traces above the niche, for the grooves of a particular period are generally parallel to each other (Fig. 4). Like the traces above the niche, the higher and older traces here are from the earliest frontal building, while the lower ones belong to

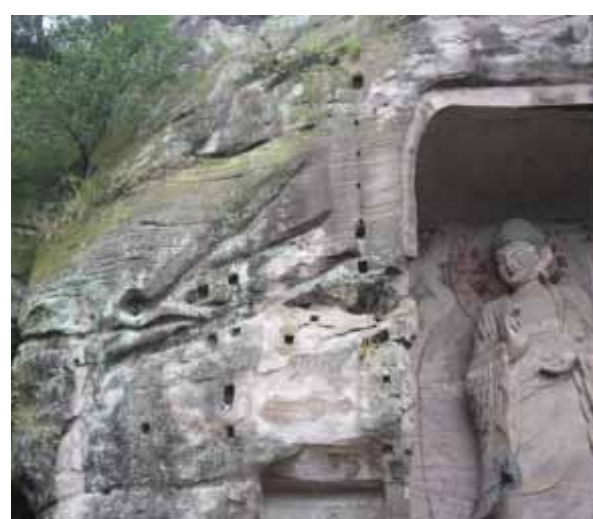


**Fig. 4:** Traces and holes on the right side of niche no.10



**Fig. 5:** Traces of frontal buildings outside niche no. 10

the wall outside and inside the niche that obviously were left by the beams of the structures.

The traces of the two frontal buildings show the profiles of two structures with a double roof (Fig. 5). Considering the practical situation, the former frontal buildings added to niche no. 10 might have been semi-hexagonal pavilions with a double roof.

Pavilions are freestanding covered structures without surrounding walls and usually seen in Chinese temples or gardens, often with varying appearance and forms. Constructed mostly from stone and wood, pavilions are often classified as round, square,

hexagonal and octagonal according to their shape. They provide visitors with a resting place or offer space for statues or bells, and as attractive structures they also become part of the scenery.

In Sichuan, pavilions as freestanding architectures – mostly of the Qing Dynasty – are preserved in plentiful numbers. One type is with a square ground plan, a closed structure and often two-storied, which is often used as a bell tower and not suitable for the Buddhist niche. Another type with a hexagonal or octagonal ground plan might be practical for niche no. 10 at Yuanjuedong. Close to Yuanjuedong there are some referable pavilions, such as Kuixingge Pavilion in Jiangjin County, Shiyiting Pavilion in Shehong County (about 100 km north of Anyue), and a pavilion about 200 metres east of the niche at Yuanjuedong (Fig. 6). A modern reference in traditional style is the Pavilion for the Script of Filial Piety built in the 1960's at Beishan in the neighbouring Dazu County (Fig. 7).

In Sichuan, many Buddhist grottoes have traces of the pavilions as the frontal buildings, although no original ones still exist. This phenomenon is not seen in North China and might be a local characteristic in Sichuan. In Anyue County, those traces are found mostly outside the niches and grottoes in Yuanjuedong as well as in other sites such as Wofoyuan, etc.

#### *A preliminary plan*

Though built on the old grooves and traces, the planned frontal building to niche no. 10 is more a modern protective building in a traditional style

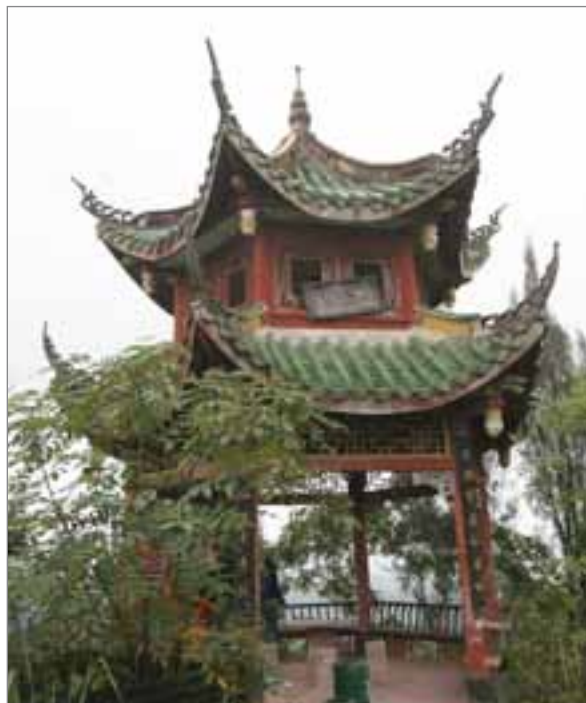


**Fig. 6:** Pavilion at Yuanjuedong



**Fig. 7:** Pavilion at Beishan

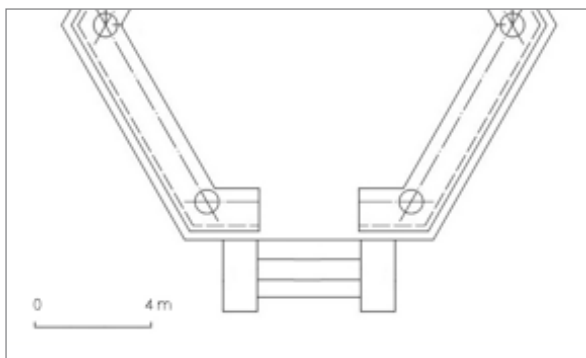


**Fig. 8:** Ground plan of the planned pavilion for niche no. 10

than a reconstruction of the original one, since no original one from the Song period is known to us. The building certainly serves for the purpose of protection without a religious function. With the holes in the wall and ground analysed and re-used, if they are still suitable for use, the appearance and style of the planned pavilion should be in accordance with the traditional architecture in the Sichuan region, whereas the extant traditional architectures there would play an important role for the designing and construction of the pavilion. Above all, the actual protective effects should be taken into consideration in the designing of the pavilion, while the experi-

ence of modern protective structures at other sites should be critically studied and referred to.

The sketch presented here is made on the basis of the grooves and traces outside the niche and drawn by modifying the Shiyi Pavilion from County Shehong, a hexagonal pavilion with a double roof built in the late Qing period.

The ground plan (Fig. 8) of the protective frontal building is a semi-hexagon with a diameter of 8 meters, about 2/3 of the height of the pavilion, the three sides 4 metres long and the distance from the frontal side to the niche 3.46 metres. Four supporting pillars stand at the corners of the half pavilion.

The profile of the pavilion is the same as a half of a double-roof pavilion of approx. 12 metres height with two raised roof corners, while the rear roofs are to be built against the rock wall using the older grooves. From the top of the roof to the top of lower roof is about 4.3 metres and from the lower roof to the platform about 7.7 metres.

Seen from the elevation (Fig. 9), the upper roof is built on the higher groove with two raised roof corners and grey roofing tiles. The roof is carried by the wood columns and beams connected by crossing brackets. No walls will be built between the columns for the sake of lighting and ventilation.



**Fig. 9:** Elevation of the planned pavilion in front of niche no. 10

The lower roof will be built in a similar way and the weight of the upper part should be carried by the four columns of the lower part through diagonal beams. The platform is about 60 cm high from the present ground with three steps leading the visitors into the pavilion. A brick or stone wall with seats and a balustrade above the platform could be built and left in its original colour in consistence with the grey roofs and red columns.

As pointed out, what is presented here is predominantly a preliminary plan and suggestions from viewpoints of art history. The ultimate plan of the protective frontal building needs to be further discussed together with the Chinese and German experts and it should finally be drawn by professional architects.

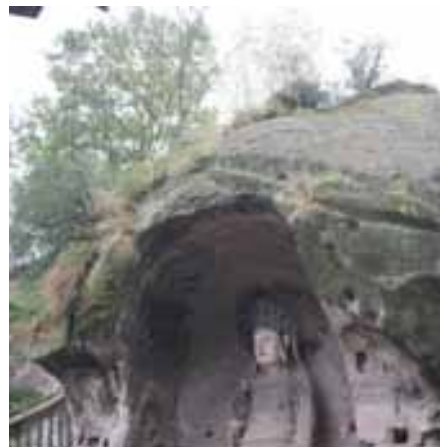
#### **Wooden construction as a protective measure for all the grottoes and niches on the north side at Yuanjuedong**

In fact, building protective constructions as an effective measure for keeping the rock carvings from further weathering has been taken in many sites in nearby Dazu County, where the groups of rock carvings were listed as a UNESCO World Cultural Heritage site in 1999.

In Yuanjuedong, the examination of other niches and grottoes shows that the former frontal wooden building for the niche no. 10 was by no means a single case; rather, there are traces of historical wooden constructions outside almost all the niches and grottoes on the north side. They are niche no. 14, the Guanyin with Lotus-bud; niche no. 12, the King of Vidya; grotto no. 8 of Complete Enlightenment; niche no. 7 of Kundika Guanyin, and niche no. 4 of 13-storied Pagoda (Fig. 10 a–d) etc.

As mentioned above, building frontal structures for the Buddhist grottoes and niches is in accordance with the Chinese tradition. In viewing this it should be pointed out here that in future all the niches and grottoes at Yuanjuedong are to be protected under the wooden protective structures, what is also to be taken into consideration while building the frontal building for the niche no. 10. To protect all the niches and grottoes on the north side at Yuanjuedong, it is practical to build pavilions for the larger niches and connect them with corridors sheltering the smaller ones between them, whereas the practices in nearby Dazu County, in Baodingshan, Beishan and Shizhuanshan, should also be further studied.

**Fig. 10 a–d:** Traces of frontal buildings outside the niches at Yuanjuedong



## Endnotes

- 1 Hu Wenhe, Sichuan daojiao fojiao shiku yishu, p. 73.
- 2 According to the earlier numbering it is no. 16. Ibid., p. 74.
- 3 All data come from the measurement made by project colleague Felix Horn.
- 4 For more information on the study of the statues in the niche in terms of art history see the article by Lin Chunmei in this publication “Die Kunst der Grotte Nummer 10 in der Grottenanlage Yuanjuedong”.
- 5 See Jean-Louis Nou : Ajanta, München: Metamorphosis Verlag, 1993, p. 213.
- 6 For the study of the four remaining frontal building of grottos in Dunhuang see Xiao, Mo: Dunhuang jianzhu yanjiu. [The Art of Architecture in Dunhuang] Beijing: Jixie gongye chubanshe, 2003, p. 335–367.
- 7 Because of the difference concerning the appearance, function and relation to the architecture between a porch and kuyan, in avoiding misunderstanding the wooden constructions to a Buddhist grottoes or niches will here be called frontal buildings.
- 8 See Pan, Yushan and Ma, Shichang: Mogaoku kuqian diantang yizhi. [Ruins of the Frontal Buildings Added to Mogao Grottoes] Beijing: wenwu chubanshe, 1985, p. 135–139.
- 9 For the study of frontal buildings in Yungang see Liu Jiajun: “Yungan di jiu shi ku kuqian liaodai jianzhu yuanzhuang tantao.” [A Study of the Original Form of the Frontal Buildings of Liao Dynasty (916–1125) before the Grottoes no. 9 and 10 in Yungang], in: Wenwe shijie (2004.5), p. 34–37, 29.
- 10 The name of Sichuan in the article refers to its historical meaning, that is, including the province Sichuan and the directly governed city region Chongqing founded in 1997.
- 11 Since no original wooden frontal buildings of the Buddhist grottoes remain, no research on the porches of Buddhist caves in Sichuan and Chongqing has ever been undertaken.
- 12 The experiences from those protective wooden constructions are no doubt meaningful references to the design of the frontal building to the niche no. 10 at Yuanjuedong. Unfortunately, no publications of such wooden constructions are available.
- 13 The niche no. 14, carved in the same period and having the same format as niche no. 10, is called kan niche, according to a contemporary inscription preserved inside. See Hu Wenhe: Sichuan daojiao fojiao shiku yishu, p. 74.
- 14 Gao Zhenming and Tan Li: Zhongguo gu ting. Taipei: Natian shuju, 1992, p. 30–72.
- 15 It is an important issue if the religious function of the statue should be taken into consideration. It is noticeable that red ribbons are donated to the Buddha and incense is frequently burnt on site. At least building a frontal construction would not hinder the worship of this kind.
- 16 The pavilion was built after 1880 according to the chronicle of the county, when the county magistrate rebuilt the site. See Chen Longzhun et al.: Shehong xianzhi [Chronicle of Shehong County.], Chengdu: Sichuan daxue chubanshe, 1990, p. 36.

